Submarine Slope Stability

Based on M.S. Engineering Thesis

Development of a Database and Assessment of Seafloor Slope Stability Based on Published Literature

By

James Johnathan Hance, B. S.
The University of Texas at Austin

Supervisor

Dr. Stephen G. Wright
The University of Texas at Austin

Project Report Prepared for the Minerals Management Service
Under the MMS/OTRC Cooperative Research Agreement
1435-01-99-CA-31003
Task Order 18217
MMS Project 421

August 2003

OTRC Library Number: 8/03B121

For more information contact:

Offshore Technology Research Center

Texas A&M University
1200 Mariner Drive
College Station, Texas 77845-3400
(979) 845-6000

or

Offshore Technology Research Center

The University of Texas at Austin
1 University Station C3700
Austin, Texas 78712-0318
(512) 471-6989

A National Science Foundation Graduated Engineering Research Center

Submarine Slope Stability

Executive Summary

Background and Context Oil and gas developments often require placing equipment, e.g., subsea wells, pipelines and flowlines, foundation systems for floating structures, in areas with sloping seafloors. Submarine slope failures can occur in such areas and create soil slides. Thus the stability of submarine slopes must be considered in selecting the site for installing and designing seafloor equipment.

Assessing submarine slope stability requires estimating the likelihood, extent, and impact of a slide during the lifetime of the facility. This assessment is difficult due to the large difference in time scales between the project life (10's of years) and the geologic processes and triggering mechanisms that cause the slides (10,000's of years) Such an assessment is best approached through a probabilistic risk analysis that considers the risks to the equipment; the causes, likelihood, and behavior of submarine slides; and the uncertainties.

A forum of experts from industry, government, and academia was held in 2002 (1, 2) to discuss the current state-of-the-art and state-of-the-practice and to identify areas where future research was needed to advance capabilities to assess submarine slope stability and the impact of submarine slides. That forum concluded that a comprehensive data base should be developed for historical slides containing information on the seafloor characteristics (soil properties, slope topography, geology), triggering mechanisms, and the characteristics and extent of the slide. This database could then be used to develop, improve, and test models for predicting slope stability, slide occurrence and behavior, and to assess the impact of uncertainties in seafloor characteristics and triggering mechanisms in predicting the likelihood and behavior of slides. By looking for similarities between a new site under investigation for a subsea installation and sites of historical slides, data from the historical slides might also be useful in assessing the slope stability and risks of a slide for the new site. This was the basis for the project reported here.

Development of a Database and Assessment of Seafloor Slope Stability based on Published Literature This work resulted from a research project conducted by J.J. Hance for his Master of Science in Engineering at the University of Texas under the supervision of Dr. Stephen G. Wright. Hance's thesis (3) is attached

Based on published literature, a database was compiled the includes 534 submarine slide events. The database contains information on the geographic location, water depth, date and type of failure, potential triggering mechanisms, dimensions, slope angle, and soil types and properties. The data were examined to identify important characteristics of seafloor slope failures. While the database is substantial, significant geotechnical information was not available for many slope failures.

Fourteen different triggering mechanisms were identified and included in the database. Earthquakes are the most commonly reported trigger.

Slope stability analyses were performed to assess the likelihood of slides being triggered by gravity, rapid sedimentation (underconsolidation) and earthquakes. The analyses revealed that it is unlikely that most of the seafloor slope failures were triggered by gravity loads alone. Earthquake loading was confirmed as a common trigger, and rapid sedimentation (underconsolidation) was also a likely trigger of many slope failures.

It is important to note that the study revealed that a relatively large number of submarine slides occurred on much flatter (less than 10 degree) slopes and traveled much greater distances than slope failures on land. This strongly suggests that different mechanisms are prevalent for submarine slides, compared to those on land.

Hydroplaning is one mechanism that may explain such large runout distances. The mechanism of hydroplaning is summarized, and a simple sliding block model is presented to illustrate how conditions for hydroplaning can be developed. Rheological models have also been developed to explain slide runout, and several models are described. However, the rheological models do not seem to explain some of the very large runout distances observed in both experiments and actual seafloor slides. For many slides, hydroplaning appears to be the mechanism that can best account for large runout distances.

References

Wright, Stephen G., "Forum on Risk Assessment for Submarine Slope Stability - Report of a Forum Held In Houston, Texas - May 10 And 11, 2002", June, 2002 (Offshore Technology Research Center Report).

Wright, Stephen G., Gilbert, Robert B., and Smith, Charles E., "Risk Assessment of Submarine Slope Stability in Deepwater - Issues and Priorities", *Proceedings*, 14th Deep Offshore Technology Conference, New Orleans, Louisiana, November 13-15, 2003.

Hance, J.J. (2003). “Development of a database and assessment of seafloor slope stability based on published literature.” M.S. Thesis, University of Texas at Austin.

Development of a Database and Assessment of Seafloor Slope Stability based on Published Literature

by

James Johnathan Hance, B.S.

Thesis

Presented to the Faculty of the Graduate School

of The University of Texas at Austin

in Partial Fulfillment

of the Requirements

for the Degree of

Master of Science in Engineering

The University of Texas at Austin

August 2003

Development of a Database and

Assessment of Seafloor Slope

Stability based on Published Literature

APPROVED BY

SUPERVISING COMMITTEE:

_____

Stephen G. Wright

_____

Robert B. Gilbert

Copyright

by

James Johnathan Hance

2003

ACKNOWLEDGEMENTS

There are several people I must thank for their efforts and encouragement during the preparation of this thesis. Without their positive involvement in this process, this thesis would not have been completed. First, I am grateful for the opportunity to work with my primary supervisor, Dr. Stephen G. Wright. His continued interest and involvement in the development of this project has been rewarding. He has offered guidance in maintaining a proper direction for this thesis while ensuring that the research process has been educational for me as a young engineer. I am thankful that Dr. Robert Gilbert became involved in this project. He was efficient in reviewing the manuscript and results from the database. I also thank Dr. Ellen Rathje who helped me with the part of my thesis that involved evaluating seismicity and pseudo-static slope stability.

I am grateful for the financial support provided by the Offshore Technology and Research Center (OTRC) during my involvement with this project. I thank the people on the 9th floor who always had a smile on their face, namely Teresa Tice-Boggs, Chris Treviño, Alicia Zapata, and Dr. Roy Olson. A special thanks also goes out to the friends I have made within the Geotechnical Engineering Program.

My parents, James Hance and Brenda Ruffner, have always been a driving force in my life, and I am thankful for their encouragement during my graduate studies at The University of Texas at Austin. I would also like to thank my stepparents, Gary Ruffner and Joan Hance, and my younger brothers, Matt, Pat and Harry.

Finally, I must acknowledge the daily support and love provided by my wonderful fiancée, Jennifer Graves. She has helped me whenever necessary, and I am forever indebted to her.

Development of a Database and

Assessment of Seafloor Slope

Stability based on Published Literature

by

James Johnathan Hance, M.S.E.

The University of Texas at Austin, 2003

SUPERVISOR: Stephen G. Wright

A database of seafloor slope failures has been created from the published literature. The database contains information on the geographic location, date and type of failure, potential triggering mechanisms, soil types, soil properties, dimensions, slope angle, and water depths for the slope failures. Data in the database have been examined to identify important characteristics of seafloor slope failures. However, while there is substantial information in the database, significant geotechnical information was lacking for many of the slope failures.

Fourteen different triggering mechanisms have been identified and are included in the database. Each of these triggers is discussed. The most common trigger reported is earthquake loading.

Seafloor slope failures (slides) can affect large areas and volumes of soil, and they tend to be larger than subaerial landslides. Also, in comparison to subaerial landslides, seafloor slides tend to travel larger distances and occur on flatter slopes.

Slope stability analyses were performed and results are presented to assess the likelihood of slides being triggered by gravity, rapid sedimentation (underconsolidation) and earthquakes. The analyses reveal that it is unlikely that most seafloor slope failures are triggered by gravity loads alone; earthquake loading and rapid sedimentation (underconsolidation) are likely triggers of many slope failures.

Many seafloor slides are accompanied by very large runout distances. Hydroplaning is one mechanism that may explain such large runout distances. The mechanism of hydroplaning is summarized, and a simple sliding block model is presented to illustrate how conditions for hydroplaning can be developed. Rheological models have also been developed to explain slide runout, and several models are described. However, the rheological models do not seem to explain some of the very large runout distances observed in both experiments and for actual seafloor slides. For many slides, hydroplaning appears to be the mechanism that best accounts for large runout distances.

TABLE OF CONTENTS

LIST OF TABLES

LIST OF FIGURES

CHAPTER 1

INTRODUCTION

Seafloor slope failures occur beneath many of the world's oceans and could impact all types of offshore and coastal facilities. In order to understand better and assess the likelihood of seafloor slope failures, this study was undertaken to compile and analyze data on such failures. Information that pertains to evaluating the potential occurrence of a landslide, such as characterizing the conditions in which landslides are known to take place, was compiled. Due to the difficulties and costs in exploring the marine environment, there is a high level of uncertainty in the stability of seafloor slopes. In an effort to reduce this uncertainty, emphasis in this project was on compiling data and creating a database of seafloor slope failures that have been reported in the literature. Much of the effort for this project was directed to forming the database.

Information related to seafloor landslides was examined in hundreds of references including textbooks, reports, magazine articles, theses, dissertations, Internet websites, maps, and technical papers from journals and conference proceedings. Information from each reference that was considered to be pertinent in describing a particular landslide event was extracted, and entered into fields in a database. The database was created as a single table in Microsoft Access, with

the fields forming columns and the landslide entries forming rows. Once the database was formed, the data were analyzed. Various types of information in the database were evaluated, and results were summarized into tables and figures.

The review of the literature used to create the database is explained in Chapter 2. Chapter 3 contains a description of the structure of the database and the content of the fields (columns) in the database table. Causes of seafloor slope failure, i.e. triggering mechanisms, are discussed in Chapter 4. Because the triggering mechanisms are complex processes, a number of fields in the database contain information pertaining to triggering mechanisms. The data are analyzed and characteristics of seafloor slope failures are examined in Chapter 5. Results of slope stability analyses performed to assess the likelihood of seafloor slides being triggered by several triggering mechanisms are presented in Chapter 6. Because some seafloor slides travel large distances, models that have been developed to explain the large movements are of interest and are examined in Chapters 7 and 8. An overview of the conclusions of this research program and recommendations for future research are presented in Chapter 9.

CHAPTER 2

LITERATURE REVIEW

2. 1 INTRODUCTION

An extensive investigation of the literature was conducted to find as many documented cases of seafloor slope failure as possible. The cases were then summarized in tabular format into a database. The body of literature and the methods used to collect the data are described in this chapter.

2.2 THE BODY OF LITERATURE

The literature investigated for this project was mainly comprised of technical papers found in geological journals and periodicals. Some of the main journals included *Marine Geotechnology, Marine Geology, Geo-Marine Letters, American Association of Petroleum Geologists Bulletin*, and the USGS Survey Bulletin (1993). About 25 papers in *Marine Geotechnology* included discussions of submarine slope failures, and about 40 papers from *Geo-Marine Letters* pertaining to seafloor slides were examined. About 25 studies of submarine slope failures in the U.S. Exclusive Economic Zone (US-EEZ) and numerous references to other studies were found in the U.S. Geological Survey Bulletin 2002.

About 257 references were used to compile the database. These references are denoted in the bibliography at the end of this thesis with an asterisk

(*). Hard copies of most of these references have been obtained from this research effort.

Two references contained compilations of a number of landslide events. In fact, approximately half of the landslide events in the database were obtained from these two references. Both of these sources were from the geology literature. The first source is McAdoo et al. (2000), who published results for areas mapped off the coasts of California, Oregon, Texas and New Jersey. McAdoo et al. (2000) reported 83 historical landslides among these four regions of the U.S. continental slopes. The second source is Booth et al. (1988), and is a detailed map and table of the U.S. – Canadian Atlantic continental slope. Booth et al. (1988) report 179 mass movements along this region based on a compilation from previous research. The sources described above and many other sources were examined to obtain the information that was entered in the database.

Submarine landslides have been documented by researchers from the United States, United Kingdom, Norway, Canada, Greece and France. The majority of the documentation is from geologists and geophysicists, and papers have been written based on findings from sonar imaging and cruise missions. Published geotechnical information is typically sparse because of the inherent cost and difficulty in acquiring this information.

2.3 HOW DATA WAS COLLECTED FROM THE LITERATURE

The majority of the literature studied was available at the Engineering and Geology Libraries at the University of Texas at Austin or was acquired electronically by means of the Internet. Information from several sources was obtained through interlibrary loans from other universities.

The Internet was a convenient tool for research. In particular, databases, accessed through the University of Texas website, such as GeoRef and Ei Compendex (Engineering Information, Inc.) were powerful search engines that were used to identify many of the technical articles. These searches were performed using keyword searches or searching by journal type or the name of a particular author. Keyword searches were helpful in narrowing search results. Examples of keywords include synonyms of slope failure such as landslide, slump, slide, debris flow, mud flow, and turbidity current as well as potential causes of seafloor slope failure such as earthquake, gas hydrate disassociation, salt, and storm wave. By searching for documents using these keywords, relevant literature could be located.

From the extensive investigation of the literature, a database of submarine slope failures was created. The structure and content of the database are described in Chapter 3.

CHAPTER 3

STRUCTURE AND CONTENT OF THE DATABASE

3.1 INTRODUCTION

This chapter focuses on the structure and content of the database and how data can be extracted for analyses. The database is an extensive synopsis of "what is known" about submarine landslides based on case histories reported in the literature and what characteristics are considered to be important. Information considered to be relevant and included in the database is discussed in this chapter. Not all data in the literature was entered into the database, and examples of excluded information are also provided in this chapter. The database is one table in Microsoft Access® and contains fields or categories that form columns of information. A description of each field (column) is provided in this chapter. A description of how data was extracted from the database is also presented.

3.2 INCLUDED AND EXCLUDED INFORMATION

Over 300 sources of information, mainly technical papers, contained relevant data for this project. Geotechnical data included in the database consists of the types and properties of the soil involved in the landslide events. Geologic information includes the approximate date of the landslide and interpretations of how the landslide was caused in the particular geologic environment. Most of the

landslides were discovered as a result of geophysical imagery. The geometry of a mass movement, e.g. length, width, and thickness, the angle of the seafloor slope, and water depths to the seafloor affected by the landslide were obtained through geophysical measurements and are included in the database.

Some data in the literature was not entered into the database. For example, references often contained a description of an entire region explored in a seafloor investigation, and the landslide represented only a portion of the findings. In such cases, only the information pertaining to the landslide was extracted. Specifically, detailed results of the bathymetry in the region of the explored seafloor were excluded because only so much bathymetric data could be entered into the database. Sometimes there was description of the geomorphology of a region, and this information was typically excluded from the database unless it was found to be helpful in describing the landslide or the potential cause of the landslide (trigger). Furthermore, geologic classifications of seafloor subsoils were typically excluded as well as estimates of the age of sediments.

3.3 STRUCTURE AND CONTENT OF THE DATABASE

The database is one table that was created using Microsoft Access® software. In this section each of the categories or “fields” that make up the database are described. The fields represent columns in the database, and each

row in the database represents an individual landslide. The fields are expressed as different data types in accordance with Microsoft Access®, and the data types included in the database are text, number and hyperlink. The availability of information for each of these fields is discussed in Chapter 5.

3.3.1 IDENTIFICATION NUMBER (ID) AND SLIDE NUMBER

A field called an identification number (ID) was assigned to each landslide event, and this field is known as the primary key field. A primary key is an important consideration in creating a table in Microsoft Access® because this field contains a unique number that sets the record entry apart from all other records in the table. The identification numbers are whole numbers that range from 1 to 534, which represents total number of seafloor slope failures, and this field is a **number** field.

The slide number is a **number** field that was assigned to each slide when this project began, prior to establishing Microsoft Access® as the database program (earlier versions of the database were created in Microsoft Word® and Excel®), and, thus is an arbitrary number. The slide number indicates the order in which the case histories were researched from the literature and entered into the database. Hard copies of the references that were used to compile the database are organized according to slide number. The slide number is used as the connection to the hyperlinked image files, which are described in Section

3.3.20. The hyperlinked image files are labeled with reference to the slide number. The slide number and the identification number rarely coincide.

3.3.2 DESCRIPTION OF EVENT LOCATION

The event location field is a **text** field that defines the location of the slope failure according to the original author(s). For example, Booth et al. (1988) defined 179 mass movements and numbered them accordingly. These numbers assigned by Booth et al. (1988) are included in the event location field for convenience. Other descriptions that may appear in this field include the landslide location with respect to an ocean, a state, a country, and a seafloor region, i.e. continental shelf, slope or rise.

3.3.3 LATITUDE

This field is a **number** field that contains the latitude for each landslide, expressed as a whole number in degrees. In the database landslides that occurred in the northern hemisphere (north latitude) have positive latitudes, and slides that occurred in the southern hemisphere (south latitude) have negative latitudes.

3.3.4 LONGITUDE

This field is a **number** field that contains the longitude for each landslide expressed as a whole number in degrees. Landslides that occurred in the western

hemisphere (west longitude) are positive numbers, and slides that occurred in the eastern hemisphere (east longitude) are negative.

3.3.5 DATE OF THE SLOPE FAILURE

This field is a **text** field that includes the date or age of the slope failure. However, this field does not include the age of the sediments within the explored seafloor region. This field represents the knowledge of the researchers at the time the papers were written. This field may contain text or numbers depending whether the landslide occurred in ancient or recent times and depending on the accuracy of the geologic dating used in the investigation. Ancient landslides are expressed either in Geologic Epochs such as Pleistocene or Holocene, or they are defined according to years (thousands to millions) before present. Recent landslides are described according to the date the event occurred.

3.3.6 SOIL TYPE

Soil type is a **text** field that describes the soils (sediments) involved in the landslide. This field contains geotechnical and geologic classifications. Examples of geotechnical classification include “clayey silt” and “silty sand,” and examples of geologic classification include “mud clasts” and “calcareous siltstones.”

3.3.7 SOIL PROPERTIES

The soil properties field is a **text** field that defines the geotechnical characteristics of the soils involved in the slope failure. Geotechnical characteristics include index properties such as water content (w) and Atterberg limits, i.e. liquid limit (LL), plastic limit (PL), and plasticity index (PI). Soil properties also include the percentage of organic material (O or OM), sensitivity (S_t), void ratio (e), porosity (n), unit weight (γ) and liquidity index (LI). Shear strength properties are also provided in this field when available. Shear strengths may be expressed as effective stress, drained parameters (ϕ' and c') or as undrained shear strengths, either s_u or a c/p ratio. All of the geotechnical information is grouped into this field because this information is scarcely available in the literature, so it was not deemed necessary to create additional fields for each soil property. It is noted that data for soil properties, as defined in this field, could be converted into a table in the future.

3.3.8 TRIGGERING MECHANISMS

An examination of the literature revealed that there were a number of causes of seafloor slope failure. These are referred to as “triggering mechanisms” in this thesis. As a result, a **text** field in the database was created to describe the potential triggering mechanism(s) reported in the literature for each landslide

event. After extensive investigation, the triggering mechanisms include the following:

- earthquakes and faulting
- rapid sedimentation
- gas and disassociation of gas hydrates
- ocean storm waves
- tidal events
- human activity
- erosion
- mud volcanoes
- magma volcanoes
- salt diapirism
- flood events
- creep
- tsunamis
- sea-level fluctuations

A discussion of each of these mechanisms and how the information related to these mechanisms is captured in the database is provided in Chapter 4.

3.3.9 LANDSLIDE DESCRIPTION

This **text** field provides a description of the landslide that was considered to be helpful for the database user. The description may include a statement about the progression of events after the landslide initially occurred. The description may also describe any damage that was caused by the slope failure. There are a number of terms that appear in the landslide description field, and definitions are provided for these terms in Table 3.1. These terms vary according to the type of landslide observed in the seafloor investigation and the investigators who created these terms to describe the various types of landslides.

Table 3.1. Description of terms that appear in the landslide description field.

Term	Definition
Slump	a landslide where the failed soil does not exceed the limit of the scar, according to Lee et al. (1993); slumps are bounded on all sides by distinct failure planes. Mulder and Cochonat (1996) noted that slumps are described as coherent or cohesive because the failed soil appears essentially undisturbed, and the downslope movement is limited.
Debris flow	a completely deformed mass that has moved as a viscous fluid, according to Booth and O'Leary (1991); from this project, this term was most widely used to distinguish the mass movement from a slump-type of failure.
Turbidity current	refers to sediment that is in suspension, as opposed to a slumped mass or a debris flow; many turbidity currents form from sediment that has failed and moved downslope. Turbidity currents often form as the last sequence of events in a mass movement that may have initiated with a slump.
Translational	type of slope movement that has a planar slip surface (rupture surface), according to Hampton et al. (1996)
Rotational	type of slope movement that has a concave-upward slip surface (rupture surface), according to Hampton et al. (1996)

Table 3.1. Description of terms that appear in the landslide description field *(continued)*.

Term	Definition
Disintegrative	according to Whitman (1985), type of failure typically associated with debris flows; involves a loss of shear strength in the soil that is produced by a loading event such as an earthquake. The remaining shear strength in the soil is less than the shear stress induced by gravitational force, resulting in large downslope displacements.
Rubble slide	a displaced mass consisting of large rock fragments or rubble; disintegrative-type slope failure, according to Booth and O'Leary (1991)
Collapse	a depression associated with sediment that has collapsed or liquefied at depth, or possibly throughout its entire thickness; disintegrative-type slope failure, according to Booth and O'Leary (1991)
Retrogressive	the sliding of sediments that occurs successively as failure progresses upslope, according to Hampton et al. (1996)
Non-disintegrative	associated with slumps; this type of failure is characterized by little deformation after the loading event, according to Whitman (1985).
Block slide	a displaced mass that is structurally intact and cubical; nondisintegrative slope failure according to Booth and O'Leary (1991)
Slab slide	a displaced mass that is structurally intact and tabular; nondisintegrative slope failure according to Booth and O'Leary (1991)
Mixed slide	shallow slides with a small circular scar (slip surface) and a huge planar body according to Booth and O'Leary (1991)
Carpet slide	intact, yet displaced masses that are typically tabular with folded or wrinkled parts according to Booth and O'Leary (1991)
Scarp	a steep slope typically formed by the removal of sediments due to slope failure; also called escarpment; headscarp is most upslope scarp
Scar	surface that is formed by the removal of sediments due to slope failure, i.e. rupture surface
Mud flow	a mass flow, i.e. debris flow, of fine-grained sediment
Hummocky	seafloor surface that appears disturbed and raised above the adjacent undisturbed region

Table 3.1. Description of terms that appear in the landslide description field *(continued).*

Term	Definition
Turbidite	soil that is deposited by turbulent flow, probably turbidity currents
Debris lobe	refers to the appearance of deposits from debris flows; debris lobes are typically elongated with a roundish shape of sediment at the end of the slide deposit

3.3.10 VOLUME

Volume is a **number** field in the database that defines the approximate volume of displaced soil, and does not include the volume of the landslide scar. The landslide volume is expressed in units of cubic kilometers (km^3). The level of precision varies from whole numbers to 10^{-6}.

3.3.11 AREA

Area is a **number** field in the database that identifies the total area influenced by the slope failure. This area is a combination of the area of the landslide scar and the region of disturbed material that may be present downslope from the scar. This area is expressed in units of square kilometers (km^2). The level of precision varies from whole numbers to 10^{-1}.

3.3.12 THICKNESS

Thickness is a **number** field in the database and represents the average thickness of the landslide based on geophysical data and, if available, geologic

dating from cores. The units of thickness are in meters (m) whereas all other dimensions in the database are in units of kilometers, i.e. km, km^2 and km^3. The level of precision varies from whole numbers to 10^{-1}.

3.3.13 LENGTH

The length of the landslide, which is commonly referred to as runout distance, is the limit of disturbed seafloor downslope from the headscarp. It is a **number** field, expressed in units of kilometers (km). The level of precision varies from whole numbers to 10^{-2}.

3.3.14 WIDTH

Width is the average width of the landslide from an aerial (plan) view. It is a **number** field in the database, expressed in units of kilometers (km). The level of precision varies from whole numbers to 10^{-2}.

3.3.15 SLOPE ANGLE

The slope angle field defines the average angle of the seafloor slope at failure. The slope angle is usually obtained by determining the angle of the unfailed adjacent seafloor slope. Slope angle is a **number** field in the database expressed in degrees. The level of precision varies from whole numbers to 10^{-2}.

3.3.16 SHALLOWEST WATER DEPTH

The “shallowest water depth” is the shallowest depth affected by slope failure, and usually refers to the water depth at the location of the headscarp, at the head of the landslide. However, landslides can retrogress upslope so the shallowest water depth does not always correspond to the location of the initial headscarp. Shallowest water depths are in units of meters below the water surface, and this field is a **number** field in the database, expressed as whole numbers. The water depths listed in the database are the water depths at the time of the site investigation.

3.3.17 DEEPEST WATER DEPTH

The “deepest water depth” field defines the greatest depth affected by slope failure, and is the water depth at the end of landslide runout or at the limit of disturbed material, at the toe of the landslide. Deepest water depths are in units of meters below the water surface, and this field is a **number** field in the database, expressed as whole numbers. The water depths listed in the database are the water depths at the time of the site investigation.

3.3.18 REFERENCES

This field is a **text** field and includes all references reported in the literature for the landslide. This field contains the author(s) and date of the

published reference, but does not contain a detailed bibliography. A detailed bibliographic list of references is included at the end of this thesis.

3.3.19 SCANNED IMAGES (1 TO 12)

There are 12 fields in the database devoted to image files, totaling over 520 files. As information about each landslide was retrieved from the literature, relevant visual images were scanned into the computer using a scanner and saved as image files (JPG files) so they could be viewed in the database. The data type represented in this field is a **hyperlink**, linking the scanned image fields to the saved JPG files. When the database user clicks on a hyperlink, a window appears with the particular image.

The image files that were created include different views of the landslide (plan view, profile view, and 3D view) and descriptions of soil properties such as tables summarizing laboratory shear strength parameters, boring logs with soil data, or shear strength profiles. The image files were saved and named according to the type of information displayed in the image. For example, a profile view of a landslide that was considered relevant from the literature was saved as “profile view” and this file appears in the scanned image field as a hyperlink.

3.4 HOW THE DATABASE WAS USED

Once the database was constructed and the relevant data from the literature was entered into the fields, the data were analyzed. Queries were written to extract information from various fields in the database. The select query was used for this project, and this query returned data according to a defined criterion(a) within specified fields. Queries were written for the following:

- Each of the 14 triggering mechanisms
- Slides located in north latitudes and south latitudes
- Slides located in east longitudes and west longitudes
- Total area influenced by slide
- Total volume of slide mass
- Runout distance
- Thickness of slide mass
- Shallowest water depths affected by slide
- Deepest water depths affected by slide
- Slides that damaged submarine cables
- Slides that have information on soil type
- Slides that have information on soil properties
- Slides that have a scanned image

- Liquefaction-type slope failures
- Slides that have information on slope angle and total area
- Slides that have information on slope angle and runout
- Slides that occurred in Holocene, Pleistocene, and Paleocene ages
- Slides described as debris flows
- Slides described as slumps

Appendix A contains a summary of how the database appears in Microsoft Access. This summary includes screen images showing the database, queries and output from the queries as they appear in Microsoft Access. Appendix A is intended as a "user's manual" for future use of the database.

The output from the queries listed above was assembled into tables, and exported to Excel for analysis. A summary of the analysis from many of the queries is presented in Chapter 5. Chapter 4 is a detailed synopsis of the causes of seafloor slope failure, i.e. triggering mechanisms, that were described in Section 3.3.8. Chapter 4 also includes how the database captures any information relevant to triggering mechanisms.

CHAPTER 4

TRIGGERING MECHANISMS

4.1 INTRODUCTION

Many geohazards and triggering mechanisms can affect seafloor slope stability. "Triggering mechanism" is used in this chapter to refer to the cause of a slope failure. Triggering mechanisms can be grouped into two broad categories. The first category encompasses triggers that reduce the shear strength of the soil and, thus, decrease the resisting forces in the slope. The second category encompasses triggers that increase the driving forces in the slope. These two categories are not mutually exclusive; both categories of triggers can occur simultaneously for the same slope.

This chapter describes the triggering mechanisms identified from the literature search and explains briefly how each mechanism affects seafloor slope stability. Although the database included a field specifically for triggering mechanisms, other fields in the database also include relevant information. All of this information is discussed in this chapter.

4.2 TYPES OF TRIGGERING MECHANISMS

There are various triggering mechanisms reported in the literature. These mechanisms and how information relevant to these mechanisms appears in the database are discussed in this section.

4.2.1 EARTHQUAKES AND FAULTING

Earthquakes and faulting are important triggering mechanisms that result from plate tectonic activity. The seismic energy induced by plate tectonics is transferred to the bedrock, and released through displacements in the Earth's crust, i.e. faults. The faulting produces earthquake ground motions in the bedrock and overlying soil deposits. Earthquakes can increase the driving stresses in the slope via seismic accelerations and also reduce the shear strength in the soil via liquefaction.

Knowledge about the seismicity of a region is important when assessing the likelihood of an earthquake or fault triggering a slope failure. A global seismic hazard map, provided by Giardini et al. (1999), is shown in Figure 4.1 to illustrate seismicity on a global scale. This map only includes the seismic hazard for regions of the continental crust and not the oceanic crust, i.e. seafloor. This map shows peak ground acceleration (PGA) values predicted with a 10 percent probability of exceedance in 50 years: The higher the PGA value, the larger the seismic hazard. This map indicates there are many areas of the world with a high

seismic hazard. A field with the geographic coordinates of the slope failures (Section 3.2.4) was included in the database so that landslides believed to be triggered by earthquakes and faulting could later be mapped on the global seismic hazard map to determine any correlations with seismicity. Results of such correlations are presented in Chapter 5.

Other information that may be pertinent to earthquakes and faulting was included in the database, and is summarized in Table 4.1. Table 4.1 also includes comments regarding the relationship of the information to earthquakes and slope instability.

Table 4.1. Information Relevant to Earthquakes or Faulting as Triggering Mechanisms.

Type of Information	Database Field(s) Containing Information	Comments
Earthquake Magnitude	Triggering Mechanism	Describes amount of energy that triggered failure. This information appeared for about 22 slides in the database.
Geographic Location of Slope Failure	Latitude; Longitude	This information enables mapping of slope failure on global seismic hazard map.
Slope failure location relative to earthquake epicenter location	Slide Description	Defines distance between earthquake epicenter and resulting slope failure; This information was available for 6 slides in the database.
Slope location relative to fault location	Triggering Mechanism	Defines distance between fault and resulting slope failure; This information was available for about 50 slides in the database.

Table 4.1. Information Relevant to Earthquakes or Faulting as Triggering Mechanisms. *(continued)*

Type of Information	Database Field(s) Containing Information	Comments
Liquefaction	Triggering Mechanism; Slide Description	Liquefaction of soil is typically caused by earthquake shaking and, thus, provides indirect evidence of earthquake-triggered slides; This information was available for about 10 slides in the database.
Geomorphologic Description	Triggering Mechanism; Slide Description	Submarine canyons have been linked to faulting and, thus, provide indirect evidence; This information was rarely provided in the literature.
Type of Slope Failure, e.g. debris flow, slump	Slide Description	The type of failure may correlate with the trigger; This information was provided for most earthquake-triggered slides in the database.
Geophysical Description	Triggering Mechanism	Geophysical surveys have revealed the presence of faulting in the subsurface in proximity to slope failure.
Description of seismic activity, e.g. number of earthquakes with magnitude greater than 5 over last 50 years	Triggering Mechanism	Earthquakes and faulting can be inferred as a trigger if the slope is located in a region with sufficient seismic activity. This information was available for about 35 slides in the database.
Date of Slope Failure	Date of Slope Failure	Knowing age can correlate with known earthquakes or periods of seismicity

Table 4.1. Information Relevant to Earthquakes or Faulting as Triggering Mechanisms. *(continued)*

Type of Information	Database Field(s) Containing Information	Comments
Number of Past Slope Failures	Triggering Mechanism	Describes quantitatively or qualitatively the history of seismically-induced slope failures; This information was rarely provided in the literature
Type of Fault	Triggering Mechanism	Defines the type of fault that induced slope failure, e.g. strike-slip; This information was available for about 5 slides in the database.

4.2.2 SEDIMENTATION PROCESSES

Sedimentation processes can affect slope stability in the offshore environment and were cited as the cause of failure for many of the case histories examined. Sedimentation processes are complex because they vary significantly with respect to time and location. Higher sedimentation rates are commonly associated with glaciation where water from the oceans is transferred to ice caps, and the sea level drops. As a result, more continental crust is exposed for erosion and transport to the oceans. Sedimentation processes are influential in most marine environments including fjords, river deltas, submarine canyon-fan systems, open continental slopes and oceanic volcanic islands and ridges. The processes depend on factors such as water depth, distance to source of sediment (rivers and river deltas), and, according to Booth et al. (1988), physiographic setting such as canyon walls, broad open slopes, and ridges.

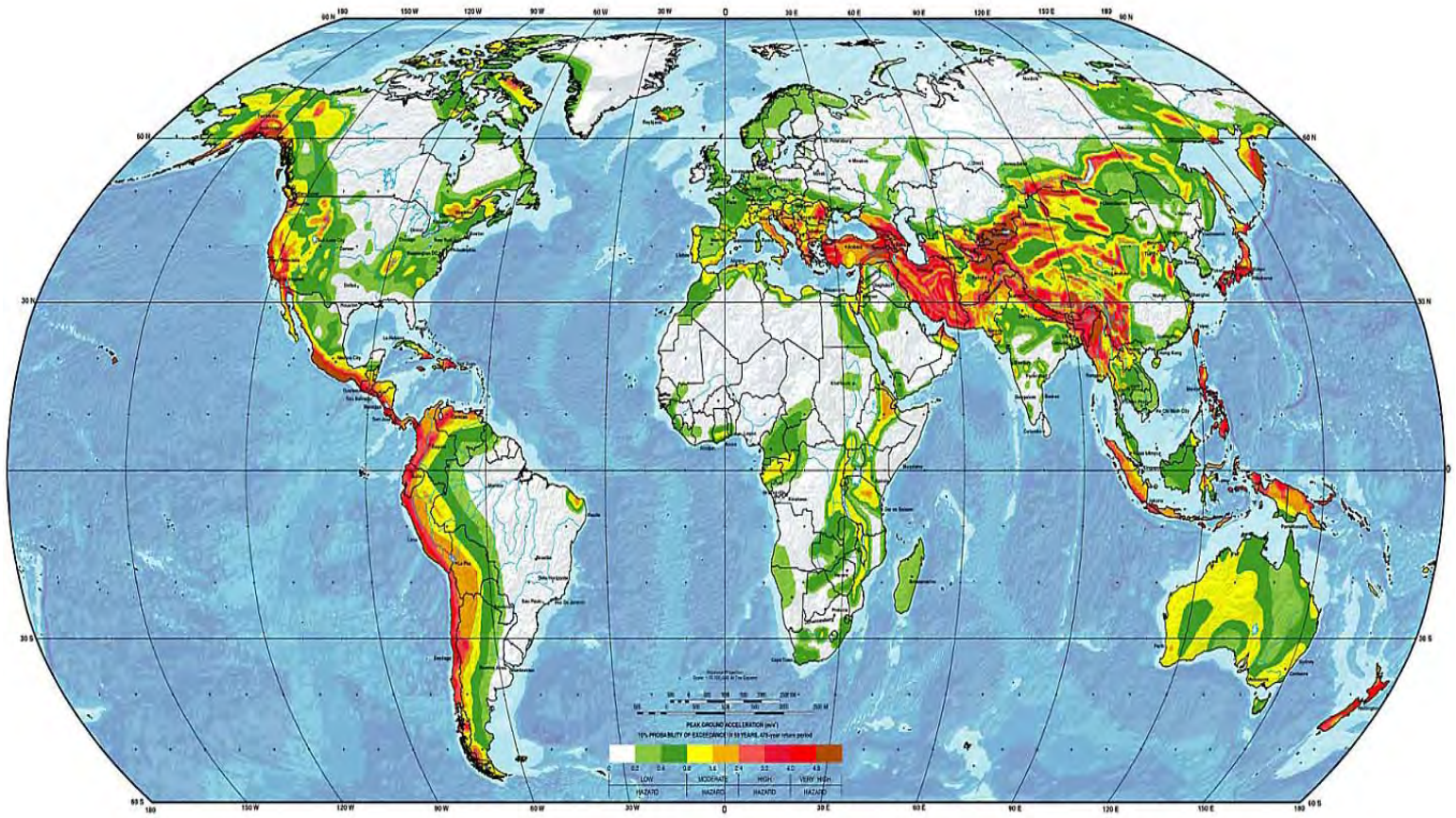

Figure 4.1: Global Seismic Hazard Map. Orange, red and brown colors indicate high levels of seismic hazard due to large peak ground acceleration (PGA) values predicted with a 10 percent probability of exceedance in 50 years. Green, light green and white colors indicate lower levels of seismic hazard (Giardini et al., 1999).

Sedimentation processes can cause slope failure in a variety of direct and indirect ways. For example, Terzaghi (1956) noted that rapid sediment deposition can produce an increase in total stresses at a rate faster than the rate of dissipation of excess pore water pressures. This leads to underconsolidation of soils and correspondingly low shear strength. Sedimentation can also indirectly trigger slope failures by creating an environment conducive to other triggering mechanisms. For example, the accumulation of sediment also contributes to formation of salt diapirs and steeper slopes (Section 4.2.9). One of the requirements for the formation of mud volcanoes described in Section 4.2.10 is rapid sedimentation. If a slope does not fail directly due to sediment loads, the excess pore water pressures that are created in the soil may leave the slope marginally stable with factors of safety near unity. If another triggering mechanism, such as fault rupture, develops, the slope may then fail due in part to the low shear strength.

Prior and Coleman (1984) noted that rapid sedimentation is typically encountered in offshore delta areas and at the base of submarine canyons. Rivers that deliver the highest sediment load to deltas are shown in Figure 4.2. This figure includes 22 rivers: Ganges, Yellow (Huangho), Amazon, Yangtze, Irrawaddy, Magdalena, Mississippi, Orinoco, Red, Mekong, Indus, MacKenzie, Godavari, La Plata, Purari, Pearl, Copper, Danube, Choshui, Yukon, Niger, Zaire. According to Milliman and Meade (1983), these rivers each deliver in excess of

40 million tons of sediment to the oceans per year. It is important to note, however, that increases in sedimentation have commonly been associated with ancient periods of glaciation, and therefore, regions of high sedimentation may not correlate with current active river deltas. Sedimentation-triggered landslides are discussed further and mapped in Chapter 5.

The database included information pertinent to sedimentation processes and the role of sedimentation as a triggering mechanism. All of this information is summarized in Table 4.2.

Table 4.2. Information Relevant to Sedimentation Processes as a Triggering Mechanism.

Type of Information	Database Field(s) Containing Information	Comments
Sedimentation rates	Triggering Mechanism	Triggering expected to increase with increase in sedimentation rate. This information appeared for about 5 slides in the database.
Cause of Sedimentation	Triggering Mechanism	Sedimentation may be caused by glaciers, rivers, snow melt, etc. This information appeared for about 23 slides in the database.
Geographic Location	Latitude; Longitude	Enables slope failures to be correlated with rivers or other geologic settings delivering high sediment load
Date of Slope Failure	Date of Slope Failure	Allows correlation of slope failure with periods of highest sedimentation.

Table 4.2. Information Relevant to Sedimentation Processes as a Triggering Mechanism. *(continued)*

Type of Information	Database Field(s) Containing Information	Comments
Number of Past Slope Failures	Triggering Mechanism	Describes quantitatively or qualitatively the history of seismically-induced slope failures; This information was rarely provided in the literature
Water depths of the slope failure	Shallowest Water Depth; Deepest Water Depth	This information may correlate with sedimentation from a river or from lowered sea level during ancient times
Type of Slope Failure, e.g. debris flow or a slump	Slide Description	The type of failure may correlate with this trigger; This information was available for most sedimentation-triggered slides in the database.

4.2.3 GAS RELATED TRIGGERING MECHANISMS

Triggering mechanisms related to gas include disassociation of gas hydrates and free gas. Both of these gas related triggers are described in this section.

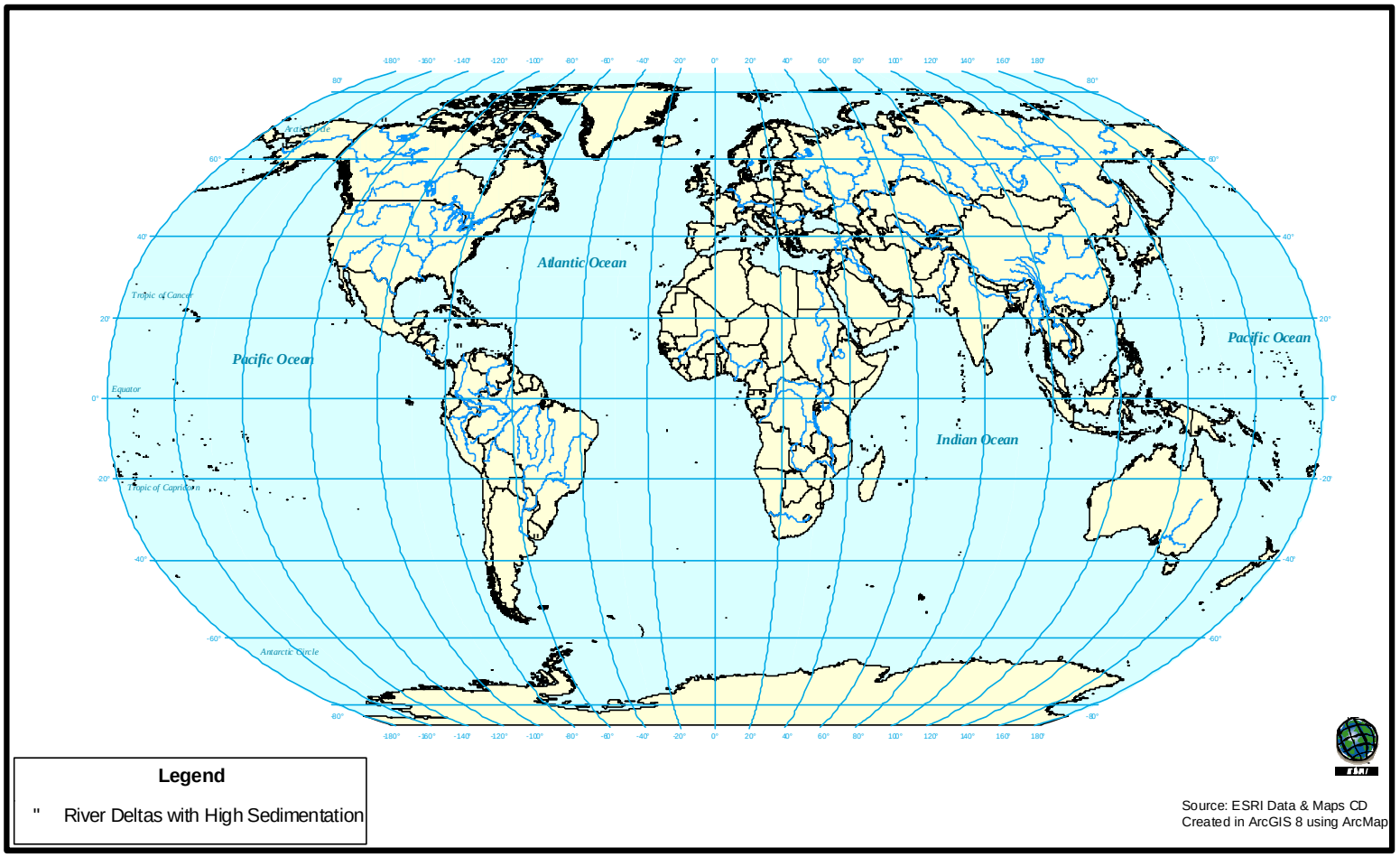

Figure 4.2. Worldwide distribution of river deltas that experience the largest sedimentation rates (sediment discharge data obtained from Milliman and Meade, 1983).

4.2.3.1 GAS HYDRATE DISASSOCIATION

Gas hydrates (clathrates) are ice-like substances consisting of natural gas and water that are stable under certain pressure and temperature conditions (Locat and Lee, 2002). If the pressure or temperature conditions change, gas hydrates may disassociate into natural gas, which can trigger slope failures. Kayen and Lee (1991) noted that the seafloor temperature and pressure in water depths exceeding about 300 to 500 m are adequate for the formation of hydrates. Gas hydrates are typically found within a range of depths below the seafloor known as a "hydrate stability field" where suitable pressure and temperature conditions exist. An ample supply of natural gas such as methane is also required for the formation of hydrates.

Gas hydrates form within seafloor subsoils when low temperature and moderate to high pressure conditions exist, as shown in Figure 4.3. The gas hydrate phase boundary, which is shown in Figure 4.3a, is the pressure-temperature boundary at which hydrate remains stable. The hydrate stability field is indicated in Figure 4.4a as the shaded region. In Figure 4.3b, the "base" for gas hydrates, which is the lowest depth below the seafloor at which gas hydrate can be present, is shown. According to Kayen and Lee (1991), gas hydrates cannot exist below the base because temperatures in the soil are too high for gas hydrates to form at the pressures that exist.

Kvenvolden and Lorenson (2000) mapped the global distribution of recovered and inferred gas hydrate occurrence. Their map is shown in Figure 4.4. Twenty locations where hydrate samples were recovered during drilling projects are shown in this figure. Another 79 locations are shown where hydrate occurrence was inferred based on geophysical, geochemical, and geological evidence. Examples of such evidence include well logs and bottom-simulating reflections, which are anomalous reflections from marine seismic records. The depths of bottom-simulating reflections range from about 100 to 1100 meters below the seafloor and correspond roughly to the base of the gas hydrate stability field, according to Kvenvolden et al. (1993).

Gas hydrates occur in only a small portion (less than 10 percent) of the area covered by oceans for two reasons: First, according to Kvenvolden et al. (1993), gas hydrates are restricted to water depths that exceed about 300 m which limits them to the relatively small area of the continental slope and rise along the margins of continents. Secondly, in these areas there are also substantial organic-rich sediments that provide an adequate source of methane.

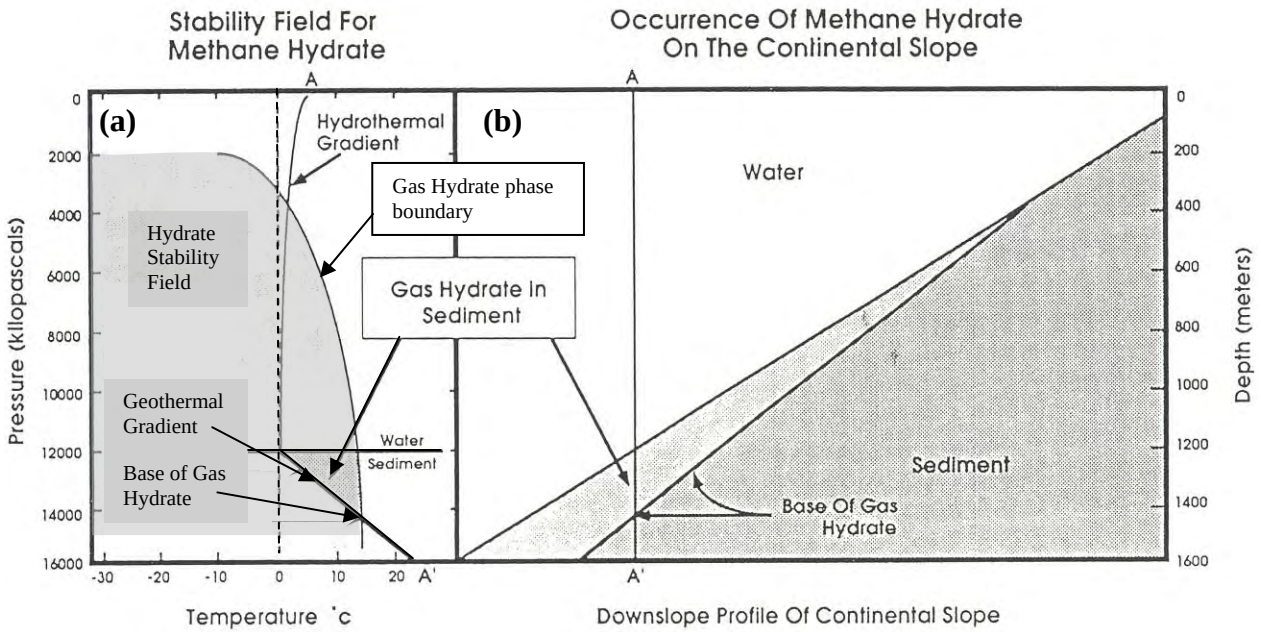

Figure 4.3. (a) A pressure-temperature phase diagram for gas hydrate. Shaded region is the hydrate stability field where gas hydrates can exist due to suitable temperature and pressure conditions. (b) A schematic of an offshore slope, indicating the zone in the subsurface where gas hydrate is present. Section A-A′, drawn through the slope, is shown in the phase diagram shown in (a) with the temperature and pressure conditions (modified from Kayen and Lee, 1991).

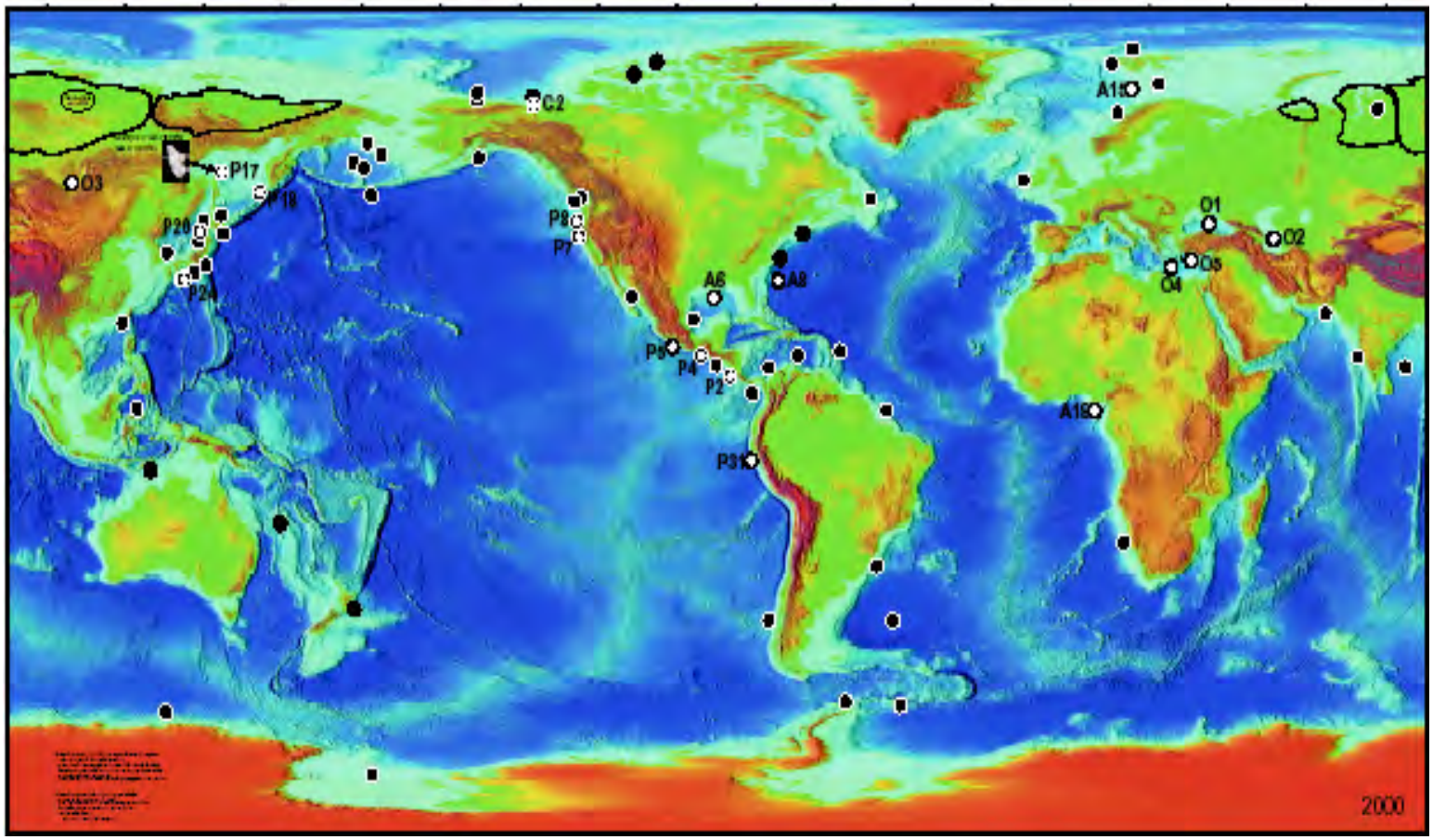

Figure 4.4. Worldwide distribution of gas hydrate occurrence. Black circles indicate inferred gas hydrate occurrence based on bottom-simulating reflections and well logs. White circles indicate recovered gas hydrate samples obtained from drilling projects (Kvenvolden and Lorenson, 2000).

Gas hydrates may be the direct trigger of a slope failure, or they may be associated with other triggering mechanisms. For example, according to Milkov (2000), gas hydrates typically form around the central part of mud volcanoes, which are described in Section 4.2.8.

Locat and Lee (2002) noted that a drop in sea level, which reduces the pressure acting on the seafloor, can cause gas hydrates to disassociate. When gas hydrates disassociate, the natural gas that is released as bubbles induces total stresses, σ, and excess pore air pressures, $\bar{u}_a$, and excess pore water pressures, $\bar{u}_w$, within the soil deposit, due to the low permeability of most marine soils. Thus, effective stresses in the sediment, σ', are reduced, i.e. $\sigma' = \sigma - u = \sigma - (\bar{u}_a + u_a + \bar{u}_w + u_w)$. The shear strength is also reduced, and slope failure occurs. A seafloor slope failure due to gas hydrate disassociation is shown in Figure 4.5.

Increased temperatures can also cause gas hydrate disassociation. For example, global warming or warming of the seafloor by changes in current flow patterns may cause gas hydrates to disassociate. These possibilities may be of more immediate interest than the next glacial age, which would be expected to be associated with a drop in sea level as discussed in Section 4.2.14.

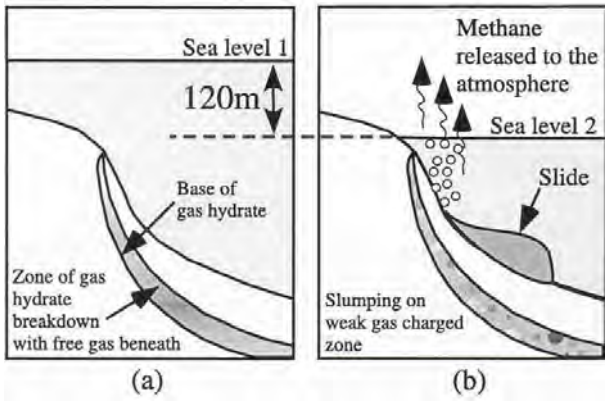

Figure 4.5: Gas Hydrates role on slope instability. (a) Time of high sea level with stable conditions for solid gas hydrate near seafloor. (b) Time of lower sea level where reduction in confining stresses causes a release of gas hydrates and a slope failure (Locat and Lee, 2002).

4.2.3.2 FREE GAS

Newton et al. (1980) noted that free gas that is present in the subsurface can accumulate in high permeability soils and form high pressure gas pockets. Newton et al. (1980) observed this in the Caspian Sea. These gas pressures may act as a loading mechanism on the soil, by adversely affecting the shear strength in the soil and/or increasing the driving forces on the soil. Information included in the database that may be pertinent to free gas and gas hydrates is summarized in Table 4.3.

Table 4.3. Information Relevant to Gas Related Triggering Mechanisms.

Type of Information	Database Field(s) Containing Information	Comments
Date of Slope Failure	Date of Slope Failure	Age can be correlated with times of low sea levels, which may cause gas hydrates to disassociate.
Geographic Location of Slope Failure	Latitude; Longitude	Enables slope failures to be mapped along with areas having gas hydrates
Water Depths of Slope Failure	Shallowest Water Depth; Deepest Water Depth	Gas hydrates exist only in certain water depths.
Physical Dimensions of Slope Failure	Area; Length; Width; Thickness	Dimensions of slope failure are expected to be correlated with dimensions of gas hydrate regions*.
Evidence of Gas	Triggering Mechanism; Slide Description	Required for gas hydrates to form; This information was provided for about 15 slides in the database.
Geomorphologic Description	Triggering Mechanism; Slide Description	Pockmarks observed on the seafloor have been linked to gas and, thus, provide indirect evidence of gas related slope failures; This information was provided for about 4 slides in the database.
Geophysical Description	Triggering Mechanism	Geophysical surveys have revealed anomalous seismic reflections and the presence of gas hydrates was inferred. This information provides indirect evidence of slope failure attributed to past gas hydrate disassociation.

* Kayen and Lee (1991, 1993) documented a slope failure triggered by gas hydrate disassociation where the thickness of the slope failure correlated with the base of the hydrate stability field, and the area of the failure correlated with the areal extent of the gas hydrate zone.

4.2.4 OCEAN WAVES

Ocean storm waves and internal waves can affect the stability of the seafloor. Storm waves primarily affect slope stability in relatively shallow water depths, less than about 150 to 300 m, which has been noted by Field and Edwards (1980) and Watkins and Kraft (1978). Large storm waves in these water depths induce increases and decreases in water pressures at the seafloor, producing a disturbing moment and increased shear stresses as illustrated in Figure 4.6 (Henkel, 1970). The increased shear stresses can cause failure if there is not sufficient shear strength to resist the stresses. Marsaglia and Klein (1983) noted that the location where large storm waves are expected depends in part on latitude as shown in Table 4.4.

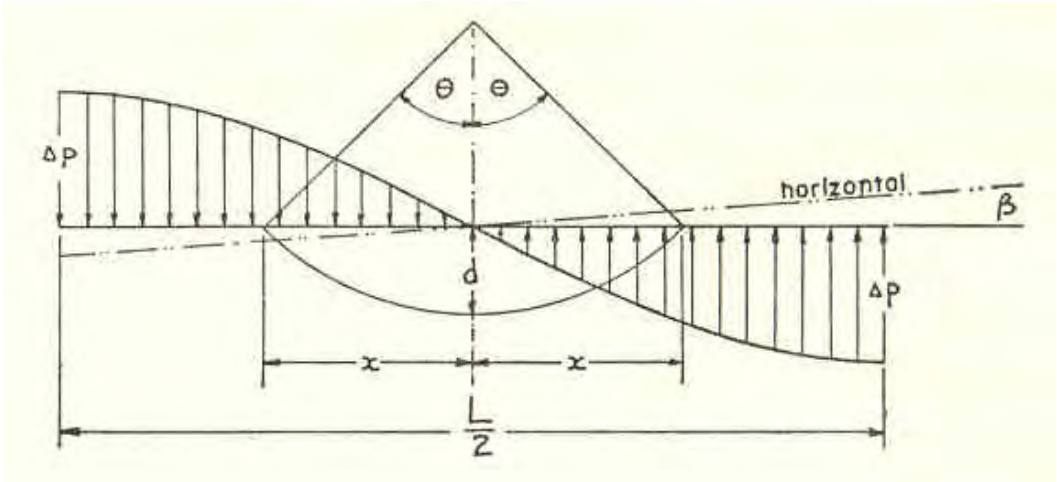

Figure 4.6. Illustration of hydrodynamic stresses imposed on the seafloor by ocean waves along with a rotational slip surface (Henkel, 1970).

Table 4.4. Frequency of storm systems according to latitude (Marsaglia and Klein, 1983).

Latitude Range (degrees)	Storm Systems
Above 45	Frequent winter storms, very rare hurricanes
25 – 45	Common winter storms, occasional* hurricanes
5 – 25	Occasional* winter storms, occasional* hurricanes
0 – 5	Very little storm activity of any kind

* "Occasional" denotes probability of occurrence. An occasional winter storms indicates one to two storms per year. An occasional hurricane occurs once in every 3,000 years. However, the Gulf of Mexico is a notable exception where hurricanes are much more frequent.

Another type of wave that can affect the stability of the seafloor is an internal wave. Internal waves are subsurface current waves. There is evidence of high velocities associated with internal waves, for example, offshore southern California as documented by Field and Edwards (1980). In deep water (greater than a few hundred meters), low-frequency internal waves can transport sediments along continental slopes and consequently, affect slope stability. However, according to Field and Edwards (1980), the quantity of sediment transported by internal waves is not known, and is expected to fluctuate over time. Information pertinent to ocean waves as a potential triggering mechanism for seafloor slides that was included in the database is shown in Table 4.5.

Table 4.5. Information in the Database Relevant to Ocean Waves as a Potential Triggering Mechanism.

Type of Information	Database Field(s) Containing Information	Comments
Oceanographic Conditions	Triggering Mechanism	Description of oceanographic conditions can relate to ocean waves as a trigger. Descriptions include "cyclic loading by storm waves" and "bottom water [soil] movements"; This information was provided for about 5 slides in the database.
Geographic Location of Slope Failure	Latitude; Longitude	Storm wave activity is related to latitude.
Water Depths of Slope Failure	Shallowest Water Depth; Deepest Water Depth	Ocean waves primarily affect seafloor stability in water depths less than about 150 to 300 m.

4.2.5 TIDAL EVENTS

Tides are natural, daily events that occur along the coastlines of oceans and seas. According to Terzaghi (1956), low tide events can trigger slope failure similar to the way that drawdown effects the upstream slope of an earth dam or the banks of a river after a flood. Considering undrained conditions, which typically apply to fine-grained soil deposits, a sudden lowering of water along a slope at the shoreline removes the resisting forces provided by the external water along the slope. The factor of safety may be reduced under these conditions by a factor of up to one half. With regard to coarse-grained soils, seepage forces can develop when the tide retreats and groundwater flows toward the ocean. Seepage

forces are additional driving forces in a slope, and can significantly reduce the factor of safety for static slope stability. Information pertinent to slope failures triggered by tidal events was included in the database when available and is summarized in Table 4.6.

Table 4.6. Information Relevant to Tidal Events as a Triggering Mechanism.

Type of Information	Database Field(s) Containing Information	Comments
Water Depths of Slope Failure	Shallowest Water Depth; Deepest Water Depth	Shallow water depths are required for failures triggered by recent tidal events.
Date of Slope Failure	Date of Slope Failure	Knowing age, in combination with soil type, could link slope failure to an ancient shoreline that was affected by this trigger.

4.2.6 HUMAN ACTIVITY

Although most seafloor slope failures are caused by natural events, several of the slope failures examined were caused by human activity, e.g. construction and dredging. The instances where failure was caused by human activity usually involved failures in reclaimed land where the soils were soft or loose. Such soils are prone to failure, especially if additional fill material is placed as overburden. Information pertinent to slope failures triggered by human activity was included in the database when available, and is summarized in Table 4.7.

Table 4.7. Information Relevant to Human Activity as a Triggering Mechanism.

Type of Information	Database Field Containing Information	Comments
Date of Slope Failure	Triggering Mechanism	Allows correlation of slope failure with times of human activity, e.g. construction.
Type of Damage	Slide Description	Damage reports from the literature of seafloor slope failures included shoreline facilities and loss of life. These reports are typically linked to slides attributed to human activity.
Type of human activity	Triggering Mechanism	Types of human activities included construction, fill placement, and dredging.

4.2.7 EROSION PROCESSES

Erosion occurs in the offshore environment due to water currents that travel along the seafloor. Erosion combines with sedimentation to change the seafloor slope by removing sediment from one area and depositing it in another area. Erosion depends on many of the same factors that affect sedimentation.

Erosion processes can produce slope failure by oversteepening a slope. Morgenstern (1967) has noted that oversteepening may be local, leading to progressive slope failure, or global.

Although no slope failures reported in the literature were definitively attributed to erosion, information pertinent to erosion processes was included in the database, and is summarized in Table 4.8.

Table 4.8. Information Pertinent to Erosion Processes as a Triggering Mechanism.

Type of Information	Database Field Containing Information	Comments
Description about oversteepening of slope	Triggering Mechanism	Oversteepening of slopes has been linked to erosion processes and slope failure. Information about oversteepening of slopes provides indirect evidence of erosion-triggered slides; This information was provided for most slides where erosion was inferred as a trigger.
Geomorphologic Description	Triggering Mechanism	Submarine canyons have been linked to erosion processes and slope failures and, thus, provide indirect evidence of erosion-induced failures; This information was rarely provided in the literature.

4.2.8 MAGMA VOLCANIC ACTIVITY

Magma volcanoes result from plate tectonics and magma in the underlying mantle. Magma volcanoes can form oceanic islands and seamounts (or guyots), and, similar to earthquakes, volcanoes continue to occur over time. Volcanoes also affect the stability of seafloor slopes. Locat and Lee (2002) described evidence of landslide activity on many volcanic islands due to the high pressures generated by magma and/or gas within the core of the volcanoes. Landsliding is a product of the growth of many volcanoes, and according to Hampton et al. (1996) landslides are believed to occur even after dormancy of the volcano. Potential

evidence of slope failure triggered by volcanic activity includes the presence of magma near the slip surface. Information pertinent to volcanic activity as a trigger for slope instability was included in the database, and is summarized in Table 4.9.

Table 4.9. Information Relevant to Magma Volcanic Activity as a Triggering Mechanism.

Type of Information	Database Field(s) Containing Information	Comments
Results of Magma Volcanoes, e.g. erupting lava	Triggering Mechanism	Rapid growth of volcanic islands, accumulation of volcanic sediments and erupting lava are a direct result of magma volcanoes and, thus, provide indirect evidence; This information was rarely provided in the literature on landslides.
Type of Slope Failure, e.g. debris avalanche, rock avalanche	Slide Description	Debris avalanches and rock avalanches are typically associated with slides triggered by magma volcanoes; This information was provided for most slides triggered by magma volcanic activity.
Water Depths of Slope Failure	Shallowest Water Depth; Deepest Water Depth	Volcano-induced slides have been observed to occur over a very large range of water depths, i.e. failures typically start above sea level and end at water depths greater than 2000 m.
Geographic Location	Latitude; Longitude	Information about geographic location enables slope failures to be correlated with locations of known magma volcanic activity
Physical Dimensions of Slope Failure	Area; Length; Volume	Volcano-induced slope failures have large physical dimensions; this information was provided for most of the slides triggered by magma volcanoes.

4.2.9 SALT DIAPIRISM

Salt diapirs can form in the subsurface of the seafloor due to cycles of flooding and evaporation over geologic time. The geologic history of the Gulf of Mexico provides a good illustration of the formation processes associated with salt diapirs. During the Jurassic period (about 213 to 144 million years ago), the Gulf of Mexico became isolated from the oceans, and a thick sequence of salt (Louann Salt) accumulated as water evaporated from the Gulf. During the Jurassic period, the Gulf was a smaller basin than today with a more restricted opening for water to enter. The Gulf would periodically flood, and then become completely dry, forming a salt plain. As sediments were later deposited in the basin by flood waters, the weight of the sediments caused the underlying salt to deform plastically. McGregor et al. (1993) noted that after the salt plains formed an enormous amount of sediment was deposited. In response to the weight of the overlying sediment, salt tended to rise to the surface, deforming plastically in the process. As this occurred, numerous fingers of salt, also known as diapirs, moved upward through the sediment. The term diapir is from the Greek word "diapeirein" which means "to pierce" according to O'Brien (1968).

Diapiric activity causes the seafloor to deform plastically over time. The growth of diapirs is proportional to the thickness of salt available for movement and the amount of overburden stresses. Overburden stresses depend on the density of the sediment and the rates of sediment accumulation and erosion. In

areas of diapiric activity, the slope of the seafloor is a result of a complex relationship between overburden sediment loading (sediment accumulation) and diapiric growth. Diapirs can create a bathymetric low by increasing slope angles, which can result in an intraslope basin. An example of such a basin created from adjacent diapiric uplifting is shown in Figure 4.7. Intraslope basins become locations where sediment can accumulate at higher rates than along higher angle, adjacent slopes. As a result, additional diapirs can then later form within this basin. Seafloor slope angles evolve over time, and the corresponding bathymetry becomes more complex. The complex bathymetry mapped along the Texas-Louisiana slope is shown in Figure 4.8, and the corresponding masses of salt and shale along the Texas-Louisiana slope are shown in Figure 4.9. Evidence of the effects of diapiric activity is shown in Figures 4.8 and 4.9.

Slope failure occurs due to diapiric activity. Soil slopes continue to fail by slumping due to the increasing slope angles in areas of diapiric activity. A slump that was mapped in a region of diapiric uplift is shown in Figure 4.7. The pressures induced by the underlying mobile salt may act as a loading mechanism on the overlying soil slope. If the soil is fine-grained and has a low permeability, excess pore water pressures would be generated. Thus, the shear strength and factor of safety for slope stability would be reduced.

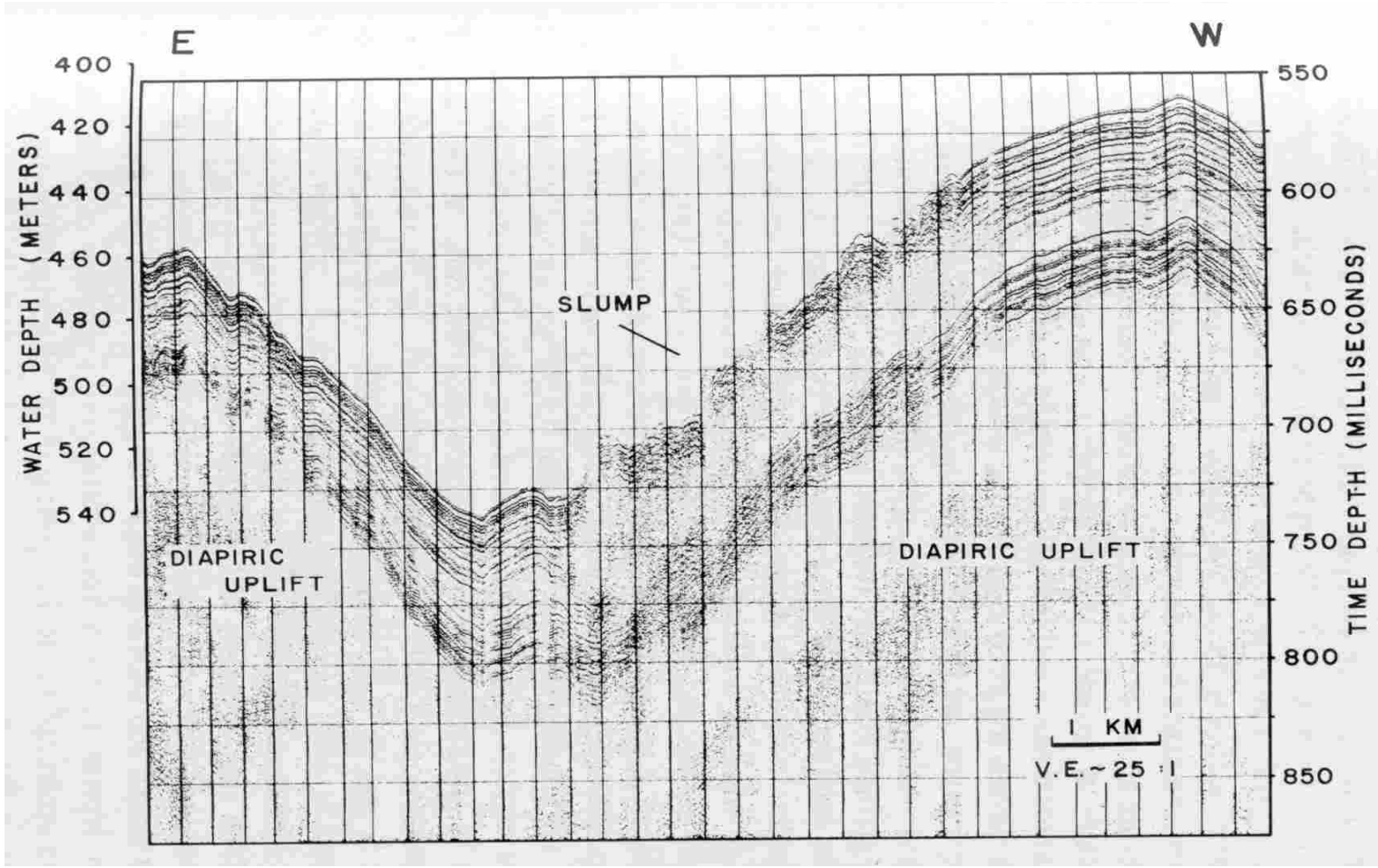

Figure 4.7: Seismic reflection profile across diapiric uplift in upper continental slope off Western Louisiana showing slumping (Martin and Bouma, 1982).

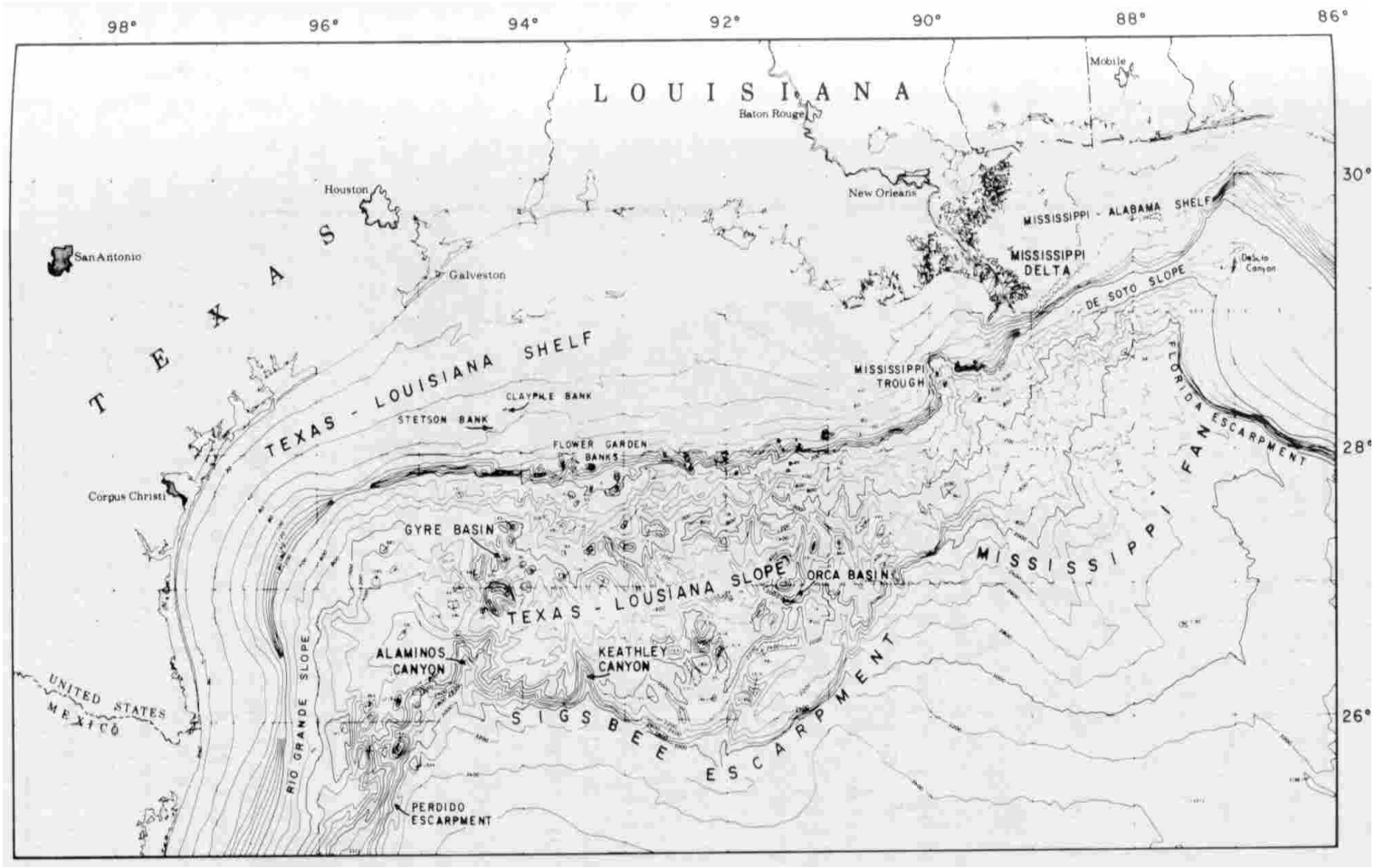

Figure 4.8: Northwestern Gulf of Mexico showing continental shelf and slope off Texas and Louisiana and bathymetry of seafloor (Martin, 1980).

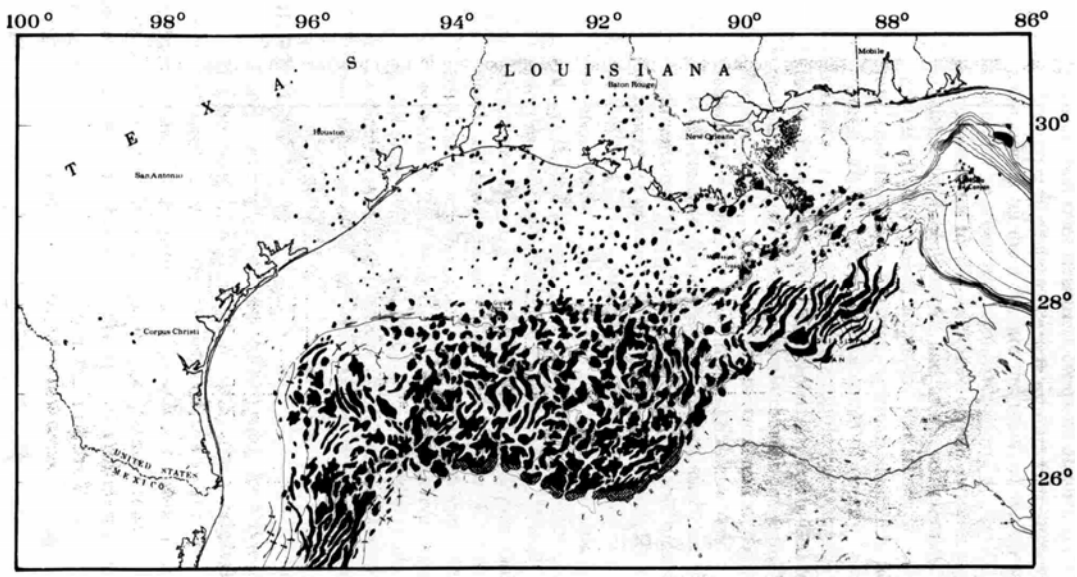

Figure 4.9: Location of structurally active thick masses of Jurassic salt and Tertiary shale (Martin and Bouma, 1982).

There are also areas other than the Gulf of Mexico where diapiric activity is evident. Diapiric activity has been reported along the South and mid-Atlantic U.S. continental slope, Norwegian-Greenland Sea, Beringian margin (Alaska), Gulf of Guinea (West Africa), northern Sinai-southern Israel continental slope, and the Sao Paulo Embayment (Brazil-Uruguay continental margin). Information pertinent to salt diapirism that was included in the database is summarized in Table 4.10.

Table 4.10. Information Relevant to Salt Diapirism as a Triggering Mechanism.

Type of Information	Database Field(s) Containing Information	Comments
Cause of Salt Diapirism	Triggering Mechanism	Causes of diapiric activity include rapid sedimentation and faulting.
Type of Slope Failure, e.g. or slump	Slide Description	Knowing the type of slope failure, e.g. slump, allows slump-type failures to be correlated with areas of salt diapirism. This information was provided for most diapir-triggered slides in the database.
Geographic Location	Latitude; Longitude	Enables slope failures to be correlated with areas of diapiric activity
Physical Dimensions of Slope Failure	Area; Length; Width	Knowing dimensions of slope failure allows "footprint" of slide to be correlated with areas of diapiric growth. This information was provided for most diapir-triggered slides in the database.
Date of Slope Failure	Date of Slope Failure	Age of slope failure can be correlated with periods of rapid sedimentation and diapirism.
Description about oversteepening of slope	Triggering Mechanism	Oversteepening of slopes has been linked to diapiric activity and slope failure and provides indirect evidence of diapiric-triggered slides. This information was frequently reported in the literature regarding slides triggered by diapiric activity.
Type of Soil, i.e. clay presence	Soil Type	Clay soils are associated with regions of diapiric activity.
Geophysical Description	Triggering Mechanism	Geophysical surveys have revealed diapirs in the subsurface in proximity to seafloor slumps.

4.2.10 MUD VOLCANIC ACTIVITY

Submarine mud volcanoes are raised features on the seafloor that erupt mud, gas and fluids such as water and oil. The possible ways mud volcanoes form are illustrated in Figure 4.10. The formation of mud volcanoes requires high gas or fluid pressures within the subsurface and fluid migration either along a compression fault (Figure 4.10c, d, e) or via a diapir that pierces the seafloor (Figure 4.10b). In addition to high pressures and fluid migration, high sedimentation rates (Section 4.2.2) are often required to promote diapiric growth so that mud volcanoes can occur. According to Newton et al. (1980), mud volcanoes can also be reactivated periodically due to gas pressures, faulting, diapirism, and sedimentation, which are all recurring triggering mechanisms.

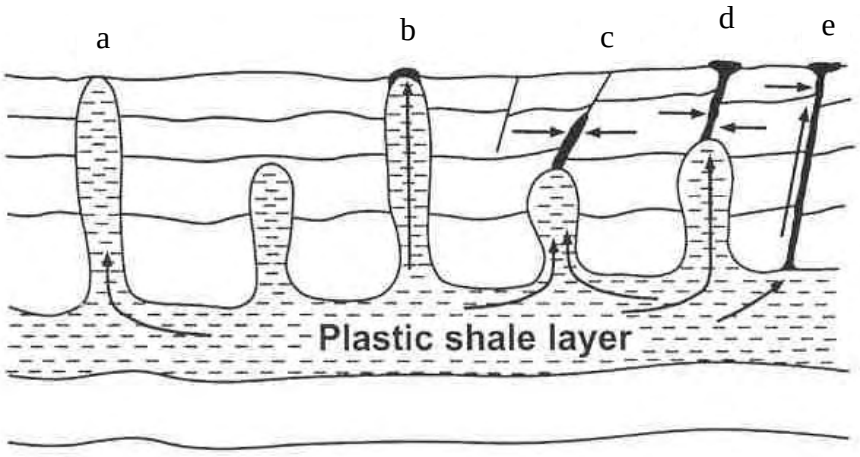

Figure 4.10. Possible ways mud volcanoes can form. (a) Diapir without a mud volcano; (b) Mud volcano formed on top of a seafloor-piercing diapir; (c) Fluid forming along a compression fault; (d, e) Mud volcanoes formed due to fluid transported up to the seafloor along compression faults. Arrows indicate path of fluid travel (Milkov, 2000).

Milkov (2000) described that evidence of submarine mud volcanoes comes from observations of subcircular elevated seafloor structures, seafloor-piercing diapirs, fluids ejected above seafloor structures, short-term mud islands, and gas bubbles at the water surface. Milkov (2000) mapped the worldwide locations of known and inferred mud volcanoes that are shown in Figure 4.11.

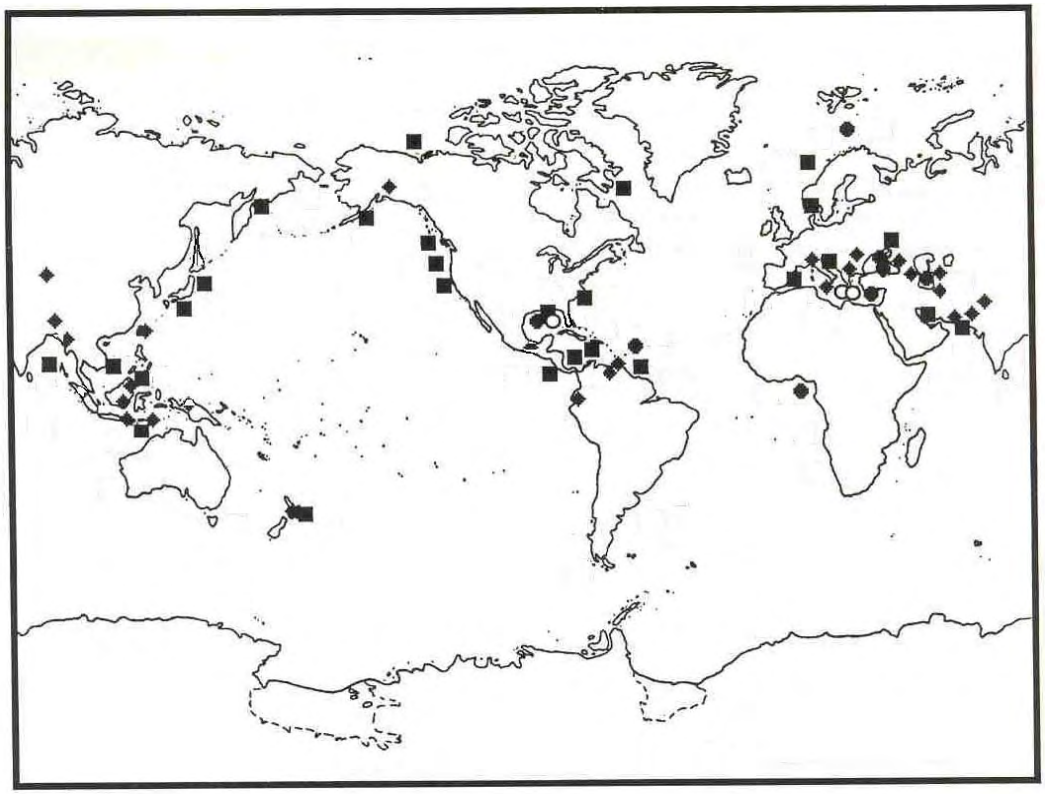

Figure 4.11. Worldwide location of known (diamonds and circles) and inferred (squares) submarine mud volcanoes (modified from Milkov, 2000).

Mud volcanoes can affect seafloor slope stability by oversteepening slopes and/or imposing additional driving stresses on the soil, which reduces the factor of safety for slope stability. Information pertinent to mud volcanoes as a

triggering mechanism that was included in the database is summarized in Table 4.11.

Table 4.11. Information Relevant to Mud Volcanoes as a Triggering Mechanism.

Type of Information	Database Field(s) Containing Information	Comments
Evidence of other triggering mechanisms	Triggering Mechanism	Rapid sedimentation, compression faulting, diapirs and high gas pressures have been linked to mud volcanoes and, thus, provide indirect evidence of mud volcanoes as a triggering mechanism.
Geographic Location	Latitude; Longitude	Geographic location of major mud volcanic activity is known, and by knowing the location of slope failures, correlations between slope failure and mud volcanic activity should be possible.

4.2.11 FLOOD EVENTS

Flood events often produce rapid sedimentation in coastal regions and river deltas (Section 4.2.2). High sedimentation rates caused by flooding may increase driving stresses on the seafloor sediments, leading to failure. Flood events may also erode river deltas, leading to turbidity currents, or low density landslides.

Only two landslides in the database were actually attributed to flood events. Information that may be relevant to flood events and was included in the database is summarized in Table 4.12.

Table 4.12. Information Pertinent to Flood Events as a Triggering Mechanism.

Type of Information	Database Field Containing Information	Comments
Cause of Flood Event	Slide Description	Snowmelt and glacier melt have been linked to flooding and, thus, may provide indirect evidence of slides triggered by flood events.
Erosion of river deltas	Triggering Mechanism	Erosion of river deltas (sand bars) has been linked to flooding and slope failure, i.e. turbidity current formation, and provides indirect evidence of seafloor slides attributed to flooding.

4.2.12 CREEP

Creep is generally defined as strain that develops under constant load. Creep is a time-dependent, slow process and can involve large masses of soil. Creep can occur under either drained or undrained loading conditions.

Although creep is poorly understood as a mechanism for seafloor slope movement, creep has been attributed to mass movement processes in the literature. For example, Field and Edwards (1980) mention sediment creep as a slope movement process offshore southern California. Information pertinent to creep that was included in the database is summarized in Table 4.13.

Table 4.13. Information Relevant to Creep as a Triggering Mechanism.

Type of Information	Database Field(s) Containing Information	Comments
Geomorphologic Description	Slide Description; Triggering Mechanism	Lack of a distinct failure scar has been linked to creep-induced sliding.
Geophysical Description	Triggering Mechanism	Geophysical surveys have revealed internal deformation within seafloor subsoils, which have been linked to creep.

4.2.13 TSUNAMIS

Tsunamis are large ocean waves triggered by seismic events or submarine landslides, rather than by ocean storm events. Tsunamis can affect slope stability in two ways: First, tsunamis can induce large hydrodynamic stresses on the seafloor. Secondly, tsunamis can also lower water levels as they approach shorelines, causing rapid drawdown (Wright and Rathje, in press). The rapid lowering of the water level without time for drainage of the soil reduces the resisting force of the body of water with no change in soil shear strength, thus reducing the factor of safety. There were no slope failures in the database directly caused by tsunamis. However, information relevant to tsunamis that was included in the database is summarized in Table 4.14.

Table 4.14. Information Pertinent to Tsunamis as a Triggering Mechanism.

Type of Information	Database Field(s) Containing Information	Comments
Linking tsunami and slope failures	Slide Description	Soils deposited by tsunamis have been linked to slope failures and, thus, provide indirect evidence of slope failures attributed to tsunamis.
Date of slope failure	Triggering Mechanism; Date of Slope Failure	Allows correlation of slope failure with periods of seismic activity, which often triggers the tsunami.

4.2.14 SEA-LEVEL FLUCTUATIONS

Sea level fluctuations are primarily caused by changes in global climate. Sea level fluctuations can cause slope failures in several ways. A fall in sea level reduces the overall pressure applied on the sea floor, which can result in disassociation of gas hydrates (Section 4.2.3) which can trigger slope failure. A fall in sea level can also promote an increase in sedimentation (Section 4.2.2), which can trigger landslides. McGuire (1992) noted that a rise in sea level can lead to erosion of the flanks of volcanic islands, which results in steepening of the slope and eventual slope failure. Sea level changes also affect the pressures acting on magma volcanoes, and McGuire (1992) noted that large changes in water pressure on the seafloor may increase magmatic activity and cause formation of volcanic islands (Section 4.2.8) and eventual landsliding.

Information pertinent to sea-level fluctuations as a potential triggering mechanism for seafloor slides was included in the database. Pertinent information is summarized in Table 4.15.

Table 4.15. Information Relevant to Sea-Level Fluctuations as a Triggering Mechanism.

Type of Information	Database Field Containing Information	Comments
Date of Slope Failure	Date of Slope Failure	Dates can be correlated with times of low or high sea level.
Other Triggers (see Comments)	Triggering Mechanism	Other triggering mechanisms such as gas hydrate disassociation, rapid sedimentation, erosion, and magmatic volcanoes could be linked to sea level fluctuations.

4.3 SUMMARY

Fourteen different triggering mechanisms are identified in the database. Most of these triggering mechanisms are complex in terms of how they form, when they occur, where they are located, and how they influence the stability of seafloor slopes. Consequently, information pertinent to triggering mechanisms often appears in several of the fields in the database, in addition to the field designated specifically for the triggering mechanism. The variety of information that is contained in the various fields of the database for each triggering mechanism has been summarized in a series of tables in this chapter.

CHAPTER 5

EVALUATION OF CHARACTERISTICS OF SLOPE FAILURES IN THE DATABASE

5.1 INTRODUCTION

Once the database was created, the data were examined to determine important characteristics of the failures and trends in the data. The following characteristics of the slopes failures were examined:

- geographic location
- date of the failure
- soil type
- triggering mechanism(s)
- distance of slide runout
- slide thickness
- slide area
- slide volume
- slope angle
- shallowest and deepest water depths for the slide mass

The database contained fields for each of these characteristics. Queries were then written to extract information from these fields. Information from the queries was then exported to Microsoft Excel® where plots of the information were made. In

addition, world maps were created showing the location of slope failures for selected triggering mechanisms. The maps were created using the geographic coordinate data in the database and the ArcGIS® software. The results of this effort are presented in this chapter.

5.2 CHARACTERISTICS OF THE DATA

A summary of the numbers of slope failures for which data were available for each particular field in the database is presented in Table 5.1. The percentage of the total number of events that contains each type of data is shown in the last column of this table.

Table 5.1. Summary of data available in the fields of the database (total of 534 seafloor slope failures).

Database Field	Number of Events with Data	Number of Events without Data	Percentage of Events with Data
Soil properties, e.g. γ, w, and Atterberg limits	70	464	13%
Soil type (clay, silt, sand, gravel, "volcanic material")	147	387	28%
Soil shear strength data (undrained)*	39	495	7%
Soil shear strength data (drained)*	15	519	3%
Maximum runout distance	434	100	81%
Total area influenced by slide	198	336	37%
Average thickness of slide	315	219	59%
Volume of failed slide mass	191	343	36%
Average angle of slope at failure	399	135	75%
Shallowest Water Depth	442	92	83%
Deepest Water Depth	408	126	76%
Slope Failure Description	514	20	96%
Triggering Mechanisms	366	168	69%
Date of Slope Failure	343	191	64%
Geographic Location (Latitude, Longitude)	524	10	98%
Scanned Image (up to 12 fields)	194	340	36%

* Shear strength data appear in the Soil Properties field and/or the Scanned Image field of the database.

The following items of information were available for at least half of the case histories:

- runout distance

- slide thickness
- average angle of slope at failure
- water depths of the failure
- slide description
- triggering mechanisms
- date of the slope failure
- geographic location

Some visual description of the slope failure was available for 194 of the slides. The visual description was captured in the Scanned Image field of the database. More than one scanned image was available for the majority of the 194 slides. The database contains over 520 images.

Although there is substantial information in the database, most slope failures lacked significant geotechnical information. Only about 10 percent of the case histories have information about the shear strength of the soil. Less than one-third of the slides have a description of the type of soil, and only about one-eighth of the slides have a description of the properties of the soil. The lack of geotechnical information can probably be attributed to the inherent cost and difficulties in obtaining this information. Site specific soil information is typically acquired and owned by oil companies, and is not published.

5.3 DATE OF SLOPE FAILURES

Information was available on the date of the slope failure for 343 of the 534 slide events in the database. The literature used to extract this information contained the date of failure in two forms. In 299 of the 343 cases, the date was reported in terms of a geologic epoch. In the remaining 44 cases, the date was reported as a specific date, and the failures generally occurred within the last few hundred years. Many of these latter 44 failures involve known earthquake events where the investigators report that the earthquake event was a possible trigger for the slope failure, i.e. the date of the slope failure was assumed to be the same as the date of the earthquake.

A plot of the frequency distribution of slope failures according to geologic epoch is shown in Figure 5.1. Figure 5.1 and the frequency distributions in the following sections of this chapter are plotted as bar charts where the slides in each interval represent a percentage of the total number of slides for which the appropriate data were available. The 44 failures that occurred (or were inferred to occur) within the last few hundred years were included in Figure 5.1 under the column for Holocene Epoch, i.e. within the last 10,000 years (10 ka). The Pleistocene Epoch is prior to the Holocene, and is between approximately 1.6 million years (1.6 Ma) and 10 ka before present. The Pliocene Epoch is before the Pleistocene, and is between approximately 5.3 Ma and 1.6 Ma before present. The case histories for which data are available are divided approximately equally

between the Holocene and Pleistocene Epochs. Only about 5 percent of the slope failures where date of failure data were available occurred in the Pliocene Epoch. Several of the triggering mechanisms such as rapid sedimentation, gas hydrate disassociation, and salt diapirism have been linked with times of low sea level which occurred during Holocene and late Pleistocene Epochs, and this may account for why most of the slope failures occurred during these epochs. Also, slides that occurred during these epochs are the most recent, so they are easier to detect than older slides.

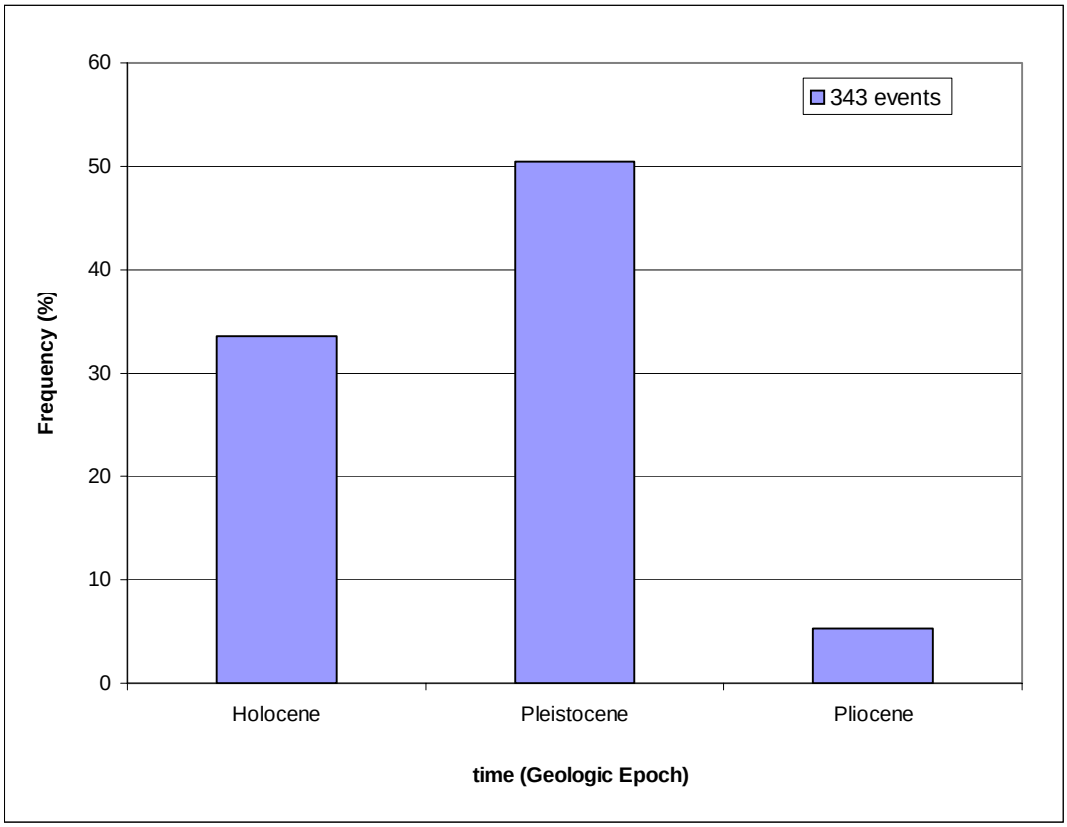

Figure 5.1. Frequency distribution of approximate date of slope failures.

The 44 slope failures with a specific date are plotted separately as a frequency distribution in Figure 5.2. Figure 5.2 indicates that most of the slides (about 80 percent) with specific dates occurred during the last 80 years, probably because of the technological advances made in detecting seafloor slides, e.g. in the fields of seismology and geophysics.

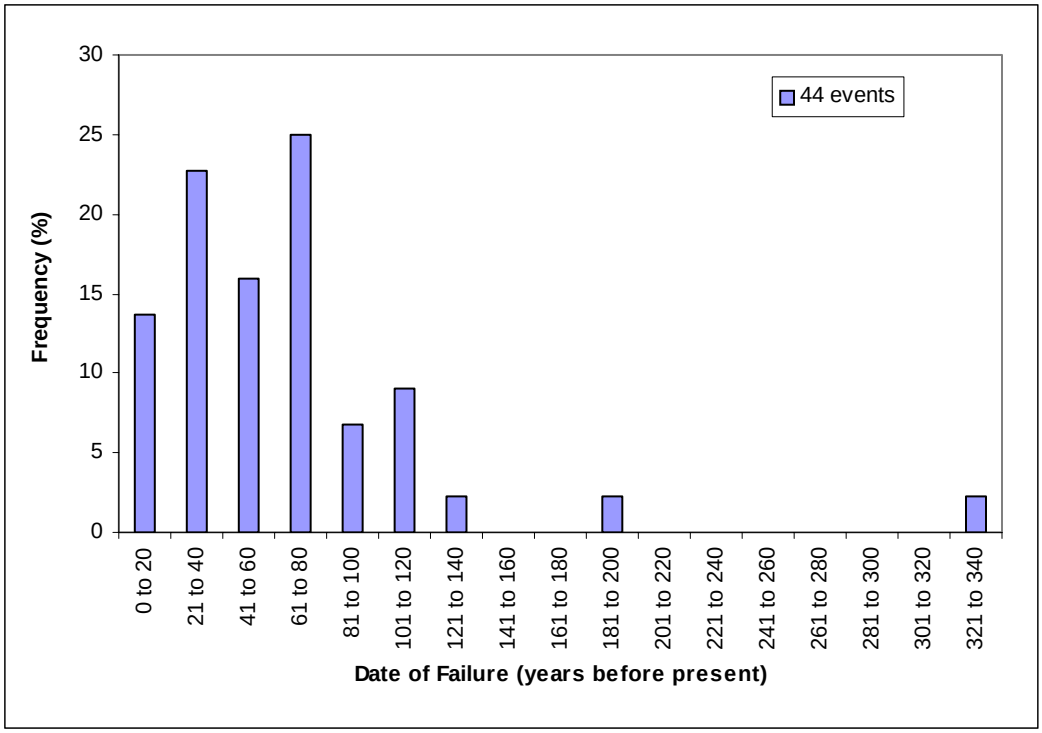

Figure 5.2. Frequency of slides for which a specific date of failure was available.

A frequency density distribution is shown in Figure 5.3 for slides that occurred or were inferred to occur on a specific date within the last 100 years and ancient slides that are believed to occur in geologic epochs. Figure 5.3 and the frequency density distributions presented in the following sections of this chapter

were plotted as bar charts where the percentage of the total number of events with information pertaining to that field (date, in this case) is divided by the range of that interval (number of years, in this case). A rate of failure (percent per year, in this case) is then plotted for frequency density distributions. As shown in Figure 5.3, the highest frequency of slope failures according to the reported literature has been in the last 100 years. It is important to note that Figure 5.3 indicates that some results from the database (date of slope failures, in this case) are biased, and do not necessarily indicate what has actually occurred in the marine environment over geologic time.

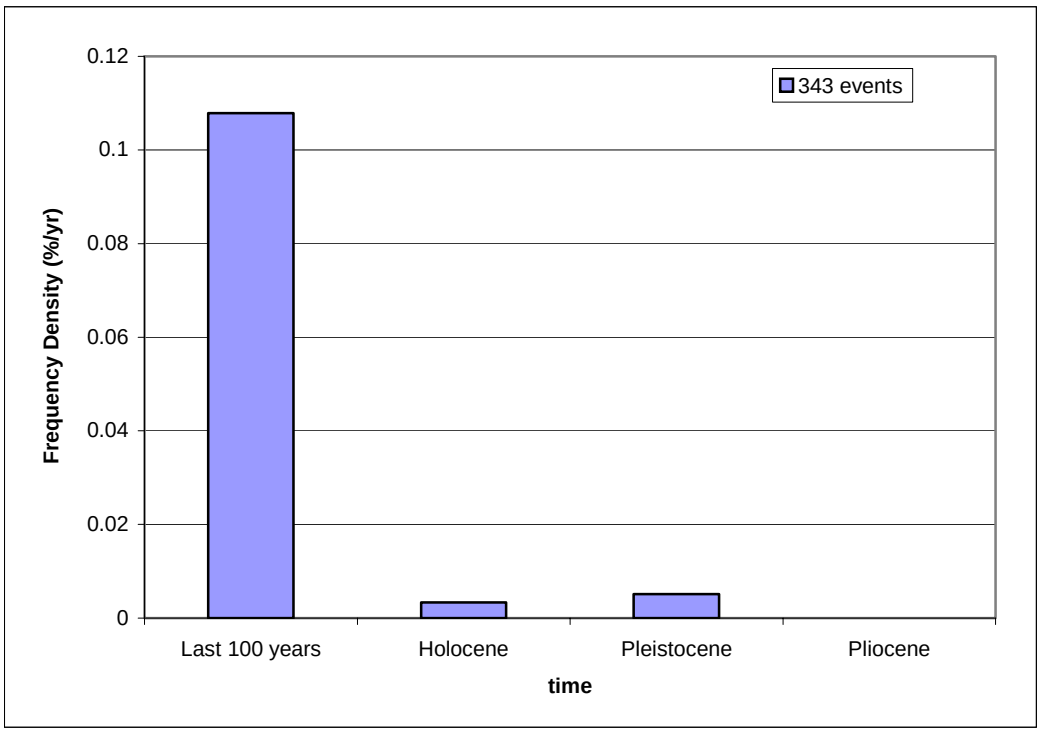

Figure 5.3. Frequency density distribution of approximate date of slope failures.

5.4 TRIGGERING MECHANISMS

Information on the triggering mechanism(s) causing the slope failure is available for 366 of the 534 landslides in the database. The following triggering mechanisms were reported in the literature:

- earthquakes and faulting
- sedimentation
- gas hydrate disassociation
- ocean storm waves
- tidal events
- human activity
- erosion
- magma volcanoes
- mud volcanoes
- salt diapirism
- flood events
- creep
- tsunamis
- sea-level fluctuations

The distribution of slope failures is plotted for each triggering mechanism in Figure 5.4. Figure 5.4 also includes 168 slope failures where no trigger was

reported. For most of the 366 slope failures where triggering mechanisms were reported, multiple triggers were cited, rather than a single, specific trigger because the trigger was uncertain. Often several triggers were listed because slides were caused by natural events that occurred in ancient times when the cause of failure (trigger) could only be inferred.

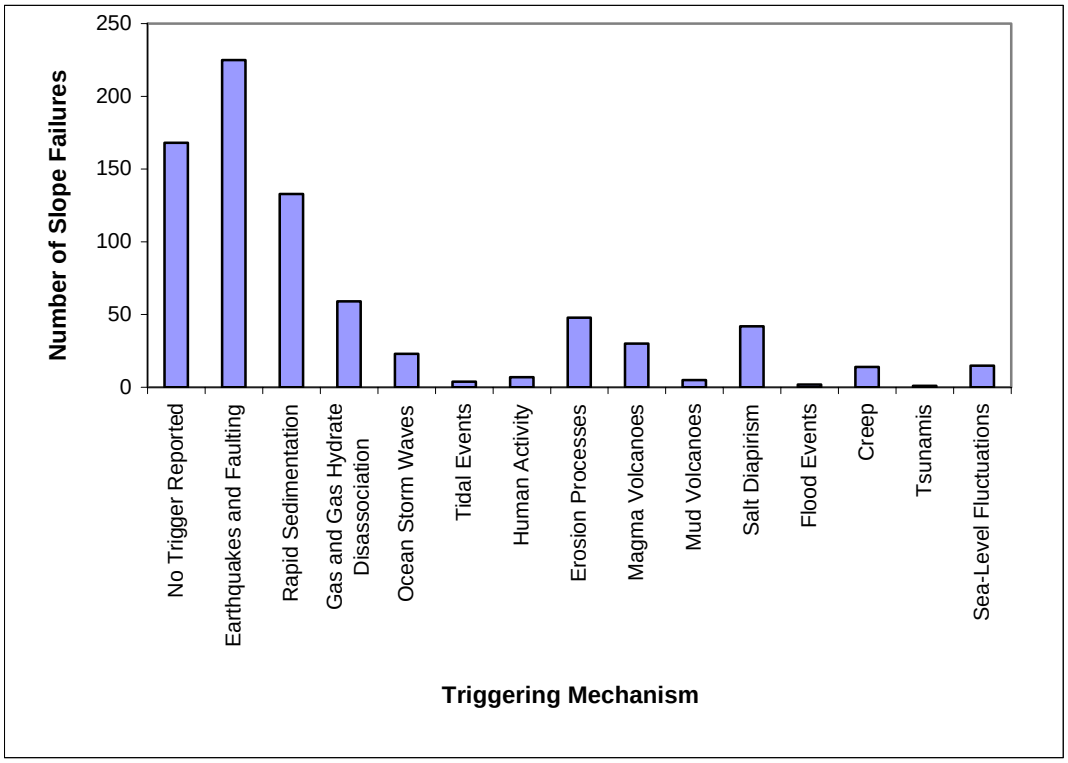

Figure 5.4. Distribution of triggering mechanisms.

The frequency distribution of triggering mechanisms is plotted in Figure 5.5. Over 40 percent of the slides where a trigger was reported were attributed to earthquake and faulting mechanisms, which represent the most common trigger reported and accounts for 225 of the slope failures.

The frequencies of slides that were inferred and were known to be triggered by earthquakes are summarized in Table 5.2. Earthquakes were inferred to be the trigger for 86 percent of the slides, but earthquakes were only known to be the trigger for 14 percent of the slides.

Table 5.2. Qualification of data regarding the 225 earthquake-triggered seafloor slope failures captured in the database.

Type of Information	Number of Events	Fraction of Total (%)
Inferred	193	86
Known	32	14

Geologic processes of sedimentation and erosion account for about 25 and 9 percent, respectively, of the potential triggers for slope failure (Figure 5.5). Ocean storm waves, tidal events, flood events and human activity were cited in less than 5 percent of the landslide events. Ocean storm waves, tidal events, flood events and human activity tend to influence slopes in water shallower than a few hundred meters. On a global scale, most ocean water is deeper than a few hundred meters, where ocean storm waves, tidal events, flood events and human activity (construction along shorelines) are not possible triggers.

Gas hydrate disassociation is cited as a possible trigger for about 11 percent of the landslides. This percentage may reflect the fact that gas hydrates are present in about 10 percent of the seafloor area covered by oceans (Chapter 4). Volcanic and diapiric activity are described as triggers in less than 10 percent

of the slope failures probably because these activities are not extensive in the marine environment. Less than 5 percent of the landslides were attributed to creep and tsunamis probably for two reasons: First, not much is known about creep as a mechanism for seafloor slope movement. Secondly, tsunamis do not occur frequently. Sea-level fluctuations are cited as a potential trigger for less than 5 percent of the landslides because investigators usually do not explicitly describe sea-level fluctuations as a trigger and, thus, sea-level fluctuations are not identified in the database.

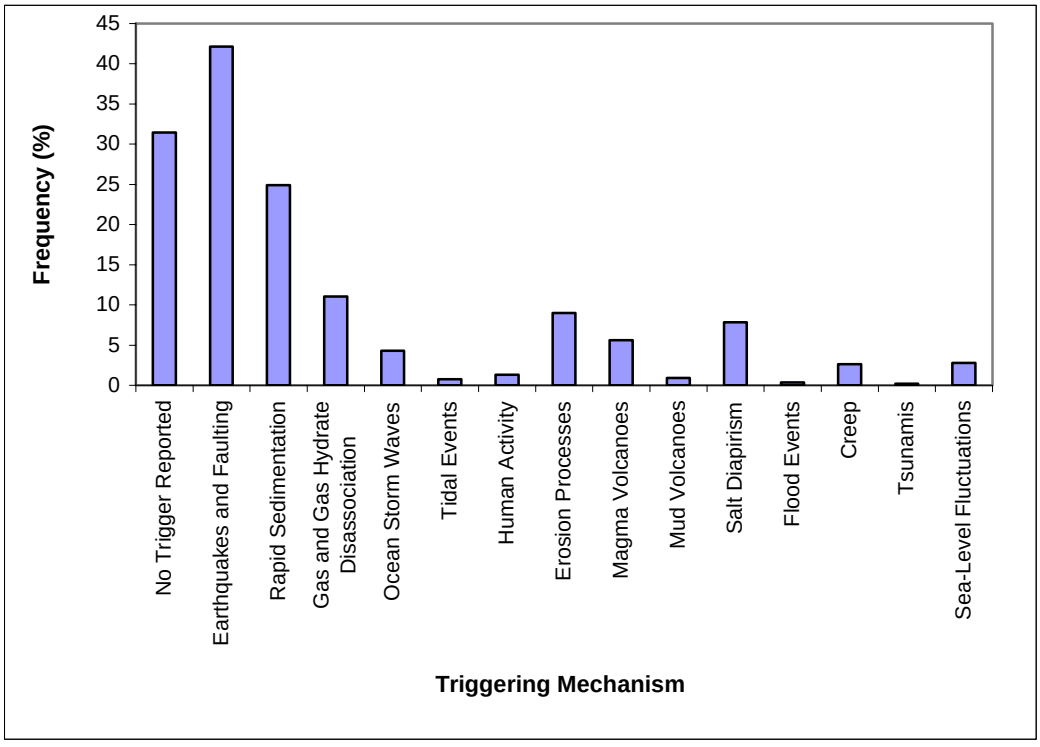

Figure 5.5. Frequency distribution of triggering mechanisms.

Among the triggering mechanisms reported above, the certainty with which the trigger is known in each case was classified as: certain, probable or potential, and completely uncertain. Case histories where no triggers were identified were considered to be completely uncertain. For each of the 534 slope failures, the certainty in the triggering mechanism(s) was classified according to these categories, and the results are summarized in Figure 5.6.

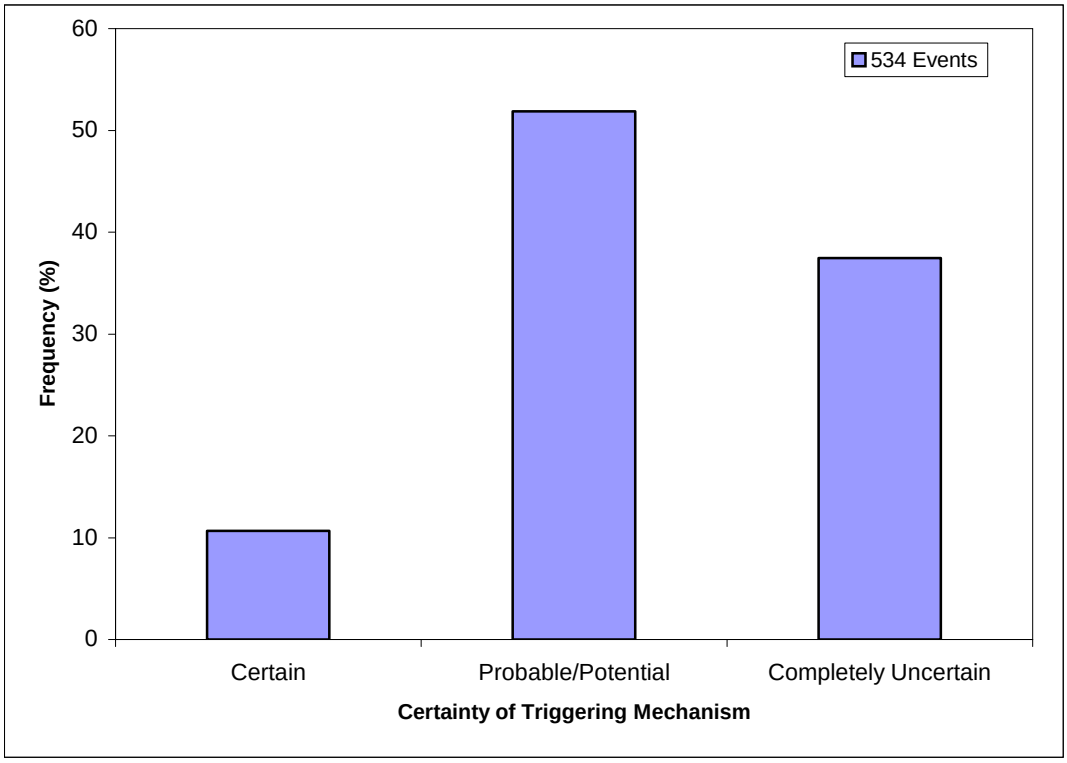

Figure 5.6. Certainty in the triggering mechanisms among the 534 slope failures.

Referring to Figure 5.6, only about 10 percent of the slope failures (57 slides) were attributed to a specific triggering event. The majority of the case histories (52 percent) cited several probable or potential triggering mechanisms, and the

cause of slope failure was completely uncertain for about 38 percent of the case histories.

Among the 57 slope failures where the triggering mechanism was certain, a breakdown of the triggering mechanism is summarized in Figure 5.7. The types of triggering mechanisms that are certain causes of slope failure are earthquakes, storm waves, tidal events, human activity, and magma volcanoes. Among these triggers, earthquakes were cited the most (about 24 percent) of cases of known triggers. Magma volcanoes were cited next for about 20 percent of the 57 slope failures. A few slope failures were attributed to storm waves, human activity, and tidal events.

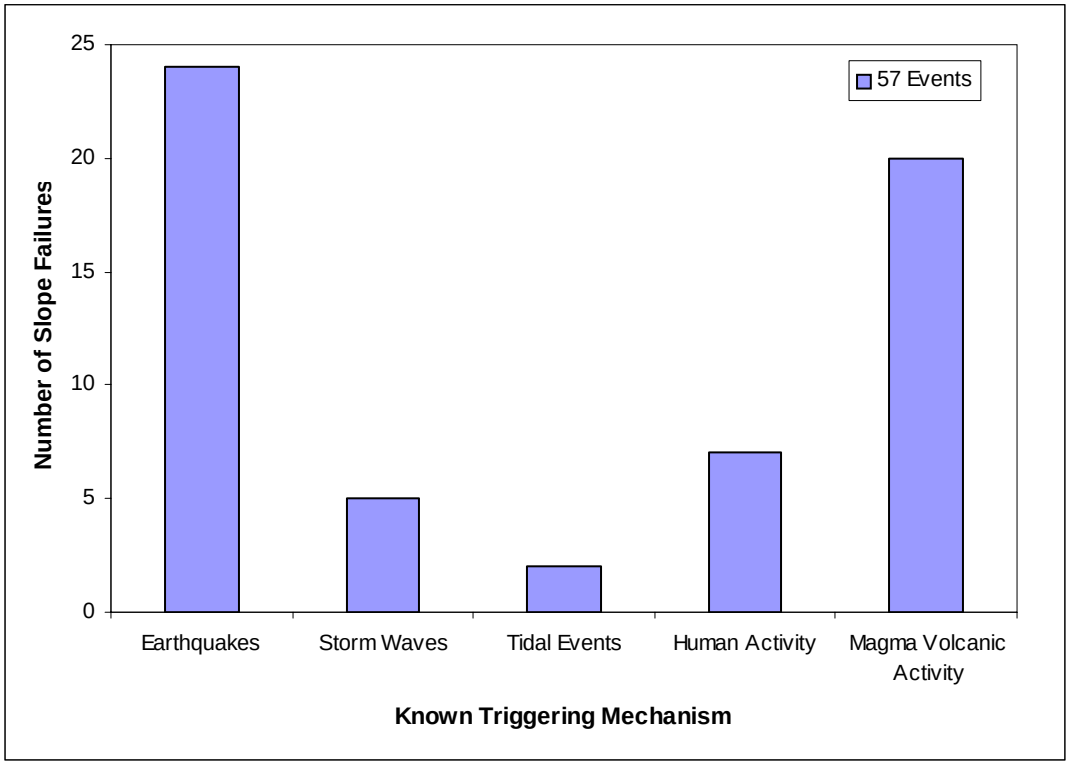

Figure 5.7. Types of triggering mechanisms among the 57 slides with known triggers.

For about 15 of the 57 slides where the trigger was certain, conclusive evidence was provided by an "eyewitness" account. Eyewitness accounts include observing damage to an offshore structure, a shoreline structure or communication cables buried in the seafloor. Linking the trigger such as a hurricane or an earthquake, with the slide that caused the damage is possible due to such eyewitness accounts.

5.5 GEOGRAPHIC LOCATION OF SLOPE FAILURES

The geographic location was reported for almost all of the seafloor slides (524 out of 534) in the database. Latitude and longitude were extracted from the literature and recorded in the database for each slope failure. The geographic coordinates were then exported from the database to Excel® to generate figures summarizing the results. The distributions of slope failures by latitude and by longitude are summarized in Figures 5.8 and 5.9, respectively.

The majority of the slope failures are located in the northern and western hemispheres of the world as shown in Figures 5.8 and 5.9, respectively. These locations are probably indicative of where offshore exploration has occurred and data have been published. Consequently, these locations are probably not indicative of the frequency of landslides worldwide.

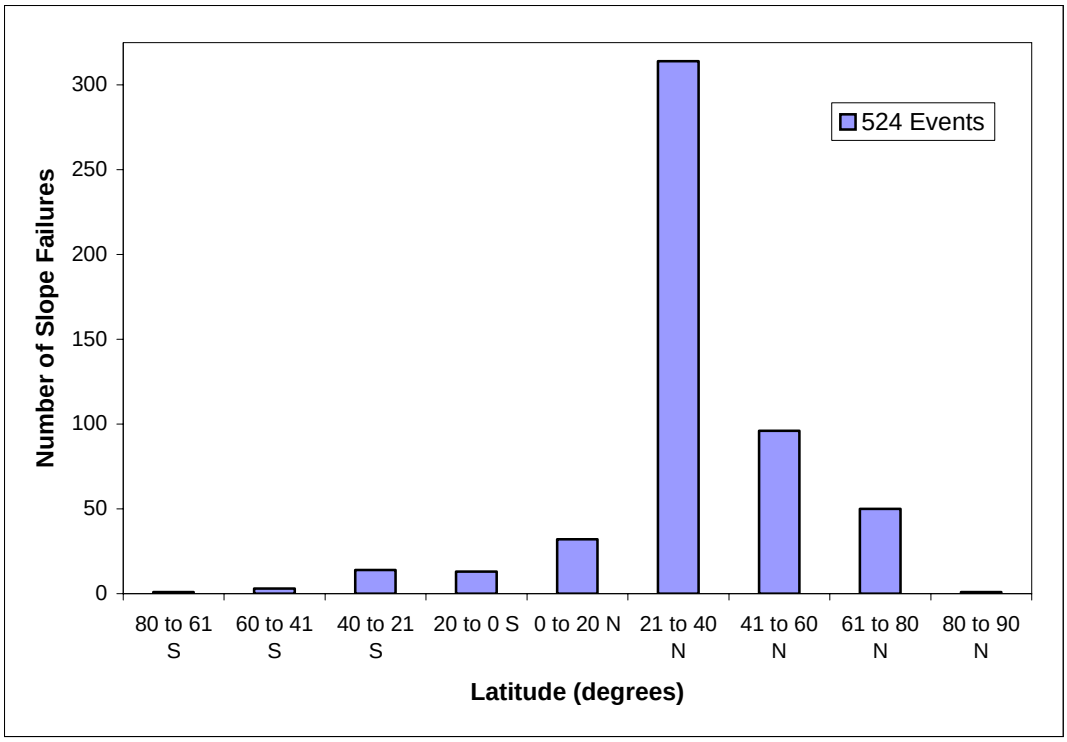

Figure 5.8. Distribution of submarine landslides by latitude.

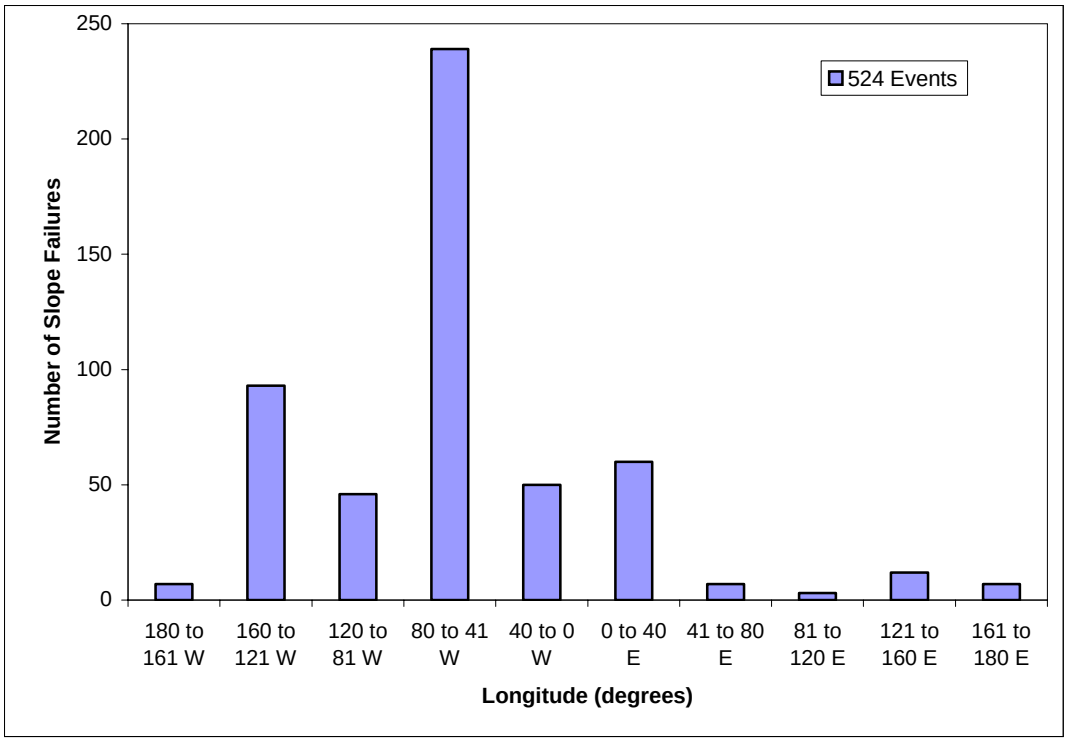

Figure 5.9. Distribution of submarine landslides by longitude.

Figure 5.10 is a world map that was generated using ArcMap (ArcGIS) software and the geographic coordinates of the slope failures. Most of the 524 slope failures shown are located in North American and European territories.

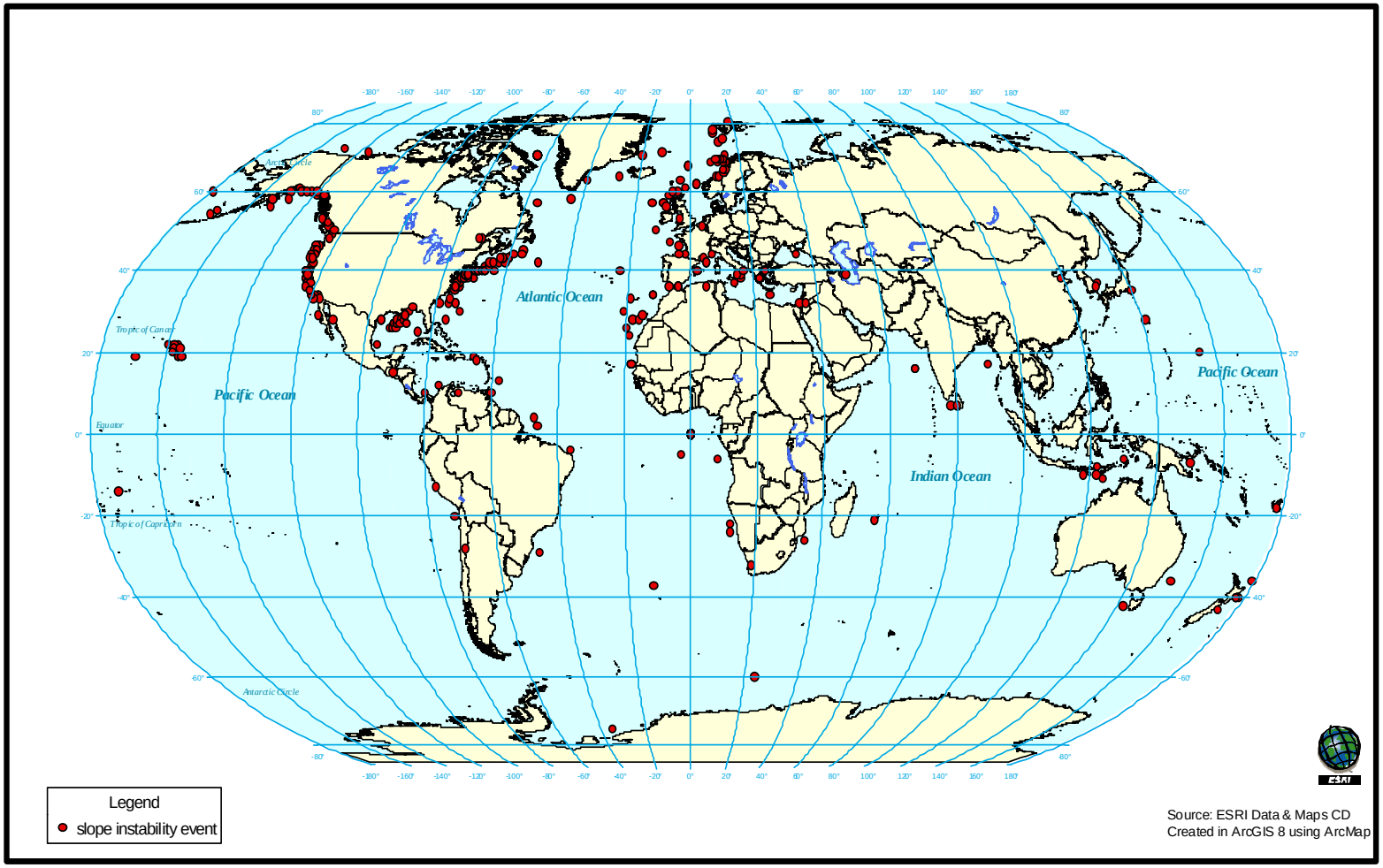

Figure 5.10. Worldwide distribution of published seafloor slope failures (524 of the 534 events).

5.6 GEOGRAPHIC DISTRIBUTION OF SLOPE FAILURES FOR VARIOUS TRIGGERING MECHANISMS

The geographic distribution of slope failures was evaluated for six triggering mechanisms: earthquakes and faulting, rapid sedimentation, gas hydrate disassociation, ocean storm waves, magma volcanoes, and mud volcanoes. World maps were created displaying the locations where triggering events are most likely and the locations of slope failures attributed to the triggers.

5.6.1 EARTHQUAKES AND FAULTING

A global seismic hazard map showing the locations of seafloor slides thought to be triggered by earthquakes and faulting is shown in Figure 5.11. Many areas of the world represent a high seismic hazard, and there is a good correlation between the seismic hazard and slides attributed to seismicity. Most of the slides shown on the map are in regions that have a moderate to high seismic hazard. For example, numerous slides believed to be triggered by earthquakes have occurred near the Pacific coast of the United States, the Gulf of Alaska, and the region of the Aleutian Islands. These areas all have moderate to high seismicity.

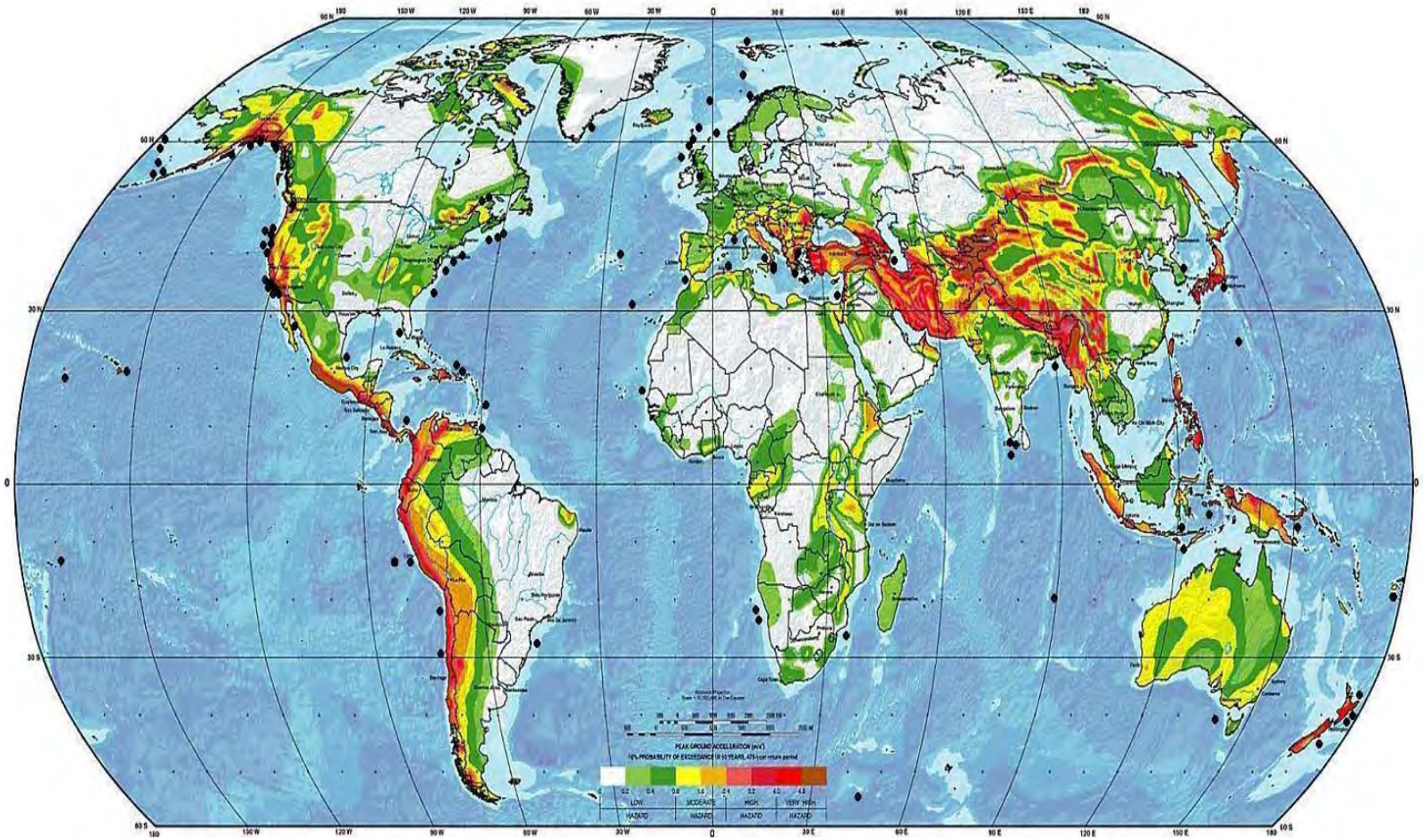

Figure 5.11. Global seismic hazard map (Giardini et al., 1999) with the worldwide distribution of published seafloor slope failures attributed to seismic loading (seafloor slides noted by black circles).

5.6.2 RAPID SEDIMENTATION

A world map showing the location of seafloor slides possibly triggered by rapid sedimentation processes and the twenty-two (22) deltas that receive the highest sediment load from rivers is presented in Figure 5.12. These rivers each deliver in excess of 40 million tons of sediment to the oceans per year (Chapter 4). The geographic coordinates of these 22 river deltas were determined from Milliman and Meade (1983). Slides believed to be triggered by sedimentation are located in proximity to deltas of the Mississippi, Amazon, Magdalena, Ganges, and Yellow (Huangho) Rivers. However, these deltas account for less than one-quarter of the deltas shown in Figure 5.12. There appears to be little correlation between major river deltas and slope failures thought to be triggered by sedimentation processes. Many of the slope failures thought to be triggered by sedimentation are located at high north latitudes such as Canada, Gulf of Alaska, Norwegian Sea, Greenland Sea and Barents Sea. High sedimentation rates have commonly been associated with ancient periods of glaciation when sea level was lower than current times. Therefore, slides triggered by high sedimentation may correlate better with ancient times rather than with current active river deltas.

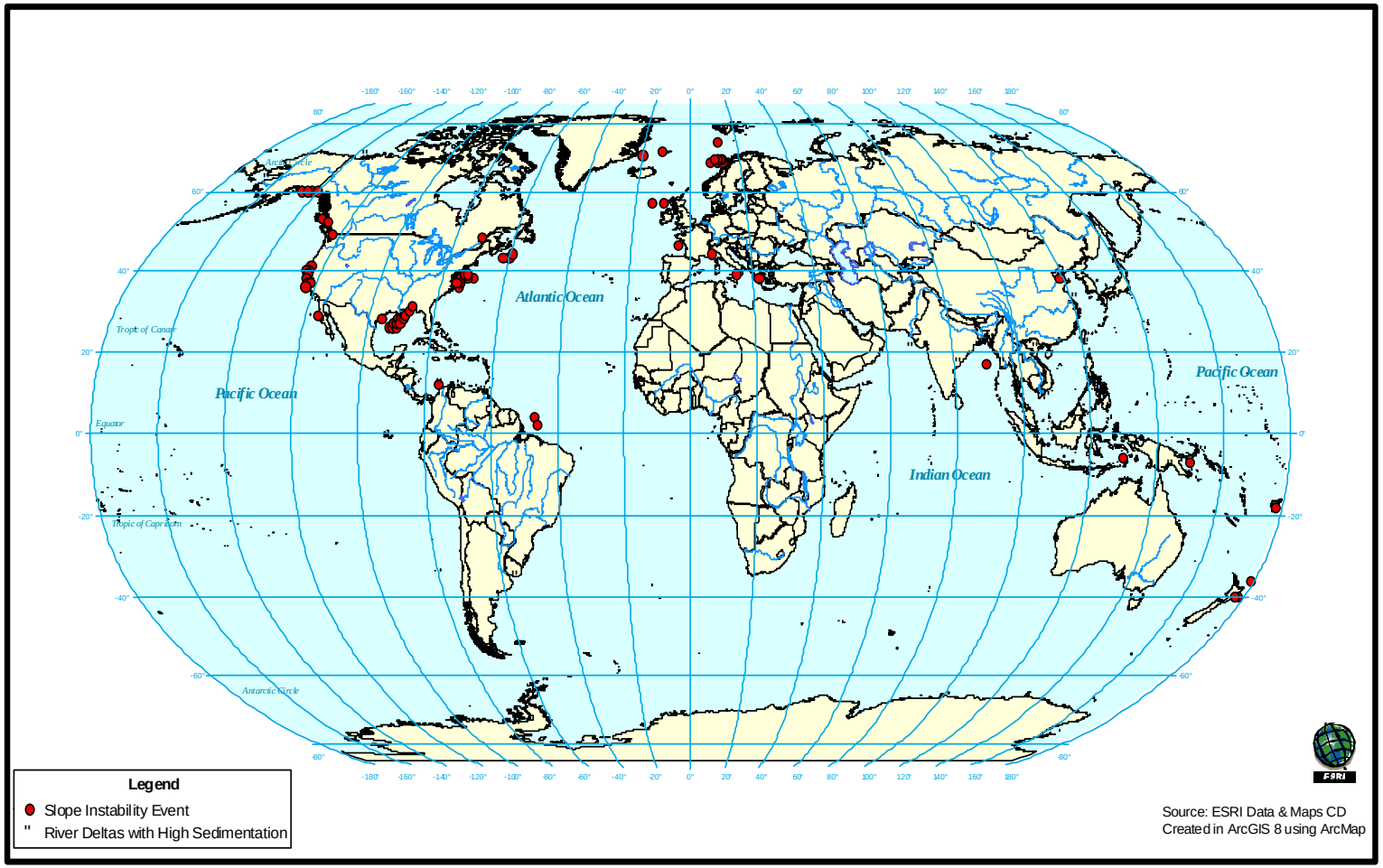

Figure 5.12. World map showing location of seafloor slope failures thought to be triggered by rapid sedimentation and location of 22 river deltas that receive highest sediment load.

5.6.3 DISASSOCIATION OF GAS HYDRATES

The areas where gas hydrates have been detected and where slope failures attributed to gas hydrate disassociation have occurred are presented in Figure 5.13. The geographic coordinates of areas where gas hydrates have been detected were determined from Kvenvolden and Lorenson (2000). In the northern latitudes, there is fairly good correlation shown in Figure 5.13 between areas where gas hydrates have been detected and slope failures attributed to gas hydrate disassociation. Areas where correlation exists include the Gulf of Mexico, offshore the southeast coast of the United States, offshore Oregon, the Beaufort Sea, the Norwegian/Barents Sea, the Caspian Sea, and the Black Sea.

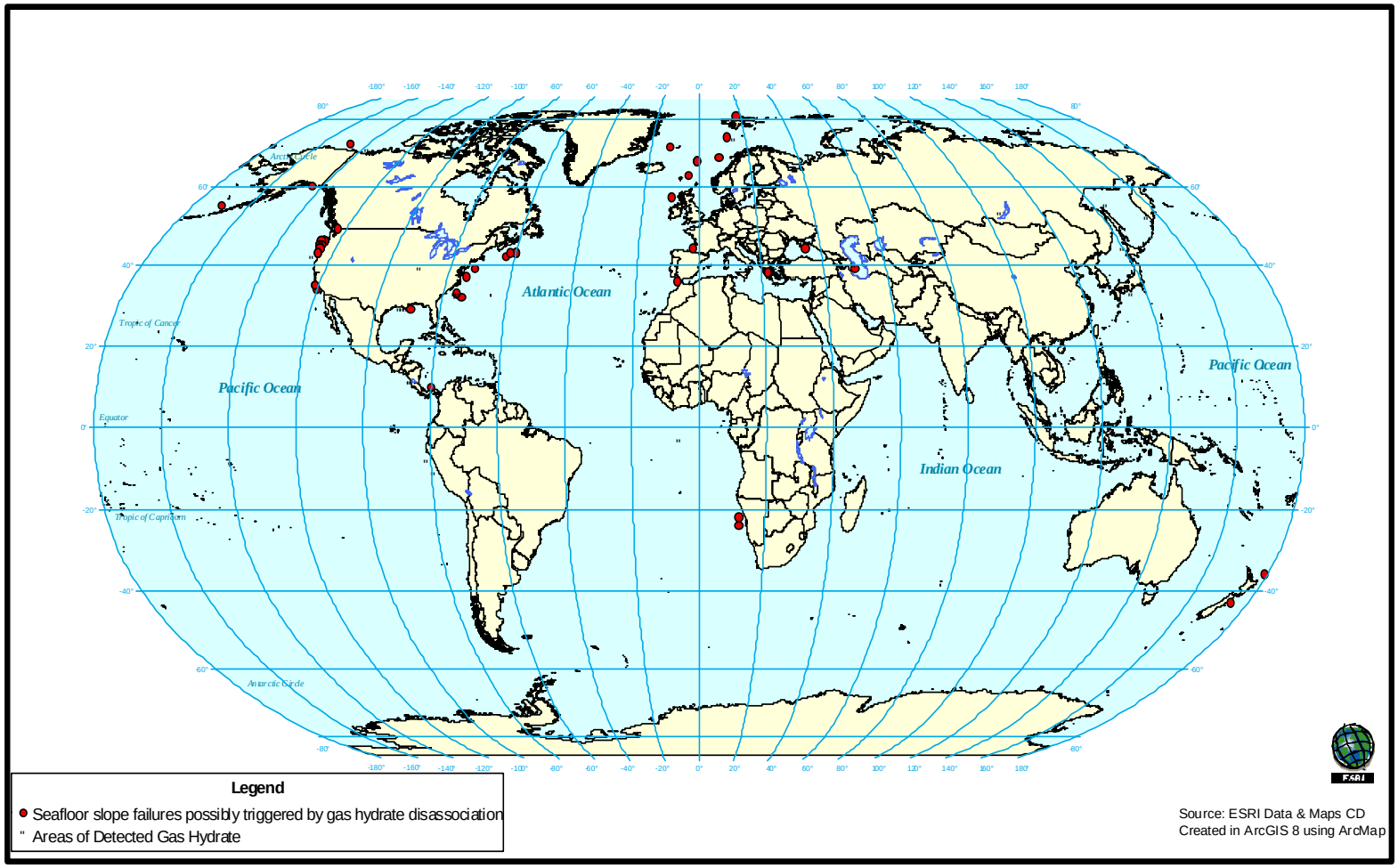

Figure 5.13. World map showing location of seafloor slope failures thought to be triggered by gas hydrate disassociation and location of detected gas hydrates.

5.6.4 OCEAN STORM WAVES

The distribution of seafloor slides associated with ocean wave loading is shown in Figure 5.14. About half of the slides shown are located above 40 degrees north latitude where winter storms are common, occurring multiple times per year. Also, three slides triggered by ocean storm waves are located in the Gulf of Mexico and along the Atlantic coast of North America where hurricane systems often travel (Marsaglia and Klein, 1983). Finally, there are several slides triggered by ocean waves in the Hawaiian Islands, where large waves occur due to tropical storms (Hayes, 1967). Overall, there is good correlation between regions of large ocean storm waves and slides attributed to storm waves.

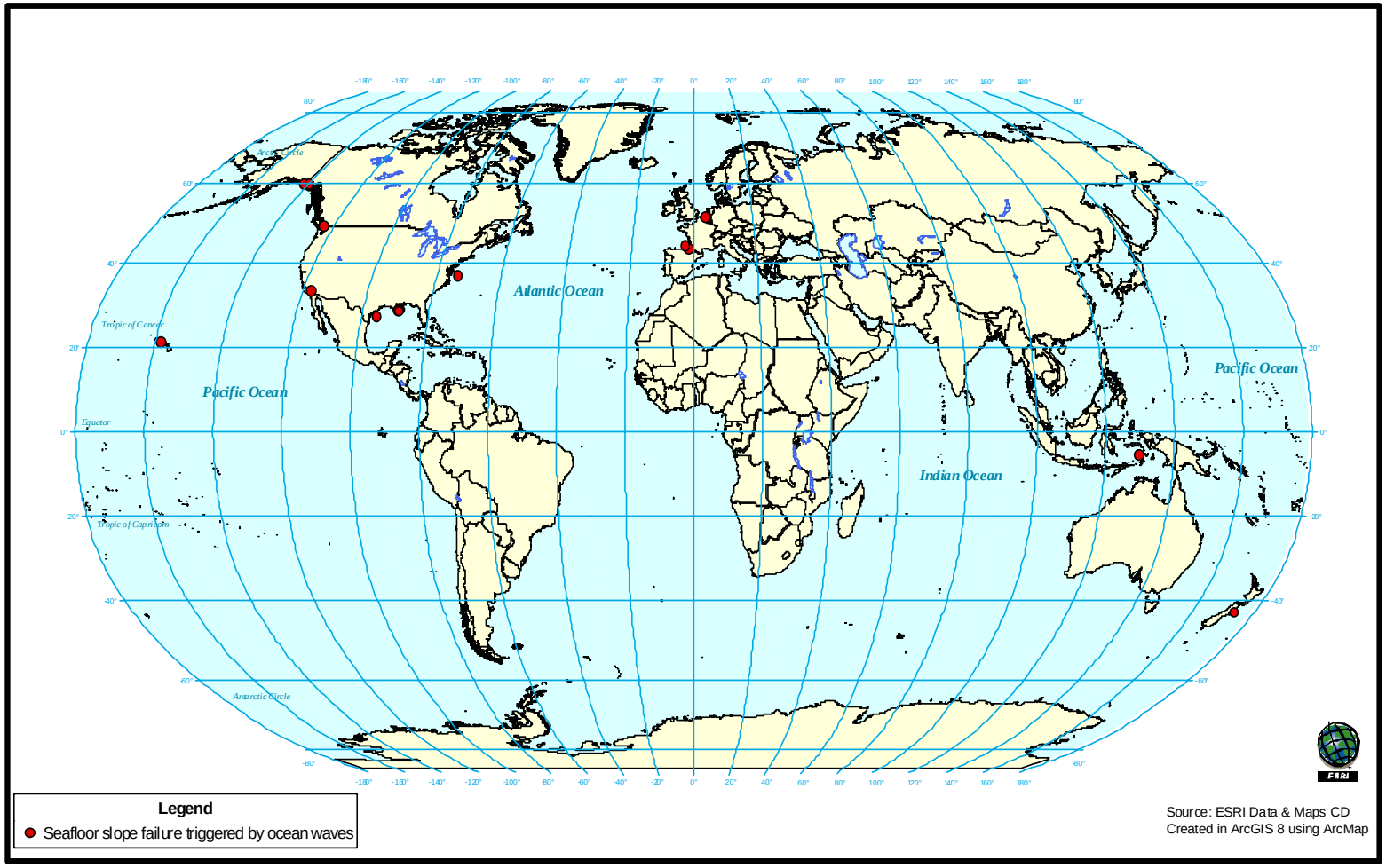

Figure 5.14. Distribution of seafloor slides attributed to ocean waves.

5.6.5 MAGMA VOLCANIC ACTIVITY

The distribution of seafloor slides associated with magma volcanic activity is shown in Figure 5.15. Slope failures are shown in the Hawaiian Islands, Canary Islands, Cape Verde Islands, Reunion Island, and Savaii Island; all of which are areas of magma volcanic activity. Thus, there is good correlation between magma volcanic activity and slides attributed to magma volcanic activity.

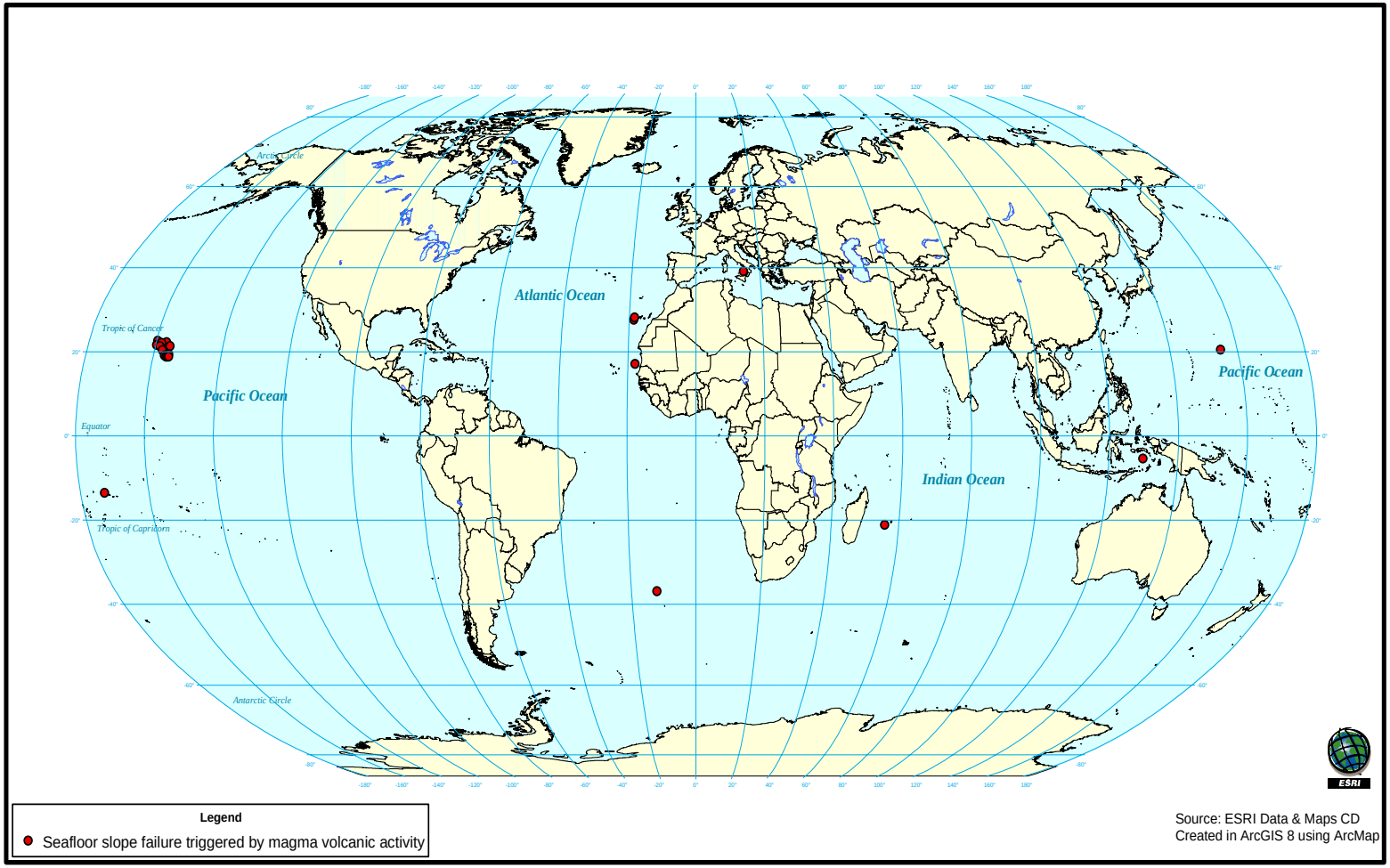

Figure 5.15. Distribution of published seafloor slope failures triggered by magma volcanic activity.

5.6.6 MUD VOLCANIC ACTIVITY

The worldwide distribution of known and inferred submarine mud volcanoes is shown with the approximate location of five seafloor slides believed to have been triggered by mud volcanic activity in Figure 5.16. All five seafloor slides are located in areas where the presence of mud volcanoes is either known or inferred. Thus, there is good correlation between mud volcanic activity and slides believed to be triggered by mud volcanoes.

5.6.7 CONCLUSION

The geographic distribution of slope failures for earthquakes and faulting, rapid sedimentation, gas hydrate disassociation, ocean storm waves, magma volcanoes and mud volcanoes correlate with the locations where these triggering mechanisms occur. Based on the maps that are shown in this section, these reported triggers seem reasonable.

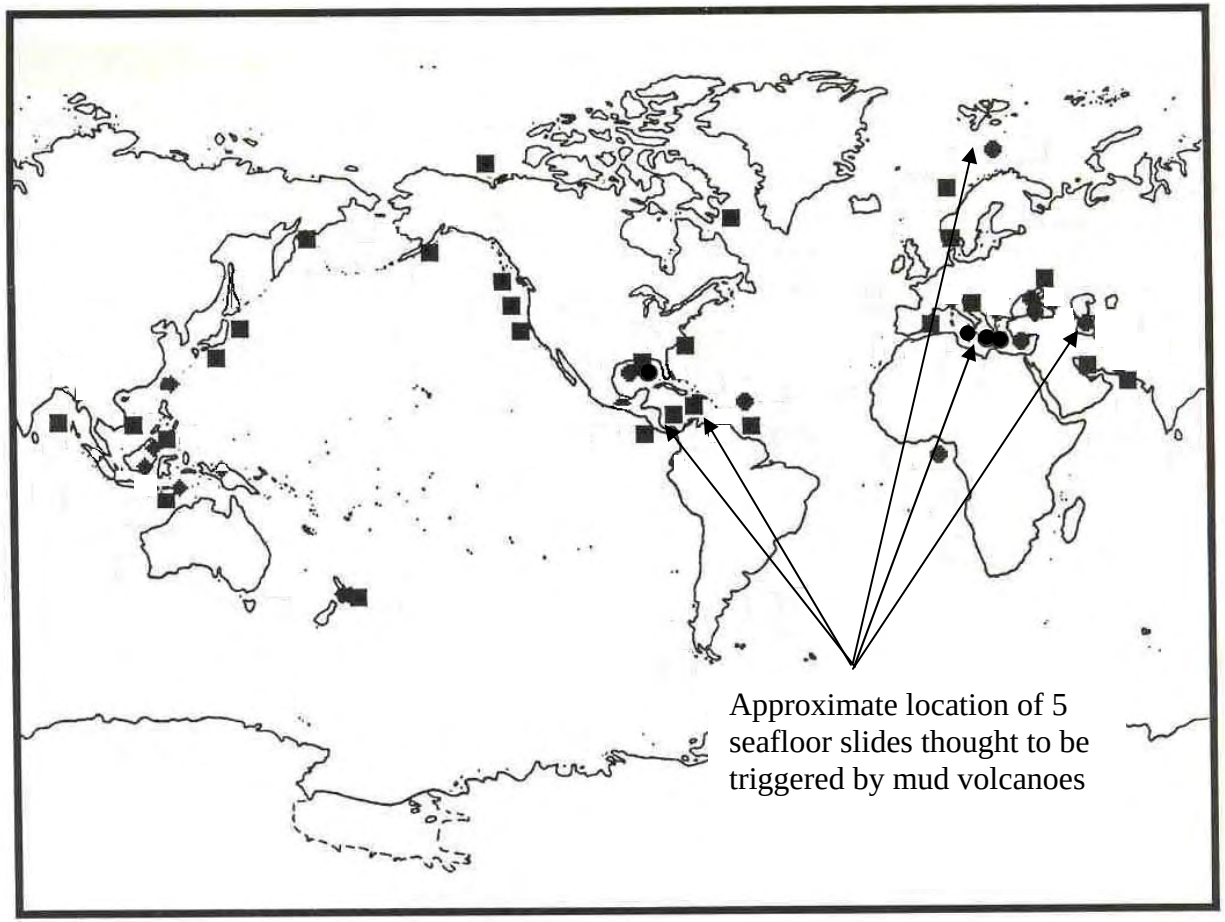

Figure 5.16. Worldwide distribution of known (circles) and inferred (squares) submarine mud volcanoes (modified from Milkov, 2000) with location of 5 seafloor slides thought to be triggered by mud volcanic activity.

5.7 SLOPE ANGLE

The average angle of the slope at failure was recorded for 399 of the 534 seafloor slope failures in the database. A frequency density distribution for the average slope angle at failure is shown in Figure 5.17. The 3 to 4 degree slope angle interval has the highest frequency of slope failures. The median slope angle for the 399 slides is 4.0 degrees, and the mean is 5.8 degrees.

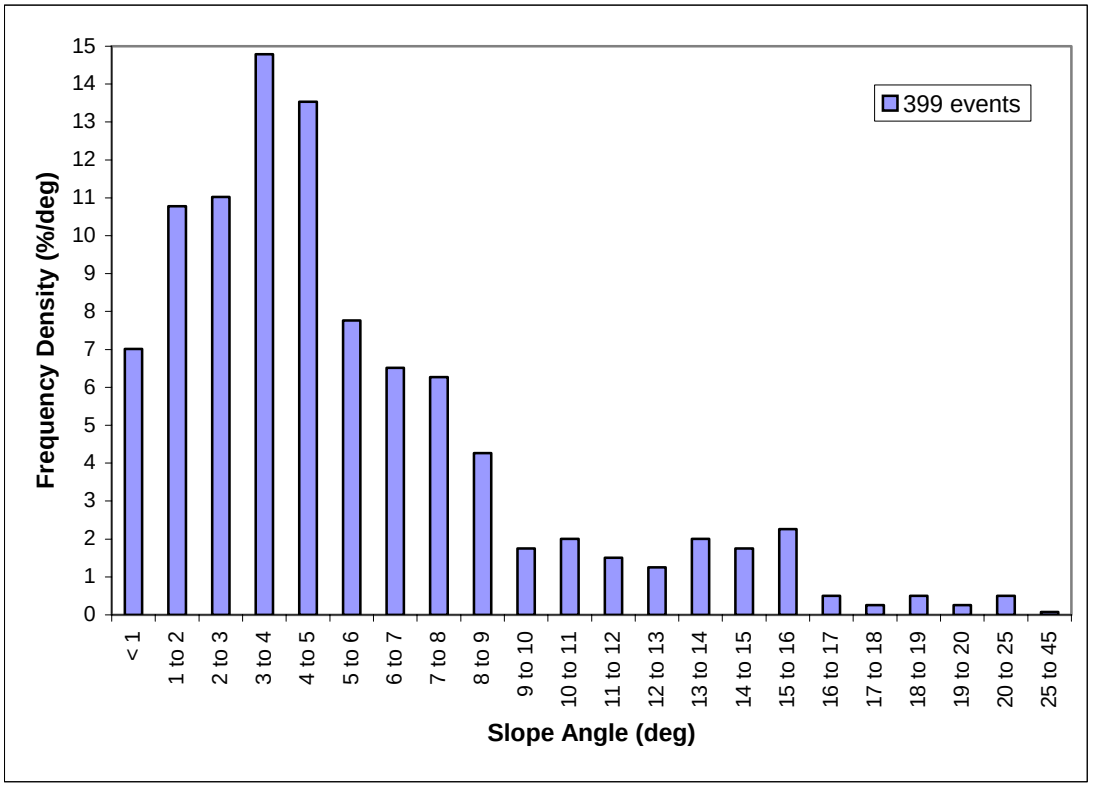

Figure 5.17. Frequency density distribution of the average angle of the slope at failure for the seafloor slope failures.

A cumulative frequency distribution for the average slope angle at failure is shown in Figure 5.18. Figure 5.18 and other cumulative frequency

distributions presented in the following sections of this chapter are line charts where the percentage of the total number of slides for which the appropriate data were available is summed consecutively. About 85 percent of the 399 slope failures (339 slides) occurred on slopes flatter than about 10 degrees (Figure 5.18). Such flat slope angles (less than 10 degrees) are much less than for most subaerial slope failures. Slope stability analyses are presented in Chapter 6 to address possible reasons why seafloor slides occur on gentle inclinations.

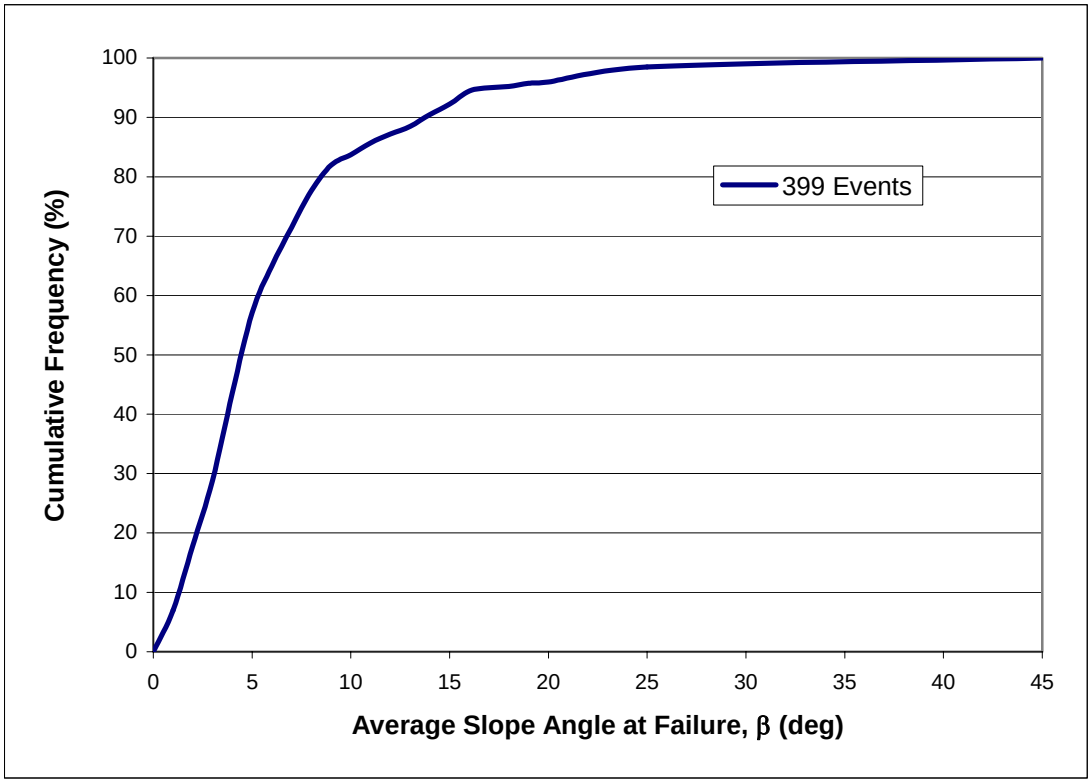

Figure 5.18. Cumulative frequency distribution of the average angle of the slope at failure for the seafloor slope failures.

5.8 DIMENSIONS OF SLOPE FAILURES

The dimensions of the slope failures were characterized by information in five fields in the database: area, length, width, thickness, and volume. This information is examined further in this section.

5.8.1 Total Area Influenced by Slope Failure

Information was available on the total area influenced by the slope failure for 198 of the 534 seafloor slides in the database. A cumulative frequency distribution of the area of the slope failures is presented in Figure 5.19. Because of the large range in area (over five orders of magnitude), a logarithmic scale is used to plot the area. The median area (50^{th} percentile) for the 198 events is approximately 200 km^2, and the mean area is approximately 3,600 km^2. The data shown in Figure 5.19 show that the area of seafloor slides can be very large, on the order of hundreds to thousands of square kilometers.

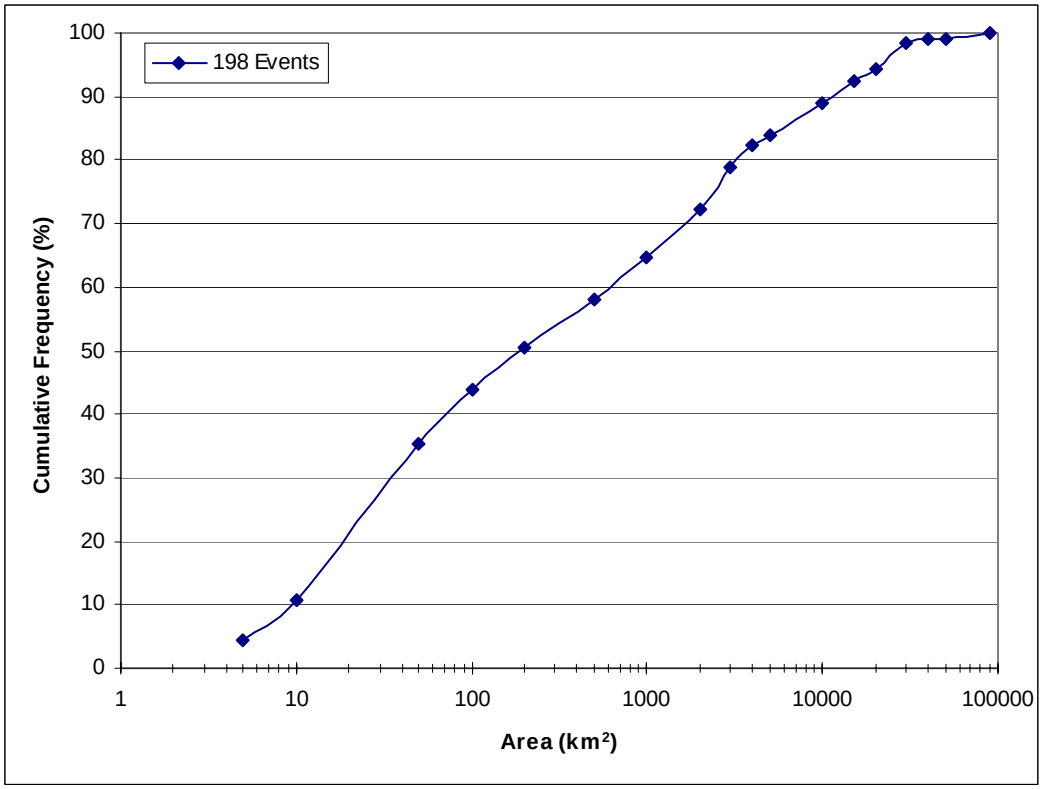

Figure 5.19. Cumulative frequency distribution of area influenced by slides.

A frequency density distribution for the total area influenced by the seafloor slides is plotted in Figure 5.20. The highest frequency of slides involve areas between about 5 and 10 km^2. The second most frequent range in areas is less than 5 km^2. The median area (200 km^2) is much smaller than the mean area (3,600 km^2) because slides of smaller areas have a much higher frequency of occurrence.

Even with the best technology, seafloor slope failures smaller than about one square kilometer are probably not detected (McAdoo et al., 2000) and, thus, are inherently excluded from the database. Furthermore, if very small slides were

detected in seafloor surveys, they would be excluded from the database if they were not reported in the literature. Despite these circumstances, seafloor slides with areas less than 5 km^2 have the second largest rate of occurrence (Figure 5.20). The data suggest that slides less than 10 km^2 occur most frequently.

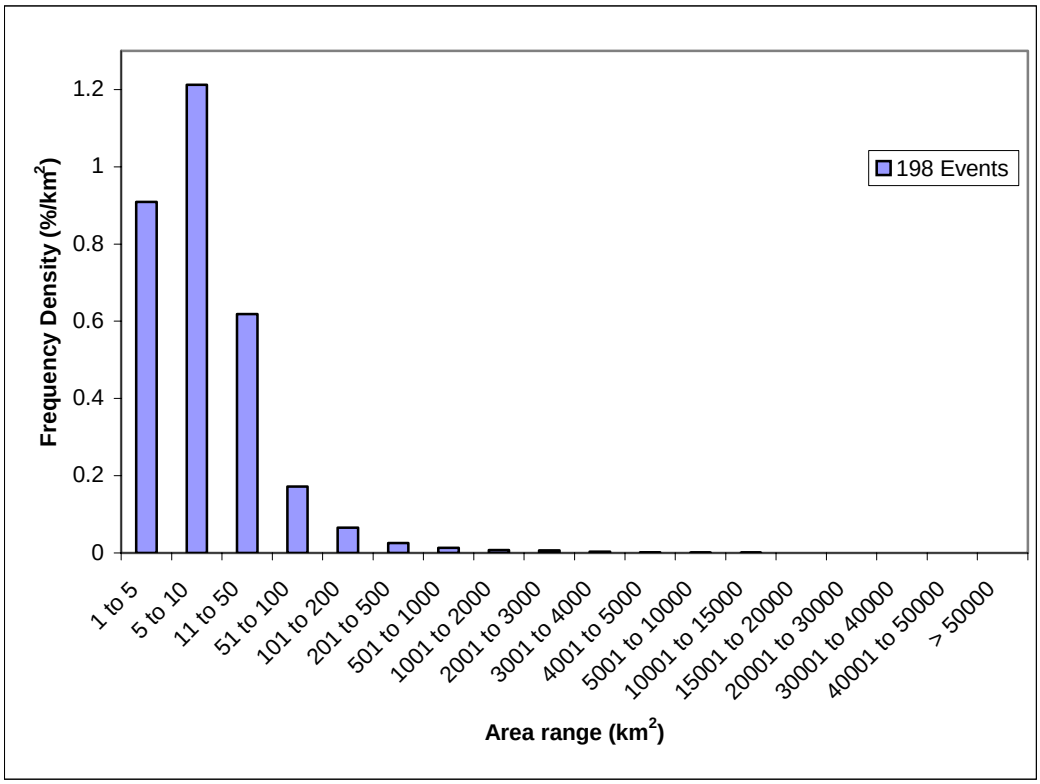

Figure 5.20. Frequency density distribution of area influenced by slope failures.

5.8.1.1 Relationship between total area influenced and average slope angle at failure

The relationship between the total area influenced by a slope failure and the average angle of the slope at failure is plotted for the 145 events where these data are available in Figure 5.21. Due to the large range in area, a logarithmic

scale is used to plot the area. The data presented in Figure 5.21 suggest that the slides with the largest areas tend to occur on the flatter slopes. This relationship is not intuitive because the inclination of the slope is typically considered a major driving mechanism for slope instability.

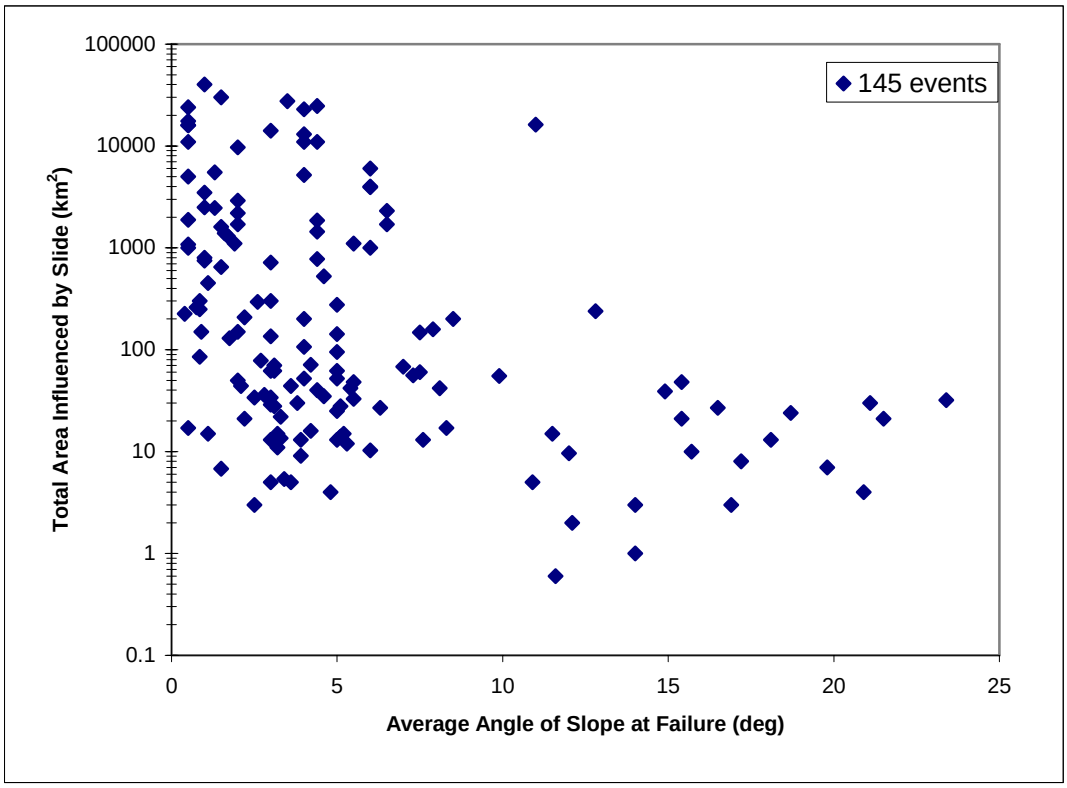

Figure 5.21. Relationship between total area influenced by a slide and average angle of the slope at failure.

5.8.2 Runout distance

A cumulative frequency distribution of the runout distance for 434 of the slope failures in the database is presented in Figure 5.22. A logarithmic scale is used to plot the runout distance due to the large range in distance involved. The

runout distance can be very large, where slides move downslope tens to hundreds of kilometers. About 10 percent of the slides (43 slides) have runout distances greater than 100 km. The median runout distance for the 434 slides is about 8 km, and the mean runout distance is about 41 km.

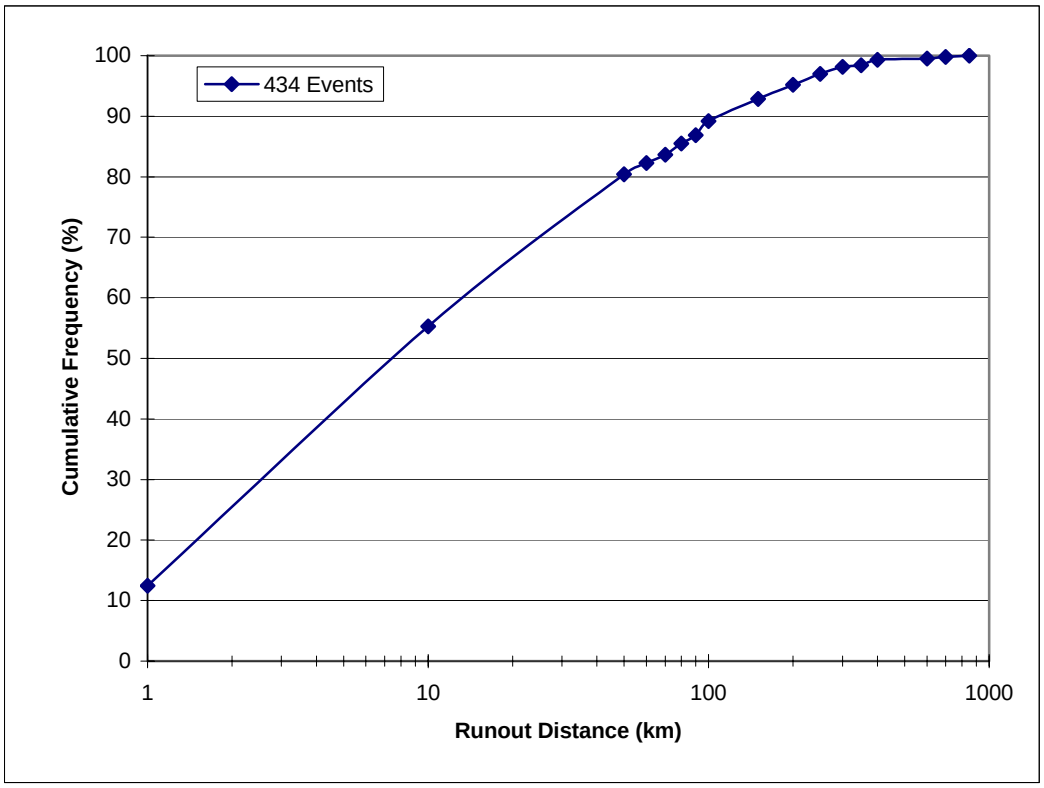

Figure 5.22. Cumulative frequency distribution of slide runout distance.

A frequency density distribution of the slide runout distance for the 434 slides is presented in Figure 5.23. The frequency of runout distance decreases almost exponentially with increasing runout distance. The most frequent runout distance is less than 1 km. The nearly exponential decrease shown in Figure 5.23

explains why the median runout distance (8 km) is much smaller than the mean (41 km).

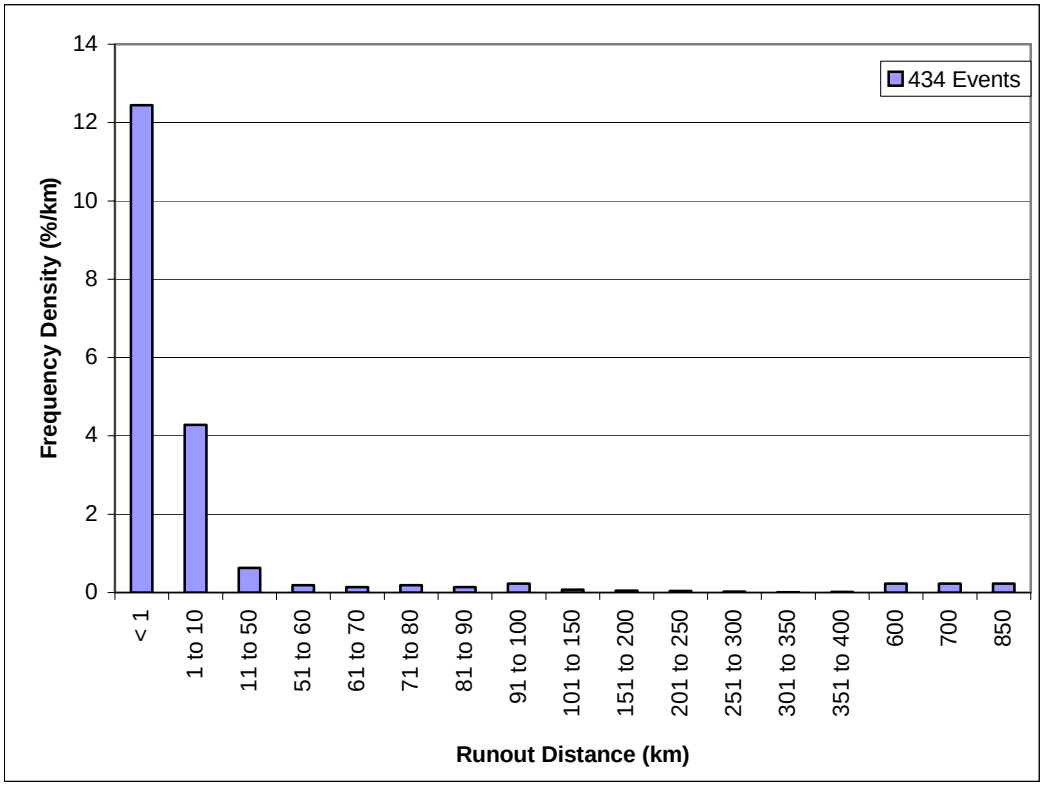

Figure 5.23. Frequency density distribution of slide runout distance.

5.8.2.1 Relationship between runout and average slope angle at failure

Information on both runout distance and slope angle at failure was available for 343 of the slides in the database. The relationship between runout distance and average slope angle for these 343 slides is shown in Figure 5.24. The runout distances in Figure 5.24 are plotted on a logarithmic scale because of the large range in the runout distance. There appears to be an almost inverse

relationship between runout distance and slope angle with the longer runout distances tending to be for flatter slopes.

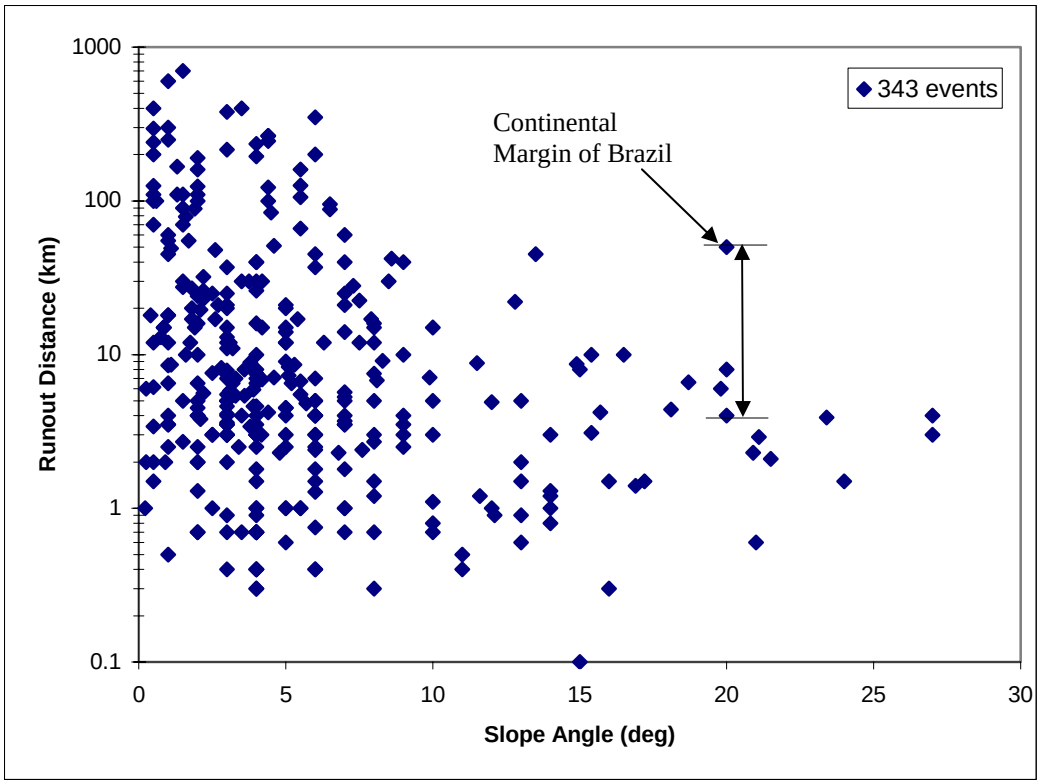

Figure 5.24. Relationship between runout distance and average slope angle at failure.

There is a large amount of "scatter" in the data in Figure 5.24. This scatter is attributed in part to the diversity of the environments where the slides have occurred. Scatter is also caused by the differences in geophysical mapping techniques. For example, one slide that is an outlier, occurred on the continental margin of Brazil and was mapped in the late 1960's using just one profile from an airgun reflection profiler (Moore et al., 1970). The slide was described as having

a runout distance of between 4 and 50 km. Such a large range in distance results from the relatively low geophysical resolution and line profiling used in the investigation. The data for this slide was plotted in Figure 5.24 using the upper limit of 50 km for the runout distance.

5.8.3 Average Thickness of Landslide

Information about the average thickness of the slide was available for 315 of the slides in the database. These thicknesses represent an average thickness of the slide obtained over the areal extent of the slide mass. The cumulative frequency distribution of slide thicknesses for the 315 slope failures is presented in Figure 5.25. There is a large range in thickness, spanning three orders of magnitude. Thus thicknesses are plotted using a logarithmic scale. The median thickness for the 315 slides is 50 m, and the mean thickness is 141 m. About 65 percent (205 slides) of the slope failures where thickness was available have an average slide thickness greater than about 30 m.

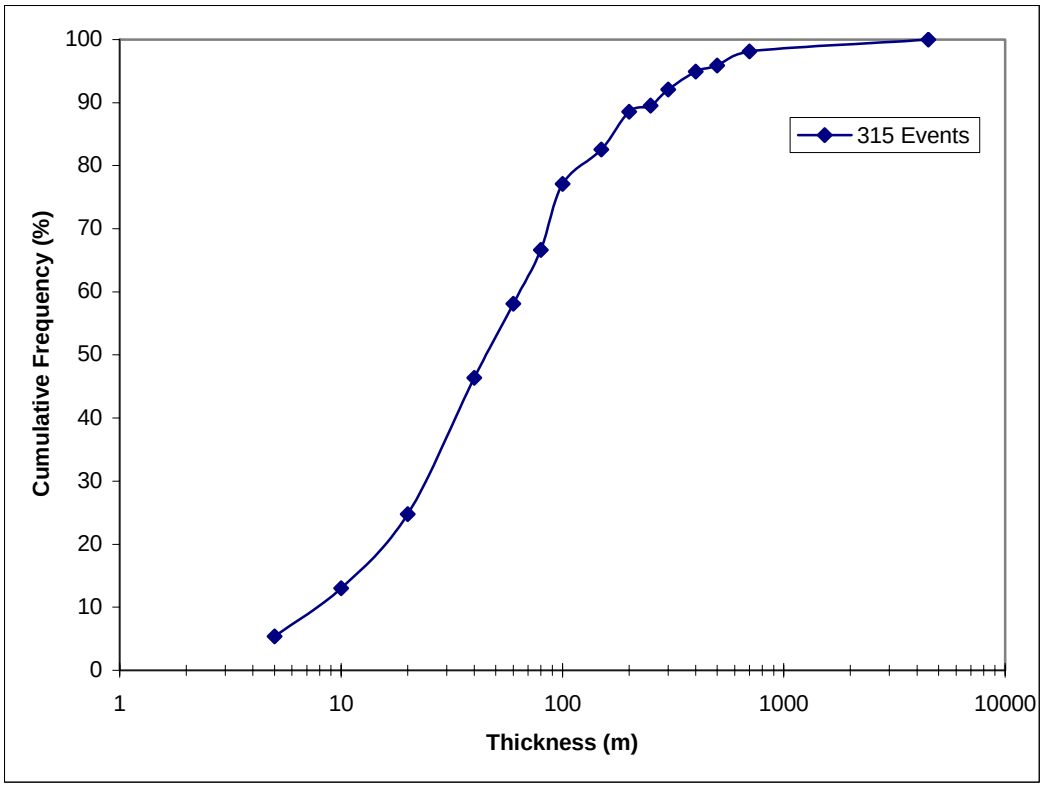

Figure 5.25. Cumulative frequency distribution of slide thicknesses.

A frequency density distribution for the 315 slides where the slide thickness was reported is presented in Figure 5.26. Thicknesses between 6 to 10 m appear most frequently in the database, which is why the median thickness (50 m) is much lower than the mean (141 m). Thicknesses up to about 40 m have similar rates of occurrence in the database. For thicknesses greater than about 100 m, the frequency density decreases significantly.

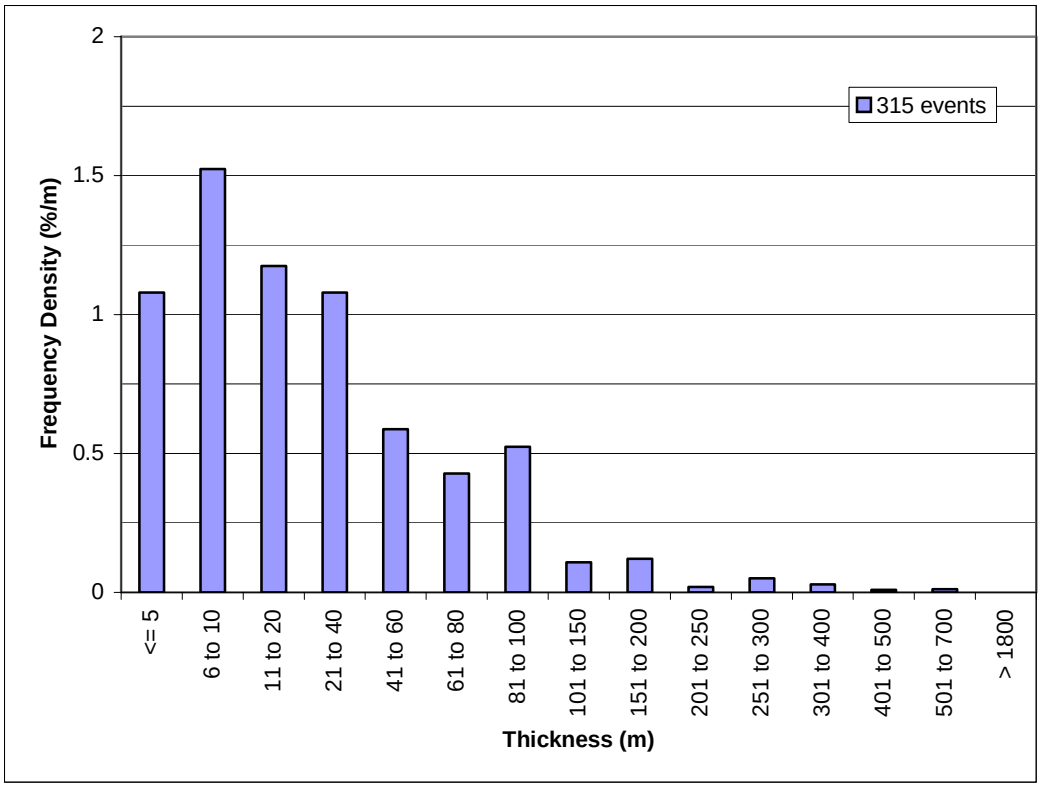

Figure 5.26. Frequency density distribution of slide thicknesses.

5.8.4 Total Volume of the Slide

Information about the total volume of the slide was available for 191 of the slides in the database, and is plotted in Figure 5.27. Almost one third of the 191 slides (61 slides) have volumes ranging from 1.1 to 10 km^3. There is a very large range in volumes, with volumes varying from less than 0.1 km^3 to greater than 20,000 km^3.

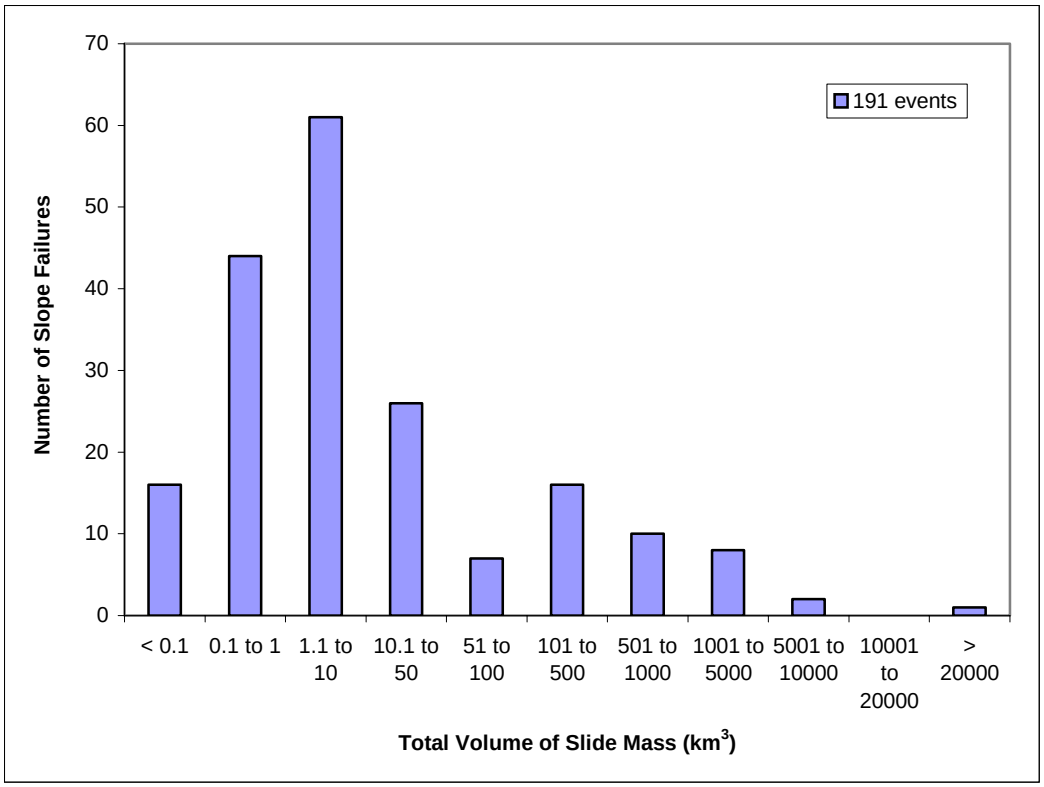

Figure 5.27. Number of seafloor slope failures according to volume of the slide.

A frequency density distribution for the 191 slides where volume data were available is plotted in Figure 5.28. Volumes between 0 and 0.1 km^3 appear most frequently in the database. Also from Figure 5.28, the frequency density decreases almost exponentially as the volumes increase. The frequency density is almost zero for slides with volumes greater than 10 km^3.

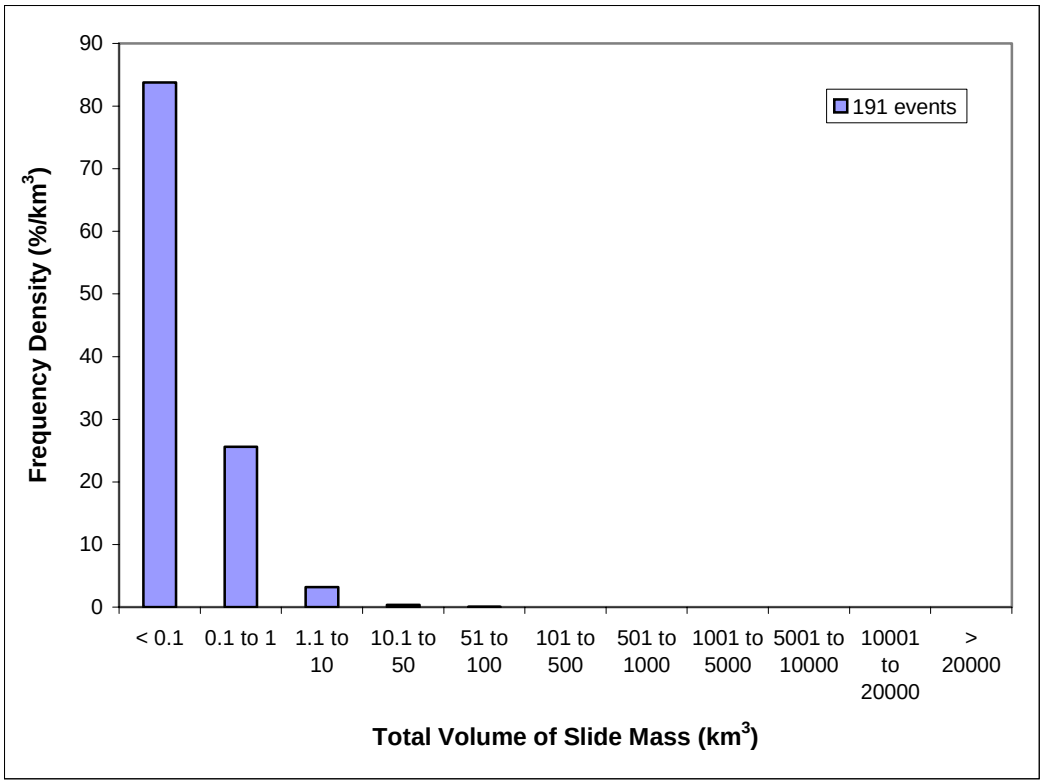

Figure 5.28. Frequency density distribution for the volume of slide mass.

A cumulative frequency distribution of the total volume of the slide mass for the 191 slides where volume data were available is presented in Figure 5.29. The volumes are plotted on a logarithmic scale because of the large range in volume, which spans over five orders of magnitude. The median volume for the 191 slides in Figure 5.29 is 3.5 km^3, and the mean volume is 354 km^3. The median is much smaller than the mean because of the much higher frequency of slides with volumes less than 1 km^2.

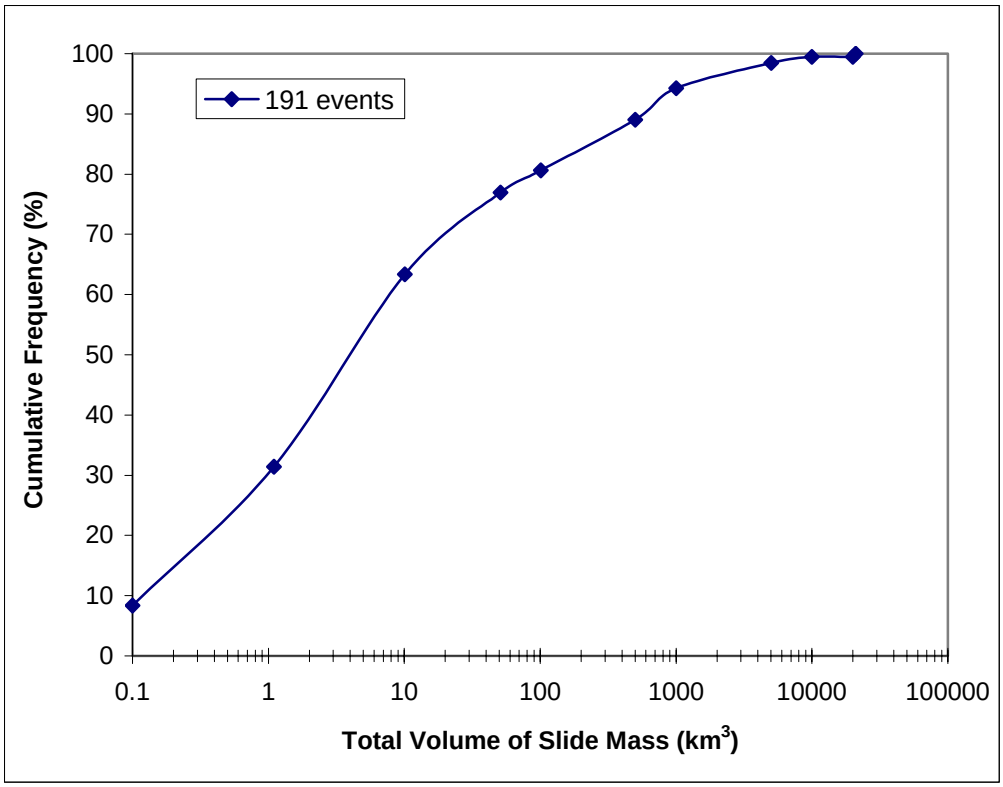

Figure 5.29. Cumulative frequency distribution for the volume of slide mass.

5.9 WATER DEPTHS

The shallowest water depth and deepest water depth affected by slope failure were recorded in the database when available. There are 442 slides in the database where the shallowest water depth affected by the slide is reported, and 408 slides where the deepest water depth affected by the slide is reported. The shallowest water depth is reported more frequently than the deepest water depth for two reasons: First, slope failures can extend into waters and depths beyond where seafloor surveys have been done. Secondly, the downslope limit of the

disturbed seafloor and slide can be difficult to determine and, thus, may not be reported.

Figure 5.30 is a cumulative frequency distribution of the shallowest and deepest water depths affected by the slides in the database. The median shallowest water depth for the 442 slides is approximately 1000 m. The median deepest water depth for the 408 slides is approximately 1750 m, which is 750 m deeper than the median shallowest water depth. Means for the shallowest and deepest water depths are about 1125 m and 1868 m, respectively, which is also a difference of about 750 m. For a slope of 10 degrees, the runout distance for a change in elevation of 750 m is about 4,250 m (4.25 km). Thus, the water depths for the slope failures suggest that failures travel long distances, e.g. at least 4 km, considering that the inclination of the seafloor is typically less than 10 degrees. About 60 percent of the slope failures in the database (260 slides) had runout distances greater than 4 km (Section 5.8.2). Thus, the runout distance results are consistent with the water depth results.

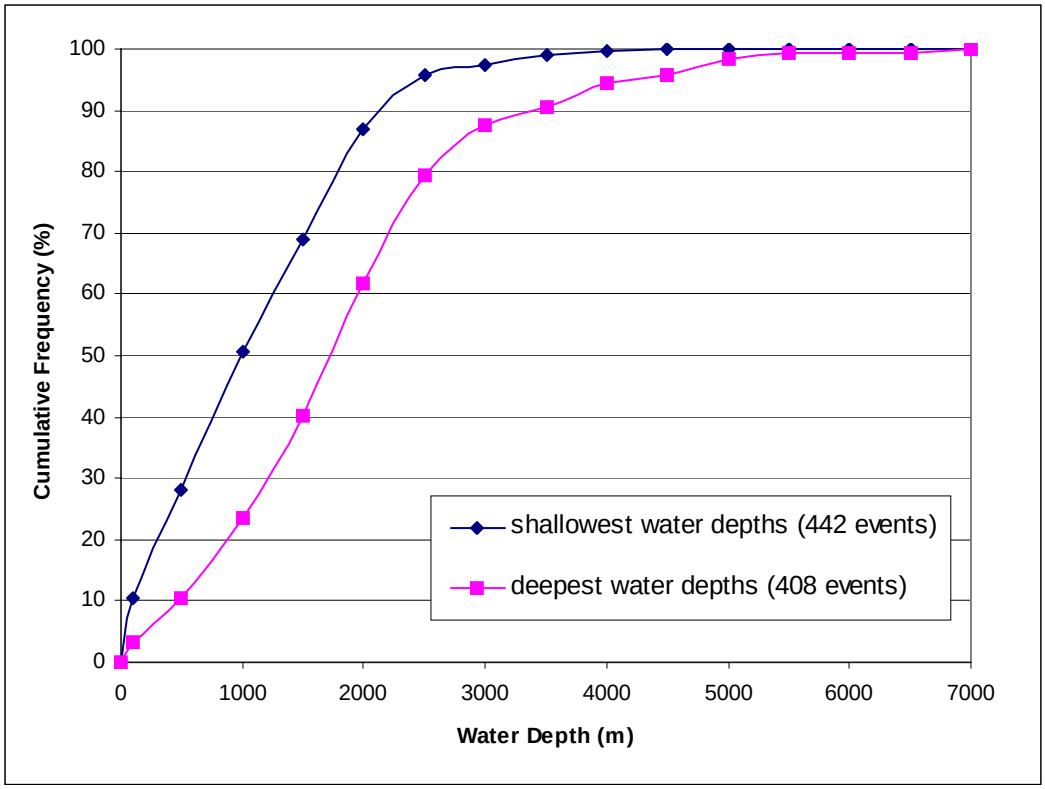

Figure 5.30. Cumulative frequency distribution of water depths affected by the seafloor slides.

Figure 5.31 is a frequency density distribution of the water depths affected by the slides in the database. The data in Figure 5.31 show there is a high frequency of slides beginning in water depths less than about 100 m and extending to water depths between 1500 and 2000 m. Hence, the most frequently reported slides tend to begin in regions of the inner continental shelf and end in water depths that correspond to the continental slope. In fact, some seafloor slides have been reported to extend out to water depths of 7,000 m, i.e. the continental rise, which are the deepest water depths on Earth.

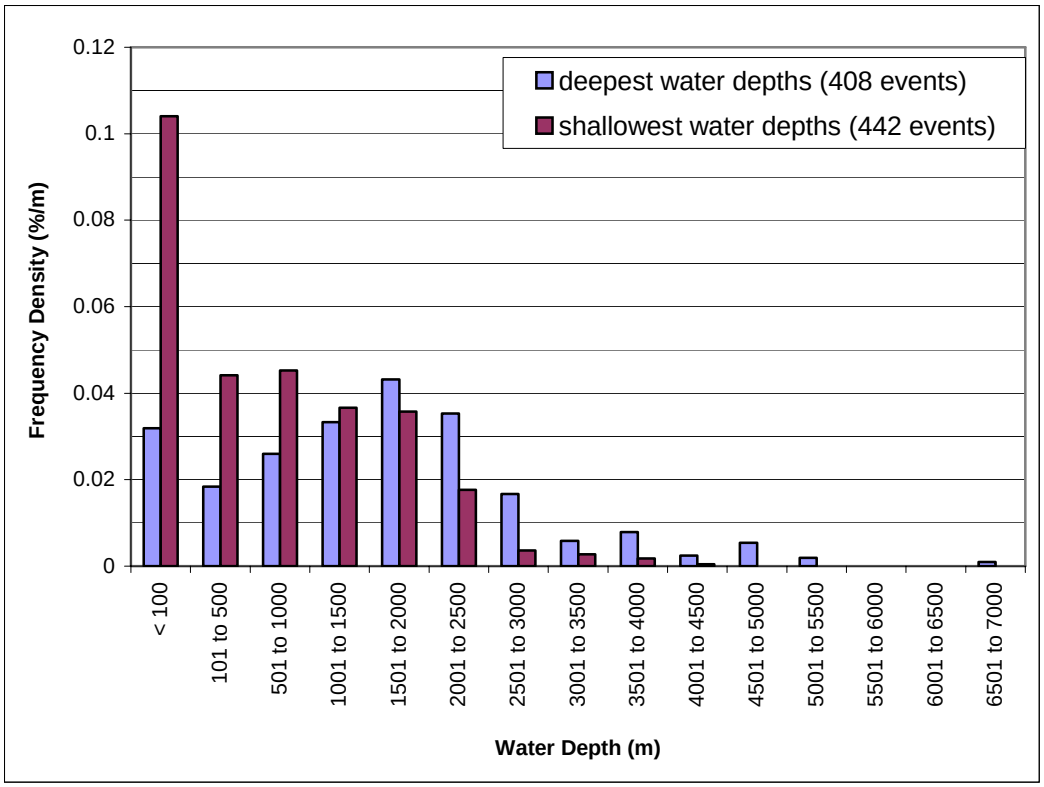

Figure 5.31. Frequency density distribution of water depths affected by the seafloor slides.

5.10 SOIL TYPE

Information about the type of soil involved in the slope failure was available for 147 of the 534 slides in the database. The frequency of slides for various soil types is shown in Figure 5.32. Soil types are categorized according to the Unified Soil Classification System (USCS), plus an additional soil type labeled “volcanic material”.

A total of 266 occurrences are shown in Figure 5.32. This number (266) exceeds the total of 147 slides because the majority of the slides (65%) involve

more than one type of soil. This occurs because soil conditions are heterogeneous and because submarine slides sometimes affect large areas and travel large distances, where the slide mass passes over more than one soil type.

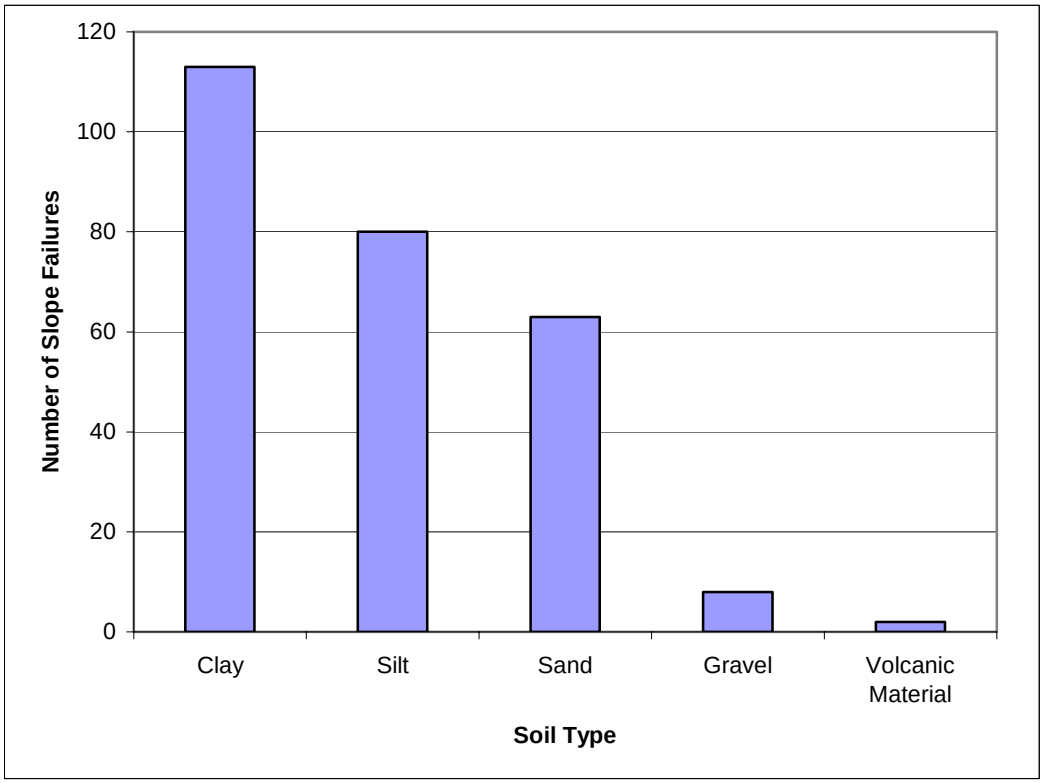

Figure 5.32. The number of slope failures according to documented soil type.

The majority of the slides where information on soil type was available involved fine-grained material, i.e. clays and silts. This characteristic is not surprising considering that most of the Earth's seafloor is composed of fine-grained material, according to Lee and Mehta (1997). Furthermore, positive excess pore water pressures can develop in marine clays and silts because of their

low permeability and their tendency to contract when sheared undrained; thus the shear strength in these soils may be lower leading to slope failure.

Sixty-three (63) of the 147 events (about 43 percent) involved sandy soils. This finding is reasonable for two reasons: First, many deltaic deposits and material on the inner continental shelf, i.e. water depths less than about 200 m, tend to contain coarse particles and are often classified as sands. More than 10 percent of the slides where water depths are known (about 50 slides) occurred in shallow water regions (Section 5.9) and account for many of the slides involving sandy soils. Secondly, earthquakes are the most common triggering mechanism in the database (Section 5.4). Liquefaction typically occurs in saturated, loose sandy deposits that experience earthquake shaking. Since earthquakes tend to liquefy saturated, loose sandy soils, the fact that sandy soils appear in 43 percent of the slides where soil data are available seems reasonable.

Gravelly soils are much less frequent than clay, silt and sand. This probably occurs for 2 reasons: First, gravelly soils are not typically present on the seafloor in water deeper than a few hundred meters because ocean currents cannot transport gravelly soils large distances offshore. Thus, gravelly soils tend to be restricted to areas near river deltas and are not generally found over other large areas of the seafloor. The second reason why gravels are not reported for most of the seafloor slides is that gravelly soils are less likely to experience adverse pore water pressure conditions than other types of cohesionless soils.

Volcanic material is the least frequent of the soil types involved in slope failures, probably because only a small portion of the slides in the database are attributed to volcanic events (Section 5.4). Also, seafloor slides triggered by volcanic activity typically did not have the soil or rock types reported.

5.11 RUNOUT CHARACTERISTICS OF SUBAQUEOUS SLIDES COMPARED TO SUBAERIAL AND QUICK CLAY SLIDES

5.11.1 INTRODUCTION

Several relationships between landslide volume and runout distance have been developed for subaerial (Scheidegger, 1973), subaerial quick clay (Edgers and Karlsrud, 1982) and subaqueous landslides (Edgers and Karlsrud, 1982; Hampton et al., 1996). The findings from this previous work are summarized in this section, and compared with data from 161 seafloor slides in the current database.

5.11.2 SUBAERIAL SLIDES

Scheidegger (1973) addressed the runout characteristics of subaerial slides. He expressed a "coefficient of friction" of the sliding material as H/L where H is the difference between the highest and lowest elevations affected by the slope failure, and L is the runout distance. Scheidegger suggested that the ratio of H/L decreases as the volume of slide material increases. Scheidegger

(1973) defined a typical relationship between H/L and slide volume for subaerial slides based on data for 33 subaerial slides, and this relationship is shown in Figure 5.33. The solid trendline is the "average" line that was calculated by the least squares regression method, and the dotted trendlines are one standard deviation from the average.

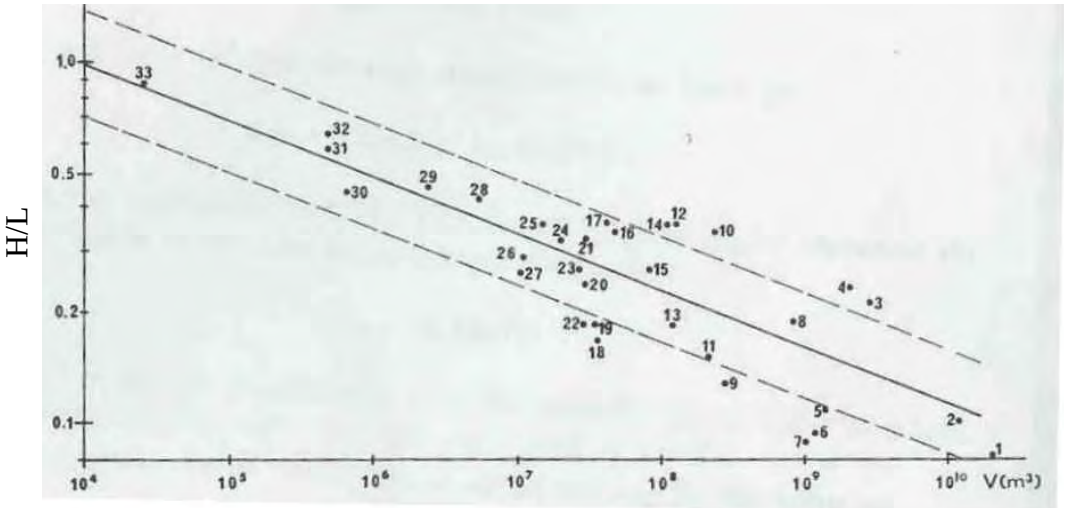

Figure 5.33. Ratio of height to runout distance (H/L) versus volume of slide mass for 33 subaerial slides (Scheidegger, 1973).

5.11.3 SCHEIDEGGER APPROACH APPLIED TO QUICK CLAY AND SUBAQUEOUS SLIDES

Edgers and Karlsrud (1982) applied the approach developed by Scheidegger (1973) to address the runout characteristics of subaerial quick clay slides and subaqueous slides. Hampton et al. (1996) updated the findings of Edgers and Karlsrud (1982). The relationships developed in these previous

studies between the ratio, H/L, and slide volume for subaerial, quick clay and subaqueous slides are summarized in Figure 5.34. In Figure 5.34, logarithmic scales are used for both axes because of the large range in values of the variables involved. This figure appears in Hampton et al. (1996) and Locat and Lee (2000, 2002). The figure includes specific data points for 15 non-volcanic and 3 volcanic submarine slides. The source data of these data points is summarized in Hampton et al. (1996).

Several trendlines are shown in Figure 5.34:

- The trendline originally proposed by Scheidegger (1973) that represents an average for subaerial slides.
- A trendline proposed by Edgers and Karlsrud (1982) based on data for 25 submarine slides. Edgers and Karlsrud (1982) showed and stated that this trendline represents a lower bound for the data of submarine slides, i.e. the lowest H/L ratio, anticipated for a particular slide volume.
- A trendline proposed by Hampton et al. (1996) based on data for 15 submarine slides. Hampton et al. (1996) showed and stated that this trendline represents an upper bound for submarine slides, i.e. the largest H/L ratio, anticipated for a particular slide volume.
- A trendline proposed by Edgers and Karlsrud (1982) based on data for 8 quick clay slides. Edgers and Karlsrud (1982) showed and stated that this trendline is a lower bound for subaerial quick clay slides, i.e. the lowest

H/L ratio, anticipated for a particular slide volume. Hampton et al. (1996) and Locat and Lee (2002) concluded that the trendline for the subaerial quick clay slides was a lower bound, i.e. the lowest H/L ratio, anticipated for a particular slide volume based on data for 15 submarine slides presented in Hampton et al. (1996).

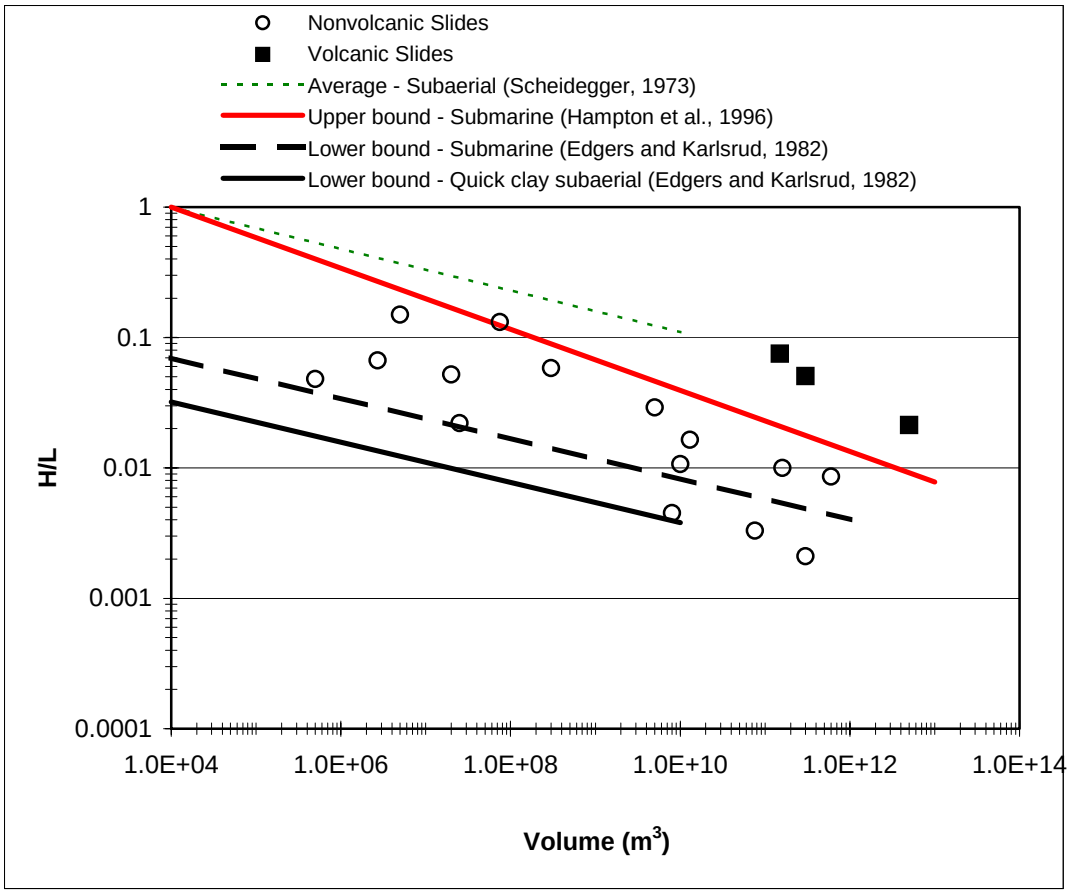

Figure 5.34. Ratio of height to runout distance (H/L) versus volume of slide mass (after Locat and Lee, 2002). There are suggested relationships by Scheidegger (1973), Edgers and Karlsrud (1982), and Hampton et al. (1996).

Edgers and Karlsrud (1982), Hampton et al. (1996), and Locat and Lee (2000) drew four conclusions from the data shown in Figure 5.34.

1) An increase in slide volume generally corresponds with an increase in runout distance (L) relative to the slope height (H), i.e. H/L decreases.
2) For the same volume of slide mass and the same change in elevation (H), submarine slides tend to have larger runout distances, i.e. lower ratios of H/L, than subaerial slides. Hampton et al. (1996) showed and stated that the trendline for subaerial slides is an upper bound for the data of the ratio, H/L, and slide volume of submarine landslides.
3) For the same volume of slide mass and the same change in elevation (H), quick clay (subaerial) slides tend to have larger runout distances, i.e. lower ratios of H/L, than submarine slides. Hampton et al. (1996) showed and stated that the trendline for quick clay (subaerial) slides is a lower bound for the data of the ratio, H/L, and slide volume of submarine landslides. Edgers and Karlsrud (1982) stated that quick clay (subaerial) slides have larger runout distances than marine soils of low to moderate sensitivity for the following reasons:
    a) the downslope gravity driving force for a subaerial slide is almost twice as large as for a subaqueous slide.
    b) there are hydrodynamic drag stresses at the top of a submarine slide due to the overlying water, which can reduce runout.

c) there is greater reduction in undrained shear strength once a slide occurs with quick clay than most marine soil, which has low to moderate sensitivity. Locat (1995) has shown that quick clay will flow as a Bingham fluid (Chapter 8) once failure occurs, resulting in large runout distances on even flat slopes, i.e. low ratios of H/L.

4) Volcanic submarine slides and subaerial slides have similar runout characteristics, i.e. the data for the ratio of H/L and volume of volcanic slides plot in the vicinity of the subaerial trendline. Hampton et al. (1996) explain the similarity between volcanic submarine slides and subaerial slides by stating that volcanic slides behave much like granular rock avalanches.

Values for the ratio, H/L, and slide volume for 155 non-volcanic and 6 volcanic submarine slides from the current database are plotted in Figure 5.35. The trendline relationships previously suggested by Edgers and Karlsrud (1982) and Hampton et al. (1996) as respective lower and upper bounds for submarine landslides are included in Figure 5.35.

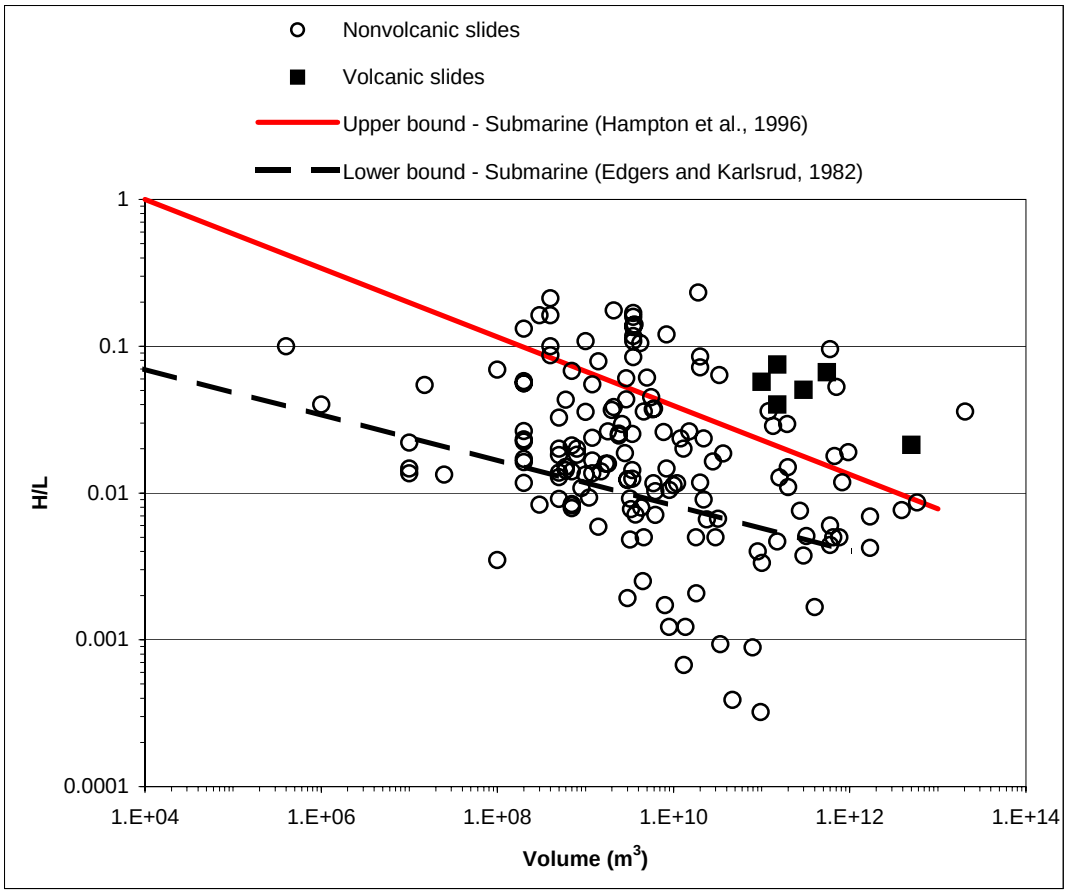

Figure 5.35. Ratio of height to runout distance (H/L) versus volume of slide mass, using 155 nonvolcanic and 6 volcanic submarine landslides from the database. There are suggested relationships by Edgers and Karlsrud (1982) and Hampton et al. (1996).

Although there is a large amount of scatter in the data in Figure 5.35, the upper bound suggested by Hampton et al. (1996) for submarine slides does not appear to be an upper bound: there are more than 30 slides for which data plot above this "upper bound". Also, the lower bound suggested by Edgers and Karlsrud (1982) for submarine slides does not appear to be a lower bound: there are approximately 39 slides for which data plot below this "lower bound". The ratio, H/L, tends to

decrease with increasing volume of slide mass, although, again, there is considerable scatter in the data. The trend is consistent with the conclusion presented by Edgers and Karlsrud (1982), Hampton et al. (1996), and Locat and Lee (2002) from Figure 5.34. After taking the logarithm of both variables, a least squares regression analysis was performed using the data to determine quantitatively the amount of scatter in the data. The analysis revealed an R-square value of only 0.09. Such a low R-square value indicates large variability between the two parameters (H/L and volume), and, reflects the considerable scatter observed in Figure 5.35.

The data shown in Figure 5.35 are plotted again in Figure 5.36, with the suggested relationships by Scheidegger (1973) for subaerial slides and by Edgers and Karlsrud (1982) for subaerial quick clay slides.

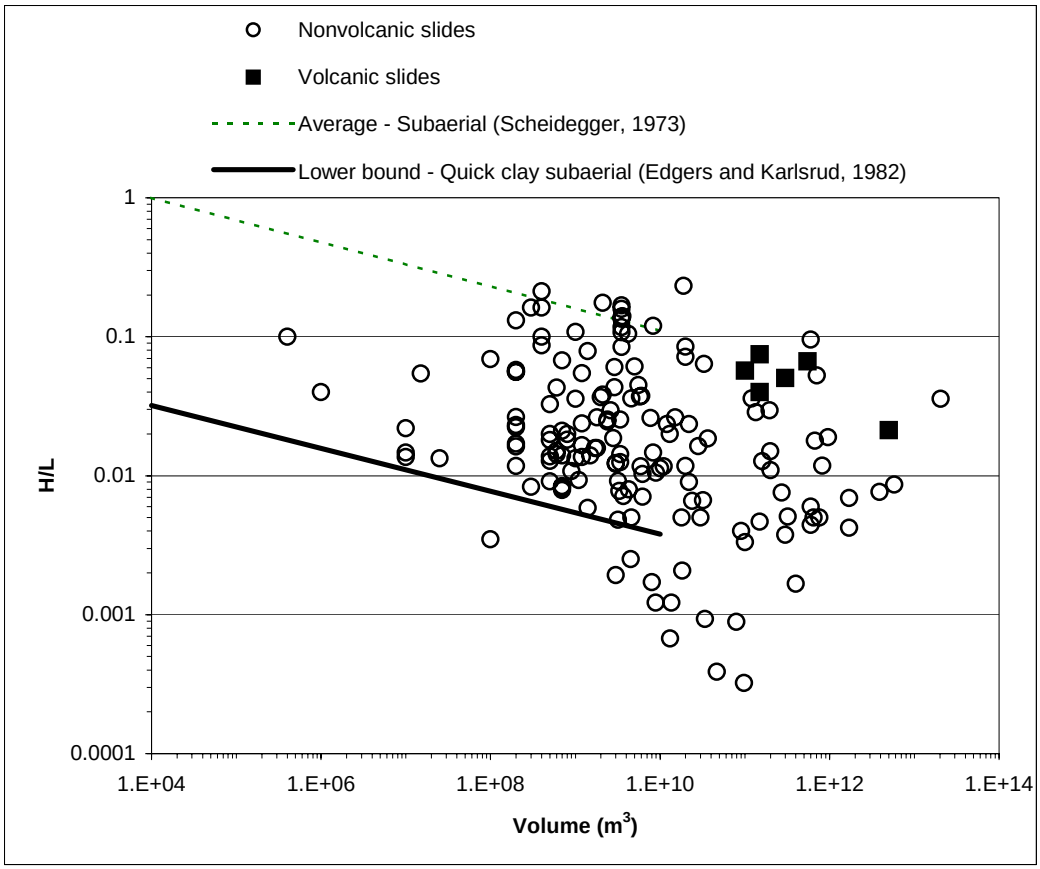

Figure 5.36. Ratio of height to runout distance (H/L) versus volume of slide mass, using 155 nonvolcanic and 6 volcanic submarine landslides from the database. There are suggested relationships by Scheidegger (1973) and Edgers and Karlsrud (1982).

The trendline for subaerial quick clay slides was suggested by Hampton et al. (1996) to be a lower bound for submarine slides. However, this trendline does not appear to be a lower bound. Approximately 13 slides have characteristics that plot below the trendline for quick clay slides. The six volcanic submarine slides shown in Figure 5.36 have similar runout characteristics to subaerial slides and the trendline suggested by Scheidegger (1973).

5.12 CONCLUSIONS

There are 14 different triggering mechanisms reported in the literature, and among these triggers, earthquakes are cited the most frequently. In terms of certainty with regard to triggering mechanisms, only about 10 percent of the slope failures in the database have a single, definitive trigger, and about 38 percent of the slope failures have a completely uncertain cause of failure. The majority of the case histories in the database (52 percent) cite several possible triggering mechanisms.

The characteristics of runout distance, slide thickness, total area influenced, slide volume, slope angle, and shallowest and deepest water depths for the seafloor slope failures examined are summarized in Table 5.3. There is a very large range between the maximum and minimum values of the characteristics shown in Table 5.3. This is attributed to the widely varying triggering mechanisms and soil types for submarine landslides. The median (50^{th} percentile) values for all the characteristics shown in Table 5.3 are smaller than the mean values. There are two reasons for this: First, a relatively large number of slides have small runout distances, slide thicknesses, total areas influenced, slide volumes, slope angles and water depths, which decrease the median values relative to the mean. Secondly, some slides have extremely large dimensions, which increases the mean values relative to the median.

Table 5.3. Summary of characteristics of seafloor slope failures in the database.

Characteristic	Units	Max	Min	Median	Mean
Runout distance	km	850	0.04	8	41
Slide thickness	m	4,500	< 1	50	141
Total Area Influenced	km^2	88,000	< 1	200	3,600
Slide Volume	km^3	20,331	0.000006	3.5	354
Slope Angle at Failure	deg	45	0.22	4.0	5.8
Shallowest Water Depth	m	4,300	0	1000	1,125
Deepest Water Depth	m	6,700	8	1750	1,868

Based on the maps that showed the geographic distribution of slope failures for earthquakes and faulting, rapid sedimentation, gas hydrates, ocean storm waves, magma volcanoes and mud volcanoes, these reported triggers seem reasonable. Thus, confidence has been gained in these triggers being the causes of reported slope failures.

In Chapter 6 results from slope stability analyses are presented to address the likelihood of various triggering mechanisms such as gravity loading, earthquakes and rapid sedimentation (underconsolidation) causing landslides.

CHAPTER 6

INFINITE SLOPE STABILITY ANALYSES AND CORRELATIONS WITH SEISMICITY

6.1 INTRODUCTION

This chapter presents the results from a series of slope stability analyses for static and pseudo-static conditions assuming an "infinite" slope. The analyses were performed to assess the likelihood of slides being triggered by gravity, earthquakes, and rapid sedimentation (underconsolidation), which are all common loading conditions for seafloor slopes. The results from the pseudo-static analyses are compared to potential seismic loads (earthquake magnitudes).

6.2 ANALYSES FOR STATIC CONDITIONS

The stability of seafloor slopes was evaluated for static conditions with only gravity loading. To evaluate slope stability for static conditions a factor of safety was computed. The factor of safety (F) was defined as:

$$F = \frac{s}{\tau} \tag{6.1}$$

where s is the available shear strength along a particular slip surface, and τ is the equilibrium shear stress along the same slip surface. A slope was generally considered stable if the factor of safety is greater than 1.0.

As shown in Chapter 5, many seafloor slides involve large distances laterally in comparison to the thickness of the slide mass. For many slides, the length of the slide is, for practical purposes, nearly infinite with respect to the thickness of the slide. Thus, the infinite slope method is a suitable and realistic method of analyses. Figure 6.1 shows a schematic of the geometry for an infinite slope with a slip surface parallel to the slope face.

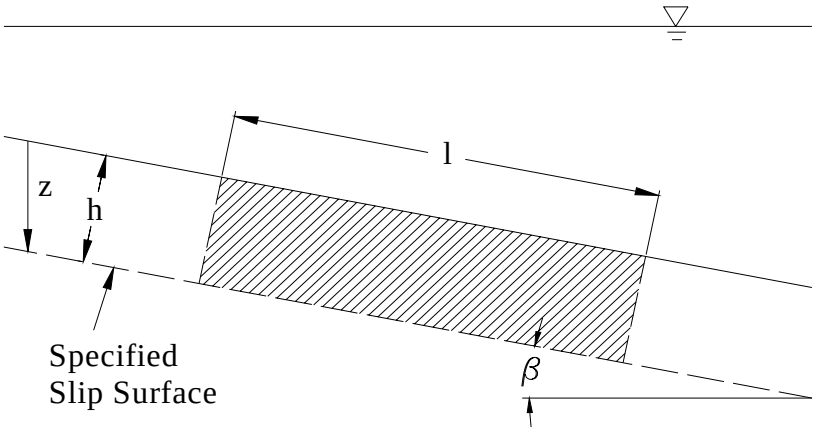

Figure 6.1. Geometry of slope and slide mass for infinite slope failure under static conditions.

6.2.1 APPROPRIATE CONDITIONS FOR STABILITY ANALYSES

Triggers such as earthquakes, ocean waves, rapid sedimentation, rapid erosion, and gas hydrate disassociation tend to influence a slope faster than it can drain, and stability should be evaluated using undrained strengths. On the other hand, triggers such as salt diapirism and faulting tend to increase gradually the inclination of a slope, and the slope tends to be loaded at a rate slow enough to

allow for dissipation of excess pore water pressures and full drainage. Thus, for these cases, stability should be evaluated using drained shear strengths. Because failures may occur under either undrained or drained conditions, it is important for slope stability analyses to address both.

For undrained conditions, the shear strength of the soil is usually expressed in terms of total stresses by an equation of the form:

$$s = c + \sigma \tan \varphi \qquad (6.2)$$

where σ is the total normal stress, c is the cohesion intercept, and ϕ is the friction angle. For saturated soil that is sheared undrained, the friction angle (ϕ) is zero, and the undrained shear strength (s_u) is expressed as a "cohesion" (c).

For drained conditions, the shear strength is expressed in terms of effective stresses by an equation of the form:

$$s = c' + \sigma' \tan \varphi' \qquad (6.3)$$

where c' and ϕ' are the cohesion intercept and friction angle expressed in terms of effective stresses, respectively, and σ' is the effective normal stress. Morgenstern (1967) and Skempton (1970) noted that many marine sediments are fine-grained, normally consolidated to slightly overconsolidated. The cohesion (c') is typically zero for this type of soil.

6.2.2 NORMALLY CONSOLIDATED SOILS

Because many marine soils tend to be normally consolidated, stability computations were first performed for normally consolidated soils. The undrained and drained stability of normally consolidated soils is summarized in the following sections.

6.2.2.1 SLOPE STABILITY FOR UNDRAINED CONDITIONS

The static factor of safety for a submerged, infinite slope for undrained conditions and total stresses was computed. The driving and resisting forces that are imposed on a submerged, infinite slope are shown in Figure 6.2.

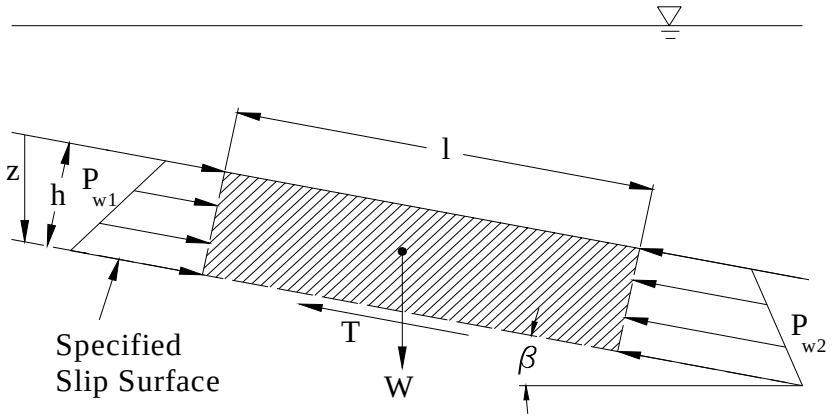

Figure 6.2. Driving and resisting forces on a submerged infinite slope.

The shear stress along the slip surface for an infinite slope can be expressed as:

$$\tau = T / l = \gamma' z \cos\beta \sin\beta \qquad (6.4)$$

where γ' is the submerged unit weight of soil, the depth below the seafloor is z, and β is the slope angle. Combining Equations 6.1 and 6.4, the factor of safety for undrained conditions can be expressed as:

$$F = \frac{s}{\tau} = \frac{s_u}{\gamma' z \cos\beta \sin\beta} \tag{6.5}$$

where s_u is the undrained shear strength. The undrained shear strength (s_u) is often normalized with respect to the in situ effective overburden stress, σ_v', i.e. s_u/σ_v', which is also referred to as a c/p ratio. For a gently sloping ground surface, the in situ effective vertical overburden stress (σ_v') can be approximated by the product of the submerged unit weight (γ') and the vertical depth (z). Thus Equation 6.5 can be written as:

$$F = \frac{c/p}{\cos\beta \sin\beta} \tag{6.6}$$

Skempton (1970) noted that c/p ratios for normally consolidated soils range from approximately 0.2 to 0.4. Using Equation 6.6 and these values for the c/p ratio, the factor of safety for normally consolidated soils was calculated for slopes ranging from 0 to 20 degrees, and is plotted in Figure 6.3.

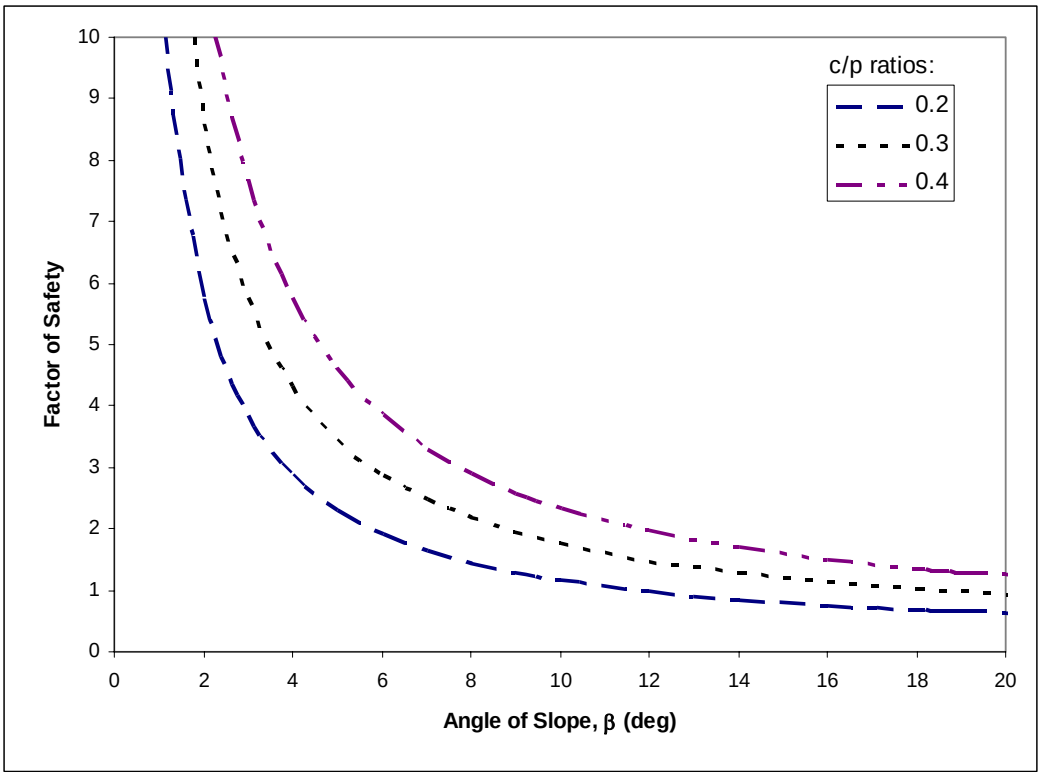

Figure 6.3. Variation in factor of safety with slope angle for infinite slope in normally consolidated soils using undrained shear strengths.

Most slope failures in the database (334 slides) occurred in slopes inclined at angles flatter than about 10 degrees. In order for such slopes to fail under static conditions ($F < 1$), the c/p ratio would need to be less than 0.17 as shown in Figure 6.4. If 0.20 represents a lower limit for the c/p ratio, there must have been a trigger other than gravity to cause most of the offshore slopes flatter than 10 degrees to fail.

6.2.2.2 SLOPE STABILITY FOR DRAINED CONDITIONS

Stability calculations for drained conditions were performed using shear strengths expressed in terms of effective stresses. The cohesion (c') was assumed to be zero, which is the case for many normally consolidated soils. The static factor of safety (F) for an infinite slope with no water flow and a cohesion of zero is expressed as:

$$F = \frac{\tan \varphi'}{\tan \beta} \qquad (6.7)$$

Based on this equation, slope failures (F < 1) are expected to occur when the slope angle (β) is greater than the friction angle expressed in terms of effective stresses (ϕ'). Most slope failures in the database (334 slides) occurred in slopes inclined at angles flatter than about 10 degrees. The effective stress friction angle (ϕ′) for many fine-grained soils is expected to be at least 20 degrees, according to Terzaghi et al. (1996). For example, for the 15 slopes in the database where effective stress friction angles were reported, the friction angles were all greater than 20 degrees. For most slopes in the database, the slope angle is less than the effective stress friction angle and slope failure (F < 1) is not expected. Therefore, failure of normally consolidated soil slopes caused only by gravity loads cannot be explained for drained conditions.

6.2.3 EFFECTIVE STRESS ANALYSES OF UNDERCONSOLIDATED SOILS

Some offshore slopes contain underconsolidated soils. For example, rapid sedimentation, the second most common trigger identified in the database, tends to generate excess pore water pressures in most underconsolidated marine soils. Many river deltas experience rapid sedimentation where the soils tend to be underconsolidated. Thus, the stability of underconsolidated soils is of interest and is examined in this section.

The infinite slope method was used to back calculate excess pore water pressures required to cause slope failure assuming a slope in underconsolidated soil. The effective cohesion (c') was assumed to be zero, and the shear strength along the slip surface (*s*) was evaluated in terms of effective stresses. In this case, the factor of safety (*F*) is computed from:

$$F = \frac{s}{\tau} = \frac{(\gamma' z \cos^2 \beta - \bar{u}) \tan \phi'}{\gamma' z \cos \beta \sin \beta} \tag{6.8}$$

where $\bar{u}$ is the excess pore water pressure. By rearranging Equation 6.8, the excess pore water pressure gradient required to trigger failure (F = 1) was computed from:

$$\frac{\bar{u}}{\gamma' z} = \frac{\cos^2 \beta \tan \varphi' - \cos \beta \sin \beta}{\tan \varphi'} \tag{6.9}$$

where $\bar{u}/\gamma' z$ is excess pore water pressure gradient. The excess pore water pressure gradient was considered to be linear with depth below the seafloor when

computing Equation 6.9. The excess pore water pressure gradient was calculated for various slope angles and effective stress friction angles, ϕ', and is plotted in Figure 6.4. The shaded region in Figure 6.4 indicates the gradients that would be required to trigger slides for most of the slopes in the database, i.e. $\beta \leq 10^{o}$ and $\phi' \geq 20^{o}$.

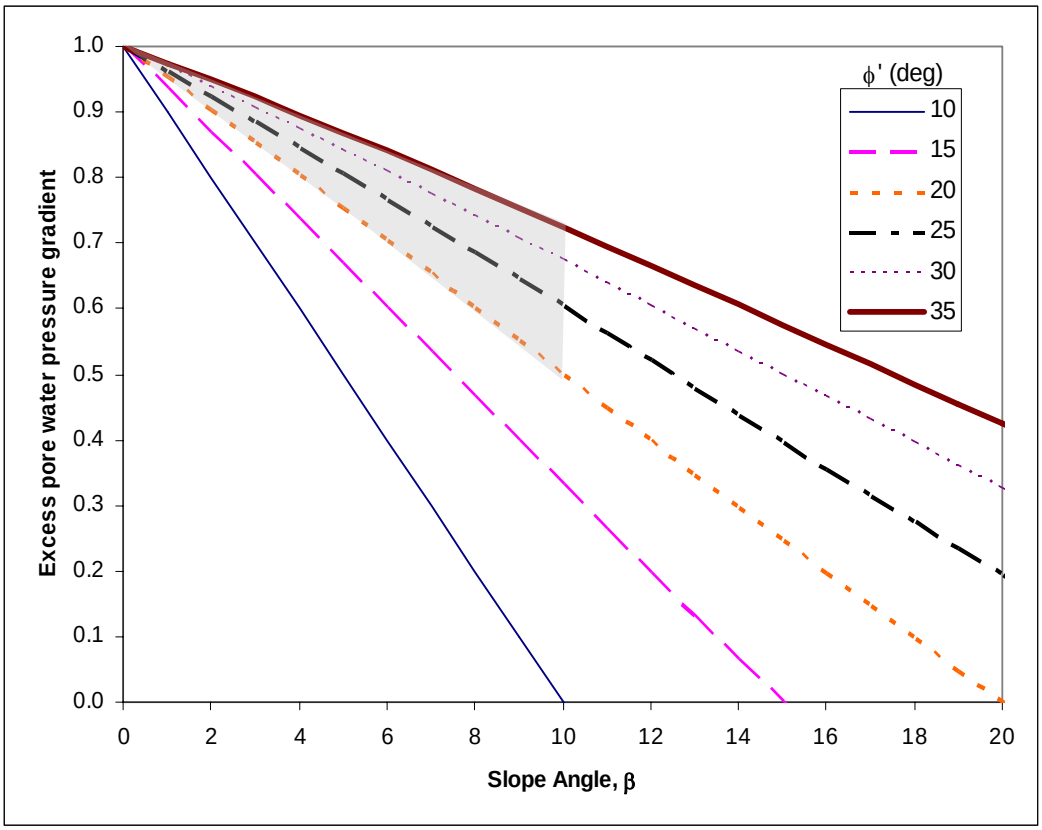

Figure 6.4. Excess pore water pressure gradients required for failure of an infinite slope for various slopes angles and friction angles ($c' = 0$).

Referring to this shaded region, excess pore water pressures greater than about 50 percent of the vertical effective stress would be required to trigger failure.

Bennett et al. (1976) have reported underconsolidated soils in the Mississippi River delta as having large excess pore water pressures ($\bar{u} \geq 0.5\sigma_v'$), yet these soils were on very flat slopes. Because such large excess pore water pressures can be developed, the above analyses indicate that underconsolidated soils are typically not stable under static gravity loads in slopes inclined at angles greater than 10 degrees.

6.2.4 SUMMARY OF ANALYSES FOR STATIC CONDITIONS

The static slope stability analyses of normally consolidated soils suggested that most seafloor slides are not likely caused by gravity loads alone. Thus, for most slopes in the database, apart from underconsolidated soils, a trigger other than gravity must have caused slope failure.

For underconsolidated soils, excess pore water pressures greater than about 50 percent of the vertical effective stress were shown to be required for failure in slopes inclined at angles flatter than 10 degrees. Since excess pore water pressures of this magnitude can be developed, it was inferred that these soils are typically not stable when inclined at angles greater than 10 degrees.

6.3 ANALYSES FOR PSEUDO-STATIC CONDITIONS

The most common triggering mechanism indicated in the database is earthquake loading, and, thus, it was deemed important to evaluate how

earthquakes might affect seafloor slope stability. A pseudo-static approach was used for this purpose. Analyses were again performed using an infinite slope.

A submerged infinite slope and slip surface are shown in Figure 6.5. The submerged weight of the sliding mass is represented by the force W′. A horizontal static force, kW, due to earthquake loading is also shown.

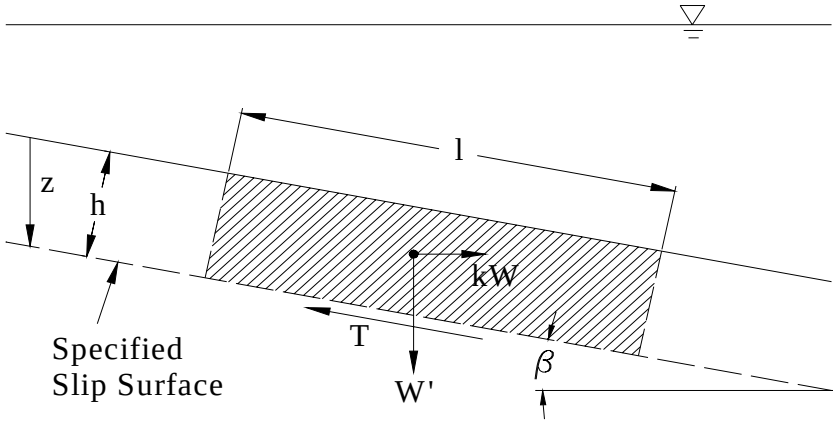

Figure 6.5. Schematic of driving and resisting forces present in a pseudo-static slope stability analysis on a submerged infinite slope.

Most marine sediments are not expected to drain immediately during seismic loading. Thus undrained shear strengths (s_u) were assumed for analyses. The shear stress along the slip surface for an infinite slope under pseudo-static conditions can be expressed as:

$$\tau = \gamma' z \cos\beta \sin\beta + k\gamma z \cos^2\beta \tag{6.10}$$

The factor of safety is then computed as:

$$F = \frac{s}{\tau} = \frac{s_u}{\gamma' z \cos\beta \sin\beta + k\gamma z \cos^2\beta} \tag{6.11}$$

Again, for a gently sloping ground surface, the in situ effective vertical overburden stress (σ_v') was approximated by the product of the submerged unit weight (γ') and the depth (z). Thus, the undrained shear strength, s_u, divided by the product of γ' and z is equal to the c/p ratio. Based on this approximation, Equation 6.11 can be written as:

$$F = \frac{c/p}{\cos^2\beta[\tan\beta + k(\gamma/\gamma')]} \tag{6.12}$$

The seismic coefficient required to trigger slope instability (F = 1) is known as the seismic yield coefficient, k_y, and was determined. By setting the factor of safety equal to one and rearranging Equation 6.12, k_y can be expressed as:

$$k_y = \frac{(c/p)(\gamma'/\gamma)}{\cos^2\beta} - (\gamma'/\gamma)\tan\beta \tag{6.13}$$

Seismic yield coefficients were calculated using Equation 6.13 and c/p ratios ranging from 0.20 to 0.40. For six of the eight slides in the database where c/p ratios were reported, the c/p ratios ranged from 0.20 to 0.40. The remaining two slides involved soil with c/p ratios greater than 0.50. This range of c/p ratios (0.20 to 0.40) was considered reasonable for most marine soils. The seismic yield coefficients that were computed from Equation 6.13 are shown in Figure 6.6 for slope angles ranging from 0 to 20 degrees. A total unit weight of 95 pcf was assumed for the soil, and a unit weight of 64 pcf was assumed for seawater. Thus, the submerged unit weight of soil was 31 pcf. Most slides in the database

(334 slides) occurred on slopes flatter than about 10 degrees. This range of slope angles and the probable range of c/p ratios is represented by the shaded region in Figure 6.6. The seismic yield coefficients (k_y) for the shaded region are 0.13 or less. In the next section, the seismic conditions required to induce permanent deformation and possibly slope failure will be evaluated and compared with the seismic conditions from several slides in the database.

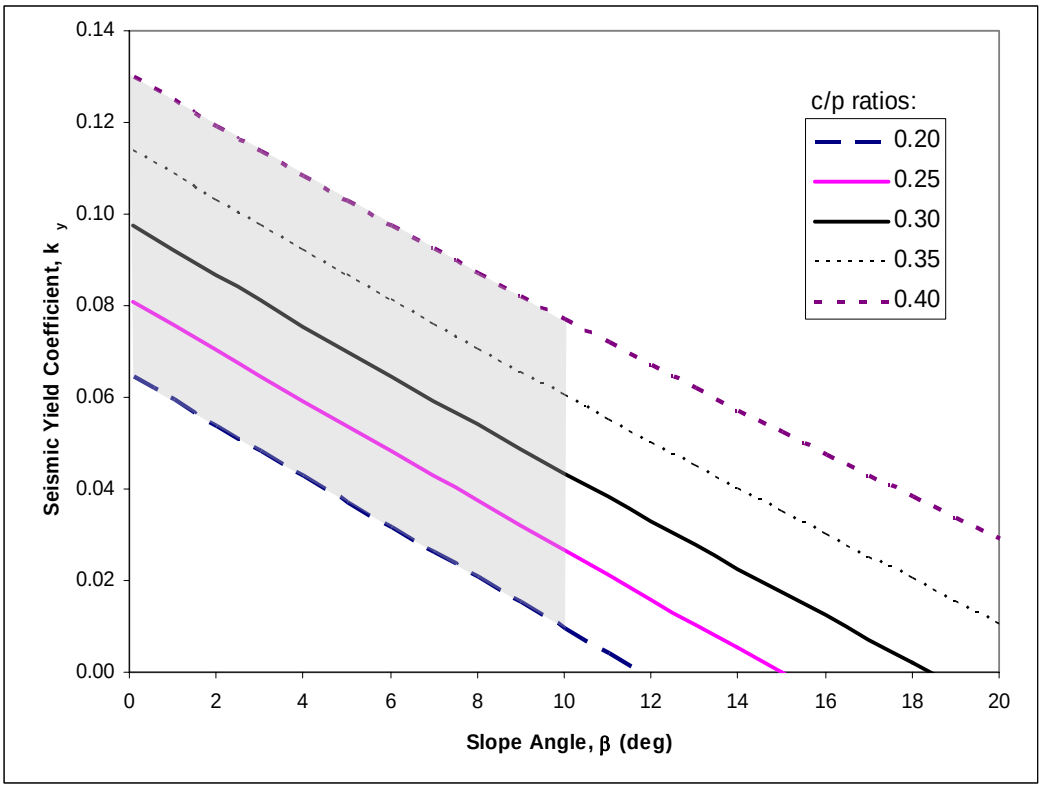

Figure 6.6. Seismic yield coefficients required for failure of a submerged infinite slope for various slope angles and c/p ratios.

6.4 CORRELATION OF RESULTS FROM PSEUDO-STATIC ANALYSES WITH SEISMICITY

In order to evaluate the feasibility of earthquakes as a trigger, a series of analyses of seismic conditions required to induce permanent deformations in a seafloor slope were conducted. The procedures used and results are presented in this section. Seismic loading can be represented by the maximum acceleration in a soil deposit, k_{max}, that is a function of the input ground motion and the geometry of the sliding mass. For this study, the input ground motion was assumed to be the peak ground acceleration in the underlying bedrock, PGA_{ROCK}, induced by an earthquake. The geometry of the sliding mass was assumed to be an "infinite" slope.

The Hynes and Franklin (1984) criterion was used as a conservative screening method for permanent displacements in a slope. The upper bound results from Hynes and Franklin's Newmark rigid sliding block analyses of 348 earthquake ground motions assuming one meter of displacement yielded a ratio of k_y to k_{max} (k_y/k_{max}) of about 0.17. Also, their criterion yielded an amplification factor, k_{max}/PGA_{ROCK}, of about 3.0, and resulted in a seismic yield coefficient of one half of the peak ground acceleration in rock, i.e. $k_y/PGA_{ROCK} = 0.17 * 3.0 \approx 0.5$. The pseudo-static analyses in Section 6.3 showed that the largest seismic yield coefficient (k_y) assuming probable conditions of shear strength and slope angle based on the database is about 0.13. Thus, PGA_{ROCK} values of at least 0.26

g would cause permanent deformation in a slope that has a seismic yield coefficient of 0.13 or less. To determine the seismic conditions required to produce these PGA_{ROCK} values (at least 0.26 g), the following analyses were performed.

6.4.1 ATTENUATION RELATIONSHIPS

The attenuation relationships developed by Abrahamson and Silva (1997) were used to determine specific seismic conditions of earthquake magnitude and distance between the earthquake (source) and the slope (site) that would induce a value of PGA_{ROCK} of at least 0.26 g. Abrahamson and Silva (1997) developed attenuation relationships for estimating peak ground accelerations based on the type of fault, earthquake magnitude, and distance between the source and site. These attenuation relationships were based on empirical site responses from a database of 655 recordings from 58 earthquakes. These attenuation relationships for estimating PGA_{ROCK} are generally consistent with other methods developed by Seed and Idriss (1982) and Boore, Joyner, and Fumal (1997).

From the attenuation relationships developed by Abrahamson and Silva (1997), a regression model was used to obtain PGA_{ROCK} as a function of earthquake magnitude and distance between the source and site. The value of PGA_{ROCK} was assumed by Abrahamson and Silva (1997) to be the spectral acceleration, S_a, at a period (time) of 0.01 seconds. The general function of the

regression model for calculating spectral acceleration at a period of 0.01 seconds, i.e. PGA_{ROCK}, is:

$$\ln S_a = f_1 \tag{6.14}$$

where S_a is the median value of spectral acceleration, and f_1 is the function of the attenuation of seismic accelerations recorded at rock sites. From Equation 6.14, spectral acceleration (S_a) can be computed as exp(f_1). The function, f_1 is expressed as:

$$f_1 = a_1 + a_2(M - c_1) + a_{12}(8.5 - M)^n + [a_3 + a_{13}(M - c_1)]\ln(R) \text{ for } M \le c_1 \tag{6.15}$$

where M is the dimensionless earthquake moment magnitude, which is approximately equal to the Richter local magnitude up to about M of 6 to 7 (Kramer, 1996). The variables a_1, a_2, a_3, a_{12}, a_{13}, c_1, and n in Equation 6.15 are functions of the time period, and are dimensionless. These variables are based on the empirical data from the database of earthquake ground motions compiled by Abrahamson and Silva (1997), and are known as regression coefficients. The quantity R in Equation 6.15 is given by:

$$R = \sqrt{r_{rup}^{\ 2} + c_4^{\ 2}} \tag{6.16}$$

where r_{rup} is the distance to fault rupture plane (km), and c_4 is a function of the time period, and is dimensionless. The regression coefficients for a period of 0.01 seconds were used to compute PGA_{ROCK}, and are summarized in Table 6.1.

Table 6.1. Regression coefficients (dimensionless) used to calculate PGA_{ROCK}.

Regression Coefficient	Value
a_1	1.640
a_2	0.512
a_3	-1.1450
a_{12}	0.0000
a_{13}	0.17
c_1	6.4
c_4	5.60
n	2

Values for PGA_{ROCK} were calculated for several earthquake magnitudes and distances (r_{rup}) using Equations 6.15 and 6.16, and these values are plotted in Figure 6.7. Earthquake magnitudes (M) shown in Figure 6.7 range from 4.5 to 6.4. Because all of the 58 earthquakes that Abrahamson and Silva (1997) used for developing their attenuation relationships had magnitudes greater than 4.5, a magnitude of 4.5 was used as the lower bound in Figure 6.7. The expression for f_1 in Equation 6.15 only applies to earthquakes with magnitudes less than or equal to 6.4. Thus, a magnitude of 6.4 was used as the upper bound. Logarithmic scales are used to accommodate the large range in values shown.

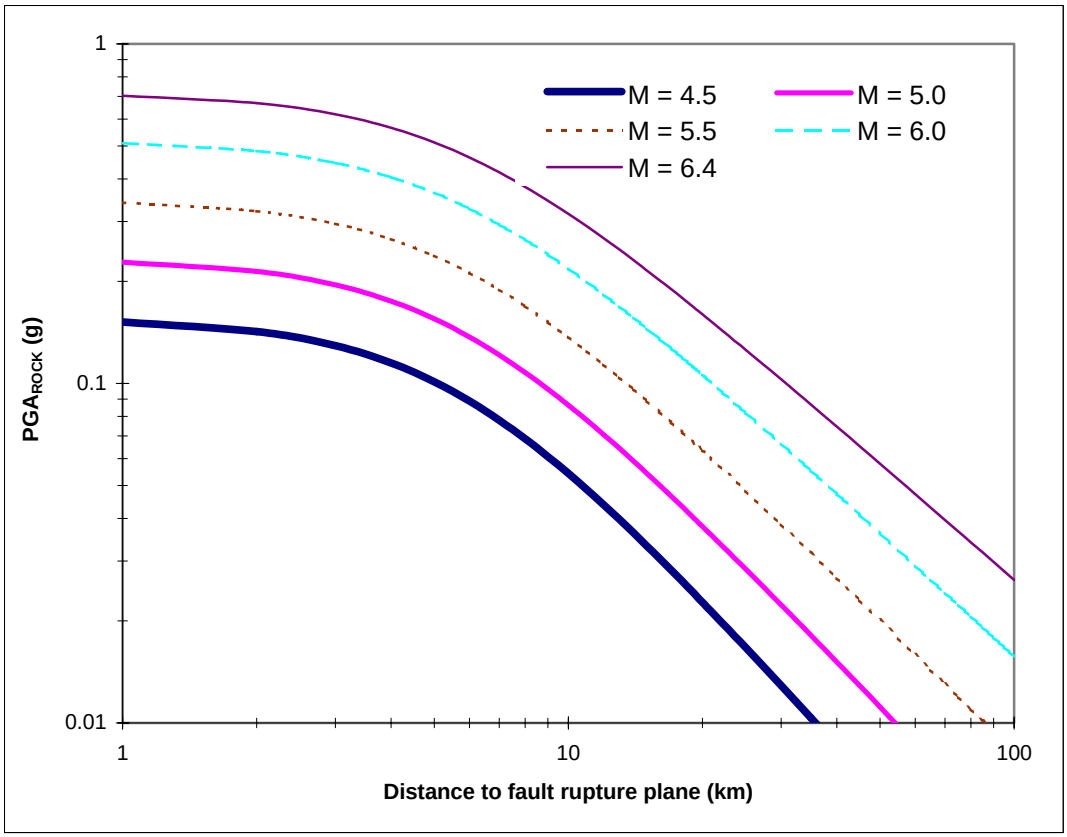

Figure 6.7. Median values of PGA_{ROCK} as a function of distance from site to fault rupture plane and earthquake moment magnitude (M) using attenuation relationships developed by Abrahamson and Silva (1997).

Referring to Figure 6.7, it can be seen that PGA_{ROCK} decreases as the distance from the source increases, and the earthquake magnitude decreases. Seismic conditions producing PGA_{ROCK} values of at least 0.26 g were calculated, and are summarized in Table 6.2. The seismic yield coefficient in Table 6.2 (k_y = 0.13) represents site conditions of an "infinite" slope inclined at greater than zero degrees and soil with a c/p ratio of 0.40. The slope angle and soil shear strength for a seismic yield coefficient of 0.13 were determined from results of the pseudo-

static analyses shown in Figure 6.6. Table 6.2 is a summary of the seismic conditions that would result in permanent deformations for any slope with a c/p ratio less than or equal to 0.40 and slopes inclined at any angle. This combination of soil shear strength ($c/p \leq 0.40$) and slope angle ($\beta > 0$ deg) represents many seafloor conditions because most seafloor slopes are inclined at these angles and most marine soils are normally consolidated to slightly overconsolidated, i.e. $0.20 \leq c/p \leq 0.40$. The PGA_{ROCK} value shown in Table 6.2 ($PGA_{ROCK} \geq 0.26$ g) is achieved when an earthquake has a magnitude of at least 5.5 and is located less than 12 km from the slope.

Table 6.2. Seismic conditions required to cause permanent deformation in a slope with $k_y = 0.13$ g.

$PGA_{ROCK} \geq 0.26$ g	
Maximum Distance, R (km)	**Earthquake Magnitude, M**
-	4.5
-	5.0
4	5.5
9	6.0
12	6.4

6.4.2 CORRELATION OF RESULTS FROM ATTENUATION RELATIONSHIPS WITH SEVERAL SLIDES IN THE DATABASE

There are a number of case histories from the database that cite earthquakes as a probably trigger, and among these case histories, there are four

that cite specific earthquake events (magnitude and/or distance) that may have caused slope failure. These four case histories are summarized in Table 6.3, and are compared to the results of earthquake magnitude and distance obtained from the attenuation relationships. Slope angles are also shown in Table 6.3.

Table 6.3. Case histories, where earthquakes are cited as a probable trigger, that include data for magnitude, distance, and seafloor slope angle.

Slide Name	M	R (km)	b (deg)	Reference
Klamath River delta (Northern California)	7.0	60	0.25	Field, 1993
San Mateo Point (Southern California)	6.0	45	3.0	Edwards et al., 1980
Mid to Northern California	San Andreas fault*	≤ 5	1.0 – 8.3	McAdoo et al., 2000
Point Arena area (Northern California)	San Andreas fault*	≤ 10 to 20	3.3	Richmond and Burdick, 1981

* San Andreas fault has high seismicity where there is a high probability of moderate magnitude (say, M ~ 5) earthquakes.

Referring to Table 6.3, the distance between earthquake source and site (R) range from a value less than 5 to 60 km. This range in distances falls within the range established from the attenuation relationships, i.e. R ≤ 12 km. The earthquake magnitudes noted for two slides shown in Table 6.3 are 6.0 and 7.0. The other two slides were probably triggered by the San Andreas fault, which is located within 20 km and where there is a high probability of moderate magnitude earthquakes (M ~ 5). The earthquake magnitudes, distances, and slope angles shown in Table 6.3 are similar to the values presented from the seismic analyses using the attenuation relationships. Based on reasonable agreement with these four case histories, the results of earthquake magnitude and distance required to

cause slope deformation and possible failure, which were obtained from the seismic analyses, are considered to be realistic.

6.5 CONCLUSIONS

The analyses of slope stability and seismicity presented in this chapter addressed the likelihood of slides being triggered by gravity, rapid sedimentation (underconsolidation), and earthquakes. Several conclusions can be drawn from the analyses:

1) It seems unlikely that most of the slope failures in the database in normally consolidated and overconsolidated soils were caused by gravity loads alone considering the slope angles and probable drained and undrained shear strengths.
2) Rapid sedimentation can produce underconsolidated soils with strengths low enough for gravity sliding to occur on slopes as flat as one degree, which includes many of the slopes in the database.
3) For slopes located less than about 12 km from an earthquake of magnitude 5.5 or greater, slope failures are likely to occur. These values of earthquake magnitude and distance are considered realistic because they are in reasonable agreement with four slides examined in the database.

Now that the cause of seafloor slope failure has been examined, mechanisms of slope movement after initial failure are addressed in the following chapters.

CHAPTER 7

HYDROPLANING MECHANISM

7.1 INTRODUCTION

Hydroplaning may explain why many submarine slides have the large runout distances that were shown in Chapter 5. Experimental evidence of hydroplaning has been presented by Mohrig et al. (1998, 1999), Harff et al. (1998), and Laval et al. (1988). This work is examined in this chapter, and where appropriate, results derived from the experimental studies are applied to slides in the database. In addition, a simple sliding block model was developed for this thesis, and is presented to illustrate how the conditions necessary for hydroplaning might be achieved.

7.2 DEFINITION OF HYDROPLANING

Hydroplaning occurs when a layer of fluid becomes entrapped between a sliding soil mass and the underlying soil. The layer of fluid significantly reduces the resistance between the moving soil mass and the underlying soil.

When a subaqueous flow advances through a body of water, a fluid pressure in excess of hydrostatic pressure is induced at the front of the sliding mass by the moving body as shown in Figure 7.1. A measure of the pressure is the fluid stagnation pressure, p_f, which is expressed as:

$$p_f = \frac{\rho_w v^2}{2} \tag{7.1}$$

where ρ_w is the mass density of water (1.94 slugs/ft^3 ≅ 1.00 x 10^3 kg/m^3), and v is the velocity of the sliding mass. This fluid pressure is hydrodynamic and depends on the velocity of the sliding mass. The excess fluid pressure developed on a moving soil mass acts from the stagnation point, shown as "s" in Figure 7.1, down to the supporting surface of the slide mass. The fluid pressure is resisted by an equivalent downward normal stress, p_d, produced by the submerged weight of the slide mass on the slope. The downward normal stress is related to a pressure, p_d, expressed as:

$$p_d = (\rho_d - \rho_w) g h_a \cos\beta \tag{7.2}$$

where ρ_d is the total mass density of the soil, and g is the acceleration due to gravity (32.2 ft/s^2 ≅ 9.8 m/s^2). The term h_a represents the average slide thickness, and β is the slope angle.

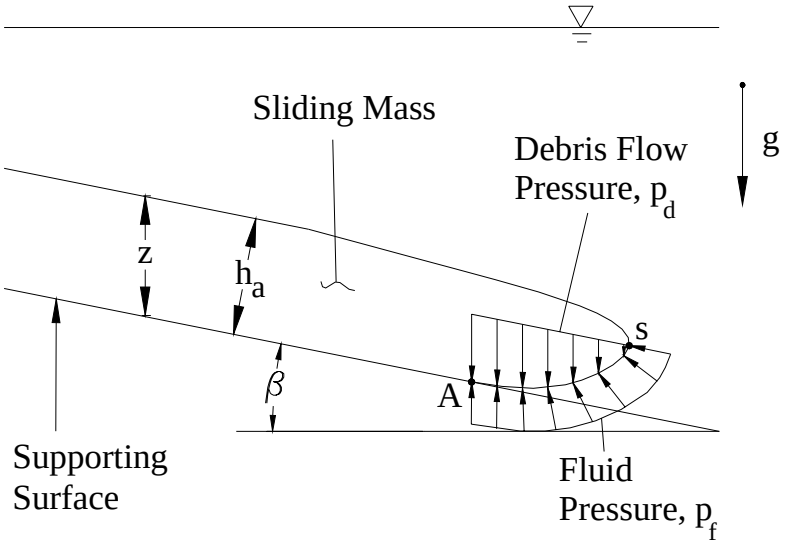

Figure 7.1. Fluid and debris flow pressures that are generated at the front of a sliding mass. "s" indicates stagnation point, above which there are no hydrodynamic pressures. "A" is the location where hydroplaning is initiated.

Hydroplaning occurs when the hydrodynamic pressure, which is proportional to p_f, exceeds the downward normal stress, which is related to p_d. The point at which hydroplaning is initiated is labeled as "A" in Figure 7.1.

7.3 OVERVIEW OF PAST EXPERIMENTS

Mohrig et al. (1998, 1999), Harff et al. (1998), and Laval et al. (1988) performed experiments to study hydroplaning of subaqueous slides. Mohrig et al. performed two sets of experiments (1998, 1999). Both experiments were performed on soil submerged in water where the soil moved down an inclined channel, thus creating subaqueous landslides or debris flows that were confined

by the sidewalls of the channel. Harff et al. (1998) performed unconfined flow experiments where soil submerged in water slid down an inclined channel and exited into a tank, simulating a debris flow exiting a submarine canyon onto an open slope. Harff et al. (1998) inferred that hydroplaning of subaqueous slides occurred because their observations were consistent with Mohrig et al.'s (1998, 1999) observations of slides where hydroplaning was actually observed. Mohrig et al.'s and Harff et al.'s observations will be described later in this chapter. Laval et al. (1988) performed experiments with sandy soil that was submerged in water. In Laval et al.'s experiments, the soil was allowed to flow down an inclined channel and resulted in subaqueous turbidity currents that were confined by the sidewalls of the channel. Laval et al.'s (1988) experiments were carried out with low density "sand flows" using various water-saline solutions, where the density of the sand was only about 1.2 to 1.3 times the density of water. Laval et al. observed a thin layer of fluid trapped between the advancing "sand flow" and the channel, and concluded that the flowing mass was hydroplaning.

Mohrig et al.'s (1998, 1999) experiments provide the most compelling and comprehensive support of hydroplaning among all of these experiments. In the following sections, their work is examined and their results are applied to data for the submarine slides in the database.

7.4 MOHRIG ET AL.'S (1998, 1999) EXPERIMENTS

The experiments of Mohrig et al. (1998, 1999) are summarized in this section. The discussion includes description of their apparatus, soil conditions, measurements, results, observations of hydroplaning, and general characteristics of slides where hydroplaning occurs.

7.4.1 APPARATUS

The setup for Mohrig et al.'s (1998, 1999) two sets of experiments consisted of a glass-walled tank that was 10 m long, 3 m high and 0.6 m wide. A rectangular channel, 0.2 m in width, was suspended in the tank as shown schematically by the cross-section in Figure 7.2. The soil was continuously mixed in a "head tank", and then fed into the channel through a "debris feed point" as shown in Figures 7.2 and 7.3. The tank was referred to as a "head tank" because it was located at the entrance to the channel.

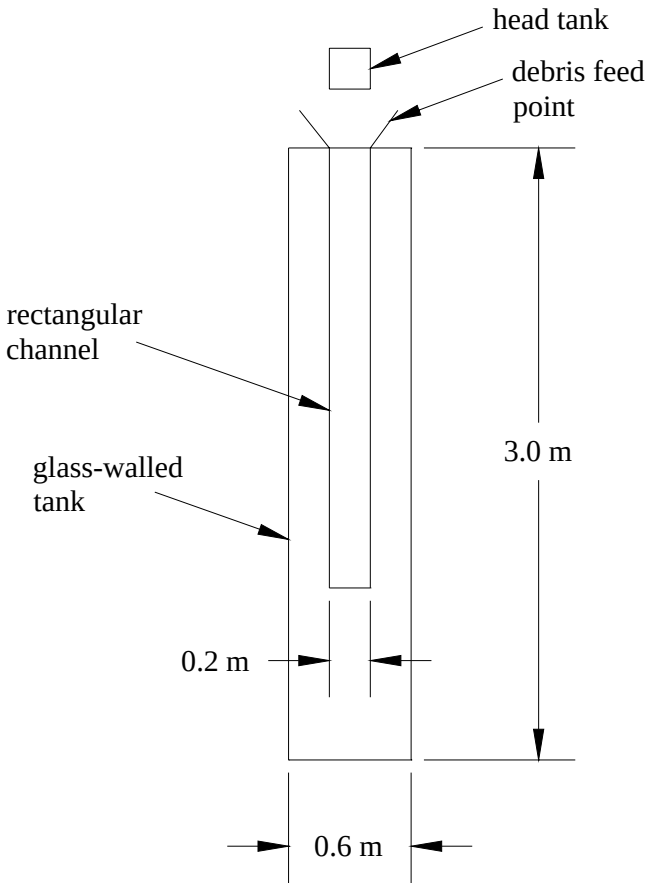

Figure 7.2. Cross section (A-A´) of experimental apparatus used by Mohrig et al. (1998, 1999).

A profile view of the experimental facility is shown in Figure 7.3. The channel had two segments and was fabricated so that each segment could be inclined at different angles. The lengths of the upper and lower segments were 5.7 m and 4.3 m, respectively. There was a gap located between the upper and lower segments so that the debris flow, which moved as a fluid-like mass, could exit the channel through a vent, as shown in Figure 7.3. A second vent was

located at the end of the lower segment so any turbidity current, which formed as suspended sediment above the slide mass, could exit the channel. All experiments were conducted with fresh water, rather than seawater.

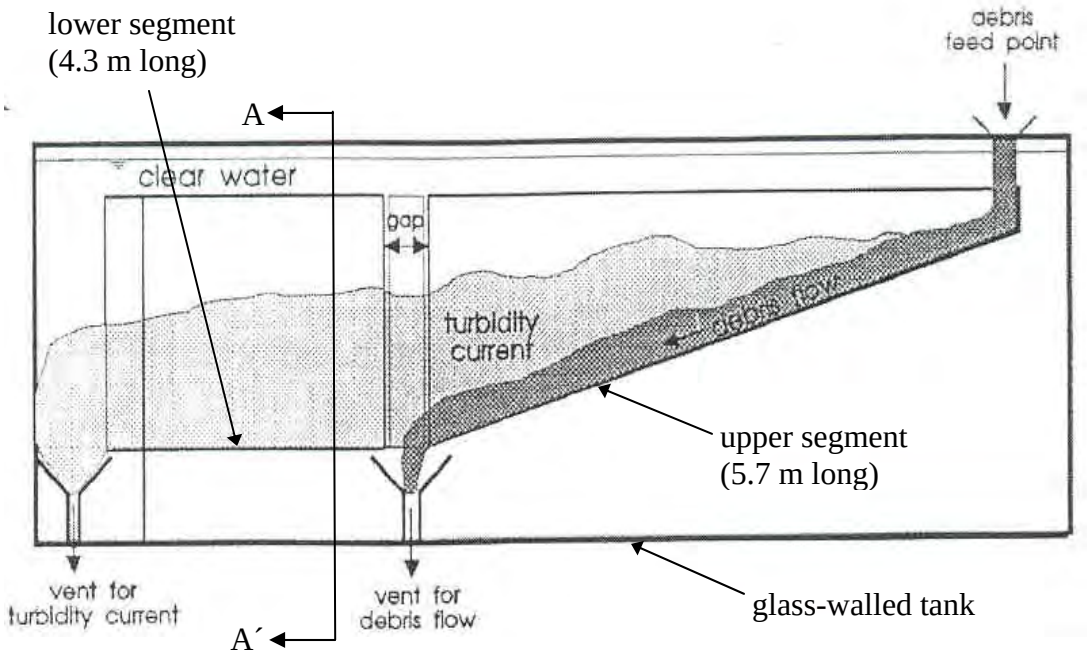

Figure 7.3. Setup (profile view) for Mohrig et al.'s (1998, 1999) experiments (modified from Mohrig et al., 1998).

The first series of tests by Mohrig and his colleagues was reported on in 1998. In these "1998" tests, the debris flows were released into the channel, and the bottom of the channel consisted of a rough, non-erodible rubber matting, i.e. a "hard" bottom.

The second series of tests by Mohrig and his colleagues was reported on in 1999. These "1999" tests were performed using two different conditions for the bottom of the channel: a "hard" bottom that, again, consisted of a rough, non-

erodible rubber matting, and a “soft” bottom that consisted of soil. For the tests with a “soft” bottom, the soil was formed on the bottom of the channel in the tank with no water by feeding soil down the channel from the “debris feed point”. The tank was then filled with fresh water slowly enough to prevent any disturbance of the soil bottom. A water-soluble dye was added to the soil representing the slide debris to distinguish the slide mass from the existing “soft bottom” soil, which had no dye. Cores were taken to determine thicknesses of the slide and the soil bottom. The procedures described for tests with a “soft” bottom were not necessary for the tests with a “hard bottom”.

7.4.2 SOIL

Grain size distribution curves for soils used in the 1998 and 1999 experiments are shown in Figure 7.4. A mixture of 55 percent silt, 45 percent sand, and no clay was used in the 1998 experiments. According to the American Society of Testing and Materials (ASTM), this soil mixture classifies as sandy silt (ML or MH). A mixture of 40 percent clay, 35 percent silt, and 25 percent sand was used in the 1999 experiments. This soil classifies as a silty clay (CL or CH).

Hydraulic conductivities (K) for the soils tested were estimated by Mohrig et al. (1998, 1999) from grain size distributions. For the sandy silt soil in the 1998 experiments, K was estimated to be 3×10^{-3} cm/s. For the silty clay soil in the 1999 experiments, K was estimated to be 1×10^{-5} cm/s. All soil used in the

tests was deposited as a slurry after being mixed in the head tank prior to being released into the channel. The soil was not compacted or densified, and no time was allowed for consolidation. The gravimetric water content of the soil was measured in the head tank prior to being released in the channel. The water content of the soil for the 1998 experiments was 16.5 percent, and was 39 percent for the 1999 experiments.

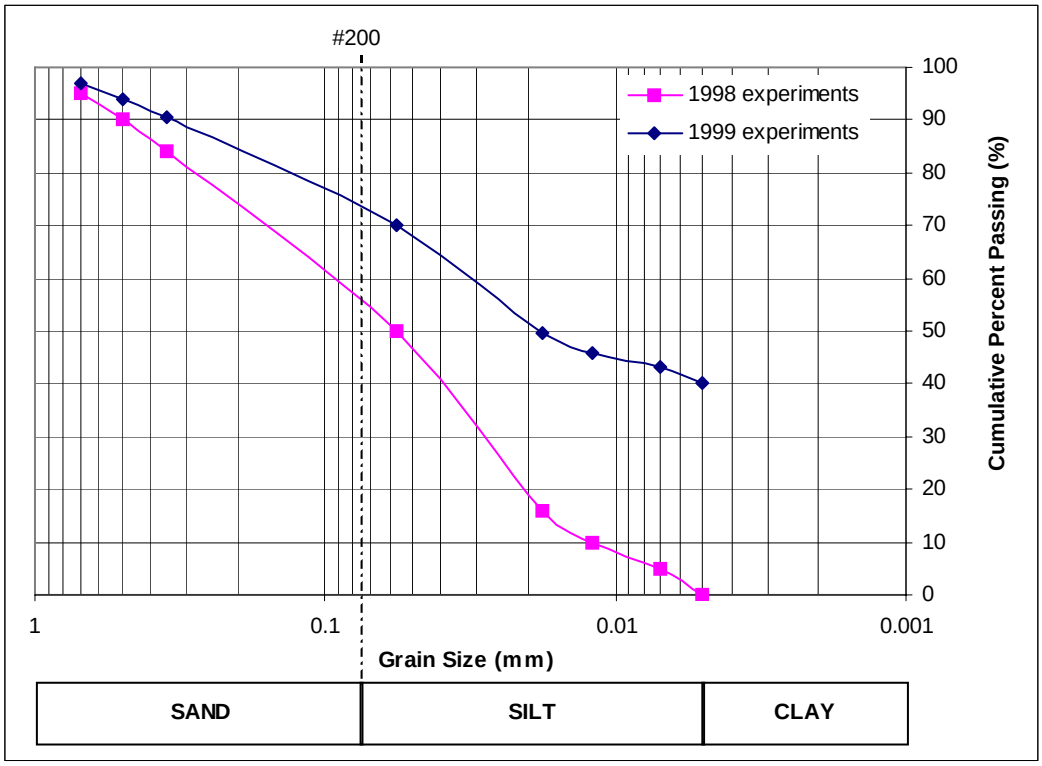

Figure 7.4. Grain size distributions for soil used in the experiments (obtained from dry weight and particle size data presented in Mohrig et al. 1998, 1999).

The dye that was used in the 1999 tests affected the consistency and rheology of the slurry. Accordingly, three consistencies of slurry were observed

and described. Mohrig et al. described these as “sticky”, “medium” and “runny”. The slurry described as “sticky” had the least amount of dye, and had the highest yield strength, τ_y, and viscosity, μ_s. The slurry described as “medium” had a moderate amount of dye, and a lower yield strength and viscosity than the “sticky” slurry. The slurry described as “runny” had the most amount of dye, and the lowest yield strength and viscosity.

7.4.3 MEASUREMENTS

For the 1998 and 1999 series of tests, slope angles of the channel segments were measured. For the 1998 tests, the upper segment was inclined at angles ranging from 1 to 20 degrees, and the lower segment was horizontal. For the 1999 tests, the upper segment was fixed at 6 degrees, and the lower segment was inclined at 1 degree.

For both tests (1998, 1999), video cameras recorded the slide motion. For the 1998 tests, a single video camera was attached to a moving carriage and followed the slide as it moved down the channel. For the 1999 tests, eight fixed video cameras were used, with each camera mounted on one of the eight panels of glass that made up the outer tank. Analysis of the video camera recordings allowed velocities to be determined. The “frontal” or “head” velocity represented the velocity at the front of the debris flow.

The average slide thickness along the 5.7 m upper segment of the channel was designated as h_a for the 1998 tests, and h_6 for the 1999 tests. The thickness of the front of the slide mass was labeled as h_h. The thicknesses (h_a, h_6, and h_h) were determined from analysis of the videotapes. For the tests with a "soft" bottom performed in 1999, the average slide thickness (h_6) was also measured with a meter stick. This thickness (h_6) was the thickness of the entire soil (slide debris plus "soft" bottom) minus the thickness of the "soft" bottom soil.

For the 1998 experiments, the typical volume of soil released during a test was approximately 0.16 m^3 (5.65 ft^3), taking about 60 seconds to flow from the head tank. A load cell measured the change of weight of soil in the head tank with time as the soil flowed into the channel. From these weight measurements, changes in volume of soil were calculated. The volumetric rate of soil discharged into the channel, Q_d, was averaged over the time required for the debris flow to travel the length of the upper segment of the channel, and was reported. For the 1999 experiments, approximately 0.03 m^3 (1.06 ft^3) of soil was released from the head gate, taking about 3.5 to 5 seconds to flow. The height of this soil in the head tank was measured with a sonic profiler versus time, and from these measurements, changes in volume were calculated. For the 1998 and 1999 tests, the total soil density, ρ_d, was measured for the slurry in the head tank and was assumed to be the same when deposited on the slope.

7.4.4 RESULTS

Results for ten of the 1998 tests were reported by Mohrig et al. (1998), and are summarized in Table 7.1. The results in Table 7.1 include the test number, slope angle, total dry density of the soil, average rate of volume discharge, average slide thickness, debris head thickness, front velocity, and "characteristic average velocity". The characteristic average velocity, v_*, of the slide is defined as the velocity at which the debris is supplied to the channel, and is expressed as:

$$v_* = \frac{Q_d}{Wh_a} \tag{7.3}$$

where W is the width of the channel in meters, h_a is the average slide thickness in millimeters, and Q_d is the average volumetric rate of soil discharged into the channel (l/s).

Table 7.1. Experimental results of sandy silt slurry (Mohrig et al., 1998).*

Test No.	β (deg)	ρ_d (x 10^3 kg/m^3)	Q_d (l/s)	h_a (mm)	h_h (mm)	v (m/s)	v_* (m/s)
2	20.0	2.10	1.4	37	---	0.179	0.19
5	16.0	2.10	3.6	48	93	0.861	0.37
6	16.0	2.10	2.6	41	75	0.776	0.31
9	15.5	2.11	10.3	55	154	1.24	0.92
11	4.9	2.06	5.31	53	73	0.743	0.49
12	4.9	2.06	3.82	58	63	0.589	0.32
13	4.9	2.06	2.46	52	40	0.326	0.23
14	6.0	2.06	6.89	54	72	0.776	0.63
15	1.0	2.06	2	67	---	0.139	0.15
17	6.0	2.05	3.56	44	71	0.732	0.40

* Yield strength (τ_y) and viscosity (μ_s) were estimated for the slurry to be 29 Pa and 13 Pa s, respectively.

Results for five of the 1999 tests were reported in Mohrig et al. (1999), and are summarized in Table 7.2. The results include the test number, slope angle, total dry density of the soil (slurry), average rate of volume discharge, average slide thickness, and front velocity. The viscosity, yield strength and rheology (consistency) of the slurry are also included in Table 7.2.

Table 7.2. Experimental results of silty clay slurry (Mohrig et al., 1999).

Test No.	β (deg)	ρ_d (x 10^3 kg/m^3)	Q_d (l/s)	h_6 (mm)	v (m/s) **	μ_s (Pa*s)	τ_y (Pa)	Rheology/ Consistency
1*	6.0	1.59	---	18	0.616	0.035	49	Sticky
2*	6.0	1.59	9.1	18	0.645	0.035	49	Sticky
3*	6.0	1.59	8.3	16	0.605	0.023	36	Medium
4+	6.0	1.59	---	6.5	0.481	0.035	49	Sticky
5+	6.0	1.60	6.4	16	0.625	0.019	33	Runny

* Test performed on 'hard' bottom (rubber matting)
+ Test performed on "soft" bottom (existing soil deposit)
** Velocities (v) were reported for the location halfway down the length of the upper segment, i.e. 2.85 m downslope from head tank.

7.4.5 DIRECT OBSERVATION OF HYDROPLANING

In a number of tests performed by Mohrig et al. (1998, 1999) a thin layer of fluid was observed being entrapped between the sliding soil mass and underlying surface. The occurrence of this water layer was considered to be evidence of hydroplaning. Evidence of entrapped water and hydroplaning was observed in all tests with the exception of tests 2 and 15 in the 1998 test series.

7.4.6 CHARACTERISTICS OF SLIDES WHERE HYDROPLANING OCCURRED

When hydroplaning occurred, Mohrig et al. (1998, 1999) observed several characteristics. When hydroplaning occurred, the front of the slide mass, i.e. the debris head, was typically deformed. Mohrig et al. (1998) hypothesized that this deformation of the debris head was due to large fluid (hydrodynamic) pressures associated with hydroplaning. Profiles of debris flows where hydroplaning did and did not occur in the 1998 tests are shown in Figure 7.5. An extreme case of deformation of the debris head is shown in Figure 7.5(c) where the debris head thickness, h_h, was 2 to 3 times the average slide thickness, h_a. The debris head thickness (h_h) was greater than the average slide thickness (h_a) in tests 5, 6, 9, 11, 12, 14 and 17 of the 1998 test series. These tests represent 7 of the 8 tests performed in 1998 where hydroplaning occurred. Slides from tests 2 and 15,

where hydroplaning did not occur, did not experience deformation of the debris head.

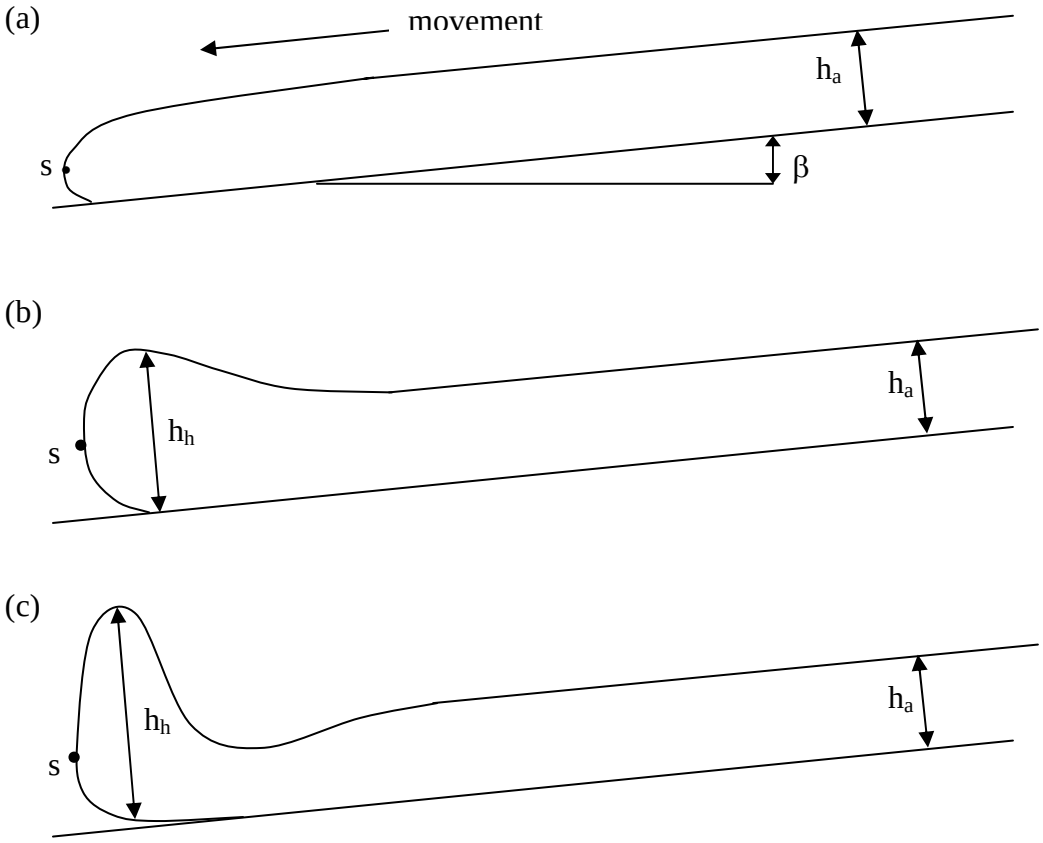

Figure 7.5. Observed debris flow profiles from the experimental subaqueous runs. The average thickness of the flow in the channel is h_a. The thickness of the debris flow head is h_h, and s is the theoretical location where the hydrodynamic pressures are stagnant. (a) A non-hydroplaning debris flow. (b) A debris flow on the verge of hydroplaning where hydrodynamic pressures have begun to deform the head of the flow. (c) A hydroplaning debris flow where a layer of fluid is observed underneath the head (Mohrig et al., 1998).

Only test 4 and 5 in the 1999 experiment had a "soft" channel bottom. Slides in tests 4 and 5 entrapped fluid between the slide and the underlying soil and hydroplaned. The soil bottom in both of these tests was not mobilized by the

passing debris flows, i.e. the existing soil deposits were not disturbed by the slides. Mohrig et al. hypothesized that the thin layer of water prevented significant shear stresses and corresponding strains from being transmitted to the seafloor.

Among all of the slides where hydroplaning occurred in the 1998 test series (tests 5, 6, 9, 11, 12, 13, 14 and 17), the frontal velocities (v) exceeded the calculated characteristic average velocities (v_*) as shown in Table 7.1. Slides in tests 2 and 15, which did not entrap fluid between the slide and the underlying soil and, thus, where hydroplaning did not occur, had frontal velocities that were less than the calculated characteristic average velocities.

For the 1999 experiments, the frontal velocity of the slide was plotted versus downslope distance from the head gate, and is shown in Figure 7.6. The channel bottom condition for each test ("soft" or "hard"), the slurry consistency ("sticky", "medium", or "runny"), and the slope angles of the upper and lower segments of the channel are also shown in Figure 7.6. Runout distances of the five tests were about the same, regardless of the differing channel bottom ("soft" versus "hard") and slurry consistencies. Frontal velocities from the five tests are approximately constant beginning about 2 m downslope from the head gate, and remain so until the bottom slope angle changes about 6 m downslope, regardless of the channel bottom ("soft" versus "hard") and slurry consistency. The velocities are similar, becoming about 55 to 60 cm/s at the end of the 6 deg slope.

Mohrig et al. (1999) hypothesized that the thin layer of water entrapped due to hydroplaning accounted for the very similar velocity profiles and runout distances among the five slides that have different soil and channel bottom conditions. Thus, Mohrig et al. (1999) also hypothesized that hydroplaning is a mechanism for large runout distances that is independent of rheology.

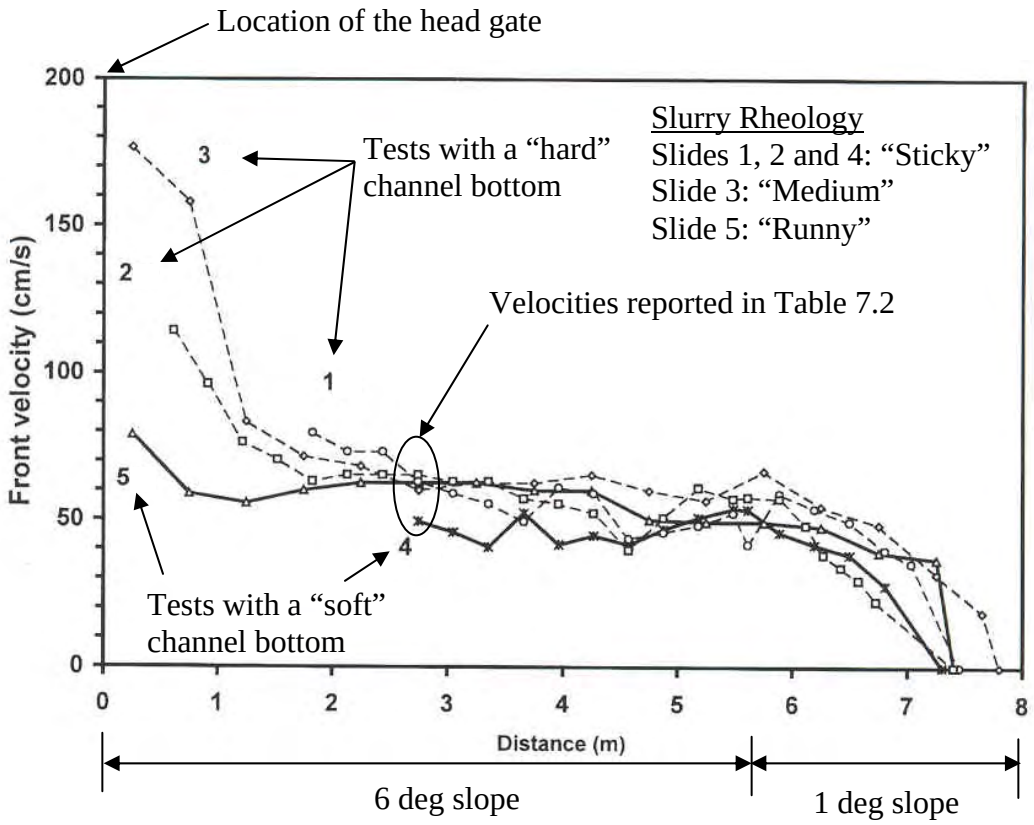

Figure 7.6. Velocity of the front of slide versus downslope distance for the Mohrig et al. (1999) experiments. Bottom of channel conditions, slurry rheology, and location of velocities reported in Table 7.2 are also noted (modified from Mohrig et al., 1999).

7.5 HYPOTHESIS OF HYDROPLANING OF SEAFLOOR SLIDES BASED ON GEOPHYSICAL IMAGERY

For a slide where hydroplaning occurs, the head of the debris flow can deform, as was shown in Figure 7.5 (c). Mohrig et al. (1998) and Harff et al. (1998) observed in the laboratory an extreme case of the profile illustrated in Figure 7.5 (c), where the debris head actually becomes completely detached from the rest of the flow. Mohrig et al. and Harff et al. hypothesized that the head of the debris flow becomes detached due to the large hydrodynamic pressures associated with hydroplaning, and the detached head then accelerates on the entrapped layer of fluid ahead of the remainder of the debris flow. There is also natural landslide evidence to support separation and detachment of a debris flow like those observed in the laboratory. Two seafloor slides, Alika debris avalanche in Hawaii (Lipman et al., 1988; Normark et al., 1993) and Kitimat Inlet in British Columbia (Prior et al., 1984; Johns et al., 1986), provide examples where the head of a debris flow detached from the rest of the flow. A three-dimensional illustration of the Kitimat Inlet landslide is shown in Figure 7.7. In this figure, blocks of sediment, labeled as outrunner blocks, are shown at the furthest downslope location in the mass movement. Prior et al. (1984) hypothesized that the outrunner blocks are heads of debris flows that detached from the rest of the flows due to hydroplaning.

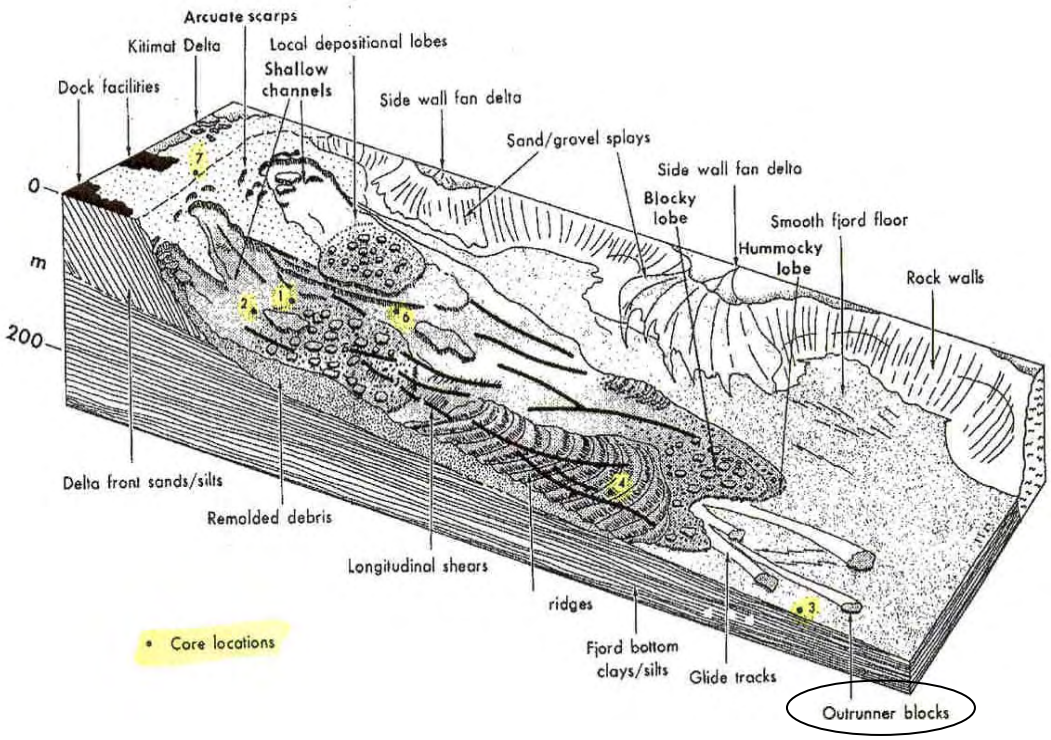

Figure 7.7. Interpretive three-dimensional image of the Kitimat Inlet landslide in British Columbia (Prior et al., 1984). The outrunner blocks are hypothesized to be heads of debris flows that detached from the rest of the flows due to hydroplaning.

7.6 DENSIMETRIC FROUDE NUMBER: INDICATOR OF HYDROPLANING BASED ON EXPERIMENTAL RESULTS

Mohrig et al. (1998) observed that there was a relationship between the "densimetric Froude number", Fr_d, and the occurrence of hydroplaning. The densimetric Froude number is a dimensionless parameter that has been used to characterize gravity-dominated flow involving two "liquids" of slightly different densities, and is expressed as:

$$Fr_d = \frac{v}{\sqrt{gL\left(\frac{\Delta\rho}{\rho}\right)}} \tag{7.4}$$

where $\Delta\rho$ is the difference in density between the two fluids, ρ is the density of one of the fluids, and L is the downslope distance traveled. Using the variables from their experiments, Mohrig et al. (1998) modified Equation 7.4 to the form:

$$Fr_d = \frac{v}{\sqrt{\left(gh_a \cos\beta\right)\left(\frac{\rho_d}{\rho_w} - 1\right)}} \tag{7.5}$$

Mohrig et al. (1998, 1999) calculated densimetric Froude numbers for their tests. The results are summarized in Table 7.3 in order of increasing densimetric Froude number, and are presented along with the experimental parameters used for the calculations.

Table 7.3. Calculated densimetric Froude numbers based on experimental measurements.

Test No.	β (deg)	ρ_d (x 10^3 kg/m^3)	h_a (mm)	v (m/s)	Fr_d
15*	1	2.06	67	0.139	0.17
2*	20	2.1	37	0.179	0.29
13*	4.9	2.06	52	0.326	0.44
12*	4.9	2.06	58	0.589	0.76
11*	4.9	2.06	53	0.743	1
14*	6	2.06	54	0.776	1
17*	6	2.05	44	0.732	1.1
5*	16	2.1	48	0.861	1.2
6*	16	2.1	41	0.776	1.2
9*	15.5	2.11	55	1.24	1.6
1**	6	1.59	18	0.616	1.9
3**	6	1.59	16	0.605	1.98
2**	6	1.59	18	0.645	1.99
5**	6	1.6	16	0.625	2.04
4**	6	1.59	6.5	0.481	2.47

* Mohrig et al. (1998) experiment
** Mohrig et al. (1999) experiment

Hydroplaning occurred in all tests except tests 2 and 15, which are shaded in Table 7.3, where a thin layer of fluid was not observed between the slide mass and underlying surface. The highest value of Fr_d for the slides where hydroplaning did not occur was 0.29, calculated for test 2. The lowest value of Fr_d for the slides where hydroplaning did occur was 0.44, calculated for test 13. Based on the results of tests 2 and 13, Mohrig et al. (1998) concluded that a minimum densimetric Froude number in the range of 0.30 to 0.40 was required for hydroplaning.

Mohrig et al. (1998) state that "instigation of hydroplaning…is suitably characterized by the densimetric Froude number". As part of this thesis, the fluid

stagnation pressure (p_f) and the average debris normal stress (p_d) were examined to determine how these quantities compare to Mohrig et al.'s densimetric Froude number criterion. By squaring both sides of Equation 7.5 and then multiplying the numerator and denominator on the right hand side by ρ_w, Equation 7.5 can be written as:

$$Fr_d^{\,2} = \frac{\rho_w v^2}{g h_a \cos\beta(\rho_d - \rho_w)} \tag{7.6}$$

Introducing Equations 7.1 ($p_f = 0.5\rho_w v^2$) and 7.2 ($p_d = gh_a\cos\beta(\rho_d - \rho_w)$) into Equation 7.6, the densimetric Froude number can be expressed in terms of the fluid stagnation pressure (p_f) and an average debris normal stress (p_d) as:

$$Fr_d = \sqrt{2\left(\frac{p_f}{p_d}\right)} \tag{7.7}$$

From Equation 7.7, it can be seen that the densimetric Froude number represents a ratio between p_d and p_f. Thus, one would expect that there is a general relationship between Froude number and when hydroplaning occurs for submarine landslides. Referring to Equation 7.7, a densimetric Froude number of 0.3 represents a fluid stagnation pressure (p_f) of about 5 percent the average debris normal pressure (p_d), while a densimetric Froude number of 0.4 corresponds to a value of p_f that is about 8 percent the value of p_d. Fluid stagnation pressures (p_f) and average debris normal pressures (p_d) were calculated based on the densimetric Froude numbers calculated by Mohrig et al. and are

shown in Table 7.4. The calculations summarized in Table 7.4 emphasize that hydroplaning occurs when the hydrodynamic pressure, which is proportional to p_f, exceeds the downward normal stress, which is related to p_d.

Table 7.4. Calculations of fluid stagnation pressures (p_f) and average debris normal pressures (p_d).

Test No.	Hydroplaning observed?	Fr_d	p_f (Pa)	p_d (Pa)	p_f/p_d (%)
15*	NO	0.17	120	696	17
2*	NO	0.29	16	375	4
13*	YES	0.44	53	538	10
12*	YES	0.76	173	600	29
11*	YES	1	276	549	50
14*	YES	1	301	558	54
17*	YES	1.1	268	450	60
5*	YES	1.2	371	497	75
6*	YES	1.2	301	425	71
9*	YES	1.6	769	576	133
1**	YES	1.9	190	104	183
3**	YES	1.98	183	92	199
2**	YES	1.99	208	104	200
5**	YES	2.04	195	93	210
4**	YES	2.47	116	37	314

* Mohrig et al. (1998) experiment
** Mohrig et al. (1999) experiment

7.7 DENSIMETRIC FROUDE NUMBERS CALCULATED FOR SEAFLOOR SLIDES

Mohrig et al.'s experiments as well as theoretical considerations indicate that the densimetric Froude number is a useful measure of when hydroplaning occurs in the laboratory. There is also sufficient information on several of the slides in the database to allow densimetric Froude numbers to be calculated. This

research effort involved examining the relationship between densimetric Froude number and hydroplaning (slide runout distances) for several seafloor slides.

Sufficient data were available to permit densimetric Froude numbers to be calculated for six of the slides in the database. Mohrig et al. (1998) calculated the densimetric Froude number for five of the six slides. The calculated densimetric Froude numbers and associated values of slope angle, thickness, and velocity used for the calculations are summarized in Table 7.5. In all cases the velocities that were reported for the case histories were based on observed damage to submarine cables. For these case histories the cables were broken at known times and locations, and velocities of the seafloor slides were then inferred. Also, slide runout distances were not included in Mohrig et al. (1998), but were obtained from the database. Runout distances are shown in Table 7.5 for comparison with the calculated densimetric Froude numbers. The densimetric Froude numbers range from 0.19 to 1.68. Based on Mohrig et al.'s (1998) criterion for hydroplaning, that densimetric Froude numbers be at least 0.30 to 0.40, hydroplaning should have occurred for five of the six landslides shown in Table 7.5. Also, the five slides where hydroplaning probably occurred had large runout distances (> 20 km) and occurred on flat slopes as shown in Table 7.5. For the one slide (Sandnessjoen slide) where the calculated Fr_d number (0.19) was less than the threshold value required for hydroplaning, hydroplaning probably did not occur due to the small runout distance and low Fr_d number. It can be seen in

Table 7.5 that the runout distance for this slide is much less than the runout distance for the other slides.

Table 7.5. Submarine slide case histories with calculated densimetric Froude numbers (Mohrig et al., 1998 with the exception of the slide in Suva, Fiji).

Slide Number	Landslide	β (deg)	h (m)	v (m/s)	Runout distance (km)	Fr_d
80	Sandnessjoen	5	2	0.7	1.2	0.19
78*	Suva, Fiji	3	30	4.47	113	0.31
57	Orkdalsford	5	10	2.6	22.5	0.31
70	Messina	3	20	6	220	0.51
10	Grand Banks	3	50	27.4	> 750	1.47
71	Orleansville	15	20	19.5	110	1.68

* indicates slide was not considered by Mohrig et al. (1998).
Note: The total soil density (ρ_d) used to calculate the densimetric Froude numbers was assumed to be 1.71 x 10^3 kg/m^3 according to Mohrig et al. (1998). The runout distances reported above were not included in Table 2 of Mohrig et al. (1998).

As part of this thesis, runout distances from Table 7.5 are plotted in Figure 7.8 versus the calculated densimetric Froude number to examine the relationship between the two quantities. Runout distances are plotted on a logarithmic scale because of the large range in distances, which spans over 2.5 orders of magnitude. The shaded region in Figure 7.8 illustrates the range in minimum Froude numbers that Mohrig et al. (1998) suggest are required for hydroplaning. Runout distance tends to increase with an increase in densimetric Froude number. Once the calculated densimetric Froude number meets the criterion for hydroplaning suggested by Mohrig et al. (shaded region), there is a significant increase in

runout distance. Also, the runout distance can be highly variable, ranging almost 1.5 orders of magnitude.

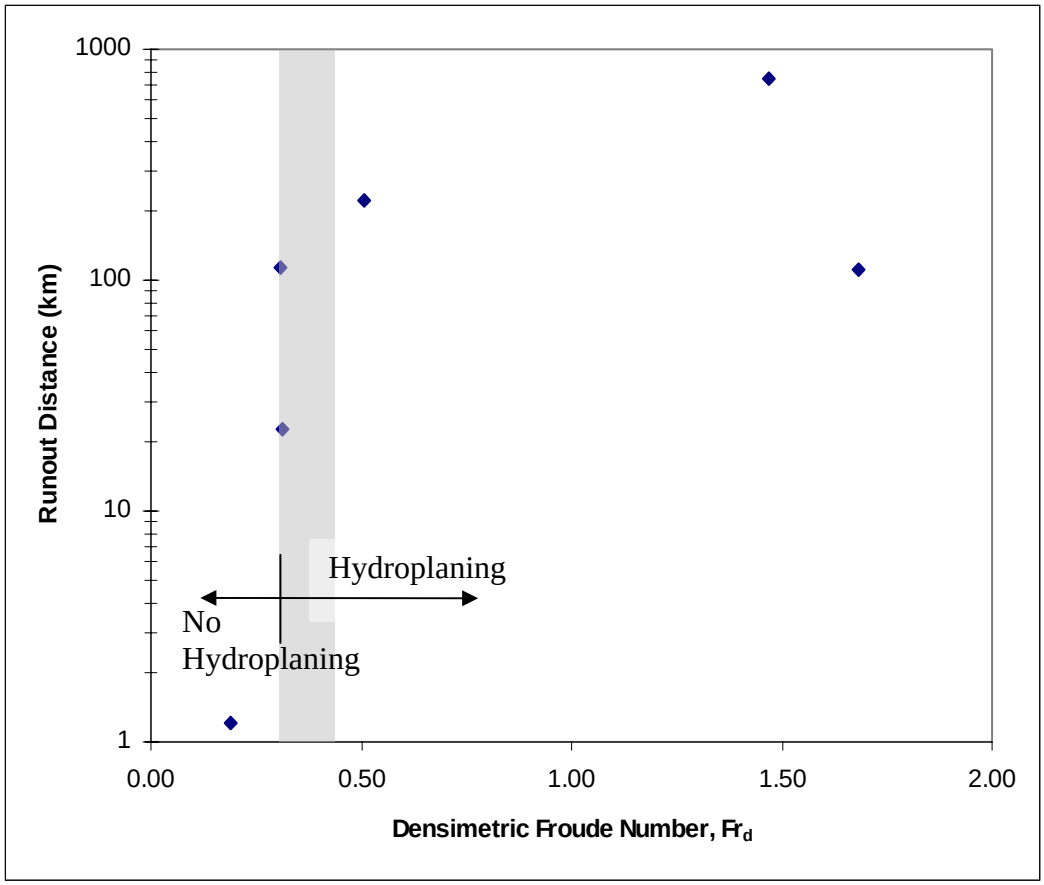

Figure 7.8. Calculated densimetric Froude numbers versus runout distance based on six seafloor slides from the database. Shaded region indicates Froude number criterion (Fr_d of 0.30 to 0.40) for hydroplaning suggested by Mohrig et al. (1998).

7.8 SLIDES FROM THE DATABASE THAT MAY HAVE HYDROPLANED

Four of the five slides examined in the previous section are believed to have hydroplaned based on the calculated densimetric Froude numbers and the large runout distances (>20 km) that were achieved on flat slopes (< 5 deg). The

fifth slide (at Orleansville) occurred on a slope inclined at 15 degrees. The characteristics of runout distance (>20 km) and slope angle (< 5 deg) for the four slides were applied to the remainder of slides in the database that have information available for runout distance and slope angle. Runout distance versus slope angle was plotted in Figure 5.24 (Chapter 5) for 343 slides in the database. This figure was plotted again to examine the slides in the database that the same characteristics of slide runout as the slides that are believed to have hydroplaned, i.e. runout distance > 20 km and β < 5 deg. This is shown in Figure 7.9 with a shaded region indicating the criteria inferred for hydroplaning. There are about 60 slides that have data that plot in this shaded region. Based on the similar runout characteristics as the four slides that are believed to have hydroplaned, hydroplaning may have also occurred for these 60 slides.

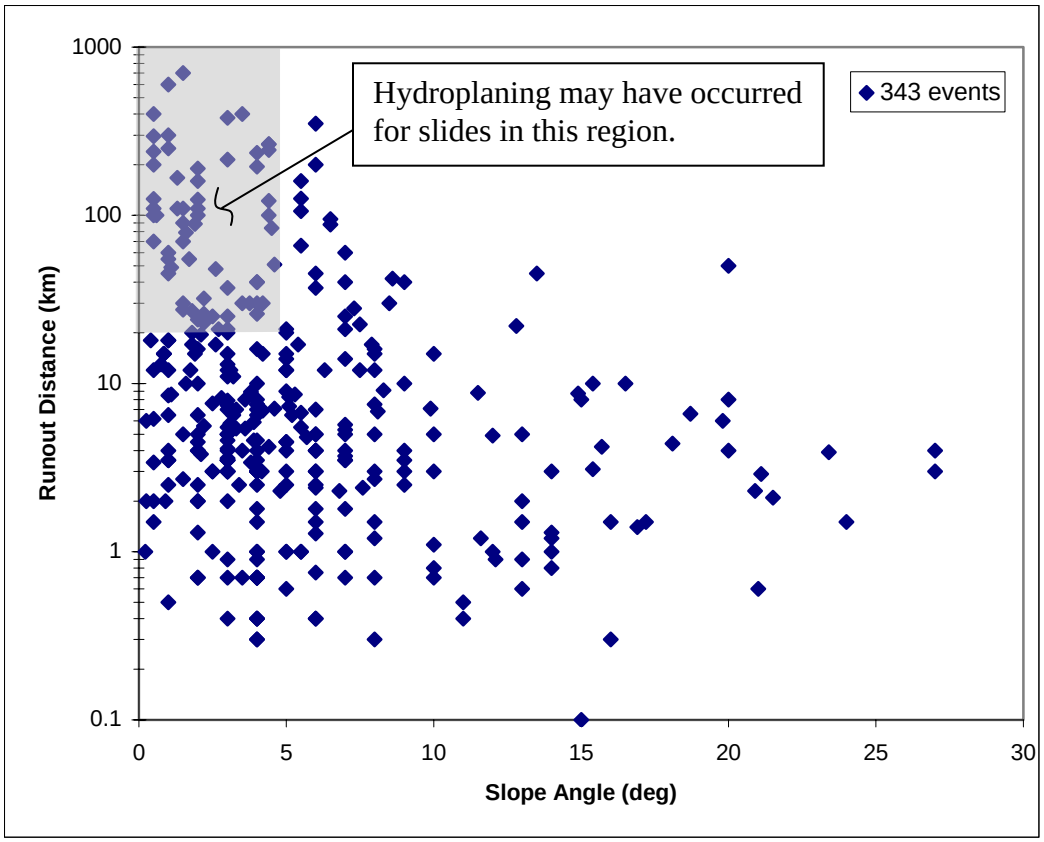

Figure 7.9. Slides that may have hydroplaned considering the characteristics of runout distance (> 20 km) and slope angle (< 5 deg).

7.9 ROLE OF SOIL STRENGTH IN PRODUCING REQUIRED VELOCITIES FOR HYDROPLANING

For hydroplaning to occur, there must be sufficient velocity of the landslide, and this is reflected in the requirement that the densimetric Froude number be at least 0.30. As part of this thesis, the role of soil strength in producing velocities required for hydroplaning was examined. The velocity of the landslide sufficient for hydroplaning was expressed as:

$$0.30 = \frac{v_{CRIT}}{\sqrt{gh_a \cos\beta\left(\frac{\rho_d}{\rho_w} - 1\right)}} \tag{7.8}$$

The "critical slide velocity", v_{CRIT}, required to attain a densimetric Froude number of at least 0.30 was computed from Equation 7.8 as follows:

$$v_{CRIT} = 0.30 * \sqrt{gh_a \cos\beta\left(\frac{\rho_d}{\rho_w} - 1\right)} \tag{7.9}$$

For this research effort, critical slide velocities, v_{CRIT}, were calculated using the data summarized for the five slides in Table 7.5, and are shown in Table 7.6 with the inferred velocities that were based on known submarine cable breaks. All five slides achieved velocities greater than the calculated "critical" slide velocity and, thus, meet the velocity requirement for hydroplaning.

Table 7.6. Inferred velocities from submarine cable breaks and "critical" slide velocities for the five slides that hydroplaned.

Landslide	**Inferred velocity from case study v (m/s)**	**"Critical" velocity v_{CRIT} (m/s)**
Grand Banks	27.4	5.6
Orkdalsfjord	2.6	2.5
Messina	6	3.5
Orleansville	19.5	3.5
Suva, Fiji	4.5	4.3

In order to reach the velocities necessary for hydroplaning to occur, the soil mass must accelerate, i.e. there must be some imbalanced force acting on the moving slide mass. The relationship between acceleration (a) and force (F) on a slide mass (m) is expressed by Newton's Second Law of Motion, F = ma. One way that an imbalanced force could be developed is by a loss in soil shear strength such that the strength remains lower than the driving stress along the slip surface. The soil conditions and triggering mechanisms for the five slides that are believed to have hydroplaned are summarized in Table 7.7. Referring to Table 7.7, four of the five slides were triggered by earthquakes or blast loading; the fifth slide (at Orkdalsfjord, Norway) was triggered by rapid loading from placement of fill during construction. Because all slides were triggered by rapid loading, the failures probably occurred under undrained conditions where excess pore water pressures could not dissipate as the slides were triggered. All of the slides in Table 7.7 involved saturated sands, loose silts, or sensitive clays, and when sheared undrained, these soils tend to lose strength.

7.10 ESTIMATING STRENGTH LOSSES REQUIRED FOR HYDROPLANING TO OCCUR

In section 7.8 it was shown that a sufficient slide velocity is required to achieve hydroplaning and a loss in soil shear strength after failure can produce the required velocities. To examine what strength losses and conditions might be

required to achieve critical velocity and hydroplaning, a simple model of a block on an inclined plane was developed as part of this study. The model is shown in Figure 7.10. The plane is inclined at the angle, β. The block has a mass, m, downslope displacement, d, from initial static position and a velocity, v, along (parallel to) the plane. The coefficient of friction between the block and plane is μ, and the change in vertical elevation corresponding to downslope displacement is h.

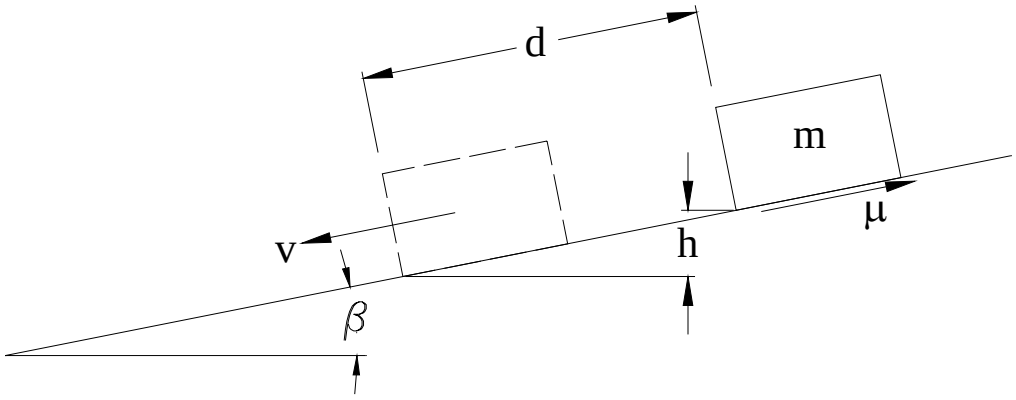

Figure 7.10. Model of block sliding on an inclined plane used to examine what conditions might be required to achieve critical velocity and hydroplaning.

The kinetic energy of the block (KE) is equal to the gravitational potential energy (GPE) less the frictional energy (FE) due to the sliding of the block along the inclined plane, i.e.

$$KE = GPE - FE \tag{7.10}$$

Table 7.7. Soil conditions and triggering mechanisms of five seafloor slides believed to have hydroplaned.*

Slide No.	Event Location	Soil Type	Soil Properties	Triggering Mechanism
10	Grand Banks	Low plasticity clayey-silty fine sands along upper slope from around 500 mbsl; Low to medium plasticity clays along slope around 1000 – 1500 mbsl	Sensitive, strain-softening clays where w > LL (i.e. LI > 1.0, ~ 1.5); high sensitivity (S > 1.5); $\varphi' = 34^o$, $c' = 0$ psf.	11/28/29 Earthquake (M = 7.2), slide occurred within epicentral region.
57	Orkdalsfjord, Norway	Failed material is very loose, soft non plastic silt	w ~ 33%; n ~ 49%, i.e. void ratio ~ 0.96	Man made slide (recent fill), Occurred on May 2, 1930
70	Messina, Italy	Sand/Silt		Earthquake loading (M = 7.5), occurred on 12/28/1908; slide occurred within epicentral region
71	El Asnam (formerly Orleansville)	Sand; well sorted (poorly graded), possibly alternating layers of sand and clay		Earthquake loading (M = 6.7), occurred on 9/9/1954; slide did not occur within epicentral region
78	Suva, Kadavu passage, Fiji	Sand		Earthquake loading (M = 6.75), occurred in 1953; slide occurred within epicentral region

* Refer to database for references.

The gravitational potential energy (GPE) can be expressed as:

$$GPE = mgh = mgd\sin\beta \tag{7.11}$$

The frictional energy (FE) is expressed as:

$$FE = \mu mgd\cos\beta \tag{7.12}$$

where μ is the coefficient of friction, or in terms of a friction angle, ϕ:

$$FE = \tan\phi mgd\cos\beta \tag{7.13}$$

Finally, the kinetic energy (KE) is expressed as:

$$KE = 0.5mv^2 \tag{7.14}$$

By combining Equations 7.10, 7.11, 7.13 and 7.14 and solving for velocity (v), the velocity of the block is calculated as:

$$v = \sqrt{2gd\sin\beta(1-\tan\phi\cot\beta)} \tag{7.15}$$

The block begins to slide (incipient failure) when the friction angle between the block and the inclined plane (ϕ) is equal to the angle of the plane (β), i.e. $\tan\phi\cot\beta = 1$ or $\phi = \beta$. Suppose now, there is a loss in strength after initiation of failure such that ϕ then becomes less than β. The loss in strength after failure can be expressed as $\beta - \phi_r$ where ϕ_r represents the reduced shear strength after failure and the angle of the inclined plane remains constant. Introducing the term $\beta - \phi_r$ into Equation 7.15, the velocity of the block is then calculated as:

$$v = \sqrt{\frac{\left(2gd\sin(\beta - \phi_r)\right)}{\cos\phi}} \tag{7.16}$$

Velocities were calculated from Equation 7.16 for various combinations of downslope displacement, d, and strength losses, $\beta - \phi_r$. The friction angle at failure, ϕ, is also a variable in Equation 7.16, and velocities were calculated varying ϕ from 20 to 30 degrees, which were considered reasonable values. Three scenarios of strength loss (1, 4, and 10 degrees) were considered in the calculations, and are also believed to be reasonable values. One degree of strength loss is a lower limit based on geotechnical testing capabilities, and ten degrees of strength loss is considered an upper limit. Using four degrees of strength loss, data for velocity as a function of downslope movement plot as an "average" between the lower and upper limits. The velocity of the sliding block, v, is plotted versus the downslope movement, d, for losses in strength of 1, 4, and 10 degrees as shown in Figure 7.10. Referring to Table 7.6, it can be seen that "critical" slide velocities tend to be less than about 10 m/s (ranging from about 3 m/s to 6 m/s) based on the five case histories. This range in velocities (3 to 6 m/s) is shown as a shaded region in Figure 7.11.

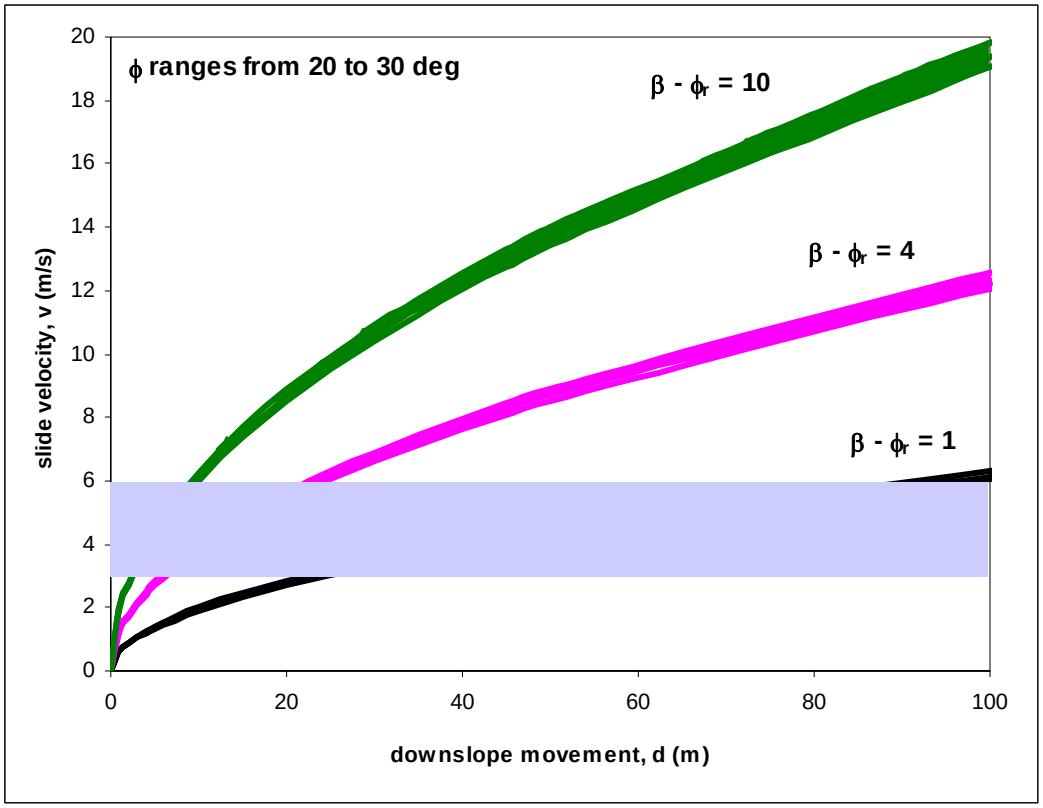

Figure 7.11. Velocity of a sliding block versus downslope movement in terms of shear strength loss after failure ($\beta - \phi_r$). Shaded region indicates the velocities required to initiate hydroplaning based on the five seafloor slides examined and Mohrig et al.'s (1998) criterion (Table 7.7).

For the range in "critical" velocities (shaded region) shown in Figure 7.11, downslope movements from about 3 to 100 m are required for the strength losses considered (1 to 10 degrees). These displacements are reasonable considering the large dimensions of typical seafloor slides (Chapter 5). For an only moderate loss in strength of 4 degrees, only about 16 to 17 m of downslope movement would be sufficient to develop a "critical" slide velocity of 5 m/s and initiate hydroplaning for the five case histories summarized in Table 7.6 and 7.7. For a large strength

loss of 10 degrees only about 6 m of downslope movement would be sufficient to initiate hydroplaning.

7.11 CONCLUSIONS

Hydroplaning of subaqueous slides occurs when a thin layer of fluid is trapped between a sliding soil mass and the underlying soil. This mechanism may account for large runout distances that have been observed for seafloor slides on flat slopes. Hydroplaning occurs when the hydrodynamic pressure acting on the front of the slide mass exceeds the normal stress exerted produced by the submerged slide mass on the slip surface. The densimetric Froude number has been shown to be a useful indicator of when hydroplaning occurs. From this study, a slide velocity of about 3 to 6 m/s appears to be sufficient for hydroplaning to occur based on five seafloor slides in the database and Mohrig et al.'s (1998) criterion for hydroplaning ($Fr_d \geq 0.30$). In order to achieve the "critical" velocity required for hydroplaning, there must be a force imbalance along the slip surface. This force imbalance could be provided by a loss in soil shear strength. Characteristics of hydroplaning slides include:

1. deformation (distortion) of the front of slide mass (debris head) during downslope movement
2. the thickness of the front of the slide mass (debris head) exceeding the average thickness of the slide

3. in extreme cases, the frontal velocity exceeding the characteristic average velocity, causing complete detachment and acceleration of the front of the slide mass
4. the underlying soil remaining largely undisturbed by the overlying slide mass
5. negligible influence of the rheological properties of the moving slide mass (yield strength and viscosity) and channel bottom conditions ("soft" versus "hard")

The simple model of a sliding block developed for this thesis provides a simple, effective way to evaluate the combinations of downslope movement, strength loss, and slide velocity required to initiate hydroplaning. Based on this model, movements of as little as 3 to 100 m accompanying a strength loss of 1 to 10 degrees could be enough to achieve "critical" velocity (3 to 6 m/s) and initiate hydroplaning.

CHAPTER 8

RHEOLOGICAL MODELS

FOR SEAFLOOR SLIDE RUNOUT

8.1 INTRODUCTION

Several rheological models have been developed by others to address the mechanics of submarine landslides during runout following the initial failure. The rheological models treat the downslope movement of debris (soil) as a flowing, fluid-like mass, rather than a sliding mass. Common rheological models are described in this chapter. A one-dimensional, finite difference numerical model that implements the rheological models in a computer program (BING) is also described. The computer program was developed by Imran et al. (2001), and was used by Imran et al. (2001) and Marr et al. (2002) to calculate runout distances and thicknesses of submarine slides. The numerical simulations of runout distance and slide thickness using the computer program have been compared by Imran et al. (2001) to runout distances and slide thicknesses observed for subaqueous slides in Mohrig et al.'s (1998, 1999) experiments reported on in Chapter 7 and have been compared by Marr et al. (2002) to seafloor slides in the Barents Sea.

8.2 RHEOLOGICAL MODELS

A description of rheology and various rheological models is presented in this section. Three rheological models based on a viscoplastic material and a "nonlinear" rheological model based on a combination of two classical types of fluids are described.

8.2.1 OVERVIEW OF RHEOLOGY

Rheology is the study of the deformation and flow of matter. Rheological models treat a moving slide mass as a flowing, fluid-like material; thus the soil described in a rheological model is typically referred to as "fluid", and fluid mechanics principles are implemented. The amount of fines (minus No. 200 sieve), clay mineralogy, grain size distribution, and water content affect the rheology of the "fluid".

With rheological models, typical quantities used to define the properties of materials are yield stress (strength), τ_y, and dynamic viscosity, η. These quantities are defined by measurements of shear stress, τ, and rates of angular deformation or shear strain, $\dot{\gamma}$ or $d\dot{u}/dy$, using a viscometer. The yield stress, τ_y, is the shear stress required to cause motion of the "fluid". Motion of the fluid stops when the shear stress falls below the yield stress. The dynamic viscosity, η,

is the slope of the shear stress-shear strain rate curve, and depends on the type of sediment and the rate of shear.

Classical types of fluids are “Newtonian”, “shear thickening”, “Bingham”, and “Herschel-Bulkley”. The behavior of each of these types is illustrated in Figure 8.1. Newtonian and Bingham fluids have a viscosity that remains constant with shear strain rate. With shear thickening fluids, the viscosity increases with increasing rate of shear strain, while Herschel-Bulkley fluids have a viscosity that decreases with increasing rate of shear strain. Newtonian fluids have no yield strength, τ_y, while shear thickening, Bingham, and Herschel-Bulkley fluids have a yield strength. The viscosity and yield stress define how a viscous material responds to forces such as friction, surface forces (frontal and drag), internal shear and gravity.

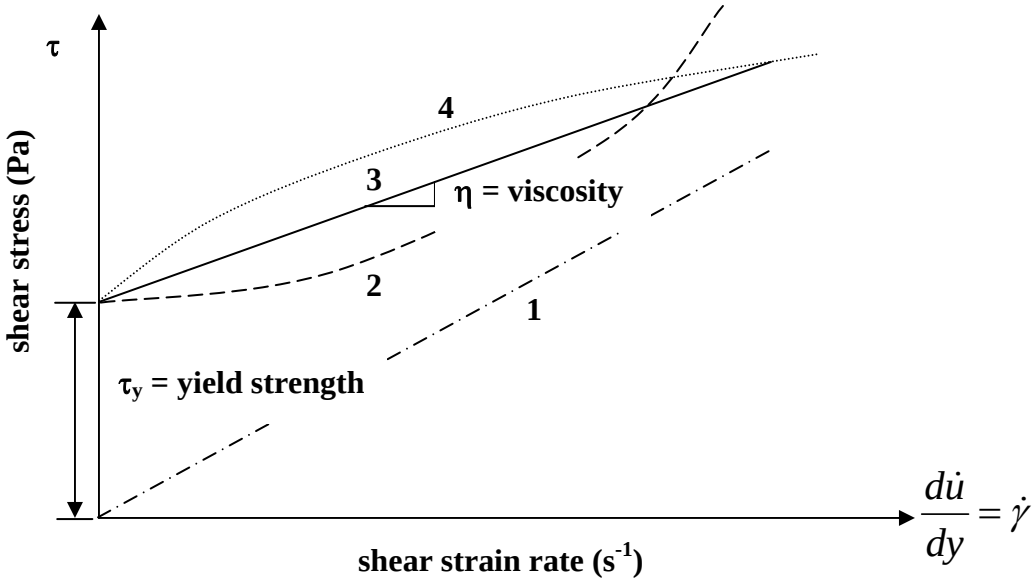

Figure 8.1. Stress-strain rate relationships. Fluid types shown are (1) Newtonian, (2) shear thickening, (3) Bingham, (4) Herschel-Bulkley.

8.2.2 VISCOPLASTIC MODELS

A representation of a soil mass flowing on a slope as a viscoplastic material is shown in Figure 8.2. The mass that is flowing downslope is assumed to have two distinct flow regimes: a plug flow region and a viscous layer. The plug flow region has two characteristics: First, the downslope velocity, $\dot{u}$, is constant within the plug. Secondly, because there is no velocity gradient ($d\dot{u}/dy = 0$) within the plug flow, there is no shearing within the plug flow layer. The viscous flow layer is a layer located below the plug flow layer, between the undisturbed seafloor and the overlying plug flow region. In the viscous layer, the

downslope velocity decreases from the velocity of the plug flow ($\dot{u}$) to zero at the base of the flow (y = 0).

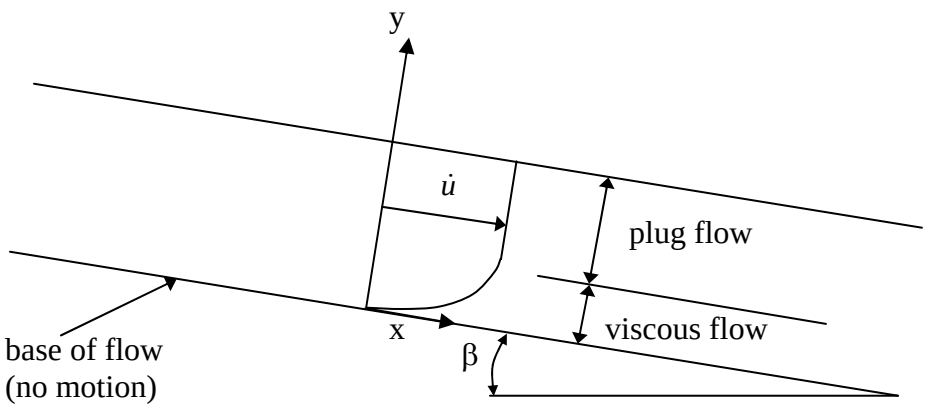

Figure 8.2. Representation of viscoplastic model with a flowing soil mass on a slope. Two flow layers are shown as plug flow and viscous flow (after Suhayda and Prior, 1978).

The Bingham, Herschel-Bulkley and Coulomb friction models are common viscoplastic models, and are described in the following subsections.

8.2.2.1 BINGHAM FLUID MODEL

A Bingham fluid is characterized by a yield strength and a viscosity that remains constant with strain rate. Thus, the relationship between shear stress and shear strain rate for a Bingham fluid can be expressed as:

$$\tau = \tau_y + \eta\dot{\gamma} \tag{8.1}$$

A Bingham fluid is the most common rheological model applied to the flow of subaqueous soil. The Bingham fluid model has various applications to

subaqueous soils. For example, Johnson (1970) studied the viscosity of silt and sand particles in water and concluded that these particles behaved as a Bingham fluid. Furthermore, Govier and Aziz (1982) found that high concentrations of clay, silt, and sand in water behave as a Bingham fluid under low shear strain rates.

8.2.2.2 HERSCHEL-BULKLEY FLUID MODEL

The Herschel-Bulkley fluid model is a modification of the Bingham model where the fluid is characterized as "pseudo-plastic" material that "thins" with increase in applied shear strain, i.e. "shear thinning". Thus, the viscosity decreases as the shear strain rate increases as shown in Figure 8.1. The shear stress-shear strain rate relationship for a Herschel-Bulkley model is expressed by an equation of the form:

$$\tau = \tau_y + \eta \dot{\gamma}^n \tag{8.2}$$

where n is less than one. This model is just the opposite of what one would expect for soils. Typically the shear strength of soil increases with increasing rate of shear strain, i.e. viscosity increases. So, most soils should be "shear thickening". However, O'Brien and Julien (1988) concluded that the Herschel-Bulkley model defines the behavior of clay-water suspensions reasonable well at high shear strain rates.

8.2.2.3 COULOMB FRICTION MODEL

Johnson (1965, 1970) utilized a model that has generally been referred to as the "Coulomb friction model". The Coulomb friction model is a modification to the Bingham and Herschel-Bulkley models, and includes a friction term as a component of the shear strength of the "fluid". The Coulomb friction model is expressed as:

$$\tau = \tau_y + \eta\dot{\gamma}^n + \sigma' \tan\phi' \qquad (8.3)$$

where σ' is the effective normal stress in the "fluid", and ϕ' is the friction angle expressed in terms of effective stresses. The first and second terms in Equation 8.3 are similar to those of the Herschel-Bulkley model described previously. The third term applies to a soil with frictional resistance that depends on effective stress. The Coulomb friction model has been applied by Suhayda and Prior (1978), Edgers and Karlsrud (1982), and Norem et al. (1990).

8.2.3 NONLINEAR ("BILINEAR") MODEL

The fourth rheological model considered is not a viscoplastic model, and, thus, differs from the Bingham, Herschel-Bulkley and Coulomb friction models. Consequently, the assumption of distinct viscous and plug flow layers does not apply. The relationship between shear stress and shear strain rate is nonlinear as shown in Figure 8.3. This model has been referred to as a "bilinear" fluid model by Locat (1997), and this designation will be used here even though the model is

actually nonlinear. The bilinear fluid is a hybrid of a Bingham and Newtonian fluid. Qualitatively speaking, at sufficiently low strain rates, the fluid behaves as a Newtonian fluid with a viscosity, η_1, and no yield strength, τ_y. At sufficiently high strain rates, the fluid behaves as a Bingham fluid with lower viscosity, η_2.

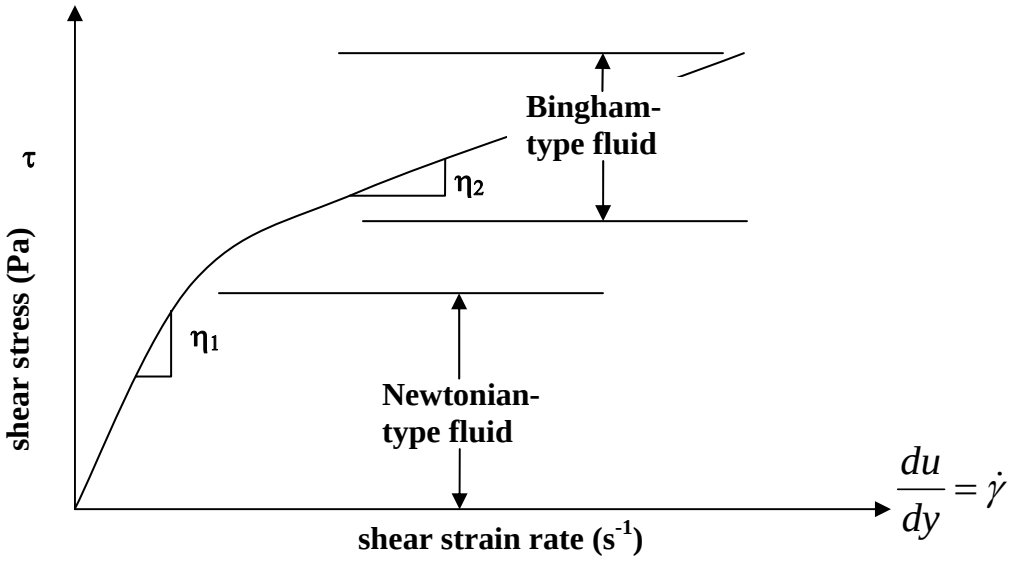

Figure 8.3. Bilinear rheological model.

The response of the bilinear fluid is expressed as:

$$\tau = \tau_y + \eta\dot{\gamma} + \left(\frac{c}{\dot{\gamma} + \dot{\gamma}_0}\right) \tag{8.5}$$

where τ_y is the apparent yield strength, $\dot{\gamma}_0$ is a rheological constant with units of the inverse of time, and c is an empirical constant that has a negative value and units of pressure divided by time. Imran et al. (2001) calculated the stress-strain rate response of a bilinear fluid like the one described by Equation 8.5. Selected

values of the parameters used by Imran et al. (2001) are summarized in Table 8.1.

The shear stress-shear strain rate relationship is plotted in Figure 8.4.

Table 8.1. Parameters for stress-strain rate relationship of bilinear fluid (Imran et al., 2001).

Parameter	**Units**	**Value**
Yield strength, τ_y	Pa	1000
Viscosity, η	Pa-sec	400
Rheological constant, γ_0	s^{-1}	0.01
Constant, c	Pa/s	-10

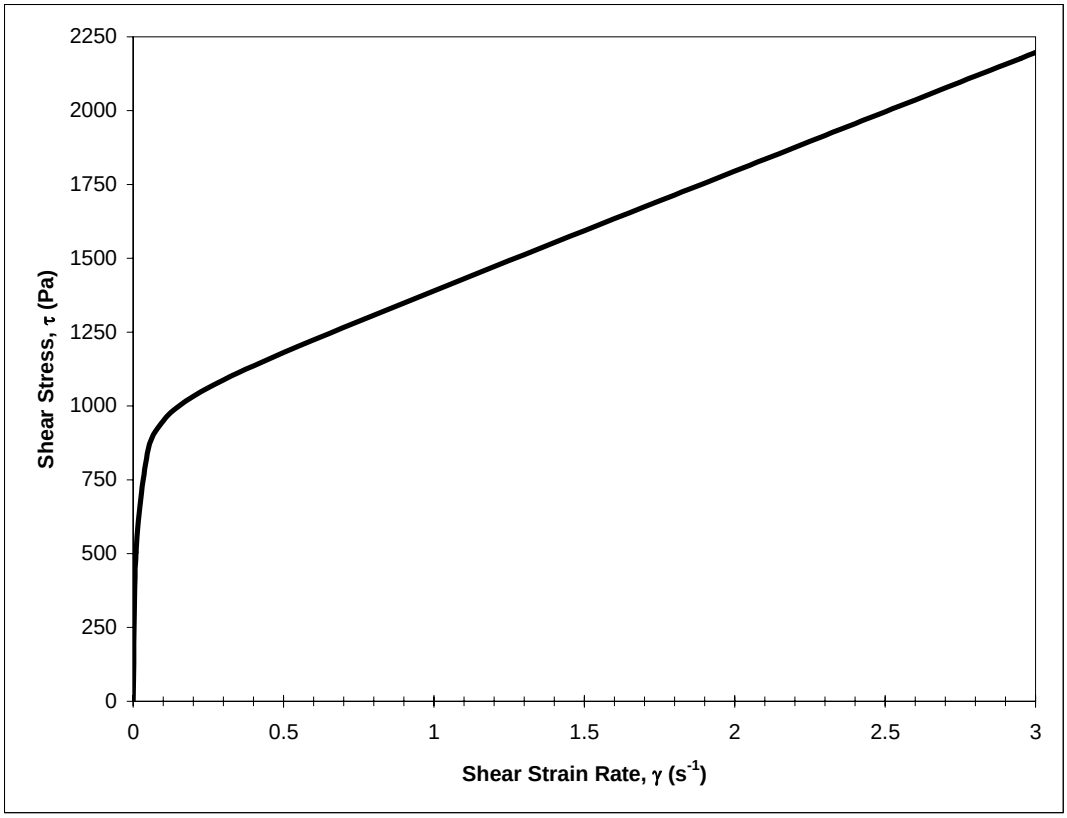

Figure 8.4. Stress-strain relationship for bilinear fluid model (after Imran et al., 2001).

8.3 NUMERICAL MODEL

A one-dimensional numerical model was developed by Imran et al. (2001) to simulate debris flows based on Bingham, Herschel-Bulkley and bilinear fluid models. The numerical model uses an explicit finite difference method to conserve mass and momentum in debris flows assuming laminar flow. The numerical model was implemented in a computer program called BING, and was written in the Microsoft Visual Basic programming language. The computer program has a graphical user interface. The program numerically simulates a flowing mass and computes the runout distance, downslope velocity and thickness of the deposit. Imran et al. (2001) studied the effect of the initial geometry of the flow mass, the rheological model, and the rheological parameters of viscosity and yield strength on the runout distance and thickness of the flow mass. They also used their model to study the effect of the density of the material that overlies the debris flow, i.e. air versus water, to examine possible differences between subaerial and subaqueous debris flows.

A summary of input parameters for their simulations from the computer program BING is shown in Table 8.2. The same values for the input parameters were used for the analyses of subaerial and subaqueous flows, with the exception of the mass density of the ambient material. For subaerial flows, the value for $\rho_{AMBIENT}$ (ρ_{AIR}) was 1 kg/m^3, and for subaqueous flows, $\rho_{AMBIENT}$ (ρ_{WATER}) was

1000 kg/m^3. Referring to Table 8.2, the initial shape of the flow mass in profile view, prior to initiating failure, is a parabola. This initial shape is expressed as:

$$D = D_o - 4D_o\left[\left(\frac{x - L/2}{L}\right)^2\right] \tag{8.6}$$

where D_o is the maximum thickness of the parabola prior to initiating the debris flow, L is the initial downslope length of the flow mass, x is the downslope distance, and D is the thickness of the flow mass at a downslope distance, x. A schematic of the geometry of the flow mass prior to downslope movement is shown in Figure 8.5. All numerical simulations were performed for a slope inclined at 2.9 degrees. The initial profile shape of the debris flow (parabola) from Equation 8.6 is plotted in Figure 8.6 for the input parameters from the simulations, i.e. D_o = 24 m and L = 600 m.

Table 8.2. Input parameters from numerical simulations (Imran et al., 2001).

	INPUT						
Debris flow	**L (m)**	**D_o (m)**	**τ_y (Pa)**	**η (Pa·s)**	**β (deg)**	**ρ_{SOIL} (kg/m^3)**	**$\rho_{AMBIENT}$ (kg/m^3)**
Subaerial	600	24	1000	400	2.9	1500	1
Subaqueous	600	24	1000	400	2.9	1500	1000

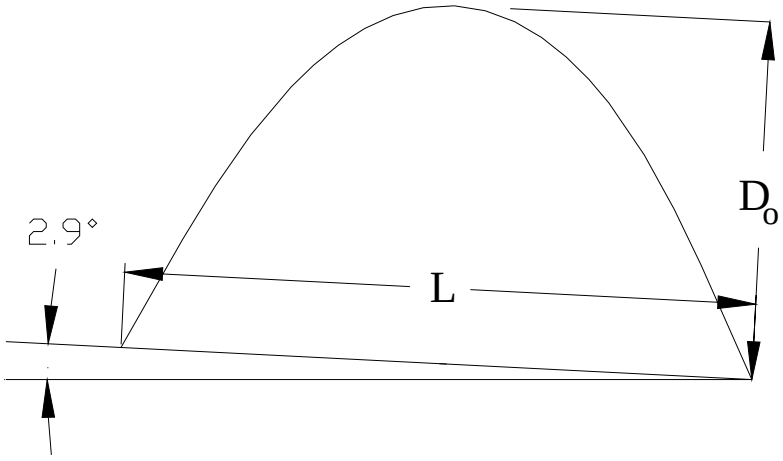

Figure 8.5. Schematic of the geometry of the flow mass prior to movement down the inclined slope.

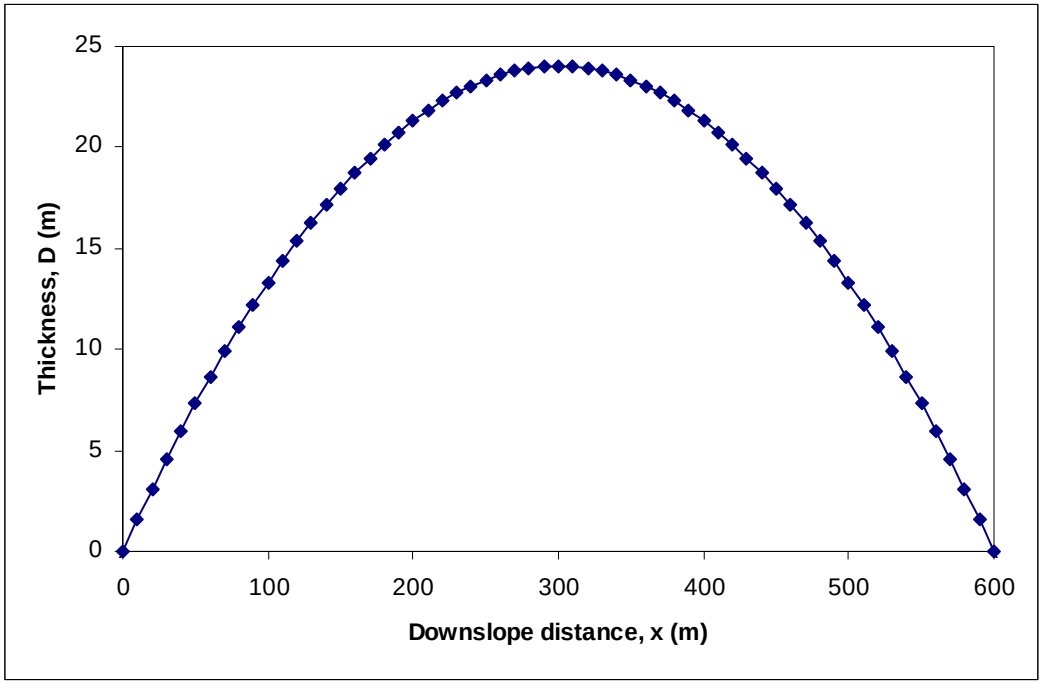

Figure 8.6. Initial shape of debris flow for numerical simulations performed by Imran et al. (2001).

A summary of the output from the numerical simulations performed by Imran et al. (2001) is shown in Table 8.3. The results presented in Table 8.3

show that the runout distance and peak velocity are greater for the subaerial debris flow than for the subaqueous debris flow. The total time for runout, i.e. from the time of initiation of downslope movement to the time the flow came to rest, is also greater for the subaerial debris flow than for the subaqueous debris flow.

Table 8.3. Output from the numerical simuations (Imran et al., 2001).

	OUTPUT		
Debris flow	**Runout distance (m)**	**Peak velocity (m/s)**	**Total Time for Runout (min)**
Subaerial	5,480	22.3	101.78
Subaqueous	1,571	9.86	21.95

The shapes of the debris flows from the simulations for the subaerial and subaqueous flows are shown in Figure 8.7 in profile view. The thickness of the debris flow is y, and is plotted normalized to the initial maximum thickness of the flow (D_o). The downslope length at time, t, is x, and is plotted normalized to the initial length of the flow mass (L). The shapes of the debris flows at a downslope travel (runout) time of 2 minutes are shown in Figure 8.7 (a), and the final shapes of the debris flows at rest are shown in Figure 8.7 (b).

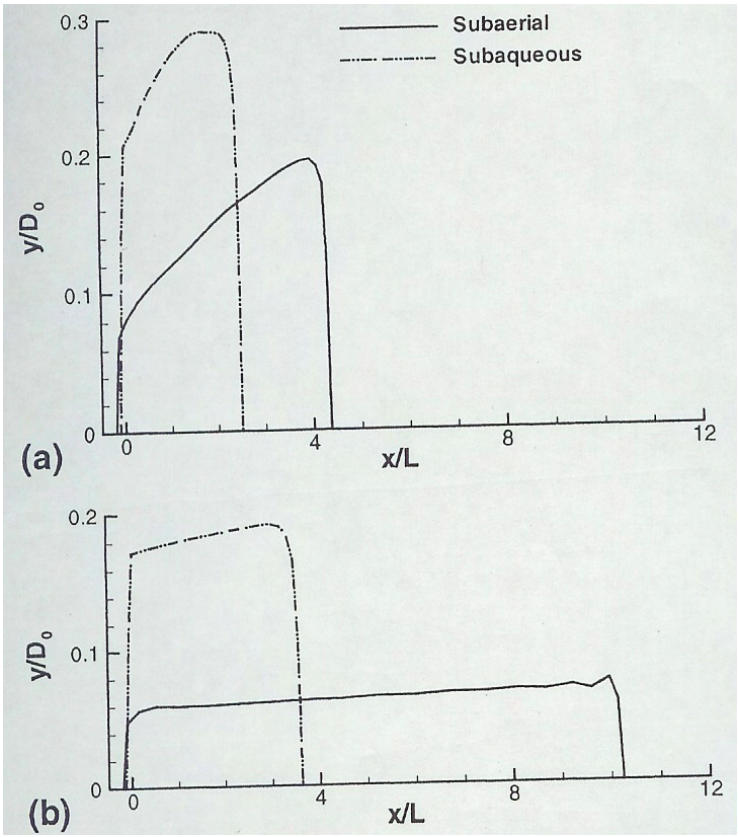

Figure 8.7. Shapes of subaerial and subaqueous debris flows that are moving down a slope inclined at 2.9 degrees (a) at a downslope travel (runout) time of 2 minutes; (b) final shape at end of simulation (Imran et al., 2001).

Imran et al. (2001) found that for a given volume of flow, the total runout distance was less for subaqueous debris flows than for subaerial debris flows (Table 8.2; Figure 8.6). They also found that the final thickness of the slide debris is greater for subaqueous debris flows than for subaerial debris flows. Imran et al. (2001) explained that the difference between subaqueous and subaerial debris flows is that water, in comparison to air, reduces the effect of

gravity and impedes flow for subaqueous flows. However, Imran et al.'s findings contradict most of the observations of Mohrig et al. (1998, 1999) who found that when hydroplaning occurs, subaqueous debris flows can produce a thinner deposit and travel longer distances than subaerial debris flows. In Chapter 7, it was shown that 13 of the 15 subaqueous slides in Mohrig et al.'s (1998, 1999) experiments were observed to hydroplane. Consequently, Imran et al. (2001) found that simulations from their numerical model were only consistent with two of the experimental observations of Mohrig et al. (1998). These were the two tests where hydroplaning did not occur.

Marr et al. (2002) used Imran et al.'s (2001) computer program (BING) to calculate runout distances and final thicknesses of slide deposits for seafloor slides on the Isfjorden fan and the Bear Island fan in the Barents Sea. Data for these seafloor slides were originally compiled by Laberg and Vorren (1993, 1995) and Elverhøi et al. (1997). Marr et al. (2002) assumed that the soils behaved as a Bingham fluid. A summary of the input parameters used for the numerical simulations is shown in Table 8.4. Marr et al. (2002) state that the yield strengths used in Cases 1 and 3 (Table 8.4) are representative of seafloor sediments in the Barents Sea. On the other hand, Marr et al. (2002) state that unreasonably low yield strengths, i.e. 1 to 5 kPa, were used as input for the numerical simulation for Case 2 of the Bear Island debris flow.

Table 8.4. Input parameters for Marr et al.'s (2002) simulations.

Debris flow	Initial shape	Slope Angle (deg)	L (km)	D_o (m)	τ_y (kPa)	η (Pa·s)
Isfjorden (Case 1)	Parabola	3 – 4	6.67	90	10 - 25	300, 30
Bear Island (Case 2)	Parabola	0.2 – 0.5	20	225	1 – 5	300, 30
Bear Island (Case 3)	Parabola	0.2 – 0.5	20	225	10 - 25	300, 30

Output from Marr et al.'s (2002) numerical simulations is summarized in Table 8.5. The observed runout distances and mean slide thicknesses are also shown in Table 8.5 for comparison with the computed values. Numerical simulations for slides on the Isfjorden fan were in good agreement with field observations (Case 1), as shown in Table 8.5. Simulations for the slides on the Bear Island fan were not in good agreement with field observations (Case 3) when reasonable values for the yield strength were used. Simulations from Case 2 were in good agreement with field observations; however Marr et al. (2002) stated that the yield strengths that were used in these computations (Case 2) were not representative of field conditions. To explain the discrepancies between the simulations and the actual observed results, Marr et al. (2002) attributed the Bear Island fan slides, which have long runout distances of 100 to 200 km on slope angles less than one degree, to a flow mechanism other than the Bingham fluid model, such as hydroplaning. Thus the Bingham model does not appear to be valid for the slides that occurred on the Bear Island fan.

Table 8.5. Observed runout characteristics and output from Marr et al.'s (2002) simulations.

	Runout distance (km)		Mean thickness (m)	
Debris flow	**Observed**	**BING**	**Observed**	**BING**
Isfjorden (Case 1)	10 - 30	13 – 44	10 – 30	10 – 22
Bear Island (Case 2)	100 – 200	77 – 355	10 – 50	8 – 30
Bear Island (Case 3)	100 - 200	7 - 35	10 - 50	50 - 130

8.4 CONCLUSIONS

Imran et al.'s (2001) and Marr et al.'s (2002) numerical simulations of runout distance and thickness of debris flows using a Bingham rheological model were in good agreement with only 3 of the 17 cases considered, i.e. 2 of the 15 cases from Mohrig et al.'s (1998, 1999) experiments and 1 of the 2 seafloor slides identified by Laberg and Vorren (1993, 1995) and Elverhøi et al. (1997). In general, the observed runout distances were larger and the observed slide thicknesses were smaller than those predicted by the numerical simulations. Imran et al. (2001) and Marr et al. (2002) attributed the discrepancies in runout distance and thickness of the debris flows to some additional mechanism such as hydroplaning.

CHAPTER 9

SUMMARY, CONCLUSIONS, AND RECOMMENDATIONS

9.1 SUMMARY AND CONCLUSIONS

An extensive review of the literature on seafloor slope failures has been conducted, and data on 534 seafloor slope failures have been compiled in a database. The database includes the date of failure, geographic location, soil types, soil properties, causes of slope failure (triggering mechanisms), distance of slide runout, slide thickness, total area influenced by slide, volume of slide mass, slope angle, and shallowest and deepest water depths affected. Fourteen different triggering mechanisms (triggers) were identified and are included in the database. The triggers have been described in Chapter 4, and relevant information pertaining to the triggers and how the information is included in the database have also been described. Although there is a large amount of information in the database, significant geotechnical information was lacking for most of the slope failures.

Characteristics of the seafloor slope failures (slides) have been evaluated and are summarized in tables and figures in Chapter 5. The data show that seafloor slides generally affect large areas and volumes of soil, and they tend to be larger than subaerial landslides. Also, in comparison to subaerial landslides,

seafloor slides tend to travel larger distances and occur on flatter slopes. In fact, it was observed that seafloor slides can have significant runout distances, traveling up to hundreds of kilometers on gentle slopes that are typically inclined at angles less than 5 to 10 degrees.

To evaluate the feasibility of various triggers causing slope failure, a series of infinite slope stability analyses was performed for both static and seismic conditions, and the results are summarized in Chapter 6. The analyses revealed that seafloor slope failures are probably not triggered by gravity alone, and earthquake loading is a likely trigger. This conclusion is consistent with information in the database from the literature where earthquake loading was the most common trigger reported. Assuming probable conditions of shear strength and slope angle based on information in the database, pseudostatic analyses showed that the largest seismic yield coefficient (k_y) for these conditions is about 0.13. Based on analyses of possible seismic conditions using the attenuation relationship developed by Abrahamson and Silva (1997), it was concluded that slopes may experience permanent deformation and possibly slope failure by earthquake loading when the earthquake source has a magnitude of at least 5.5 and is located less than 12 km from the slope. In fact, if the soil experiences a loss in shear strength due to earthquake loading, slope failure is even more likely.

One of the most probable explanations for the large runout of seafloor slides is hydroplaning, which was discussed in Chapter 7. Hydroplaning occurs

when a thin layer of fluid is trapped between a sliding soil mass and the underlying soil. One of the characteristics of hydroplaning is that the deformation properties of the moving slide mass have negligible influence. The densimetric Froude number, Fr_d, is a useful indicator of when hydroplaning is likely to occur. It was shown that a slide velocity of about 3 to 6 m/s could initiate hydroplaning based on Mohrig et al.'s (1998) criterion for hydroplaning ($Fr_d \geq 0.30$) and the characteristics of five seafloor slides where densimetric Froude numbers were able to be calculated. In order for hydroplaning to occur, it was shown that a force imbalance could be caused by a loss in shear strength along the slip surface. A simple model of a sliding block was presented to illustrate how the relationship between strength loss, slide velocity, and downslope movement could initiate hydroplaning. Specifically, it was shown that slide movements of as little as 3 to 100 m accompanying a reasonable loss in shear strength after failure could be enough to initiate hydroplaning.

In addition to hydroplaning, several rheological and numerical models have been developed to study slide runout. These rheological models treat the moving slide mass as a flowing, fluid-like material. However, numerical simulations of runout distance and slide thickness are not in good agreement with observations of actual seafloor slides that achieved large runout distances on flat slopes and the majority of a series of experiments by Mohrig et al. where hydroplaning occurred. Thus, the use of rheological models to explain large

seafloor slide movements is probably not valid in many instances. Hydroplaning, which Mohrig et al. (1999) suggest is independent of rheology, is the most likely mechanism to account for the large runout distances observed for some seafloor slides.

9.2 RECOMMENDATIONS FOR FUTURE WORK

Recommendations are provided in this section to refine the database that was created as part of this thesis, to develop models that account for hydroplaning, to develop a methodology for risk assessment, and to continue experimental studies of hydroplaning.

9.2.1 THE DATABASE

The database is currently in the form of one, large table in Microsoft Access®. It is recommended that this database be refined into smaller tables, e.g. by the addition of tables for shear strengths and plasticity indices. Additional information should also be obtained from existing literature and incorporated into the database. This includes determining the area of seafloor surveyed in the geophysical investigation for each case study and the reasons the investigations occurred, i.e. who funded the investigation. A new field containing an overall "data quality" factor that is a function of the certainty of the cause(s) of slope failure and the geophysical information is also recommended. It is recommended

that further statistical analyses of data in the database be performed to determine correlations among the triggering mechanisms, site conditions and subsequent extent of seafloor slide movement.

9.2.2 MODELS

It is recommended that numerical, theoretical and analytical models be developed that account for the hydroplaning mechanism that has been observed in the laboratory by Mohrig et al. (1998, 1999) and has been inferred to occur in some seafloor slides from the database. Important properties and parameters required for the models, e.g. slide velocity, soil shear strength (and potential for strength loss), and type of loading, should be identified. These models should be calibrated so that results of runout distance and slide thickness are in agreement with observations of actual seafloor slides.

9.2.3 RISK ASSESSMENT

Because seafloor slope failures can impact oil and gas production in deepwater, the formulation and testing of a methodology for risk assessment of seafloor slope instability is important and recommended. Selected offshore sites should be used to demonstrate how a risk assessment can be applied, to show how existing data on submarine slope failures may be used, and to determine the value of obtaining additional site-specific information. The risk assessment should

begin with a decision tree framework that outlines the potential triggering mechanisms for the site, the history of seafloor slope instability in the vicinity of the site, and various consequences of slope failure. For example, the decision of where to construct an oil pipeline is a practical example that might be used to establish the decision tree. The decision could be to position the pipeline through a region susceptible to slope failure (low cost of construction, yet large risk of damage to pipe) or to re-route the pipeline through a region where there is little indication of future slope instability (high cost of construction, yet small risk of damage to pipe). As part of this decision tree framework, the value of obtaining additional site-specific information to reduce the risk should then be determined.

9.2.4 EXPERIMENTAL STUDIES

Several further experimental studies are needed to understand hydroplaning better. Following the work of Mohrig et al. (1998, 1999), improvements and additional tests could include:

(1) developing an experimental facility with a length of at least 20 m and slopes of less than 5 degrees; Mohrig et al.'s facility was only 10 m long, and slope angles for the channel were 4.9, 6.0, 15.5, 16.0 and 20.0 degrees. Mohrig et al. (1998) performed one test on a 1-degree slope, which represents actual seafloor conditions better, yet hydroplaning did not occur.

(2) performing more tests where the bottom of the channel is an existing soil deposit ("soft" bottom) to simulate actual seafloor conditions prior to filling with water and introducing a subaqueous slide; Mohrig et al. (1999) only performed 2 tests with a "soft" bottom.

(3) performing additional tests to better delineate when hydroplaning occurs and when it does not and to define better the densimetric Froude number required for hydroplaning to occur. Mohrig et al.'s (1998) criterion based on the densimetric Froude number was developed based on results from only eight tests where hydroplaning occurred and two tests where hydroplaning did not occur.

APPENDIX A:

USER'S GUIDE FOR DATABASE OF SEAFLOOR SLOPE FAILURES

A.1 INSTALLATION

1. In order to use the database, Microsoft Access97® (or later) must be installed on the computer. Since visualization and analysis is generally done outside of Access, it is desirable that Microsoft Excel®, or other visualization software, be installed as well.

2. There is only one file that *must* be installed: "Database of Seafloor Slope Failures.mbd" which is an Access database. Copy "Database of Seafloor Slope Failures.mbd" to a chosen work directory. Also, in order to view scanned images from the database, the 524 image files must be installed. This is done by copying the folders, which contain the image files, labeled "JPG image files", "JPG image files 2", and "JPG image files 3" to the same directory as the database file.

3. Open the database to use it.

A.2 MICROSOFT ACCESS® DATABASE

The relevant data are stored in a Microsoft Access® relational database. In general, data in the Access database can be queried, sorted, placed in a report, or exported for analysis and visualization. Once exported, data can be analyzed with a spreadsheet program or modeled with modeling or visualization software. The database contains one "Table", numerous "Queries", and two "Forms". These components are each described separately below.

A.2.1 Table—Data Storage and Entry

The data are organized in one Table. A portion of this table is shown below.

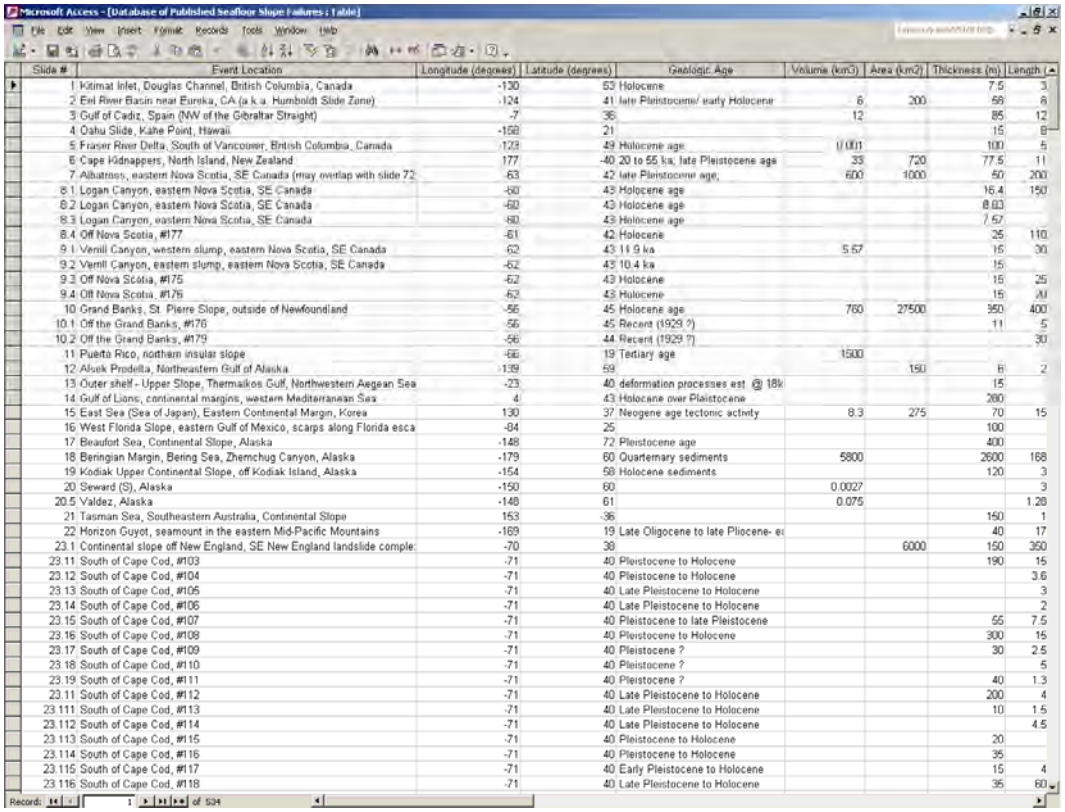

Slide #	Event Location	Longitude (degrees)	Latitude (degrees)	Geologic Age	Volume (km3)	Area (km2)	Thickness (m)	Length (km)
1	Kitimat Inlet, Douglas Channel, British Columbia, Canada	-130	53	Holocene			7.5	3
2	Eel River Basin near Eureka, CA (a.k.a. Humboldt Slide Zone)	-124	41	late Pleistocene/ early Holocene	6	200	68	8
3	Gulf of Cadiz, Spain (NW of the Gibraltar Straight)	-7	36		12		85	12
4	Oahu Slide, Kahe Point, Hawaii	-158	21				15	8
5	Fraser River Delta, South of Vancouver, British Columbia, Canada	-123	49	Holocene age	0.001		100	5
6	Cape Kidnappers, North Island, New Zealand	177	-40	20 to 55 ka; late Pleistocene age	33	720	77.5	11
7	Albatross, eastern Nova Scotia, SE Canada (may overlap with slide 72	-63	42	late Pleistocene age;	600	1000	50	200
8.1	Logan Canyon, eastern Nova Scotia, SE Canada	-60	43	Holocene age			16.4	150
8.2	Logan Canyon, eastern Nova Scotia, SE Canada	-60	43	Holocene age			8.03	
8.3	Logan Canyon, eastern Nova Scotia, SE Canada	-60	43	Holocene age			7.57	
8.4	Off Nova Scotia, #177	-61	42	Holocene			35	110
9.1	Verrill Canyon, western slump, eastern Nova Scotia, SE Canada	-62	43	11.9 ka	5.57		16	30
9.2	Verrill Canyon, eastern slump, eastern Nova Scotia, SE Canada	-62	43	10.4 ka			16	
9.3	Off Nova Scotia, #175	-62	43	Holocene			16	25
9.4	Off Nova Scotia, #176	-62	43	Holocene			16	40
10	Grand Banks, St. Pierre Slope, outside of Newfoundland	-56	45	Holocene age	760	27500	350	400
10.1	Off the Grand Banks, #176	-56	45	Recent (1929 ?)			11	5
10.2	Off the Grand Banks, #179	-56	44	Recent (1929 ?)				30
11	Puerto Rico, northern insular slope	-66	19	Tertiary age	1500			
12	Alsek Prodelta, Northeastern Gulf of Alaska	-139	59			150	6	2
13	Outer shelf - Upper Slope, Thermaikos Gulf, Northwestern Aegean Sea	-23	40	deformation processes est @ 18k			15	
14	Gulf of Lions, continental margins, western Mediterranean Sea	4	43	Holocene over Pleistocene			280	
15	East Sea (Sea of Japan), Eastern Continental Margin, Korea	130	37	Neogene age tectonic activity	8.3	275	70	15
16	West Florida Slope, eastern Gulf of Mexico, scarps along Florida esca	-84	25				100	
17	Beaufort Sea, Continental Slope, Alaska	-148	72	Pleistocene age			400	
18	Beringian Margin, Bering Sea, Zhemchug Canyon, Alaska	-179	60	Quarternary sediments	5800		2600	168
19	Kodiak Upper Continental Slope, off Kodiak Island, Alaska	-154	58	Holocene sediments			120	3
20	Seward (S), Alaska	-150	60		0.0027			3
20.5	Valdez, Alaska	-148	61		0.075			1.28
21	Tasman Sea, Southeastern Australia, Continental Slope	163	-36				150	1
22	Horizon Guyot, seamount in the eastern Mid-Pacific Mountains	-169	19	Late Oligocene to late Pliocene- e			40	17
23.1	Continental slope off New England, SE New England landslide comple	-70	38			6000	150	350
23.11	South of Cape Cod, #103	-71	40	Pleistocene to Holocene			190	15
23.12	South of Cape Cod, #104	-71	40	Pleistocene to Holocene				3.6
23.13	South of Cape Cod, #105	-71	40	Late Pleistocene to Holocene				3
23.14	South of Cape Cod, #106	-71	40	Late Pleistocene to Holocene				2
23.15	South of Cape Cod, #107	-71	40	Pleistocene to late Pleistocene			55	7.5
23.16	South of Cape Cod, #108	-71	40	Pleistocene to Holocene			300	15
23.17	South of Cape Cod, #109	-71	40	Pleistocene ?			30	2.5
23.18	South of Cape Cod, #110	-71	40	Pleistocene ?				5
23.19	South of Cape Cod, #111	-71	40	Pleistocene ?			40	1.3
23.11	South of Cape Cod, #112	-71	40	Late Pleistocene to Holocene			200	4
23.111	South of Cape Cod, #113	-71	40	Late Pleistocene to Holocene			10	1.5
23.112	South of Cape Cod, #114	-71	40	Late Pleistocene to Holocene				4.5
23.113	South of Cape Cod, #115	-71	40	Pleistocene to Holocene			20	
23.114	South of Cape Cod, #116	-71	40	Pleistocene to Holocene			35	
23.115	South of Cape Cod, #117	-71	40	Early Pleistocene to Holocene			15	4
23.116	South of Cape Cod, #118	-71	40	Late Pleistocene to Holocene			35	60

Figure A.1. View of a portion of database Table.

Data can be entered directly into the Table, and data can be extracted from the Table to create smaller tables. Data can also be modified and deleted. To modify data, highlight the incorrect entry and type a new one in its place. Records can be deleted by highlighting the entire record(s), and then Access will prompt you "do you really want to delete" the selected text. Data can also be entered into the Table from a spreadsheet by cutting and pasting. Entering data from a spreadsheet involves highlighting the data in the spreadsheet, copying it (to the clipboard), selecting the last record in the Access Table, and choosing "Paste Append" from the "Edit" menu. In pasting operations, it is necessary that the fields (columns) line up properly such that the widths of the columns are the same.

A.2.2 Queries—Data Manipulation

Queries are used to refine data from a dataset or to select certain types of information according to a specified criteria. There are two views for a Query:

"design" view and "table" view. An example Query for obtaining all case histories that have information available for slope angle and runout distance is shown below as it appears in the "design" view.

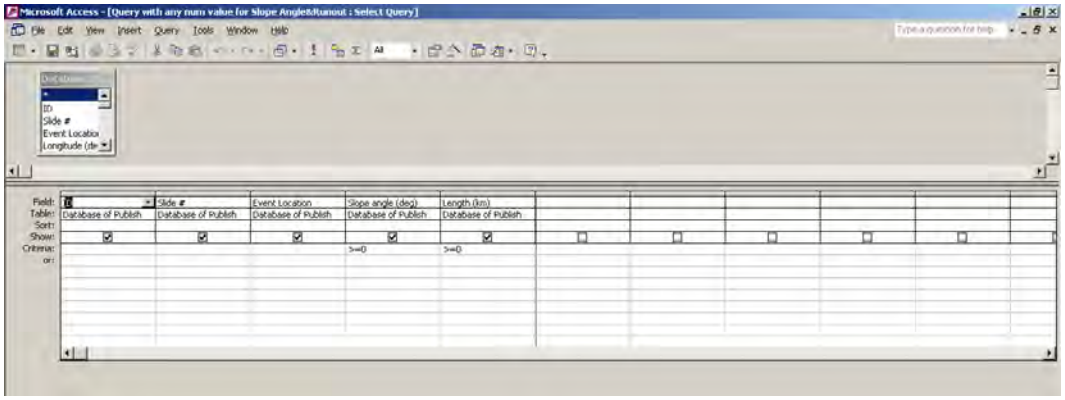

Figure A.2. "Design" view of query to extract all records with information available for average slope angle at failure and runout distance.

Queries can retrieve information either from Tables or other Queries, and data can be modified through Queries. For example, if an error is detected during a Query it can be corrected in the Query and the corrections will be reflected in the Table and other Queries that contain that data.

Design of a Query is generally a point and click operation with logical operators used to narrow down a selection. Access provides an "expression builder" when the user right clicks in the "criteria" field of the Query "design" view. For non-routine Queries, the on-line help is useful.

Each field in the database has a specific type. The types of fields in the database are "number", "text", and "hyperlinks", and there are several queries that were implemented for this database. For example, each "number" field was queried with a ">0" criterion to determine what slope failures have information in the specified field. Also, each "text" and "hyperlink" field was queried with a "* *" criterion. A space is always placed between the asterisks, which signifies there is data in that particular field. Another query method used for "text" and "hyperlink" fields is the "Is Null" criterion, which signifies there is no data in that particular field. If records are returned for the "Is Null" criterion, then these records do not have information for that particular field. The results from these search criteria (">0", "* *", and "Is Null") were noted and compared to the total number of slope failures in the database (534) in Table 5.1 in Chapter 5 of the thesis.

More than 50 Queries were created for the database. The queries that were used to extract information that was presented and summarized in this thesis are listed in Table A.1 along with a summary of the information that each query provides. The Queries for this database involve only the one Table that comprises the database.

A.2.3 Forms—Automation

Forms are used to make using the database more convenient. For example, forms may be used to automate common processes, or display data from a Table in a way more pleasing to the eye. A Form is based upon one or more Tables or Queries. The data in a Form may be displayed in datasheet mode (looks like a Table) or in standard form mode, which shows only one record at a time. You can toggle between the two modes by right-clicking the title bar of the Form and selecting the other view from the menu. Data may be entered or modified directly in a Form. While a Form is based on a Table or Query, the format of a Form is not automatically updated. For example, if you created a new field in a Table, that field would not automatically appear on an old Form. A standard form view for a landslide case history is shown below.

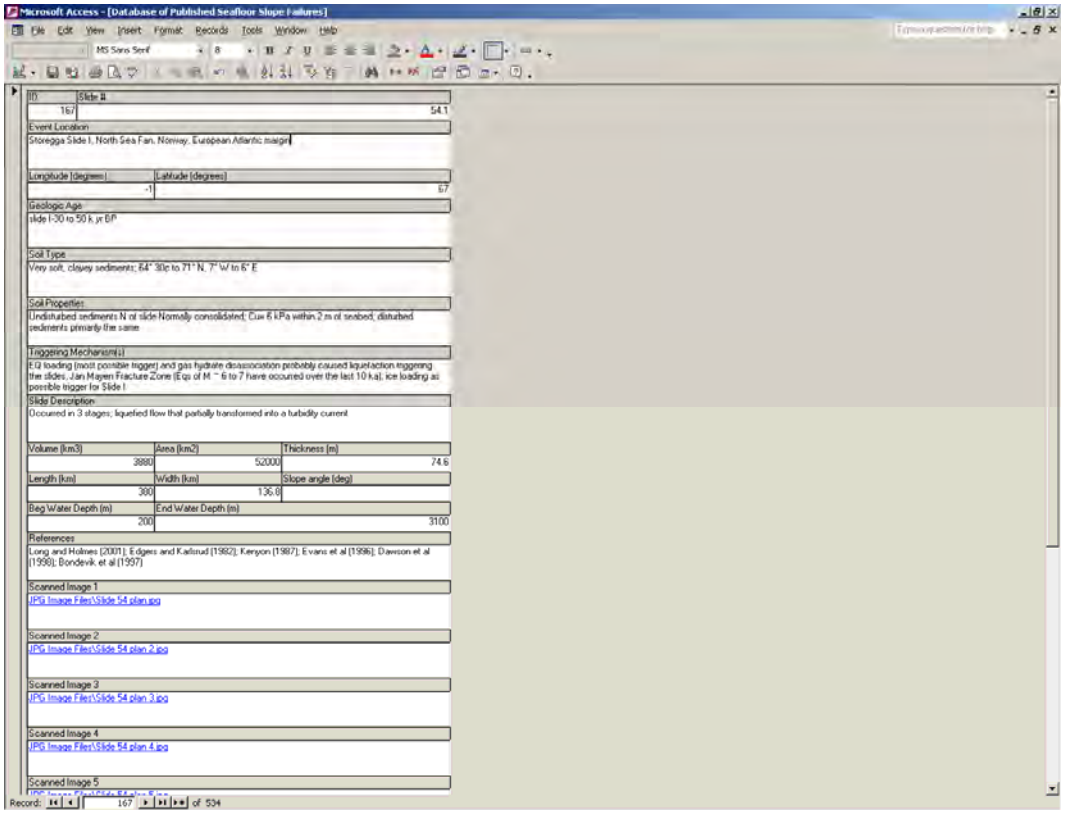

Figure A.3. Standard form view of a landslide case history.

Table A.1. Summary of the significant Queries that were used in the Database.

Query Name	Type of Data
EQ and Faulting as Trigger	Returns all slides triggered by “EQ” or “faulting”
Sedimentation as Trigger	Returns all slides triggered by “sedimentation”
Gas as Trigger	Returns all slides triggered by “gas”
Storm Waves as Trigger	Returns all slides triggered by “storm waves”
Tidal Events as Trigger	Returns all slides triggered by “tidal events”
Human Activity as Trigger	Returns all slides triggered by “human activity”
Erosion as Trigger	Returns all slides triggered by “erosion”
Magma Volcanoes as Trigger	Returns all slides triggered by “magma volcanoes”
Salt as Trigger	Returns all slides triggered by “salt”
Mud Volcanoes as Trigger	Returns all slides triggered by “mud volcanoes”
Flood Events as Trigger	Returns all slides triggered by “flood[s]”
Creep as Trigger	Returns all slides triggered by “creep”
Tsunamis as Trigger	Returns all slides triggered by “tsunamis”
Sea-level Change as Trigger	Returns all slides triggered by “sea-level change”
No Trigger Query	Returns all slides with no trigger assigned
Any num value for Area	Returns all slides with information on Area
Any num value for Runout Distance	Returns all slides with information on Runout Distance
Any num value for Volume	Returns all slides with information on Volume
Any num value for Width	Returns all slides with information on Width
Any num value for Thickness	Returns all slides with information on Thickness
Any num value for Slope Angle	Returns all slides with information on Slope Angle
Any num value for Shallowest Water Depth	Returns all slides with information on Shallowest Water Depth
Any num value for Deepest Water Depth	Returns all slides with information on Deepest Water Depth
East Longitude Query	Returns all slides with east longitudes
West Longitude Query	Returns all slides with west longitudes
North Latitude Query	Returns all slides with north latitudes
South Latitude Query	Returns all slides with south latitudes
“Debris flow” or “Disintegrative”	Returns all slides described as such
“Slump” or “Nondisintegrative”	Returns all slides described as such
Any num value for Slope Angle and Area	Returns all slides with this information
Any num value for Slope Angle and Runout Distance	Returns all slides with this information
Holocene Geologic Age Query	Returns all slides that occurred in Holocene
Pleistocene Geologic Age Query	Returns all slides that occurred in Pleistocene
Paleocene Geologic Age Query	Returns all slides that occurred in Paleocene
No Soil Type Query	Returns all slides that have no defined soil type
Soil Type Query	Returns all slides that have any defined soil type
No Scanned Image Query	Returns all slides that have no scanned images
No Soil Properties Query	Returns all slides that have no defined soil properties
Soil Properties Query	Returns all slides that have any defined soil properties

A.3 QUERY EXAMPLE

To illustrate a typical Query, the following example is provided. The "design" view for this Query was shown previously in Figure A.2. This Query extracts all landslides that have information on slope angle and runout distance. In this example, the data are exported into an Excel® spreadsheet to be plotted.

To create this Query, click the New button on the main Queries list. Select Design View and click OK. This brings up the Show Table window, which contains a list of available Tables and Queries that can be added to the Query. Select the *Database of Seafloor Slope Failures* Table by clicking Add since this is where the information of slope angle and runout distance is located. The fields of slope angle and runout distance are then queried by clicking-and-dragging from the Table in the upper half of the screen to a location in the lower half as shown in Figure A.4. Logical operators are then used to establish the criteria in the lower half. Criteria placed on the same row are "AND" criteria, while those on different rows are "OR" criteria. Criteria for this Query are placed in two fields. In this case, we want slides with any value for "Slope Angle (deg)" and "Runout Distance (km)". In the row for criteria, type ">=0" for "Slope Angle (deg)" and for "Runout Distance (km)" on the same line (Figure A.4). This Query is then saved, named as *Any num value for Slope Angle and Runout Distance*, and viewed by clicking the Query View button on the upper left-hand corner of the screen.

When the Query is complete, the output is then reviewed after clicking the Query View button. This output is shown in Figure A.5. The output is then exported into Excel. Since the cut and paste operation includes formats, it is often desirable to clear the formats after pasting into the spreadsheet (on the pull-down menu: Edit/Clear/ Formats). Figure A.6 shows the exporting command used from the "File" option on the toolbar.

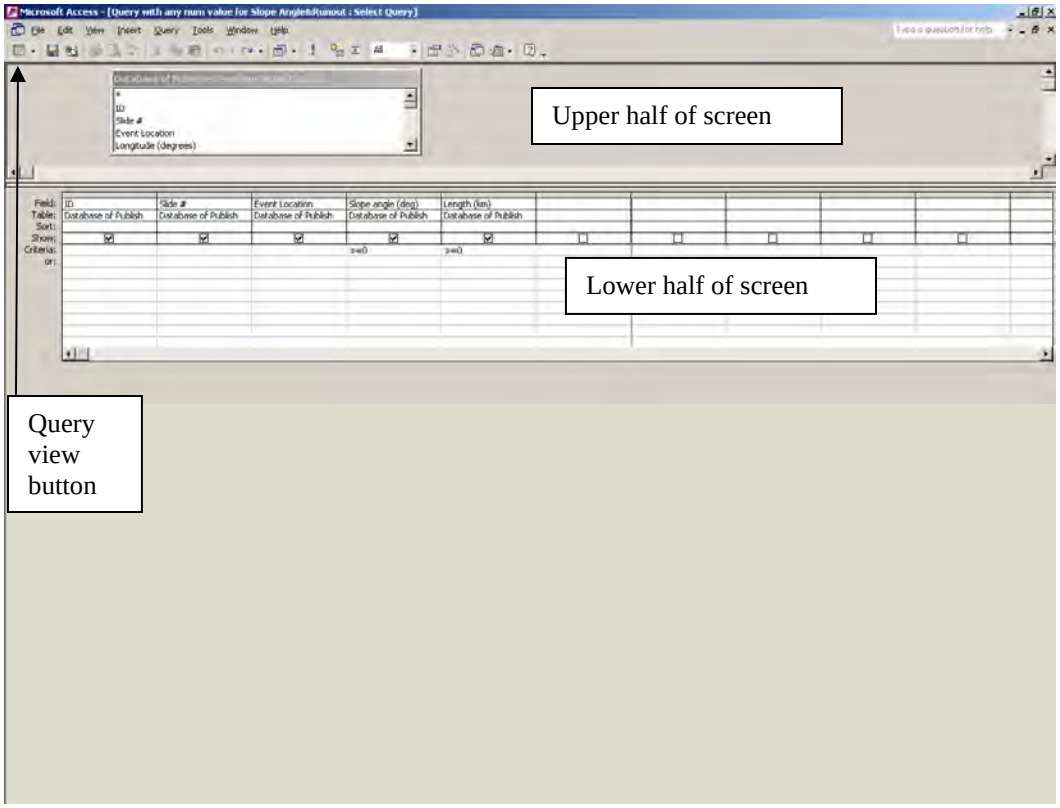

Figure A.4. Illustration of upper half and lower half of screen in Query "design" view.

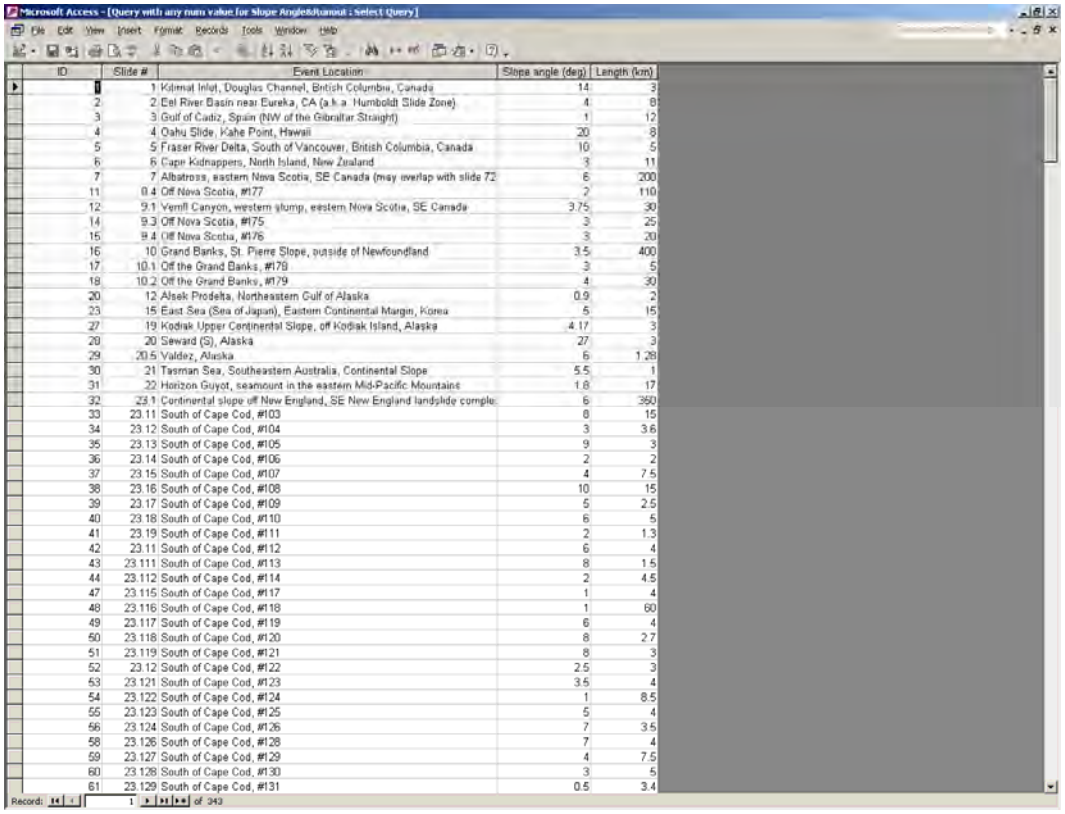

ID	Slide #	Event Location	Slope angle (deg)	Length (km)
1	1	Kitimat Inlet, Douglas Channel, British Columbia, Canada	14	3
2	2	Eel River Basin near Eureka, CA (a.k.a. Humboldt Slide Zone)	4	8
3	3	Gulf of Cadiz, Spain (NW of the Gibraltar Straight)	1	12
4	4	Oahu Slide, Kahe Point, Hawaii	20	8
5	5	Fraser River Delta, South of Vancouver, British Columbia, Canada	10	5
6	6	Cape Kidnappers, North Island, New Zealand	3	11
7	7	Albatross, eastern Nova Scotia, SE Canada (may overlap with slide 72	6	200
11	9.4	Off Nova Scotia, #177	2	110
12	9.1	Verrill Canyon, western slump, eastern Nova Scotia, SE Canada	3.75	30
14	9.3	Off Nova Scotia, #175	3	25
15	9.4	Off Nova Scotia, #176	3	20
16	10	Grand Banks, St. Pierre Slope, outside of Newfoundland	3.5	400
17	10.1	Off the Grand Banks, #178	3	5
18	10.2	Off the Grand Banks, #179	4	30
20	12	Alsek Prodelta, Northeastern Gulf of Alaska	0.9	2
23	15	East Sea (Sea of Japan), Eastern Continental Margin, Korea	5	15
27	19	Kodiak Upper Continental Slope, off Kodiak Island, Alaska	4.17	3
28	20	Seward (S), Alaska	27	3
29	20.5	Valdez, Alaska	6	1.28
30	21	Tasman Sea, Southeastern Australia, Continental Slope	5.5	1
31	22	Horizon Guyot, seamount in the eastern Mid-Pacific Mountains	1.8	17
32	23.1	Continental slope off New England, SE New England landslide comple	6	350
33	23.11	South of Cape Cod, #103	8	15
34	23.12	South of Cape Cod, #104	3	3.6
35	23.13	South of Cape Cod, #105	9	3
36	23.14	South of Cape Cod, #106	2	2
37	23.15	South of Cape Cod, #107	4	7.5
38	23.16	South of Cape Cod, #108	10	15
39	23.17	South of Cape Cod, #109	5	2.5
40	23.18	South of Cape Cod, #110	6	5
41	23.19	South of Cape Cod, #111	2	1.3
42	23.11	South of Cape Cod, #112	6	4
43	23.111	South of Cape Cod, #113	8	1.5
44	23.112	South of Cape Cod, #114	2	4.5
47	23.115	South of Cape Cod, #117	1	4
48	23.116	South of Cape Cod, #118	1	60
49	23.117	South of Cape Cod, #119	6	4
50	23.118	South of Cape Cod, #120	8	2.7
51	23.119	South of Cape Cod, #121	8	3
52	23.12	South of Cape Cod, #122	2.5	3
53	23.121	South of Cape Cod, #123	3.5	4
54	23.122	South of Cape Cod, #124	1	8.5
55	23.123	South of Cape Cod, #125	5	4
56	23.124	South of Cape Cod, #126	7	3.5
58	23.126	South of Cape Cod, #128	7	4
59	23.127	South of Cape Cod, #129	4	7.5
60	23.128	South of Cape Cod, #130	3	5
61	23.129	South of Cape Cod, #131	0.5	3.4

Figure A.5. Table of Output from Query for Slope Angle and Runout Distance.

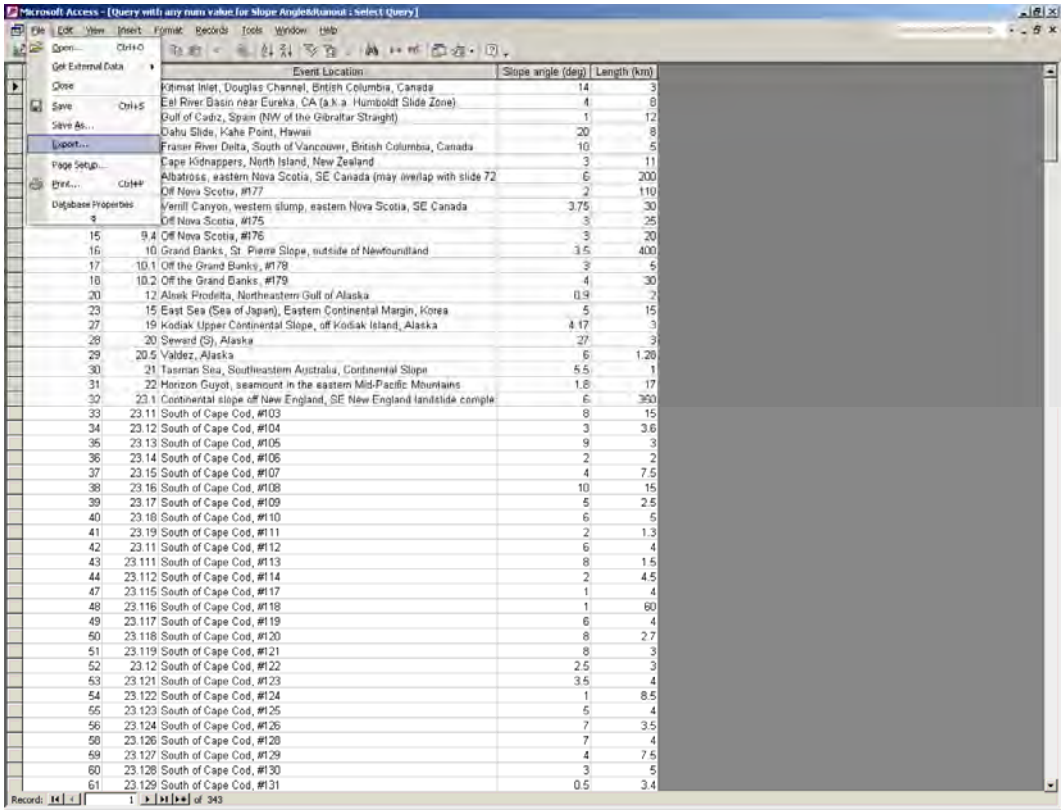

Figure A.6. Export Command: Method Used to export table to Excel®.

BIBLIOGRAPHY

Abrahamson, N.A., and Silva, W.J., 1997. Empirical Response Spectral Attenuation Relations for Shallow Crustal Earthquakes. *Seismological Research Letters*, v. 68, no. 1.

Almagor, G., 1978. Submarine slumping as a major agent of downslope sediment transport on the continental margin of Israel. *International Congress on Sedimentology, 10th*, v. 1, p. 15. *

Almagor, G., 1980. Halokinetic deep-seated slumping on the Mediterranean slope of northern Sinai and southern Israel. *Marine Geotechnology*, v. 4, p. 83 – 105. *

Almagor, G., and Wiseman, G., 1991. Analysis of submarine slumping in the continental slope off the southern coast of Israel. *Marine Geotechnology*, v. 10, p. 303-342. *

Alonso, B., Kastens, K.A., Maldonado, A., Maliverno, A., Nelson, C.H., O'Connell, S., Palanques, A., and Ryand, W.B.F., 1985. Morphology of the Ebro fan valleys from SeaMARC and SeaBeam profiles, *Geo-Marine Letters*, v. 5, p. 141 – 148.

Andersen, A., and Bjerrum, L., 1967. Slides in subaqueous slopes in loose sand and silt. *Marine Geotechnique*, p. 221 – 239.

Andersen, E.S., Solheim, A., and Elverhoi, A., 1994. Development of a glaciated Arctic continental margin: Exemplified by the western margin of Svalbard. *Proceedings, International Conference on Arctic Margins, 1992 (ICAM)*, p. 155 – 160.

Assier-Rzadkieaicz, S., Heinrich, P., Sabatier, P.C., Savoye, B., Bourillet, J.F., 2000. Numerical Modelling of a Landslide-generated Tsunami: The 1979 Nice Event. *Pure and Applied Geophysics*, v. 157, issue 10, p. 1707-1727. *

Bailey, E.B., Collet, L.W., and Field, R.M., 1928. Paleozoic submarine landslips near Quebec City. *Journal of Geology*, v. 36, p. 577 – 614. *

Baltuk, M., Taylor, E. and McDougall, K., 1985. Mass movement along the inner wall of the Middle America Trench, Coast Rica, *Initial Report of the Deep Sea Drilling Project*, v. 84, p. 551 – 565. *

Baltzer, A., Cochonat, P., and Piper, D.J.W., 1994. In situ geotechnical characterization of sediments on the Scotian Slope, Eastern Canadian continental margin. *Marine Geology*, v. 120, p. 291-308. *

Baltzer, A., Holmes, R. and Evans, D., 1998. Debris flows on the Sula Sgeir Fan, NW of Scotland. In *Geological Processes on Continental Margins: Sedimentation, mass-wasting and stability*, edited by M.S. Stoker, D. Evans, and A. Cramp, Geological Society, London, Special Publications, no. 129, p. 105-115. *

Baraza, J., Ercilla, G., and Nilson, C.H., 1999. Potential geologic hazards on the eastern Gulf of Cadiz slope (SW Spain). *Marine Geology*, v. 155, p. 191 – 215. *

Barnes, P.M., Cheung, K.C., Smits, A.P., Almagor, G., Read, S.A.L., Barker, P.R., and Froggatt, P., 1991. Geotechnical Analysis of the Kidnappers slide, upper continental slope, New Zealand. *Marine Geotechnology*, v. 10, p. 159-188. *

Bartolini, C., Gehin, C., and Stanley, D.J., 1972. Morphology and recent sediments of the Alboran Basin in the Mediterranean Sea. *Marine Geology*, v. 13, p. 159-224. *

Baumgartner, T., Ferreira, V., Soutar, Andrew, Schrader, H., and Moreno, F., 1985. Sedimentological implications of the reconstructed twentieth century varve record from the central Gulf of California. *Eos, Transactions, American Geophysical Union*, v. 66, no. 46, p. 917. *

Bea, R.G., and Arnold, P., 1973. Movements and forces developed by wave-induced slides in soft clays, *Offshore Technology Conference*, Preprints, v. 2, p. 731 – 742.

Bellaiche, G., Droz, L., Aloisi, J.-C., Bouye, C., Got, H., Monaco, A., Maldonado, A., Serra-Raventos, J., and Mirabile, L., 1981. The Ebro and the Rhone deep-sea fans: First comparative study. *Marine Geology*, v. 43, p. M75 – M85. *

Bennett, R.H., Bryant, W.R., Dunlap, W.A., and Keller, G.H., 1976. Initial results and progress of the Mississippi Delta sediment pore water pressure experiment. *Marine Geotechnology*, v. 1, no. 4, p. 327 – 344.

Bennett, R.H., Lambert, D.N., and Hulbert, M.H., 1977. Geotechnical properties of a submarine slide area on the U.S. continental slope northeast of Wilmington Canyon. *Marine Geotechnology*, v. 2, p. 245-261.

Bjerrum, L., 1971. Subaqueous slope failures in Norwegian fjords, *International Conference on Port and Ocean Engineering under Arctic Conditions, Proceedings*, v. 1, p. 24 – 47. *

Bohlke, B.M., and Bennett, R.H., 1980. Mississippi prodelta crusts: a clay fabric and geotechnical analysis, *Marine Geotechnology*, v. 4, p. 55-82.

Bondevik, S., Svendsen, J.I., Johnsen, G., Mangerud, J., and Kaland, P.E., 1997. The Storegga tsunami along the Norwegian coast, its age and runup. *Boreas*, v. 26, p. 29 – 53. *

Booth, J.S., and O'Leary, D.W., 1991. A statistical overview of mass movement characteristics on the North America Atlantic Outer Continental Margin. *Marine Geotechnology*, v. 10, p. 1-18. *

Booth, J.S., O'Leary, D.W., Popenoe, P., and Danforth, W.W., 1993. U.S. Atlantic Continental Slope Landslides: Their Distribution, General Attributes, and Implications. *U.S. Geological Survey Bulletin 2002*, Submarine Landslides: Selected Studies in the U.S. Exclusive Economic Zone, p. 14 – 22. *

Bornhold, B.D., Ren, P., and Prior, D.B., 1994. High-frequency turbidity currents in British Columbia fjords. *Geo-Marine Letters*, v. 14, p. 238 – 243. *

Bouma, A.H., Stelting, C.E., and Coleman, J.M., 1984. Mississippi Fan: Internal structure and depositional processes. *Geo-Marine Letters*, v. 3, p. 147 – 153.

Buffler, R.T., Shaub, F.J., Watkins, J.S., and Worzel, J.L., 1979. Anatomy of the Mexican Ridges, Southwestern Gulf of Mexico. *The American Association of Petroleum Geologists Special Publication*, M 29: Geological and Geophysical Investigations of Continental Margins, p. 319 – 327. *

Bugge, T., Befring, S., Belderson, R.H., Eidvin, T., Jansen, E., Kenyon, N.H., Holtedahl, H., and Sejrup, H.P., 1987. A giant three-stage submarine slide off Norway. *Geo-Marine Letters*, v. 7, p. 191 – 198. *

Bunn, A.R. and McGregor, B.A., 1980. Morphology of the North Carolina continental slope, Western north Atlantic, shaped by deltaic sedimentation and slumping, *Marine Geology*, v. 37, p. 253-266. *

Butenko, J., and Barbot, J.P., 1979. Geological hazards related to offshore drilling and construction in the Orinoco river delta of Venezuela, *Offshore Technology Conference, Proceedings*, v. 1, p. 323 – 329. *

Butler, L.W., 1979. Shallow structure on the continental margin, southern Brazil and Uruguay, *Geological Society of America Bulletin*, v. 81, p. 1079 – 1096. *

Canals, A. M., and Chassefiere, B., 1989. Slump scars and eroded canyon walls on continental margins; implication for their geotechnical and mass physical properties; Gulf of Lions, Western Mediterranean Sea, *Giornale di Geologia*, v. 51, no. 1, p. 147 - 163. *

Carlson, P.R., Karl, H.A., and Edwards, B.D., 1982. Puzzling mass movement features in the Navarinsky Canyon head, Bering Sea. *Geo-Marine Letters*, v. 2, p. 123 – 127. *

Carlson, P.R., Karl, H.A., and Edwards, B.D., 1991. Mass sediment failure and transport features revealed by acoustic techniques, Beringian Margin, Bering Sea, Alaska. *Marine Geotechnology*, v. 10, p. 33-51. *

Carlson, P.R., Karl, H.A., Edwards, B.D., Gardner, J.V., and Hall, R., 1993. Mass movement related to large submarine canyons along the Beringian Margin, Alaska. *U.S. Geological Survey Bulletin 2002*, Submarine Landslides: Selected Studies in the U.S. Exclusive Economic Zone, p. 104 - 116. *

Carlson, P.R. and Molnia, B.F., 1977. Submarine Faults and slides on the continental shelf, northern Gulf of Alaska. *Marine Geotechnology*, v. 2, p. 275-290. *

Carpenter, G.B., 1981a. Potential geologic hazards and constraints for blocks in proposed South Atlantic OCS Oil and Gas Lease Sale 56. *U.S. Geological Survey Open-File Report 81-019*, 286 p.

Carpenter, G.B., 1981b. Coincident slump/clathrate complexes on the U.S. Atlantic continental slope, *Geo-Marine Letters*, v. 1, p. 29 - 32. *

Carpenter, G.B., Cardinell, A.P., Francois, D.K., Good, L.K., Lewis, R.L., and Stiles, N.T., 1982. Potential geologic hazards and constraints for blocks in proposed oil and gas lease sale 52. *U.S. Geological Survey Open-File Report 82-36*, 51 p.

Carter, L., 2001. A large submarine debris flow in the path of the Pacific deep western boundary current off New Zealand. *Geo-Marine Letters*, v. 21, p. 42 – 50. *

Carter, L., and Carter, R.M., 1985. Current modification of a mass failure deposit on the continental shelf, North Canterbury, New Zealand. *Marine Geology*, v. 62, p. 193 – 211. *

Cashman, K.V. and Popenoe, P., 1985. Slumping and shallow faulting related to the presence of salt on the Continental Slope and Rise off North Carolina, *Marine and Petroleum Geology*, v. 2, p. 260 – 271. *

Chamberlain, T.K., 1964. Mass transport of sediment in the heads of Scripps Submarine Canyon, California. In: *Papers in marine geology; Shepard commemorative volume. Ed.: Miller, R.L.*, p. 42 – 64. *

Chassefiere, B., and Monaco, A., 1989. Role of organic matter and particle fabric in mass-physical and geotechnical properties: Implications for undrained slumping in Aegean Sea and Ionian Sea modern sediments, *Marine Geology*, v. 87, p. 165 – 182. *

Chen, M.-P., and Tian, W.-M., 1982. Marine geotechnical properties and stability of the continental margin deposits off Hua-Lien, northeast of Taiwan, *Acta Oceanography Taiwanica*, no. 13, p. 23 – 68. *

Cherkis, N.Z., Max, M.D., Vogt, P.R., Crane, K., Midthassel, A., and Sundvor, E., 1999. Large-scale mass wasting on the north Spitsbergen continental margin, Arctic Ocean. *Geo-Marine Letters*, v. 19, p. 131 – 142. *

Chough, S. K., Yoon, S. H., and Lee, H. J., 1992. Submarine slides in the eastern continental margin, Korea, *Marine Geotechnology*, v. 10, p. 71-82. *

Chough, S. K., and Lee, H. J., 1987. Stability of sediments on the Ulleung Basin slope, *Marine Geotechnology*, v. 7, p. 123-132. *

Christian, H., Piper, D.J.W., and Armstrong, R., 1991. Geotechnical properties of seabed sediments from Flemish Pass. *Deep Sea Research*, v. 38, p. 663-676.

Christian, H.A. et al, 1994. Slope instability on the Fraser River Delta Foreslope, Vancouver, British Columbia. *Proceedings of the 47th CGS Conference* in Halifax, p. 115-165. *

Christian, H.A., Woeller, O.J., Robertson, P.K., and Courtney, R.C., 1997. Site investigations to evaluate flow liquefaction slides at Sand Heads, Fraser River delta, *Canadian Geotechnical Journal*, v 34, n 3, p. 384-397. *

Cochonat, P., Bourillet, J.F., and Savoye, B., 1993. Geotechnical characteristics and instability of submarine slope sediments, the Nice slope (N-W Mediterranean Sea), *Maine Georesources Geotechnology*, v. 11, p. 131-151. *

Cochonat, P., Ollier, G., and Michel, J.L., 1989. Evidence for slope instability and current-induced sediment transport, the RMS *Titanic* wreck search area, Newfoundland Rise, *Geo-Marine Letters*, v. 9, p. 145 – 152. *

Coleman, J.M., and Garrison, L.E., 1978. Geological aspects of marine slope stability, northwestern Gulf of Mexico, *Marine Geotechnology*, v. 2, p. 9 - 44. *

Corthay, J.E. II, and Aliyev, A.A., 2000. Delineation of a mud volcano complex, surficial mudflows, slump blocks, and shallow gas reservoirs, offshore Azerbaijan. *Proceedings of the Annual Offshore Technology Conference*, v. 1, 32nd Annual Offshore Technology Conference - OTC 2000, p. 327 – 354. *

Coulter, H.W., and Migliaccio, R.R., 1966. Effects of the earthquake of March 27, 1964, at Valdez, Alaska. *U.S. Geological Survey Professional Paper 542-C*, 36 p. *

Coumes, F., 1987. Seismic stratigraphy of giant mass movements, including megaturbidites, on recent continental margins. *Geo-Marine Letters*, v. 7, p. 113 – 117. *

Damuth, J.E., and Flood, R.D., 1984. Morphology, sedimentation processes, and growth pattern of the Amazon deep-sea fan, *Geo-Marine Letters*, v. 3, p. 109 – 117. *

Davis, S.N., and Karzulovic, K.J., 1963. Landslides at Lago Rinihue, Chile. *Seismological Society of America Bulletin*, v. 53, no. 6, p. 1403 – 1414. *

Davies, T.L., Van Niel, B., Kidd, R.B., and Weaver, P.P.E., 1997. High-resolution stratigraphy and turbidite processes in the Seine Abyssal Plain, northwest Africa. *Geo-Marine Letters*, v. 17, p. 147 – 153. *

Daviess, S.N., 1971. Barbados: a major submarine gravity slide, *Geological Society of America Bulletin*, v. 82, p. 2593 – 2602. *

Dawson, A.G., Long, D., and Smith, D.E., 1988. The Storegga slides: Evidence from eastern Scotland for a possible tsunami. *Marine Geology*, v. 82, p. 271 – 276. *

Dengler, A.T., Wilde, P., Noda, E.K., and Normark, W.R., 1984. Turbidity currents generated by Hurricane Iwa. *Geo-Marine Letters*, v. 4, p. 5-11. *

Desgagnes, P., Locat, J., Lee, H.J., Leroueil, S., Alexander, C., Mountain, G.,and Pratson, L., 2000. Geotechnical properties of a mass flow deposit on the Hudson Apron, off New Jersey, U.S.A., *53rd Canadian Geotechnical Conference*, v. 1, p. 137 – 144. *

Dillon, W.P., Popenoe, P., Grow, J.A., Klitgord, K.D., Swift, B.A., Paull, C.K., and Cashman, K.V., 1982. Growth faulting and salt diapirism—their relationship and control in the Carolina trough, eastern North America, *in* Watkins, J.S. and Drake, C.L. (eds.), Studies in continental margin geology. *American Association of Petroleum Geologists Memoir 34*, p. 31 – 46.

Dillon, W.P., Risch, J.S., Scanlon, K.M., Valentine, P.C., and Huggett, Q.J., 1993. Ancient Crustal Fractures Control the Location and Size of Collapsed Blocks at the Blake Escarpment, East of Florida. *U.S. Geological Survey Bulletin 2002*, Submarine Landslides: Selected Studies in the U.S. Exclusive Economic Zone, p. 54 - 59. *

Dimakis, P., Elverhøi, A., Hoeg, K., Solheim, A., Harbitz, C., Laberg, J.S., Vorren, T.O., and Marr, J., 2000. Submarine slope stability on high-latitude glaciated Svalbard-Barents Sea margin, *Marine Geology*, v. 162, p. 303-316. *

Dingle, R. V., 1977. The anatomy of a large submarine slump on a sheared continental margin (SE Africa), *Journal of the Geological Society of London*, v. 134, Part 3, p. 293-310. *

Droz, L., Rigaut, F., Cochonat, P., and Tofani, R., 1996. Morphology and recent evolution of the Zaire turbidite system (Gulf of Guinea). *Geological Society of America Bulletin*, v. 108, p. 253-269. *

Edgers, L., and Karlsrud, K., 1982. Soil flow generated by submarine slides – Case studies and consequences. In: C. Chryssostomidis and J.J. Connor (Eds.), *Proceedings of the Third International Conference on the Behavior of Offshore Structures*, Hemisphere, Bristol, Pa, p. 425-437.

Edgers, L., and Karlsrud, K., 1985. Viscous analysis of submarine flows. Behaviour of Offshore Structures, p. 773 – 784.

Edwards, B.D., Lee, H.J., and Field, M.E., 1993. Seismically Induced Mudflow in Santa Barbara Basin, California. U.S. Geological Survey Bulletin 2002, Submarine Landslides: Selected Studies in the U.S. Exclusive Economic Zone, p. 167-175. *

Edwards, B.D., Field, M.E., and Clukey, E.C., 1980. Geological and geotechnical analysis of a submarine slump, California borderland, paper presented at *12th Annual Offshore Technology Conference, Proceedings*, v. 1, p. 399-410. *

Egloff, J., and Johnson, G.L., 1982. Growth fault on insular slope/rise of western Iceland; comparison with SE Greenland canyons and slumps. *Geo-Marine Letters*, v. 2, p. 143 – 148. *

Elverhøi, A., Norem, H., Andersen, E.S., Dowdeswell, J.A., Fossen, I., Haflidason, H., Kenyon, N.H., Laberg, J.S., King, E.L., Sejrup, H.P., Solheim, A., and Vorren, T., 1997. On the origin and flow behavior of submarine slides on deep-sea fans along the Norwegian-Barents Sea continental margin. *Geo-Marine Letters*, v. 17, p. 119 – 125. *

Embley, R.M., 1980. The role of mass transport in the distribution and character of deep-ocean sediments with special reference to the North Atlantic. *Marine Geology*, v. 38, p. 25-50. *

Embley, R.M., 1976. New evidence for occurrence of debris flow deposits in the deep sea. *Geology*, v.4, n. 6, p. 371-374. *

Embley, R.W., and Hayes, D.E., 1974. Giant submarine slump south of the Canaries, *Geological Society of America*, v. 6, p. 721. *

Embley, R.W. and Jacobi, R., 1977. Distribution and morphology of large submarine sediment slides and slumps on Atlantic continental margins. *Marine Geotechnology*, v. 2, p. 205-228. *

Embley, R.W. and Morley, J., 1980. Quarternary sedimentation and paleoenvironmental studies off Namiba (southwest Africa). *Marine Geology*, v. 36, p. 183-204. *

Emery, K.O., Uchupi, E., Phillips, J.D., Bowin, C.O., Bunce, E.T., and Knott, S.T., 1970. Continental rise off eastern North America. *American Association of Petroleum Geologists Bulletin*, v. 54, no. 1, p. 44 – 108. *

Emery, K.O., Uchupi, E., Bowin, C.O., Phillips, J., and Simpson, E.S.W., 1975a. Continental margin off western Africa: Cape St. Francis (South Africa) to Walvis Ridge (South West Africa), *American Association of Petroleum Geologists, Bulletin*, v. 59, p. 3 - 59. *

Emery, K.O., Uchupi, E., Phillips, J., Bowin, C.O., and Mascle, J., 1975b. Continental margin off Western Africa: Angola to Sierra Leone. *American Association of Petroleum Geologists, Bulletin*, v. 59, no. 12, p. 2209 – 2265. *

Emmel, F.J., and Curray, J.R., 1984. The Bengal submarine fan, Northeastern Indian Ocean. *Geo-Marine Letters*, v. 3, p. 119 – 124. *

Evans, D., King, E.L., Kenyon, N.H., Brett, C., and Wallis, D. 1996. Evidence for long-term instability in the Storegga Slide region off western Norway. *Marine Geology*, v. 130, p. 281-292. *

Ferentinos, G., Brooks, M., and Collins, M., 1982. Gravity-induced deformation on the north flank and floor of the Sporadhes basin of the North Aegean sea trough, *Marine Geology*, v. 44, p. 289 – 302.

Field, M.E., and Barber, J.H., 1993. A Submarine Landslide Associated with Shallow Sea-Floor Gas and Gas Hydrates off Northern California. *U.S. Geological Survey Bulletin 2002*, Submarine Landslides: Selected Studies in the U.S. Exclusive Economic Zone, p. 151-157. *

Field, M.E., and Edwards, B.D., 1993. Submarine Landslides in a Basin and Ridge Setting, Southern California. *U.S. Geological Survey Bulletin 2002*, Submarine Landslides: Selected Studies in the U.S. Exclusive Economic Zone, p. 176 - 183. *

Field, M.E., and Edwards, B.D., 1980. Slopes of the southern California borderland: A regime of mass transport, *in* Field, M.E., Bouma, A.H., Colbourn, I.P., Douglas, R.G., and Ingle, J.C., eds., Pacific Section SEPM, Pacific Coast Paleogeography Symposium No. 4, Los Angeles, Calif., p. 169 – 184. *

Field, M.E., and Gardner, J.V., 1990. Plio-Pleistocene growth of the Rio Ebro margin, NE Spain: A prograding slope model. *Geological Society of America Bulletin*, v. 102, p. 721 – 733. *

Field, M.E., and Clarke, S.H., Jr., 1979. Small slumps and slides and their significance for basin slope processes, southern California borderland. *Geology of continental slopes, Special Publication – Society of Economic Palentologists and Mineralogists*, v. 27, p. 223 – 230. *

Flaate, K., and Janbu, N., 1975. Soil exploration in a 500 m deep fjord, western Norway. *Marine Geotechnology*, v. 1, p. 117 – 139.

Flood, R.D., Hollister, C.D. and Lonsdale, P., 1979. Disruption of the Fedi sediment drift by debris flows from Rockall Bank. *Marine Geology*, v. 32, p. 311-334. *

Fortuin, A.R., Roep, Th.B., Sumosusatro, P.A., van Weering, Tj.C.E., and van der Werff, W., 1992. Slumping and sliding in Miocene and Recent developing arc basins, onshore and offshore Sumba (Indonesia), *Marine Geology*, v. 108, p. 345 – 363. *

Fryer, G.J., 1996. Hawaiian tsunamis and small submarine landslides, AGU 1996 fall meeting, *Eos, Transactions, American Geophysical Union*, v. 77, no. 46, Suppl., p. 511. *

Fryer, G.J., 1997. Landslides triggered by storm waves and tsunamis triggered by landslides: Unrecognized coastal hazards in Hawai'i, *Abstracts with Programs - Geological Society of America,* v. 29, no. 5, p. 14.

Gardner, J.V., Prior, D.B., and Field, M.E., 1999. Humboldt Slide – a large shear-dominated retrogressive slope failure. *Marine Geology*, v. 154, p. 323 – 338. *

Giardini, D., Grynthal, G., Shedlock, K., and Zhang, P., 1999. http://seismo.ethz.ch/GSHAP/.

Ginsburg, G.D., Kremlev, A.N., Grigor'vev, M.N., Pavlenkin, A.D., Larkin, G.V., and Tsar'kov, V.Ye., 1989. Discovery of solid gas hydrate in the rock at the foot of the continental slope of the Crimea. *Transactions (Doklady) of the USSR Academy of Sciences: Earth Science Sections*, v. 309, no. 6, p. 83 – 85.

Goldfinger, C., Kulm, L.D., and McNeill, L.C., 1997. Super-scale slumping of the southern Oregon Cascadia margin; tsunamis and tectonic erosion of the forearc, *Abstracts with Programs - Geological Society of America,* v. 29, no. 5, p. 17. *

Goldfinger, C., Kulm, L.D., McNeill, L.C., and Watts, P., 2000. Super-scale failure of the southern Oregon Cascadia margin. *Pure and Applied Geophysics*, v. 157, p. 1189-1226. *

Gorsline, D.S., and Emery, K.O., 1959. Turbidity current deposits in San Pedro and Santa Monica Basins off southern California, *Geological Society of America, Bulletin*, v. 70, p. 279 – 290. *

Grass, M., Watters, R., Karlin, R., and Holmes, M., 1997. Submarine and subaerial landslides as tools for paleoseismic analysis in the Puget Sound region, Washington State, *Eos, Transactions, American Geophysical Union*, v. 78, no. 46, Suppl., p. 440. *

Grass, M., Watters, R., and Karlin, R., 1997. Paleoseismic analysis using submarine landslides in Puget Sound, Washington, *Abstracts with Programs - Geological Society of America,* v. 29, no. 5, p. 17. *

Greene, H.G., Clarke, S.H., Field, M.E., Linker, F.I., and Wagner, H.C., 1975. Preliminary report on the environmental geology of selected areas of the Southern California Continental Borderland. *U.S. Geological Survey Open-File Report 75-596.* *

Gutmacher, C.E., and Normark, W.R., 1993. Sur Submarine Landslide, a Deep-Water Sediment Slope Failure. U.S. Geological Survey Bulletin 2002, Submarine Landslides: Selected Studies in the U.S. Exclusive Economic Zone, p. 158-166. *

Hampton, M.A., 1972. The role of subaqueous debris flow in generating turbidity currents. *Journal of Sedimentary Petrology*, v. 42, no. 4, p. 775 – 793. *

Hampton, M.A., 1989. Geotechnical properties of unconsolidated sediment on the Kodiak continental shelf and upper slope, Gulf of Alaska. *Marine Geotechnology*, v.8, p. 159-180. *

Hampton, M.A., 1993. Comparison of Tectonic and Stratigraphic Control of Submarine Landslides on the Kodiak Upper Continental Slope, Alaska. U.S. Geological Survey Bulletin 2002, Submarine Landslides: Selected Studies in the U.S. Exclusive Economic Zone, p. 117-122. *

Hampton, M.A., Lemke, R.W., and Coulter, H.W., 1993. Submarine Landslides that had a Significant Impact on Man and his Activities: Seward and Valdez, Alaska. U.S. Geological Survey Bulletin 2002, Submarine Landslides: Selected Studies in the U.S. Exclusive Economic Zone, p. 123-134. *

Hampton, M.A., Lee, H.J., and Locat, J., 1996. Submarine Landslides. *Reviews of Geophysics*, v. 34, no. 1, p. 33-59.

Hampton, M.A., and Bouma, A.H., 1977. Slope instability near the shelf break, western Gulf of Alaska. *Marine Geotechnology*, v.2, p. 309-331. *

Hampton, M.A., Bouma, A.H., Carlson, P.R., Molnia, B.F., Clukey, E.C., 1978. Quantitative study of slope instability in the Gulf of Alaska, *Offshore Technology Conference, 10. Houston 1978. Proceedings*, v. 4, p. 2307 – 2318. *

Hampton, M.A., and Winters, W.J., 1981. Environmental geology of Shelikof Strait, OCS Sale Area 60, Alaska, *Offshore Technology Conference, 13. Houston 1981. Proceedings*, p. 19 – 31. *

Haner, B. E., and Gorsline, D. S., 1978. Processes and morphology of continental slope between Santa Monica and Dume submarine canyons, southern California, *Marine Geology,* v. 28, p. 77-87. *

Heezen, B.C. and Ewing, M., 1952. Turbidity currents and submarine slumps, and the 1929 Grand Banks earthquake, *American Journal of Science*, v. 250, p. 849 – 873. *

Heezen, B.C. and Ewing, M., 1955. Orleansville earthquake and turbidity currents, *American Association of Petroleum Geologists Bulletin*, v. 39, no. 12, p. 2505 – 2514. *

Heezen, B.C. and Drake, C.L., 1964. Grand Banks slump. *American Association of Petroleum Geologists Bulletin*, v. 48, p. 221 – 233. *

Henkel, D.J., 1970. The role of waves in causing submarine landslides, *Geotechnique,* v. 20, p. 75 – 80.

Herzer, R.H., 1979. Submarine landslides and submarine canyons on the slope off Canterbury, New Zealand, *Journal of Geology and Geophysics,* v. 22, no. 3, p. 391 – 406. *

Herzer, R.H. and Lewis, D.W., 1979. Growth and burial of a submarine canyon off Motunau, North Canterbury, New Zealand, *Sedimentary Geology,* v. 24, no. 1, p. 69 – 83. *

Hill, P.R., Moran, K.M., and Blasco, S.M., 1982. Creep deformation of slope sediments in the Canadian Beaufort Sea. *Geo-Marine Letters,* v. 2, p. 163 – 170. *

Hill, P.R., 1983. Detailed morphology of a small area on the Nova Scotian Continental Slope. *Marine Geology,* v. 53, p. 55 – 76. *

Hiscott, R.N., and Aksu, A.E., 1994. Submarine debris flows and continental slope evolution in front of Quaternary ice sheets, Baffin Bay, Canadian Arctic, *American Association of Petroleum Geologists Bulletin*, v. 78, no. 3, p. 445 – 460. *

Holcomb, R., and Searle, R., 1991. Large landslides from oceanic volcanoes. *Marine Geotechnology*, v. 10, p. 19-32. *

Holmes, R., Long, D., Dodd, L.R., 1998. Large-scale debrites and submarine landslides on the Barra Fan, west of Britain. In *Geological Processes on Continental Margins: Sedimentation, mass-wasting and stability,* edited by M.S. Stoker, D. Evans, and A. Cramp, Geological Society, London, Special Publications, no. 129, p. 67-79. *

Holtedahl, H., 1965. Recent turbidites in the Hardangerfjord, Norway. *Colston Research Society Proceedings*, Bristol, v. 17, p. 107 – 141. *

Hoskin, C.M., and Burrell, D.C., 1972. Sediment transport and accumulation in a fjord basin, Glacier Bay, Alaska. *Journal of Geology*, v. 80, p. 539 - 551. *

Houtz, R.E., 1962. The 1953 Suva earthquake and tsunami. *Bulletin of the Seismological Society of America*, v. 52, p. 1-12. *

Houtz, R.E., and Wellman, H.W., 1962. Turbidity current at Kadavu passage, Fiji. *Geological Magazine*, v. 99, p. 57 – 62. *

http://walrus.wr.usgs.gov/globalhydrate

Huson, W.J. and Fortuin, A.R., 1985. The Lithinon Slide: A large submarine slide in the South Cretan Trough, eastern Mediterranean. *Marine Geology*, v. 65, p. 103 – 111. *

Hwang, I.G., and Chough, S.K., 2000. The Maesan fan delta, Miocene Pohang Basin, SE Korea: architecture and depositional processes of a high-gradient fan-delta-fed slope system. *Sedimentology*, v. 47, p. 995 – 1010. *

Hynes, M.E., and Franklin, A.G., 1984. Rationalizing the Seismic Coefficient Method. Miscellaneous Paper GL-84-13. US Army Engineer Waterways Experiment Station, Vicksburg, MS.

Imamura, F., and Kikuchi, M., 1994. Moment release of the 1992 Flores Island earthquake inferred from tsunami and teleseismic data. *Sci. Tsunami Hazards*, v. 12, p. 67 – 76. *

Imran, J., Parker, G., Locat, J., and Lee, H., 2001. 1D numerical model of muddy subaqeuous and subaerial debris flows, *Journal of Hydraulic Engineering*, v. 127, no. 11, p. 959 – 968.

Jacobi, R. 1976. Sediment slides on the northwestern continental margin of Africa, *Marine Geology*, v. 22, p. 157-173. *

Jacobi, R. and C.L. Mrozowski, 1979. Sediment slides and sediment waves in the Bonin Trough, western Pacific. *Marine Geology*, v. 29, no. ¼, p. M1 – M9. *

Jenkins, C.J. and Keene, J.B., 1992. Submarine slope failures of the southeast Australian continental slope: a thinly sedimented margin. *Deep-Sea Research*, v. 39, no. 2, p. 121-136. *

Johns, et al, 1986. Geotechnical aspects of a submarine slope failure, Kitimat Fjord, British Columbia. *Marine Geotechnology*, v. 6, no. 3, p. 243-279. *

Jones, O.T., 1937. On sliding and slumping of submarine sediments in Denbighshire, North Wales during the Ludlow period. *Geological Society of London Quarterly Journal*, v. 93, p. 241 – 284. *

Josenhans, H.W., Barrie, J.V., and Kiely, L.A., 1987. Mass wasting along the Labrador shelf margin: Submersible observations. *Geo-Marine Letters*, v. 7, p. 199 – 205. *

Karig, D.E., Barber, A.J., Charlton, T.R., Klemperer, S., and Hussong, D.M., 1987. Nature and distribution of deformation across the Banda Arc-Australian collision zone at Timor, *Geological Society of America Bulletin*, v. 98, p. 18 – 32.

Karlin, R.E., Watters, R.J., Grass, M.J., Prunier, C.F., Holmes, M.L., 1996. Seismic landslides in Puget Sound (SLIPS); II, Quaternary faulting and submarine mass-wasting, AGU 1996 fall meeting, *Eos, Transactions, American Geophysical Union*, 77 (46, Suppl.), p. 499.

Kayen, R.E., Schwab, W.C., Lee, H.J., Torresan, M.E., Hein, J.R., Quinterno, P.J., and Levin, L.A., 1989. Morphology of sea-floor landslides on Horizon Guyot: application of steady-state geotechnical analysis. *Deep-Sea Research*, v. 36, no. 12, p. 1817-1839. *

Kayen, R.E., and Lee, H.J., 1991. Pleistocene slope instability of gas hydrate-laden sediment on the Beaufort Sea margin, *Marine Geotechnology*, 10 (1-2), p. 125-141. *

Kayen, R. E., and Lee, H. J., 1993. Slope stability in regions of sea-floor gas hydrate; Beaufort Sea continental slope. *U.S. Geological Survey Bulletin 2002*, Submarine Landslides: Selected Studies in the U.S. Exclusive Economic Zone, p. 97-103. *

Keating, B.H., Helsley, C.E., and Karogodina, I., 2000. Sonar studies of submarine mass wasting and volcanic structures off Savaii Island, Samoa. *Pure and Applied Geophysics*, v. 157, p. 1285 – 1313. *

Keefer, D.K., 1984. Landslides caused by earthquakes. *Geological Society of America Bulletin*, v. 95, p. 406 – 421. *

Keer, F.R. and Cardinell, A.P., 1981. Potential geologic hazards and constraints for blocks in proposed mid-Atlantic OCS oil and gas lease sale 59. *U.S. Geological Survey Open-File Report 81-725*, 109 p., 5 maps. *

Keller, G.H., 1982. Organic matter and the geotechnical properties of submarine sediments. *Geo-Marine Letters*, v. 2, p. 191 – 198.

Kenyon, N.H., R.H. Belderson, and A.H. Stride, 1978. Channels, canyons and slump folds on the continental slope between South-West Ireland and Spain. *Oceanologica Acta*, v. 1, no. 3, p. 369 – 380. *

Kenyon, N.H., 1987. Mass-wasting features on the continental slope of northwest Europe. *Marine Geology*, v. 74, p. 57-77. *

King, E.L., Sejrup, H.P., Haflidason, H., Elverhøi, A., and Aaresth, I., 1996. Quarternay seismic stratigraphy of the North Sea Fan: Glacially-fed gravity flow aprons, hemipelagic sediments, and large submarine slides. *Marine Geology*, v. 130, p. 293-315. *

Knapp, J.H., and Diaconescu, C.C., 2000. Evidence for buried gas hydrates and their role in seafloor instability in the South Caspian Sea, Azerbaijan. *Geological Society of America, 2000 annual meeting, Abstracts with Programs - Geological Society of America*, v. 32, no. 7, p. 102. *

Knebel, H. and Carson, B., 1979. Small-scale slump deposits, middle Atlantic continental slope off eastern United States, *Marine Geology*, v. 29, p. 221-236. *

Kolla, V., and Buffler, R.T., 1984. Morphologic, acoustic, and sedimentologic characteristics of the Magdalena Fan. *Geo-Marine Letters*, v. 3, p. 85 – 91. *

Kolla, V., and Coumes, F., 1984. Morpho-acoustic and sedimentologic characteristics of the Indus Fan. *Geo-Marine Letters*, v. 3, p. 133 – 139. *

Kostaschuk, R.A., and McCann, S.B., 1983. Observations on delta-forming processes in a fjord-head delta, British Columbia. *Sedimentary Geology*, v. 36, p. 269 – 288. *

Koppejan, A.W., van Wamelen, B.M., and Weinberg, L.J.H., 1948. Coastal flow slides in the Dutch province of Zeeland. *Proceedings from the 2nd Conference of Soil Mechanics and Foundation Engineering*, Rotterdam, Holland, V. p. 89-96. *

Kraft, L.M. Jr., Gavin, T.M., and Bruton, J.C., 1992. Submarine flow slide in Puget Sound, *Journal of Geotechnical Engineering*, ASCE, v 118, n 10, p. 1577-1591. *

Kramer, S., 1996. Geotechnical Earthquake Engineering, Prentice-Hall, Inc., Upper Saddle River, New Jersey.

Krastel, S., Schmincke, H.-U., and Jacobs, C.L., 2001. Formation of submarine canyons on the flanks of the Canary Islands. *Geo-Marine Letters*, v. 20, p. 160 – 167. *

Krause, D.C., W.C. White, K.J.W. Piper, and B.C. Heezen, 1970. Turbidity currents and cable breaks in the Western New Britain Trench. *Geological Society of America. Bulletin*, v. 81, p. 2153 – 2160. *

Kvenvolden, K. A., Ginsburg, G. D., and Soloviev, V. A., 1993. Worldwide distribution of subaquatic gas hydrates. *Geo-Marine Letters*, v. 13, no. 1, p. 32 - 40. *

Laberg, J.S., and Vorren, T.O., 2000a. The Trænadjupet Slide, offshore Norway – morphology, evacuation and triggering mechanisms. *Marine Geology*, v. 171, p. 95-114. *

Laberg, J.S., and Vorren, T.O., 2000b. Flow behaviour of the submarine glacigenic debris flows on the Bear Island Trough Mouth Fan, western Barents Sea. *Sedimentology*, v. 47, p. 1105 – 1117. *

Laberg, J.S., Vorren, T.O., and Knutsen, S.-M., 1999. The Lofoten Contourite Drift off Norway. *Marine Geology*, v. 159, p. 1 – 6. *

Laberg, J.S., and Vorren, T.O., 1995. Late Weichselian submarine debris flow deposits on the Bear Island Trough Mouth Fan. *Marine Geology*, v. 127, p. 45 – 72. *

Laberg, J.S., Vorren, T.O., Dowdeswell, J.A., Kenyon, N.H., and Taylor, J., 2000. The Andøya Slide and the Andøya Canyon, north-eastern Norwegian – Greenland Sea. *Marine Geology*, v. 162, p. 259 – 275. *

Labazuy, P., 1996. Recurrent landslide events on the submarine flank of Piton de la Fournaise volcano (Reunion Island). In: *Volcano Instability on the Earth and Other Planets, Geological Society of London Special Publication*, v. 110, p. 295 – 306. *

Lee, H.J., Edwards, B.D., and Field, M., 1981. Geotechnical Analysis of a Submarine Slump, Eureka, California. *Offshore Technology Conference, 13*, Houston, TX, May 4-7. p. 53-65. *

Lee, H.J., and Edwards, B.D., 1986. Regional method to assess offshore slope stability, *Journal of Geotechnical Engineering,* ASCE, v. 112, p. 489-509.

Lee, H.J., Schwab, W.C., Edwards, B.D., and Kayen, R.E., 1991. Quantitative controls on submarine slope failure morphology, *Marine Geotechnology*, v. 10, p. 143-157.

Lee, H.J., and Baraza, J., 1999. Geotechnical characteristics and slope stability in the Gulf of Cadiz. *Marine Geology*, v. 155, p. 173-190. *

Lee, H.J., Locat, J., Dartnell, P., Israel, K., and Wong, F., 1999. Regional variability of slope stability: application to the Eel margin, California. *Marine Geology*, v. 154, p. 305-321. *

Lee, S.C., and Mehta, A.J., 1997. Problems in characterizing dynamics of mud shore profile. *Journal of Hydraulic Engineering. ASCE 123*, p. 351 – 361.

Lehner, P., 1969. Salt tectonics and Pleistocene stratigraphy on the continental slope of northern Gulf of Mexico. *American Association of Petroleum Geologists Bulletin*, v. 53, p. 2431 - 2479.

Leroueil, S., Vaunat, J., Picarelli, L., Locat, J., Lee, H., and Faure, R., 1996. Geotechnical characterization of slope movements. *In* Proceedings of the International Symposium on Landslides, Trondheim. v. 1, p. 53 –74.

Lewis, K.B., 1971. Slumping on a continental slope inclined at 1°-4°. *Sedimentology*, v. 16, p. 97-110. *

Lewis, D.W., 1978. Subaqueous debris flow deposits in Cenozoic neritic sequences, South Island, New Zealand. *International Congress on Sedimentology, 10th*, v. 1, p. 388. *

Li, C., and Clark, A., 1991. SeaMARC II study of a giant submarine slump on the northern Chile continental slope, *Marine Geotechnology*, v. 10, p. 257-268. *

Lipman, P.W., Normark, W.R., Moore, J.G., Wilson, J.B., and Gutmacher, C.E., 1988. The giant submarine Alika Debris Slide, Mauna Loa, Hawaii. *Journal of Geophysical Research*, v. 93B, p. 4279 – 4299. *

Locat, J., and Demers, D., 1988. Viscosity, yield stress, remolded strength, and liquidity index relationships for sensitive clays, *Canadian Geotechnical Journal*, v. 25, p. 799 – 806.

Locat, J., and Lee, H.J., 2002. Submarine landslides: advances and challenges. *Canadian Geotechnical Journal*, v. 39, p. 193-212.

Long, D., and Holmes, R., 2001. Submarine landslides and tsunami threat to Scotland, ITS 2001 Proceedings, Session 1, Number 1-12, p. 355-365. *

Lowe, D.R., 1982. Sediment gravity flows. II. Depositional models with special reference to the deposits of high-density turbidity currents. *Journal of Sedimentary Petrology*, v. 52, p. 279 – 297. *

Lucchi, F.R., Colella, A., Gabbianelli, G., Rossi, S., and Normark, W.R., 1984. The Crati Submarine Fan, Inonian Sea. *Geo-Marine Letters*, v. 3, p. 71 – 77. *

Luternauer, J.L., Barrie, J. V., Christian, H. A., Clague, J. J., Evoy, R. W., Hart, B. S., Hunter, J. A., Killeen, P. G., Kostaschuk, R. A., Mathewes, R. W., Monahan, P. A., Moslow, T. F., Mwenifumbo, C. J., Olynyk, H. W., Patterson, R. T., Pullan, S. E., Roberts, M. C., Robertson, P. K., Tarbotton, M. R., and Woeller, D. J., 1994. Fraser River Delta: Geology, geohazards and human impact, Southwestern British Columbia, (ed) J.W.H. Monger: *Geological Survey of Canada, Bulletin*, v. 481, p. 197 – 220. *

Lykousis, V., 1991. Submarine slope instabilities in the Hellenic Arc region, northeastern Mediterranean Sea, *Marine Geotechnology*, v. 10, p. 83-96. *

McAdoo, B. G., Pratson, L. F., and Orange, D. L., 2000. Submarine landslide geomorphology, US continental slope, *Marine Geology*, v. 169, no. 1-2, p. 103-136. *

McGregor, B.A., 1977. Geophysical assessment of a submarine slide northeast of Wilmington Canyon, *Marine Geotechnology*, v. 2, Marine Slope Stability, p. 229 – 244. *

McGregor, B.A., and Bennett, R.H., 1977. Continental-slope sediment instability north-west of Wilmington Canyon, *American Association Petroleum Geologists Bulletin*, v. 61, p. 918-928. *

McGregor, B.A., and R.H. Bennett, 1979. Mass movement of sediment on the continental slope and rise seaward of the Baltimore canyon trough. *Marine Geology*, v. 33, no. 3/4, p. 163 – 174. *

McGregor, B.A., and R.H. Bennett, 1981. Sediment failure and sedimentary framework of the Wilmington geotechnical corridor, U.S. Atlantic Continental margin. *Sedimentary Geology*, v. 30, p. 213 – 234. *

McGregor, B.A., 1981. Smooth seaward-dipping horizons—an important factor in seafloor stability, *Marine Geology*, v. 39, p. M89 – M98. *

McGregor, B.A., Rothwell, R.G., Kenyon, N.H., and Twichell, D.C., 1993. Salt tectonics and slope failure in an area of salt domes in northwestern Gulf of Mexico. U.S. Geological Survey Bulletin 2002, *Submarine Landslides: Selected Studies in the U.S. Exclusive Economic Zone*, p. 92 - 96. *

McIllvaine, J.C., 1973. Sedimentary processes on the continental slope off New England, Woods Hole Oceanographic Institute (WHOI) Technical Report. 73-58, 211 pp. *

McIllvaine, J.C. and Ross, D.A., 1979. Sedimentary processes on the Continental slope off New England. *Journal of Sedimentary Petrology*, v. 49, p. 563 – 574. *

Maisey, G.H., 1979. Submarine slumping on the Weddell Sea Continental slope. *Continental Shelf Institute*, Trondheim. Report, P-204/2/79. 6 p. *

Malahoff, A., Embley, R.W., Perry, R.B., and Fefe, C., 1980. Submarine mass-wasting of sediments on the Continental Slope and upper Rise south of Baltimore Canyon. *Earth and Planetary Science Letters*, v. 49, p. 1 – 7. *

Marchetti, M.P., 1957. The occurrence of slide and flowage materials (olistromes) in the Tertiary series of Sicily. *International Geol. Cong. Rept., 20th*, Mexico City, sec. 5, tomo 1, p. 209 – 225. *

Marsaglia, K.M., and Klein, G.D., 1983. The Paleography of Paleozoic and Mesozoic storm depositional systems. *Journal of Geology*, v. 91, no. 2, p. 117 - 139.

Martin, R.G., 1980. Distribution of salt structures in the Gulf of Mexico: Map and descriptive text. U.S. Geological Survey Miscellaneous Field Studies Map, MF-1213, 2 plates, 8 pp.

Martin, R.G., and Bouma, A.H., 1982. Active diapirism and slope steepening, Northern Gulf of Mexico continental slope, *Marine Geotechnology*, v. 5, p. 63 - 91. *

Masson, D.G., Gardner, J.V., Parson, L.M., and Field, M.E., 1985. Morphology of upper Laurentian Fan using GLORIA long-range side-scan sonar. *American Association of Petroleum Geologists Bulletin*, v. 69, no. 6, p. 950 – 959. *

Masson, D.G., Canals, M., Alonso, B., Urgeles, R., and Huhnerbach, V., 1998. The Canary Debris Flow: source area morphology and failure mechanisms. *Sedimentology*, v. 45, issue 2, p. 411 – 432. *

Milkov, A. V., 2000. Worldwide distribution of submarine mud volcanoes and associated gas hydrates. *Marine Geology*, v. 167, no. 1-2, p. 29 – 42.

Milliman, J.D., and Meade, R.H., 1983. World-wide delivery of river sediment to the ocean. *Journal of Geology*, v. 91, no. 1, p. 1 – 21.

Mohrig, D., Whipple, K.X., Hondzo, M., Ellis, C., and Parker, G., 1998. Hydroplaning of subaqueous debris flows. *Geological Society of America Bulletin*, v. 110, no. 3, p. 387 – 394.

Mohrig, D., Elverhoi, A., and Parker, G., 1999. Experiments on the relative mobility of muddy subaqeous and subaerial debris flows, and their capacity to remobilize antecedent deposits. *Marine Geology*, v. 154, p. 117 – 129.

Moore, T.C., van Andel, Tj. H., Blow, W.H., and Heath, G.R., 1970. Large submarine slide off northeastern continental margin of Brazil. *American Association Petroleum Geologists Bulletin*, v. 54, p. 125-128. *

Moore, D.G. and Curray, J.R., 1963. Sedimentary framework of continental terrace off Norfolk, Virginia and Newport, Rhode Island. *American Association Petroleum Geologists Bulletin*, v. 47, p. 2051-2054. *

Moore, D.G, Curray, J.R., and Emmel, F.J., 1976. Large submarine slide (olistostrome) associated with Sunda arc subduction zone, north-east Indian Ocean. *Marine Geology*, v. 21, p. 211-226. *

Morelock, J., 1969. Shear strength and stability of continental slope deposits, western Gulf of Mexico. *Journal of Geophysical Research*, v. 74, p. 465 – 482.

Morgenstern, N.R., 1967. Submarine slumping and the initiation of turbidity currents, *Marine Geotechnique*, p. 189 – 220.

Mosher, D.C., Moran, K., and Hiscott, R.N., 1994. Late Quarternary sediment, sediment mass-flow processes and slope stability on the Scotian Slope. *Sedimentology*, v. 41, p. 1039-1061. *

Mulder, T., and Alexander, J., 2001. The physical character of subaqueous sedimentary density currents and their deposits. *Sedimentology*, v. 48, p. 269 – 299.

Mulder, T. and Cochonat, P., 1996. Classification of offshore mass movements. *Journal of Sedimentary Research*, v. 66, p. 43 – 57.

Mulder, T., Berry, J.A. and Piper, D.J.W., 1997. Links between the morphology and geotechnical characteristics of large flow deposits in the albatross area on the Scotian slope (SE Canada). *Marine Georesources and Geotechnology*, v. 15, p. 253-281. *

Mulder, T., Tisot, J.P., Cochonat, P., and Bourillet, J.F., 1994. Regional assessment of mass failure events in the Baie des Anges, Mediterranean Sea, *Marine Geology*, v. 122, p. 29 – 45. *

Mulder, T., Weber, O., Anschutz, P., Jorissen, F.J., and Jouanneau, J.-M., 2001. A few months-old storm-generated turbidite deposited in the Capbreton Canyon (Bay of Biscay, SW France). *Geo-Marine Letters*, v. 21, p. 149 – 156. *

Murty, T.S., and Brown, R.E., 1979. The submarine slide of 27 April, 1975 in Kitimat Inlet and the water wave that accompanied the slide, Pacific Marine Science Report 79-11. *

Nardin, T.R., Edwards, B.D., and Gorsline, D.S., 1979. Santa Cruz Basin, California borderland; dominance of slope processes in basin sedimentation. *Geology of continental slopes, Special Publication – Society of Economic Paleontologists and Mineralogists*, v. 27, p. 209 – 221. *

Nelson, C.H., Maldonado, A., Coumes, F., Got, H., and Monaco, A., 1983. The Ebro deep-sea fan system, *Geo-Marine Letters*, v. 3, p. 125 – 131. *

Newton, R.S., Cunningham, R.C., and Schubert, C.E., 1980. Mud volcanoes and pockmarks: Seafloor engineering hazards or geologic curiosities? *Proceedings - Annual Offshore Technology Conference*, v. 1, May 5-8 1980, Houston, TX, USA, p. 425 – 435.

Niemi, T. M., and Ben-Avraham, Z., 1994. Evidence for Jericho earthquakes from slumped sediments of the Jordan River delta in the Dead Sea, *Geology* (Boulder), v. 22, no. 5, p. 395 - 398. *

Nitzsche, M., 1989. Submarine slope instability, eastern Banda Sea, *Netherlands Journal of Sea Research*, v. 24, p. 431 – 436. *

Norem, H., Locat, J., and Schieldrop, B., 1990. An approach to the physics and the modeling of submarine flowslides, *Marine Geotechnology*, v. 9, p. 93 – 111.

Normark, W.R., 1974. Ranger Submarine Slide, Northern Sebastian Vizcaino Bay, Baja California, Mexico. *Geological Society of America Bulletin*, v. 85, p. 781-784. *

Normark, W.R., Moore, J.G., and Torresan, M.E., 1993a. Giant Volcano-Related Landslides and the Development of the Hawaiian Islands. In: *Submarine landslides: Selected Studies in the U.S. Exclusive Economic Zone*, U.S. Geological Survey Bulletin 2002, p. 184-196. *

Normark, W.R., Wilde, P., Campbell, J.F., Chase, T.E., and Tsutsui, B., 1993b. Submarine slope failure initiated by Hurrican Iwa, Kahe Point, Oahu, Hawaii. In: *Submarine landslides: Selected Studies in the U.S. Exclusive Economic Zone* (Eds. Schwab, W.C., Lee, H.J., and Twichell, D.C.), U.S. Geological Survey Bulletin 2002, p. 197-204. *

Normark, W.R., Barnes, N.E., and Coumes, F., 1984a. Rhone Deep-Sea Fan: A review. *Geo-Marine Letters*, v. 3, p. 155 – 160. *

Normark, W.R., Gutmacher, C.E., Chase, T.E., and Wilde, P., 1984b. Monterey Fan: Growth pattern control by basin morphology and changing sea levels. *Geo-Marine Letters*, v. 3, p. 93 – 99. *

Normark, W.R., and Piper, D.J.W., 1991. Initiation processes and flow evolution of turbidity currents: Implications for the depositional record. SEPM Special Publication 46, p. 207 – 230. *

Normark, W.R., and Hess, G.R., 1980. Quaternary growth patterns of California submarine fans, *in* Field, M.E., Bouma, A.H., Colbourn, I.P., Douglas, R.G., and Ingle, J.C., eds., Pacific Section SEPM, Pacific Coast Paleogeography Symposium No. 4, Los Angeles, Calif., p. 201 – 210. *

O'Leary, D.W., 1986a. Seismic structure and stratigraphy of the New England continental slope and the evidence for slope instability. *U.S. Geological Survey Open-File Report 86-118*, 7 maps, scale 1:250,000. *

O'Leary, D.W., 1986b. The Munson-Nygren slide, a major lower-slope slide off Georges Bank. *Marine Geology*, v. 72, p. 101 – 114. *

O'Leary, D.W., 1993. Submarine mass movement, a formative process of passive continental margins: the Munsen-Nygren landslide complex and the southeast New England landslide complex. In: *Submarine landslides: Selected Studies in the U.S. Exclusive Economic Zone* (Eds. Schwab, W.C., Lee, H.J., and Twichell, D.C.), U.S. Geological Survey Bulletin 2002, p. 23-39. *

O'Leary, D.W., and Twichell, D.C., 1981. Potential geologic hazards in the vicinity of Georges Bank Basin, *in* Schlee, J.S. (ed.), Summary report of the sediments, structural framework, petroleum potential, and environmental considerations of the United States middle and northern continental margin in area of proposed oil and gas lease sale no. 82. *U.S. Geological Survey Open-File Report 81-1353*, p. 55 – 75.

Palmer, H.D., 1979. Man's activities on the continental slope. *The Society of Economic Paleontologists and Mineralogists, Special Publication No. 27*, p. 17 – 24.

Papatheodorou, G., and Ferentinos, G., 1997. Submarine and coastal sediment failure triggered by the 1995, M_s = 6.1 R Aegion earthquake, Gulf of Corinth, Greece, *Marine Geology*, v. 137, p. 287 – 304. *

Paul, M.A., Talbot, L.A., and Stoker, M.S., 1998. Shallow geotechnical profiles, acoustic character and depositional history in glacially influenced sediments from the Hebrides and West Shetland Slopes. In *Geological Processes on Continental Margins: Sedimentation, mass-wasting and stability*, edited by M.S. Stoker, D. Evans, and A. Cramp, Geological Society, London, Special Publications, no. 129, p. 117-131. *

Perret, D., Locat, J., and Leroueil, S., 1995. Strength development with burial in fine-grained sediments from the Saguenay Fjord, Quebec. *Canadian Geotechnical Journal*, v. 32, p. 247-262. *

Piper, D.J.W., and Normark, W.R., 1982. Effects of the 1929 Grand Banks earthquake on the continental slope off eastern Canada. Geological Survey of Canada, Paper 82-1B, p. 147-151. *

Piper, D.J.W., Stow, D.A.V., and Normark, W.R., 1984. The Laurentian Fan: Sohm Abyssal Plain. *Geo-Marine Letters*, v. 3, p. 141 – 146. *

Piper, D.J.W., Farre, J.A., and Shor, A.N., 1985a. Late Quaternary slumps and debris flows on the Scotian Slope. *Geological Society of America Bulletin*, v. 96, p. 1508 – 1517. *

Piper, D.J.W., Shor, A.N., Farre, J.A., O'Connell, S., and Jacobi, R.D., 1985b. Sediment slides and turbidity currents on the Laurentian fan—sidescan sonar investigations near the epicenter of the 1929 Grand Banks earthquakes. *Geology*, v. 13, p. 538 – 541. *

Piper, D.J.W., Cochonat, P., and Morrison, L., 1999a. The sequence of events around the epicenter of the 1929 Grand Banks earthquake: Initiation of debris flows and turbidity current inferred from sidescan sonar. *Sedimentology*, v. 46, issue 1, p. 79 – 97. *

Piper, D.J.W., Skene, K.I. and Morash, N., 1999b. History of major debris flows on the Scotian Rise. Geological Survey of Canada, Current Research, 1999-E, p. 203-212. *

Piper, 2000. The Geological Framework of Sediment Instability on the Scotian Slope: Studies to 1999. Geological Survey of Canada (Atlantic). Draft of open file. *

Pirmez, C., and Ercilla, G., 1998. Contrasting submarine fans off the Amazon and Magdalena Rivers. *AAPG Bulletin*, v. 82, no. 10, p. 1883. *

Ploessel, M.R., S.C. Crissman, J.H. Rudat, R. Son, C.F. Lee, R.G. Randall, and M.P. Norton, 1979. Summary of potential hazards and engineering constraints, proposed OCS lease sale no. 48, offshore southern California. *Offshore Technology Conference, 11*. Houston, 1979. Proceedings, v. 1, p. 355 – 363.

Popenoe, P., Schmuck, E.A., and Dillon, W.P., 1993. The Cape Fear Landslide: Slope Failure Associated with Salt Diapirism and Gas Hydrate Decomposition. In: *Submarine landslides*: *Selected Studies in the U.S. Exclusive Economic Zone*, U.S. Geological Survey Bulletin 2002, p. 40-53. *

Popenoe, P., Coward, E.L., and Cashman, K.V., 1982. A regional assessment of potential environmental hazards and limitations on petroleum development of the southeastern United States Atlantic continental shelf, slope, rise, offshore North Carolina: U.S. Geological Survey Open-File Report 82-126, 67 p.

Popenoe, P. 1983. Environmental considerations for OCS development, lease sale 90 call area, *in* Dillon, W.P. (ed.), Geology report for proposed oil and gas lease no. 90, Continental margin off the southeastern United States. *U.S. Geological Survey Open-File Report 83-136*, p. 67 – 88.

Popenoe, P. 1984. Summary geology report for the South Atlantic Outer Continental Shelf (OCS) Planning Area (a supplement to U.S. Geological Survey Open-File Report 83-136). *U.S. Geological Survey Open-File Report 84-476*, 17 p., 10 maps, scale 1:1,000,000.

Pratson, L.F., Ryan, W.B.F., Mountain, G.S., and Twichell, D.C., 1994. Submarine canyon initiation by downslope-eroding sediment flows: Evidence in late Cenozoic strata on the New Jersey continental slope. *Geological Society of America Bulletin*, v. 106, p. 395 – 412. *

Prior, D.B., 1984. Subaqueous landslides. *In* Proceedings of the 4th International Symposium on Landslides, Toronto, v. 2, p. 179 – 196.

Prior, D.B., Suhayda, J.N., Lu, N.Z., Bornhold, B.D., Keller, G.H., Wiseman, W.J., Wright, L.D., and Yang, Z.-S., 1989. Storm wave reactivation of a submarine landslide. *Nature*, v. 341, p. 47 – 50.

Prior, D.B., Bornhold, B.D., Coleman, J.M., and Bryant, W.R., 1982. Morphology of a submarine slide, Kitimat Arm, British Columbia. *Geology*, v. 10, p. 588-692. *

Prior, D.B., Bornhold, B.D., and Johns, M.W., 1986a. Active sand transport along a fjord bottom channel, Bute Inlet, British Columbia. *Geology*, v. 14, p. 581 – 584. *

Prior, D.B., Yang, Z.-S., Bornhold, B.D., Keller, G.H., Lu, N.Z., Wiseman, W.J., Wright, L.D., and Zhang, J., 1986b. Active slope failure, sediment collapse, and silt flows on the modern subaqueous Huanghe (Yellow River) Delta. *Geo-Marine Letters*, v. 6, p. 85 – 95. *

Prior, D.B., Bornhold, B.D., Wiseman, W.J., Jr., and Lowe, D.R., 1987. Turbidity current activity in a British Columbia fjord. *Science*, v. 237, p. 1330 – 1333. *

Prior, D.B., Bornhold, B.D., and Johns, M.W., 1984. Depositional characteristics of a submarine debris flow. *Journal of Geology*, v. 29, p. 707 – 727. *

Prior, D.B., and Coleman, J.M., 1984. Submarine slope instability. Slope Instability, Chapter 10, John Wiley & Sons, Inc., New York, NY, p. 419 – 455.

Prior, D.B., and Coleman, J.M., 1979. Submarine landslides – Geometry and nomenclature, *Zeitschrift fur geomorphologie*, v. 23, p. 415-426.

Prior, D.B., and Coleman, J.M., 1978. Disintegrating retrogressive landslides on very-low-angle subaqueous slopes, Mississippi delta. *Marine Geotechnology*, v. 3, p. 37-60. *

Prior, D.B., Doyle, E.H., and Neurauter, T., 1986. The Currituck Slide, mid-Atlantic continental slope – revisited. *Marine Geology*, v. 73, p. 25 – 45. *

Prior, D.B., Wiseman, W.J., and Gilbert, R., 1981. Submarine slope processes on a fan delta, Howe Sound, British Columbia. *Geo-Marine Letters*, v. 1, p. 85 – 90. *

Reed, D.L., Silver, E.A., Tagudin, J.E., Shipley, T.H., and Vrolijk, P., 1990. Relations between mud volcanoes, thrust deformation, slope sedimentation, and gas hydrate, offshore North Panama. *Marine and Petroleum Geology*, v. 7, p. 44 – 54.

Renz, O.R., Lakeman, R., and Van de Meulen, E., 1955. Submarine sliding in western Venezuela. *American Association of Petroleum Geologists Bulletin*, v. 39, p. 2053 – 2067. *

Richmond, W.C., and Burdick, D.J., 1981. Geologic Hazards and constraints of offshore Northern and Central California, *Offshore Technology Conference, 13. Houston 1981. Proceedings*, p. 9 – 17.

Richmond, W.C., Cummings, L.J., Hamlin, S., and Nagaty, M.E., 1981. Geologic Hazards and Constraints in the Area of OCS Oil and Gas Lease Sale 48, Southern California (Sale held June 29, 1979). *U.S. Geological Survey Open File Report 81-307*, 37 p.

Robb, J.M., Hampson, J.C., Jr., Kirby, J.R., and Twichell, D.C., 1981. Geology and potential hazards of the Continental Slope between Lindenkohl and South Toms Canyons offshore mid-Atlantic United States, *U.S. Geological Survey Open File Report 81-600*, 21 p., 22 figs., 3 maps. *

Roberson, J., Cassidy, J., and Chaudhry, M., 1988. Hydraulic Engineering, Houghton Mifflin Company, Boston, Massachusetts.

Roberts, D.G., 1972. Slumping on the eastern margin of the Rockall Bank, North Atlantic Ocean. *Marine Geology*, v. 13, p. 225-237. *

Roberts, D.G., and A.H. Stride, 1968. Late tertiary slumping on the continental slope of southern Portugal. *Nature*, v. 217, no. 5123, p. 48 – 50. *

Rona, P.A., 1969. Middle Atlantic Continental Slope of the United States; deposition and erosion, *American Association of Petroleum Geologists Bulletin*, v. 53, p. 1453 – 1465. *

Rona, P.A., and C.S. Clay, 1967. Stratigraphy and structure along a continuous seismic reflection profile from Cape Hatteras, North Carolina, to the Bermuda Rise. *Journal of Geophysical Research*, v. 72, p. 2107 – 2130. *

Ryan, W.B.F., and B.C. Heezen, 1965. Ionian sea submarine canyons and the 1908 Messina turbidity current. *Geological Society of America Bulletin*, v. 76, p. 915 – 932. *

Sættem, J., Poole, D.A.R., Ellingsen, L., and Sejrup, H.P., 1992. Glacial geology of outer Bjørnøyrenna, southwestern Barents Sea, *Marine Geology*, v. 103, p. 15 – 51. *

Sangrey, D.A. and Knebel, H.J., 1979. Geotechnical studies in the Baltimore canyon trough area. *Offshore Technology Conference, 11*. Houston 1979. Proceedings, v. 1, p. 331 – 341. *

Sangrey, D.A., Clukey, E.C., and Molnia, B.F., 1979. Geotechnical engineering analysis of underconsolidated sediments from Alaska coastal waters. *Offshore Technology Conference, 11.* Houston 1979. Proceedings, v. 1, p. 677 – 682.

Sassen, R., Robert, H., Milkov, A.V., and DeFreitas, D.A., 2001. Sea floor vents, seeps, and gas hydrate: Relation to Flux rate from the deep Gulf of Mexico petroleum system. *Gulf Coast Section Society of Economic Paleontologists and Mineralogists Foundation, 21st Annual Research Conference.*

Savoye, B., and Piper, D.J.W., 1991. The Messinian event on the margin of the Meditteranean Sea in the Nice area, southern France. *Marine Geology*, v. 97, p. 279-304. *

Savoye, B., Cochonat, P., and Piper, D.J.W., 1990. Seismic evidence for a complex slide near the wreck of the Titanic: model of an instability corridor for non-channeled gravity events. *Marine Geology*, v. 91, p. 281 – 298. *

Schafer, C.T., and Smith, J.N., 1987. Hypothesis for a submarine landslide and cohesionless flows resulting from a 17th century earthquake-triggered landslide in Quebec, Canada. *Geo-Marine Letters*, v. 7, p. 31 – 37. *

Scheidegger, A.E., 1973. On the prediction of the reach and velocity of catastrophic landslides. *Rock Mechanics*, v. 5, p. 231 – 236.

Scherreiks, R., 2000. A note on turbidites and debrites in the vicinity of the Aeolian Islands, SE Tyrrhenian Sea. *Geo-Marine Letters*, v. 20, p. 58 – 61.

Schwab, W.C., 1986. Sedimentologic study of Horizon Guyot, Mid Pacific Mountains. *U.S. Geological Survey Open File Report 86-433*, 137 pp. *

Schwab, W.C., and Lee, H.J., 1983. Geotechnical analyses of submarine landslides in glacial marine sediment, northeast Gulf of Alaska, in Molnia, B.F., Glacial Marine Sedimentation: New York, Plenum Press, p. 145-184. *

Schwab, W.C., and Lee, H.J., 1988. Causes of two slope-failure types in continental shelf sediment, northeastern Gulf of Alaska, *Journal of Sedimentary Petrology*, v. 58, p. 1-11. *

Schwab, W.C., Lee, H.J., Kayen, R.E., Quinterno, P.J., and Tate, G.B., 1988. Erosion and slope instability on Horizon Guyot, Mid-Pacific Mountains. *Geo-Marine Letters*, v. 8, p. 1 – 10. *

Schwab, W.C., Lee, H.J., and Molnia, B.F., 1987. Causes of varied sediment gravity flow types on the Alsek prodelta, northeast Gulf of Alaska. *Marine Geotechnology*, v. 7, p. 317-342. *

Schwab, W.C., and Lee, H.J., 1993. Processes Controlling the Style of Mass Movement in Glaciomarine Sediment: Northeastern Gulf of Alaska, In: *Submarine landslides: Selected Studies in the U.S. Exclusive Economic Zone*, U.S. Geological Survey Bulletin 2002, p. 135-142. *

Schwab, W.C., Danforth, W.W., Scanlon, K.M., and Masson, D.G., 1991, A giant slope failure on the northern insular slope of Puerto Rico, *Marine Geology*, v. 96, p. 237-246. *

Shanmugam, G., 1997. The Bouma sequence and the turbidite mind set. *Earth Science Rev.*, v. 42, p. 201 – 229. *

Shannon and Wilson, Inc., 1964a. Report on subsurface investigation for city of Seward, Alaska and vicinity: Seattle, Washington, Shannon and Wilson, Inc., 26 p. *

Shannon and Wilson, Inc., 1964b. Report on subsurface investigation for Mineral Creek townsite, city of Valdez, Alaska: Seattle, Washington, Shannon and Wilson, Inc., 12 p. *

Shepard, F.P., 1933. Depth changes in Sagami Bay during the great Japanese earthquake. *Journal of Geology*, v. 41, p. 527-536. *

Shepard, F.P., 1955. Delta front valleys bordering the Mississippi tributaries. *Geological Society of America Bulletin.* v. 66, p. 1489 – 1498.

Shepard, F.P., 1979. Submarine slopes and canyons on north side St. Croix Island, *Marine Geology*, v. 32, p. M69 – M76.

Shepard, F.P., 1981. Submarine canyons: Multiple causes and long-time persistence. *American Association Petroleum Geology Bulletin*, v. 65, p. 1062 – 1077.

Shepard, F.P., Dill, R.F., and Heezen, B.C., 1968. Diapiric intrusions in foreset slope sediments off Magdalena delta, Colombia. *The American Association of Petroleum Geologists Bulletin*, v. 52, no. 11, p. 2197 – 2207. *

Shepard, F.P., Niino, H. and Chamberlain, T.K., 1964. Submarine canyons and Sagami Trough, Central Honshu, Japan, *Geological Society of America Bulletin.* v. 75, p. 1117 – 1130. *

Shipley, T.H., Houston, M.H., Buffler, R.T., Shaub, F.J., McMillen, K.J., Ladd, J.W., and Worzel, J.L., 1979. Seismic Evidence for Widespread Possible Gas Hydrate Horizons on Continental Slopes and Rises, *AAPG Bulletin*, p. 2204 – 2213.

Shor, A.N., and Piper, D.J.W., 1989. A large late Pleistocene blocky debris flow on the central Scotian slope. *Geo-Marine Letters*, v. 9, p. 153 – 160. *

Skempton, A.W., 1970. The consolidation of clays by gravitational compaction. *Journal of Geological Society of London*, v. 125, p. 373 – 411.

Stanley, D.J., and Silverberg, N., 1969. Recent slumping on the continental slope off Sable Island Bank, southeast Canada. *Earth and Planetary Science Letters,* v. 6, p. 123 – 133. *

Sterling, G.M., and Strohbeck, E.E., 1973. The failure of the south pass 70 'B' platform in Hurricane Camille. *Offshore Technology Conference, 5.* Houston 1973. Preprints, v. 2, p. 719 – 730. *

Summerhayes, C., Bornhold, B., and Embley, R.W., 1979. Surficial slides and slumps on the continental slope and rise off Southwest Africa, *Marine Geology*, v. 31, p. 265-277. *

Swift, S.A., 1985. Late Pleistocene sedimentation on the Continental Slope and Rise off western Nova Scotia, *Geological Society of America Bulletin*, v. 96, p. 832 – 841. *

Syvitski, J.P.M., and Farrow, G.E., 1989. Fjord sedimentation as an analog for small hydrocarbon-bearing fan deltas, *in* Whately, M.K.G., and Pickering, K.T., eds., Deltas – Sites and Traps for Fossil Fuels. *Geological Society of London Special Publication 41*, p. 21 – 43. *

Syvitski, J.P.M., and Hein, F.J., 1991. Sedimentology of an Arctic Basin: Itirbilung Fjord, Baffin Island, Northwest Territories. *Geological Survey of Canada Paper 91-11*, 61 p. *

Tappin, D.R., Matsumoto, T., Watts, P., Satake, K., McMurtry, G.M., Matsuyama, M., Lafoy, Y., Tsuji, Y., Kanamatsu, T., Lus, W., Iwabuchi, Y., Yeh, H., Matsumotu, Y., Nakamura, M., Mahoi, M., Hill, P., Crook, K., Anton, L., and Walsh, J.P., 1999. Sediment slump likely caused 1998 Papua New Guinea tsunami, *Eos, Transactions, American Geophysical Union*, v. 80, no. 30, p. 329, 334, 340. *

Taylor, J., Dowdeswell, J.A., and Kenyon, N.H., 2000. Canyons and late Quaternary sedimentation on the North Norwegian margin, *Marine Geology*, v. 166, p. 1 – 9. *

Terzaghi, K., 1956. Varieties of submarine slope failures. *Texas Conference on Soil Mechanics and Foundation Engineering, 8.* Austin 1956. Proceedings. 41 p.

Terzaghi, K., Peck, R.B., Mesri, G., 1996. Soil Mechanics in Engineering Practice, 3rd Edition, John Wiley & Sons, Inc., New York, NY.

Tinti, S., and Bortolucci, E., 2000. Energy of water waves induced by submarine landslides. *Pure and Applied Geophysics*, v. 157, p. 281 – 318.

Trincardi, F., and Argnani, A., 1990. Gela submarine slide: A major basin-wide event in the Plio-Quarternary foredeep of Sicily. *Geo-Marine Letters*, v. 10, p. 13 – 21. *

Trincardi, F., and Normark, W.R., 1989. Pleistocene Suvero slide, Paola basin, southern Italy, *Marine and Petroleum Geology*, v. 6, p. 324 – 335. *

Tucholke, B.E., 1987. Submarine geology, *in* Milliman, J.D., and Wright, W.R., eds., Marine Environment of the U.S. Atlantic Continental Slope and Rise: Jones and Bartlett Publishers, Boston, p. 56 - 113. *

Twichell, D.C., Roberts, D.G., and Teleki, P.G., 1980. Long-range side-scan sonar views of the U.S. Continental slope and rise between the Hudson and Baltimore Canyons, *Abstracts with Programs - Geological Society of America*, v. 12, no. 7, p. 538 – 539. *

Uchupi, E., 1967. Slumping on the continental margin southeast of Long Island, New York, *Deep-Sea Research*, v. 14, p. 635-639. *

Van Weering, Tj.C.E., Nielsen, T., Kenyon, N.H., Akentieva, K., and Kuijpers, A.H., 1998. Large submarine slides on the NE Faeroe continental margin. In:

Stoker, M.S., Evans, D. & Cramp, A. (eds) *Geological Processes on Continental Margins: Sedimentation, Mass-Wasting and Stability.* Geological Society, London, Special Publications, no. 129, p. 5-17. *

Vestal, W., and Lowrie A., 1982. Large-scale slumps off southern India and Sri Lanka. *Geo-Marine Letters*, v. 2, p. 171 – 177. *

Vogt, P.R., Gardner, J., and Crane, K., 1999. The Norwegian-Barents-Svalbard (NBS) continental margin: Introducing a natural laboratory of mass wasting, hydrates, ands ascent of sediment, pore water, and methane. *Geo-Marine Letters*, v. 19, p. 2 – 21.

Walker, J.R., and Messingill, J.V., 1970. Slump features on the Mississippi Fan, Northeastern Gulf of Mexico. *Geological Society of America Bulletin*, v. 81, issue 10, p. 3101-3108. *

Woodbury, H.O., 1977. Movement of sediment on the Gulf of Mexico, continental slope and upper continental shelf. *Marine Geotechnology*, v. 2, p. 263 – 273.

Woodcock, N.H., 1979. Sizes of submarine slides and their significance, *Journal of Structural Geology*, v.1, p. 137-142.

Wright, L.D., Yang, Z.-S., Bornhold ,B. D., Keller, G.H., Prior, D.B., and Wiseman, W.J., 1986. Hyperpycnal plumes and plume fronts over the Huanghe (Yellow River) delta front. *Geo-Marine Letters*, v. 6, p. 97 – 105. *

Wright, R., and Anderson, J.B., 1980. Intercanyon mass flow transition on the continental slope of the Weddell Sea, Antarctica, *Abstracts with Programs - Geological Society of America,* v. 12, no. 7, p. 553. *

Wright, S.G., and Rathje, E.M., in press. Triggering mechanisms of slope stability and their relationship to earthquakes and tsunamis.

www.usgs.gov/, United States Geological Survey, Geophysical Long Range ASDIC (GLORIA) mapping project

Zeng, J., Lowe, D.R., Prior, D.B., Wiseman, W.J., Jr., and Bornhold, B.D., 1991. Flow properties of turbidity currents in Bute Inlet, British Columbia. *Sedimentology*, v. 38, p. 975 – 996. *

VITA

James Johnathan Hance was born in Washington, D.C. on December 3, 1976, the son of Brenda Hance Ruffner and James Joseph Hance. After completing his work at Gonzaga College High School, Washington, D.C., in 1994, he entered Bucknell University in Lewisburg, Pennsylvania. During the spring semester of 1997, he attended Nottingham University in Nottingham, England on a study abroad program. He earned the degree of Bachelor of Science in Civil Engineering from Bucknell University in May, 1998. During the following years, he was employed as a staff engineer with Schnabel Engineering Associates, Inc. in Maryland. In January, 2002, he entered The Graduate School at The University of Texas.

Permanent Address: 1833 Soniat Street
New Orleans, LA 70115

The thesis was typed by the author.